Modelling and Analysis of Variable Speed Wind Turbines with Induction Generator during Grid Fault

Bolik, Sigrid Mechthild

Publication date:
2004

Document Version
Publisher's PDF, also known as Version of record

AALBORG UNIVERSITY

Modelling and Analysis of Variable Speed Wind Turbines with Induction Generator during Grid Fault

SIGRID M. BOLIK

Institute of Energy Technology
Aalborg University

Danish Academy of Technical Sciences

Risø National Laboratory

Vestas Wind Systems A/S

Modelling and Analysis of Variable Speed Wind Turbines with Induction Generator during Grid Fault

by

Sigrid M. Bolik

Institute of Energy Technology
Aalborg University, Denmark
October 2004

Aalborg University
Institute of Energy Technology
Pontoppidanstraede 101
DK – 9220 Aalborg East

ISBN 87-89179-55-2

“Twenty years from now
you will be more disappointed
by the things that you didn't do than
by the ones you did do.
So throw off the bowlines.
Sail away from the safe harbor.
Catch the trade winds in your sails.
Explore. Dream. Discover.”

-Mark Twain

Abstract

During recent years wind turbine technology has undergone rapid developments. Growth in size and the optimization of wind turbines has enabled wind energy to become increasingly competitive with conventional energy sources. As a result today's wind turbines participate actively in the power production of several countries around the world. These developments raise a number of challenges to be dealt with now and in the future. The penetration of wind energy in the grid raises questions about the compatibility of the wind turbine power production with the grid. In particular, the contribution to grid stability, power quality and behaviour during fault situations plays therefore as important a role as the reliability.

The introduction of the present work briefly presents the development of wind turbine technology. Several wind turbine types are discussed and the motivations for this project are stated. The main motivations are the challenges related to the grid connection of wind turbines.

The second chapter elucidates recent thinking in the area of grid connection by discussing several grid codes or grid requirements. In the discussion it is tried to present the view of the transmission line operators as well as the challenges wind turbine manufacturers such as Vestas faced.

Modelling has an important role in the research and development of system changes because it allows many difficult questions to be answered. The varieties of challenges that must be addressed in such modelling are not met by any single modelling software program. In addition a huge range of in-house programs from different companies exist, the most widely known software for current research on the power grid are PSS/E, EMTDC/PSCAD and DigSilent. In general research and especially for control developments the software Matlab/ Simulink is used. In all these programs simplified general models for different research purposes or specific detailed models have been developed and are used today. However, since wind turbine technology only has recently had to address grid related problems, models do not satisfy the demands peculiar to this technology. In particular, the role of both the wind turbine itself and the grid with respect to their influences, interaction and behaviour under grid faults or asymmetrical operation need further investigation. The present thesis therefore deals with the development of an improved wind turbine model. For the modelling the well known and widely used program Matlab/ Simulink has been chosen. The program is a powerful tool for solving and representing mathematical differential equations and therefore provides the opportunity to combine a wide range of different modelling issues.

The improvement of the large doubly-fed induction generator model as an interface between the mechanical and electrical characteristics of a wind turbine takes a central part in this research process. Chapter 3 presents the development and implementation of a detailed analytical three-phase induction machine model. The model uses only a minimum set of parameters as supplied by the generator manufacturers of Vestas. The accuracy of the simulation is improved by including the saturation of the main and the leakage inductances, which has been validated by test bench measurements. The influence of the generator saturation effects are discussed with respect to the behaviour of the machine itself and to the complete wind turbine behaviour.

Although the generator model is of primary interest for improving the wind turbine model, the implementation of the other elements completing a total wind turbine model have been challenging as well. In chapter 4 the development of a three-phase transformer model and especially a three-phase autotransformer as used in a Vestas Turbine is shown.

Chapter 5 deals with the development of transmission lines and electrical elements connecting the transformer and generator and giving the possibility to create a small

electrical network and thereby give the possibilities to research the dynamics introduced by a fault in the grid.
The wind turbine models are completed by modelling the mechanical and aerodynamical parts of the wind turbine and include the control system. In this thesis models of the two different wind turbine types, one with pulsed rotor resistance control (Vestas OptiSlip control) and another one with doubly-fed control (Vestas OptiSpeed control) have been implemented.
Finally two fault situations have been studied with the two developed wind turbine models. The influences on the generator as well as the behaviour of the wind turbine during these faults are briefly discussed based on the simulation results.
It can be concluded, that it has been possible to build advanced wind turbine models in Matlab/ Simulink for researching fault situations. However, one conclusion of this thesis is that Matlab/ Simulink might not be the ideal tool for studying a detailed complete model of a wind turbine including a small power system. The complexity of the differential equations combined with a huge number of iteration processes leads to instabilities, which limit the use of the model. Investigations in optimisation of the implemented models are advised. Otherwise the presented models can be seen as basis for further modelling investigations. The developed models are open for further extension for different purpose, e.g. research of the harmonics.
The introduced saturation effects of the machine definitely have an influence especially during the simulation of asymmetric fault situations and should be included in models for investigations into the fault situations for wind turbines, even though the influence is much less than expected at the beginning of this work. The reduced influence of saturation is related to the control of the machine, which basically compensates for the error caused by the machine's natural behaviour. The saturation effect is decreased particular during the doubly-fed operation with a very strong control. It does however increase again, if the control system is disabled, as it is initiated for converter protection during fault situations, the effects related to saturation of the machine increases again. Further work may be done on the investigation on the influences of the protection systems or further validation of the whole turbine system.
Furthermore it can be said, that the developed two wind turbine models can be used for the research of grid faults. The model is amenable to further development for different research interests, for instance the development of control strategies or the development of a detailed gear model for the research of stresses.

Acknowledgements

This thesis is initiated from my daily work with Vestas Wind System A/S and is carried out under the Industrial PhD fellowship EF 940. The project started on the 1.10.2001 and ended at the 30.9.2004, where the writing of this thesis has been finished as well. The project got financially supported by Vestas and Oticon through the Danish Academy of Technical Science (ATV). The thesis is submitted to the Faculty of Engineering and Science at Aalborg University as partial fulfilment of the requirements for gaining the PhD degree in Electrical Engineering.

There have been three main supervisors following the progress of the project. Professor Frede Blaabjerg from Aalborg University, Poul Soerensen from Risoe National Laboratory and Torben W. Moeller from Vestas Wind System A/S. I would like to thank all three for their support, patient and help in finishing this ambitious project in the given time.

I want to thank Lars Helle, Poul Brandt Christensen and Thomas Krueger for providing parts of wind turbine models to this study, which made it possible to achieve two complete wind turbine models.

Furthermore I like to thank all the people I met on my way from countries all over the world, giving me the possibility to discuss my ideas and giving me feedback to my work and therewith having participated in the work. Especially I like to highlight the wonderful possibilities given by the Nordic Network for Multi Disciplinary Optimised Electric Drives (NorMUD; http://www.normud.auc.dk/) actively supported by Professor Ewen Ritchie (Aalborg University).

I like to give further thanks to the R&D department of ABB in Vaasa and Helsinki to help me clarifying some question around machine technology and Vestas, who made this possible.

Especially I want to thank Professor Robert E. Betz and the PhD students from Newcastle University, helping me during my 4 month stay abroad. They participated actively to reflect on my accomplished work and broaden my view not only in scientific matters.
Other thanks is to the Australians I became friends with during my stay abroad and who helped me staying motivated during the last phase of my work.

Personally I want to thank Pia Salminen (Lappeenranta University of Technology), Ana-Mari Tataru (Aalborg University) and Julija Matevosyan (Royal Institute of Technology in Stockholm), who during my PhD became very good friends.

Finally I apologies for all the people they feel forgotten in this list.

Ringkøbing, September 2004

Sigrid M. Bolik

TABLE OF CONTENTS

Chapter 1

1. Introduction

The produced electrical power from wind has dramatically increased in the last years. Therefore today's wind turbines, which typically are centralised in wind parks, have a significant influence on the power production. Besides the merge of several wind turbines into bigger units in wind farms for increasing the production from wind energy the wind turbine itself has developed in size and technology rapidly in order to extract more energy form the wind and reduce the cost per produced kWh. During these developments the wind turbine has to overcome various kinds of problems and master new challenges.

1.1 Wind turbine technology

There exist a huge range of possible wind turbine configurations. Most commonly wind turbines are sorted into the two major categories of "fixed speed turbines" and "variable speed turbines". There is a wide range of topologies classified into these groups. A comparison and discussion of a few concepts can be found in /32/, /34/, /35/, /36/, /101/. The most commonly used concepts are pictured in Figure 1

Fixed speed wind turbines equipped with asynchronous or induction generators directly connected to the grid is one of the oldest and simplest concepts, which was first used in Denmark, and therefore known as the "Danish concept" (see Figure 1 a).
Variable speed turbines with induction or synchronous generator, directly or indirectly connected to the grid have become more and more important in recent years (see in Figure 1 concepts b) – f)). Possibilities such as mechanical load reduction and more efficient energy production, due to intelligent control strategies, make these concepts a beneficial economic solution. Furthermore these types are better grid compliant compared to the fixed speed turbines. The possibility to independently control the speed decoupled from the grid, gives the possibility to decouple frequencies resulting from the wind fluctuations from the grid, which reduces flicker contribution. The converter integrated in variable speed wind turbines gives the possibility to actively control the power output of the wind turbine, which is increasingly important for the integration of wind turbines into the grid /3/, /12/, /41/.
The fixed speed wind turbine is a self controlled concept. With increasing wind speed the laminar wind current flow around the fixed blade profile breaks and the turbine loses the possibility to obtain energy from the wind, the turbine stalls. The squirrel cage induction generator which transforms the obtained mechanical energy into electrical energy is directly connected to the grid. The speed of the generator may differ from the grid frequency due to the slip variation of the generator, which is up to 1%.
The variable speed wind turbine is usually equipped with a pitch control, where the blade can be turned to increase or decrease lift forces on the blade profile and thereby continuously control energy absorption from the wind. The active pitch control is designed to optimize the power obtained from the wind by changing the rotation speed of the rotor and the pitch angle and therewith gain an optimum current flow around the blade. The therewith achieved variable speed range at the turbine shaft or generator axes is different from the fixed frequency of the power system to 50Hz or 60Hz. A direct coupling of a

synchronous generator to the grid is therefore not possible, and a squirrel cage induction machine is too small in speed variation possibilities (<1%), which would limit power production only in a synchronism of the shaft speed and grid frequency. To enable an efficient power production at a huge range of different wind speeds the mechanical speed has to be decoupled from the grid frequencies. One method to decouple the two systems is to use a full scale power converter between the generator and the grid. This may give a speed variation up to 120%. The success of this concept has been limited over many years due to technical development in the area of power electronics and associated costs.

a) direct grid connected asynchonous generator with short circuit rotor

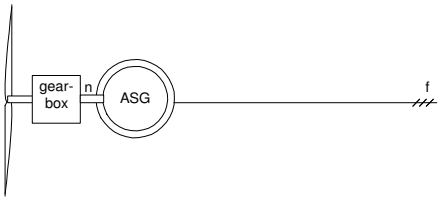

n = (1-s) f / p s = 0...0.08
(output dependent)
inductive power consumer

b) grid connection via converter of an asynchonous generator with short circuit rotor

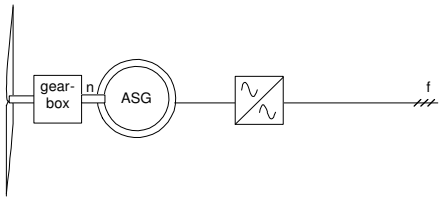

n = 0.8 ... 1.2 f / p (controllable)
inductive power consumer

c) dynamic slip control with slip ring generator

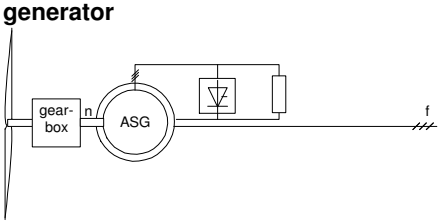

n = (1-s) f / p s = 0...0.1...(0.3)
(output dependent, dynamic)
inductive power consumer

d) grid connection via converter and synchonous generator with excitation system

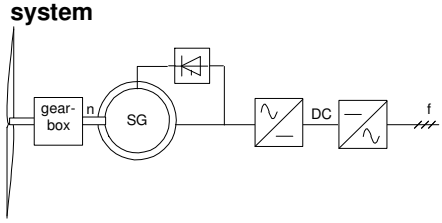

n = 0.5...1.2 f / p (controllable)
1) with thyristor converter - inductive power consumer
2) with pulse inverter - controllable reactive power output

e) grid connection via converter and synchonous generator with excitation system

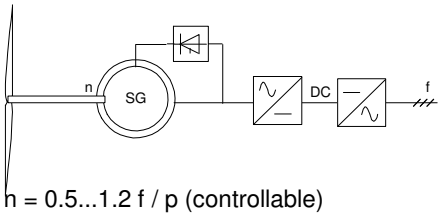

n = 0.5...1.2 f / p (controllable)
1) with thyristor converter - inductive power consumer
2) with pulse inverter - controllable reactive power output

f) doubly-fed slip ring asynchonous generator

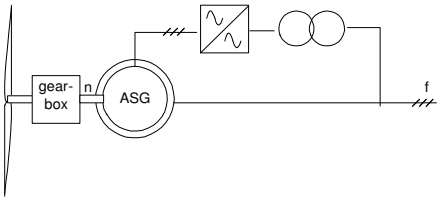

n = 0.7...1.3 f / p
(output dependent, dynamic)
inductive power consumer

Figure 1 Examples of generator concepts for wind turbines /35/
(note the used figure from the book defines positive slip values for generator operation)

Another way to connect a variable speed wind turbine to the grid is to use a doubly fed induction generator (DFIG). Wind turbines equipped with DFIG have become more and more common during the last years. It combines the advantages of pitch control with an efficient transmission of the power to the grid and the possibility of dynamic control of active and reactive power. Wind turbine technology benefits from the developments in the area of drive control. Essential progress in the dynamical control of machines brought the introduction of field oriented control by Blaschke /7/. In the following years until today research to improve the principle has been done /6/, /33/, /36/ - /38/, /59/, /64/, /70/, /80/.

In a system with DFIG the converter is placed to feed into the rotor of the machine while the stator is direct connected to the grid. Through the converter it is possible to control the supply, or extract the energy to the rotor of the induction machine. Thereby the machine can be controlled to run between sub synchronous speed and over synchronous speed (speed higher than synchronous speed). Usually a variation from -40% to +30% of synchronous speed is chosen. The total speed variation is between 60% and 70%. Under these conditions the power converter has only the size of a thirty, maximum a forty of the rated power, which is beneficial both economically and technically. In the world leading company Vestas the wind turbine concept with DFIG control is known as the *OptiSpeed®* turbine (Figure 2).

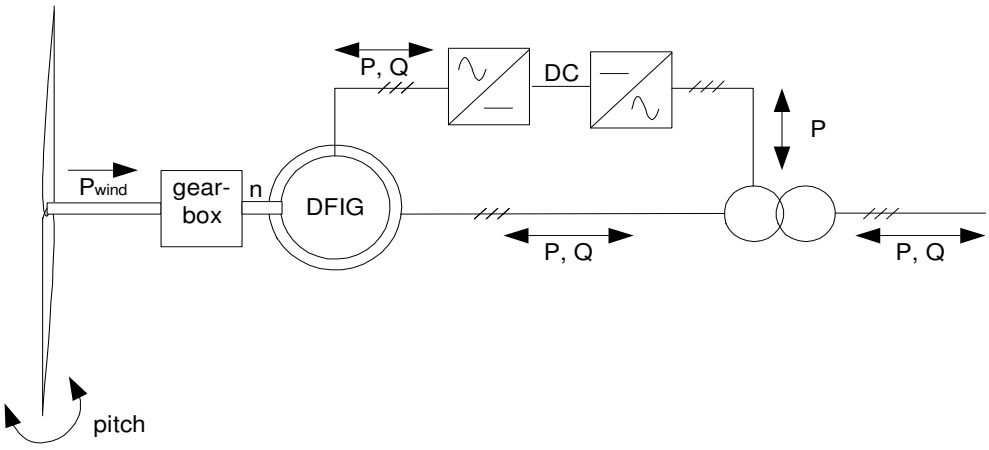

Figure 2 Vestas OptiSpeed wind turbine with Doubly Fed Induction Generator

Beside this concept Vestas also uses another concept, which technically is a variant between the fixed speed turbine and a variable speed turbine. The so called *OptiSlip®* is based on the concept of speed or torque control while using variable impedance at the rotor of the induction machine (similar as Figure 1 c). Vestas uses this concept to achieve a speed variation of 10% (sub synchronous). The benefits are the simplicity of the system, as in a fixed speed turbine but at the same time having the possibility of flicker regulation and load minimisation especially at high wind speeds.

1.2 Motivation and Aim of the Project

A wide range of research and development in the field of wind turbine technology to find the optimal concepts for wind turbine operation has been done in the past. The main focus thereby was the maximisation of energy production from the wind and cost reduction.
The increasing number of wind turbines connected to the grid shifted the focus of the research towards grid stabilisation. With the preferred broad use of the Danish concept the awareness of new power quality issues has risen. The fixed speed wind turbine couples the dynamics of the wind directly to the grid through the induction generator, which causes a poor quality power output of the turbine. An increased number of this wind turbine type integrated into the grid affects the power quality of the whole system.
Even the variable speed wind turbines are generally better grid compatible than fixed speed wind turbines, Network operators, who have to ensure well function power transmission and supply to their customers have given the wind turbines more and more attention. Induction generators for energy production are not known, especially not of the

size today used in today wind turbines (NEG Micon 4.2MW, Vestas 3.0MW). Historically power production is made by synchronous generators. Therefore there are no experiences with the integration of a large number of induction generators into the grid.
For answering these questions, measurements have been carried out and simulation models developed, mainly for the fixed speed wind turbines with squirrel cage induction generator. Results of the research from impact on the voltage quality and power fluctuation are shown in /5/, /15/, /29/, /45/, /73/, /89/, /101/. Important tasks are the grid connection and thereby connection and disconnection of the wind turbines, grid disappearance, short circuit power contribution, voltage dips and power quality during the production /1/, /44/, /56/, /58/, /76/, /77/, /85/. Network operators started to introduce grid connection requirement for the connection of wind turbines all over the world /12/, /16/, /17/, /61/, /67/, /90/.
However, the requirements are for all turbine types and the development of wind turbine models for the study of variable speed wind turbines with DFIG is still being developed. Wind turbines with DFIG have the advantage of fast electrical control. This gives the opportunity to use a wind turbine like a power plant. With special control strategies the wind turbine can even support the grid e.g. the power factor /84/, /90/, /93/. However existing models are mainly made with the purpose to develop control strategies and therefore do not express the dynamic behaviour of the whole turbine on the grid, e.g. influence of drive train oscillations and transformer asymmetry is missing /1/, /75/, /84/.

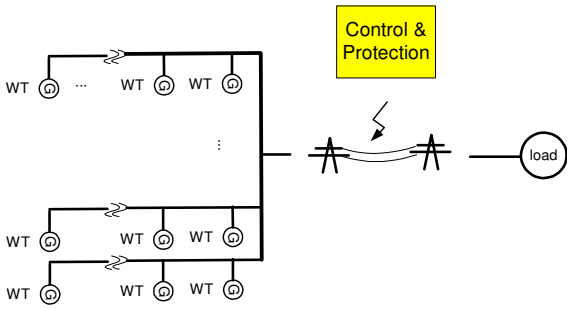

Figure 3 Power System Stability research with a wind farm connected to a larger grid

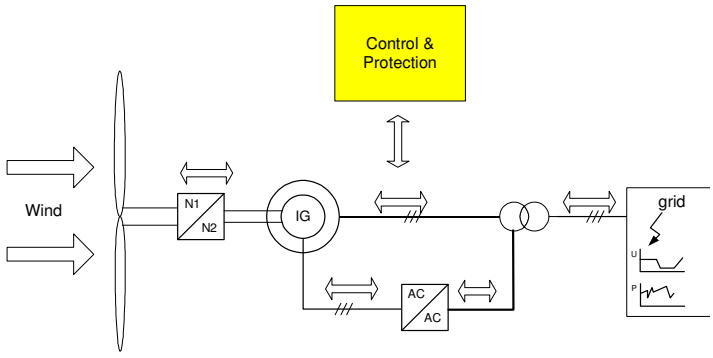

Figure 4 Wind Turbine stress research

Where on one side the network operators need wind turbine models to ensure well functioned power system (Figure 3) on the other side wind turbine manufacturers have to design a high quality product for a reasonable price. As the wind turbine affects the grid, the grid affects the function of the wind turbine itself. Determining the load caused by voltage dips, asymmetries or short circuits on the electrical as well as mechanical system require detailed models (Figure 4). These models contribute with a detailed knowledge about e.g. the torque on the wind turbine shaft caused by faults in the grid or transient current rises which is important for the estimation of the load on the wind turbines. An accurate as possible knowledge ensures the availability of the turbine for the estimated life time and low costs as well as help for the design of new wind turbines. The typical model studies requirements are summarized in Table 1-1.

Table 1-1 Typical study description for wind turbines models

	Network operator models	**Wind turbine manufacturer**
Type of analysis	Power system stability /55/ - Steady state (load flow) - Transient dynamics (large disturbances) - Small signal stability (small disturbances) - Stability studies including short and long term dynamics (angular, frequency, voltage stability)	Wind turbine stability - Transient dynamics - Load analysis
Time scale	0…ms…10s…min	0…us…ms…s
Model type	- turbine model as wind turbine unit -> several units in wind farm	- detailed turbine model with e.g. detailed transformer model, generator model

Wind turbine modelling is therefore an important part in the study of control, design, production and grid integration of wind turbines. One important issue while developing models is the clarification of the purpose of the model. Any assumptions made during the model development, which lead to simplifications of the model itself, are important in order to validate the correctness of the results. Creating a complete wind turbine model with predefined elements in the available professional software like EMTDC/ PSCAD, DigSilent or PSS/E can introduce a difficult task to find the assumptions during the development of the program. Furthermore some elements are not represented in the software packages and force either modification of the model with an equivalent design while using available elements or the creation of own models. Validation of the correct behaviour of the total wind turbine model under these circumstances can be quite a difficult task. The most common way for clarifying the correctness of the model is the use of measurements, although, in some operations it might be difficult to obtain useable measurements e.g. short-circuit of a 3MW wind turbine. But especially these abnormal situations have recently come in the focus.
Although network operators and wind turbine manufacturers have a lot of similar interests and requirements, wind turbine producers have an additional focus on the product itself, which requires the use of additional software tools. The effectiveness of the model in terms of simulation speed is thereby not that as important as the quality of the simulation result. With considering the different aspects towards wind turbine simulations for a wind turbine manufacturer such as Vestas the following requirements to a wind turbine model can be stated as.

- Development of a total wind turbine model which is appropriate for fault simulations into one programme.
- Development of an open wind turbine model with an ability to add features for future wind turbine development.
- Development of a detailed generator model able to handle asymmetries, fault operations, a huge range of different generators and a minimum data input.
- Possible research on different generator models to gain knowledge about generator effects e.g. saturation influences.

The main goals of the project can be concluded in the following points:

1. Clarification about the requirements due to wind turbines operation with focus on non-normal operation modes.
2. Achievement of a generator model in Matlab/ Simulink handling the above mentioned requirements.
3. Implementation of two total specific wind turbine models in Matlab/ Simulink appropriate for grid fault simulation studies.
4. Research of the generators, grid fault influences to the wind turbine.

1.3 Thesis outline

This thesis deals with the development and research of wind turbine models for the simulation of wind turbine operation in normal and especially abnormal operations. The models are developed with the special focus on simulation of the turbine in grid fault situations and other tough operation modes (grid codes). A self developed model has the advantages that assumptions and limitations are known. This model can be used additionally to verify models in other programs and reveal potential differences, which would otherwise be overlooked. Another advantage is the freedom to develop the model expressing the wind turbine as it exists in reality, while using the available data.
For the present work the known tool Matlab/ Simulink has been chosen. Matlab is a world known and recognised program. The graphical user interface – Simulink is widely known from the research in control strategies and gives the advantage to solve time dependent mathematical equations without deeper programming skills and seems therefore useable software for the solving the task.
The main parts of the thesis therefore deal with the modelling and implementation of different components of the wind turbine in the form of a library, which gives a variety of simulation possibilities.
Special focus has been given to the modelling of the generator. Detailed modelling of the generator is crucial in order to gain realistic behaviour of the wind turbines during faults. Simplification of the model is therefore only limited possible. The main limitation to the model is the available set of data and the software itself. A three – phase generator model implementation is a further focus of the work, but other known simplified models will be discussed as well.
The transformer model and the network models are implemented in different grade of details and can be arbitrarily exchanged in the total wind turbine model.
The two common Vestas turbine types OptiSlip and OptiSpeed have been implemented as example for the wind turbine modelling study. In Figure 5 modelling focus is visualised.

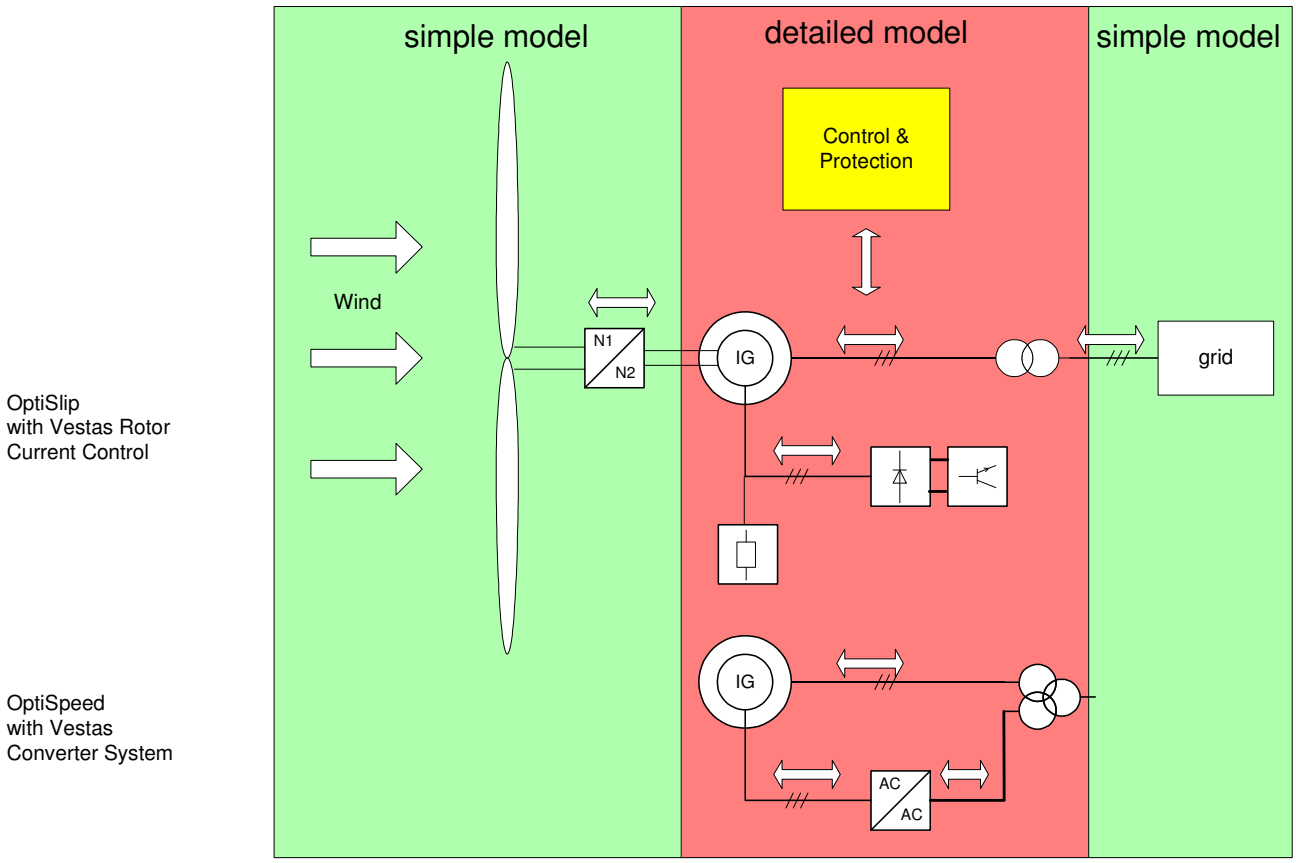

Figure 5 Schematic of modelling the Vestas OptiSlip and OptiSpeed system

With these two wind turbine models examples of the stresses occurring during a standard fault will be shown. The type of the fault is a typical situation as discussed in grid connection requirements, which will be discussed in the beginning of the thesis.

Following one main focus of this work, which is the development of a generator model for a wind turbine under grid faults, the thesis starts with the clarification of the requirements with looking at the recent grid code discussion. To point out the main research area this study is followed directly by the developments of the detailed models; the electrical components (see Figure 5). To continue the detailed modelling of the electrical components of the wind turbine and finish the electrical development issues the thesis will describe the grid, before shifting to the less discussed topic of mechanical component modelling of the wind turbine. The mechanical and aerodynamical model of wind turbines are the focus in many other investigations and therewith will not be discussed as much, although it is important for the completion of a total wind turbine model and can therefore not be left out of the description. The similar matter is the control strategies. The both presented control strategies are not the focus of the research, although have an important influence on the behaviour of the wind turbine, and therewith are briefly discussed in the end part of the thesis before setting the focus towards the fault simulations with the wind turbine models.

The content of the thesis in chapters after this introduction is:

Chapter 2 Grid connection of Wind Turbines gives an overview over the main points in the recent grid connection discussion.

Chapter 3 Induction Machine Models shows the development of induction machine models, including saturation effects. In this chapter space vector theory is introduced and applied for machine modelling.

Chapter 4 Modelling of Transformers explains the development of three-phase transformer models.

Chapter 5 Power system modelling in Matlab/ Simulink describes a solution to connect electrical elements in Simulink. Additionally transmission line theory and modelling are introduced.

Chapter 6 Wind Turbine modelling shows the modelling of the non-electrical components of a wind turbine exclusive the control system.

Chapter 7 Control of a wind turbine with controlled rotor resistance explains on the used example of the Vestas OptiSlip turbine control systems and therewith concludes one complete wind turbine model.

Chapter 8 Wind turbine with a doubly-fed induction generator control completes the second wind turbine model with using the arrangement of the Vestas OptiSpeed control system. An overview of the most important control features of this turbine is given.

Chapter 9 Fault simulations with total wind turbine models present two fault simulations with both the achieved Vestas models.

Chapter 10 Conclusion summarizes and concludes the most important results obtained in this work and sketches the perspective and future work regarding the wind turbine models.

Appendix includes all references used in this theses as well as symbol explanation and as well as copies of two published papers during the Ph.D. work.

Chapter 2

2. Grid connection of Wind Turbines

In the introduction the importance of grid connection issues were briefly introduced. The following chapter will highlight two major viewpoints to this issue. The first point is the view from the system operators or the responsible institution for power transmission and production in a country. As an example five different countries are studied. The second view is from the wind turbine manufacturer, who is producing the “power plant” and therefore the product to the energy supplier companies. Finally a closing discussion states some of the points, which should be considered for the grid connection of wind turbines.

2.1 Transmission system operator view

Even though power production from wind turbines has been known for several years the discussion for connection of wind turbines has arisen in recent years as the produced power by wind turbines increases. Furthermore, it became more and more common to install several wind turbines connected in wind farms or wind parks, which changes the view from wind power as a supplementary power source to the issue of possible substitution of conventional power plants with wind power.
Connection requirements for electrical devices to the grid have a long history in order to ensure stable operation of the grid. These requirements are besides juristic terms concerning frequency, voltage, power production and many others characteristics of the system.
Because common power plants are usually equipped with large synchronous machines, grid connection requirements are fitted to meet the operation from electrical networks with synchronous machines. Most commonly wind turbines are equipped with induction machines. Historically induction machines have been treated as consumer of the electrical grid and not as supplier. Experiences with induction machines connected in large numbers of wind turbines as energy supplier on the grid have just recently been studied /3/, /41/, /84/ and there are still many questions to answer.
Another important difference from conventional power plants is the energy resource for production. Unlike power production from nuclear power plants or coal power plants, where the possible power production is dependent on the mass of raw material and the consumed power, wind turbines are dependent on wind forecasting to guarantee a predicted power production. This forecasting of power production from wind turbines is not a simple task. However it is quite important for system operators, who need to have reliable energy sources. They have to ensure the produced power offer is fitting to the power demand, in order to keep the power system stable. Varying power demands can cause voltage and frequency changes in the system. These changes can be normalised with controlling the active and reactive power supply and therewith is another requirement the transmission system operators have towards power plants.

2.2 Wind turbine producers view

A wind turbine is a state of the art product, which all the time should meet the market demands. In addition, the cost per kilowatt should be low. Therefore it is important to know the loads in the turbine and the behaviour of the turbine exactly. Only with precise knowledge is it possible to avoid over- or under sizing of the product, which will lead to either rather expensive solutions or of not holding the life time expectancies of 20 years for the turbine. It takes typically three to five years to develop a new wind turbine type fitting to the new demands from design to sale. As an example, the Vestas products over the past years are shown in Figure 6.

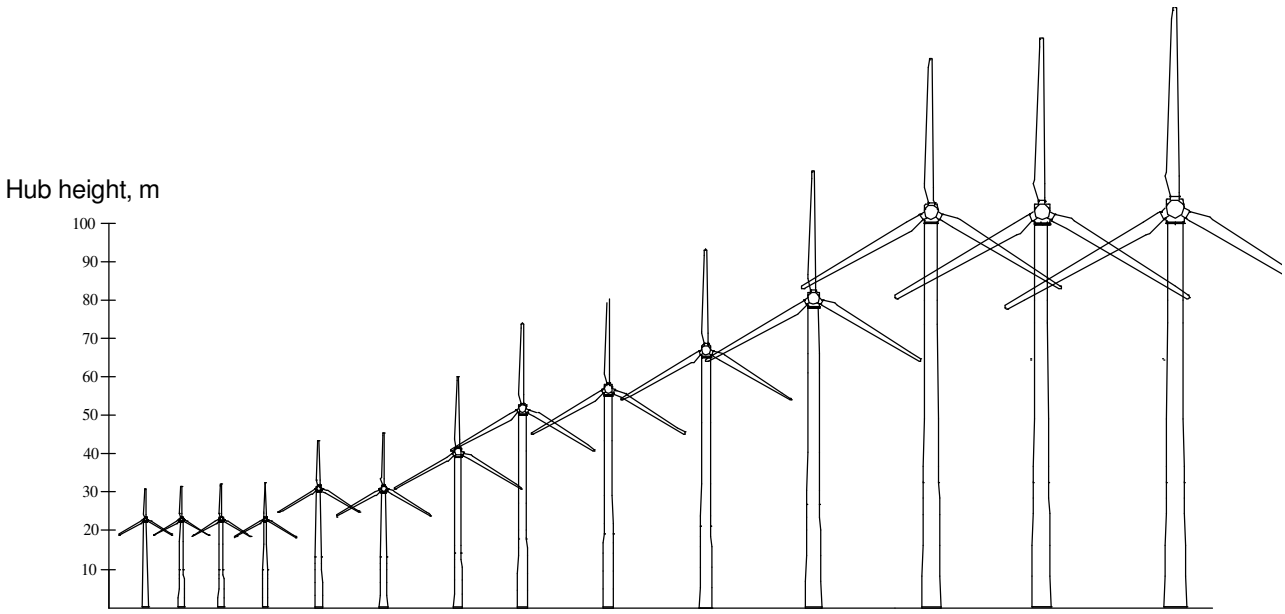

Capacity	55 kW	75 kW	90 kW	100 kW	200 kW	225 kW	500 kW	600 kW	660 kW	850 kW	1750 kW	2000 kW	3000 kW
First install.	1981	1984	1986	1987	1988	1989	1991	1995	1997	2000	1999	2000	2002
Rotor	15/16 m	17 m	19 m	20 m	25 m	27/29 m	39 m	44 m	47 m	52 m	66 m	80 m	90 m
Control	Stall	Stall	Stall	Stall	Stall	Pitch	Pitch/OptiSlip	Pitch/OptiSlip	Pitch/OptiSlip	Pitch/OptiSpeed	Pitch/OptiSpeed	Pitch/OptiSpeed	Pitch/OptiSpeed
Tower	22 m	22 m	22 m	31 m	31 m	39 m	50 m	50 m	55 m	49- 65 m	60-78 m	60-100 m	80 m
MWh/year	217	265	301	346	662	860	1671	1904	2372	2998	5303	7041	

Figure 6 Vestas Type Development during the last 23 years

While the development demands in recent years have been driven by mainly extracting most power out of the wind, the recent developments moved the focus to grid compliancy. Unfortunately the recent requirements to wind turbines or wind farms acting like conventional power plants are not necessarily easy to combine with the ideas and challenges that wind turbines have been designed in line with in years. A balance between the wind turbines handling the fluctuating wind energy resource and on the other hand being a reliable energy source supporting the electrical network has to be found. In this process the general requirements to produce a cheap product with low maintenance costs and high reliability have to be met.

2.3 Connection Requirements

However, the lack of experience enforces the use of existing grid codes of common generating units or power plants, which can be quite challenging for wind turbines. Special connection conditions for wind turbines have to be discussed. A few countries are already working on grid codes specifically for wind turbines or wind farms, or a modification of the existing code, which also meets wind turbine characteristics /23/. Figure 7 is visualises the grid code development compared to the turbines development and approximate turbine development time. The Horns Reef project is illustrated as an example.

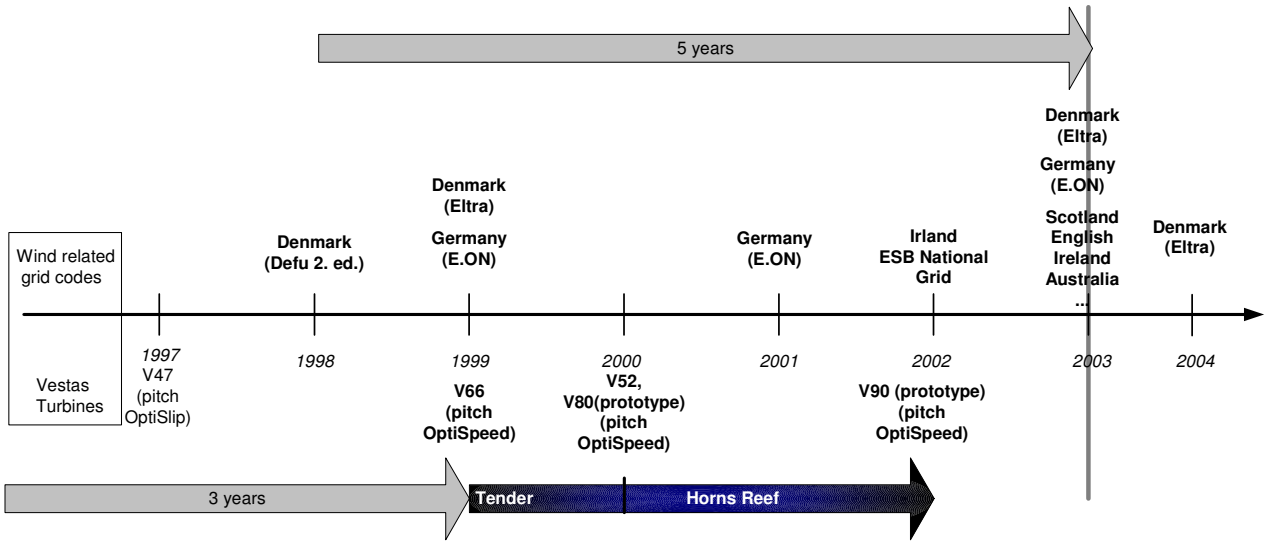

Figure 7 Wind Turbine development time and grid code demands

Unfortunately not all countries where wind turbines are installed have specific or modified grid codes. This makes the development of future wind turbines very difficult. There is a big risk involved in developing new techniques to fulfil unspecified demands.
Most wind turbine producers today deliver wind turbines to an international market and are faced with various numbers of grid requirements. Looking at a few of the existing grid codes it appears that they are very different in the most important characteristics. To visualise the state of the art technique, the different grid codes will be compared to the standard Vestas V80 2MW OptiSpeed turbine. The same turbine type is chosen for the modelling example in this Thesis.

2.3.1 Voltage criteria

The voltage in power systems can vary due to e.g. load changes or fault occurrence. To avoid loss of power generation in especially critical situations a voltage operation range is defined. The voltage tolerances can be seen from two aspects. Firstly, how much voltage variation should the wind turbine system be able to withstand, without tripping out and secondly, when and how should the disconnection from the grid occur. Figure 8 present the limits in terms of connection of the wind turbine to the grid for different countries and the performance of the Vestas V80 turbine.

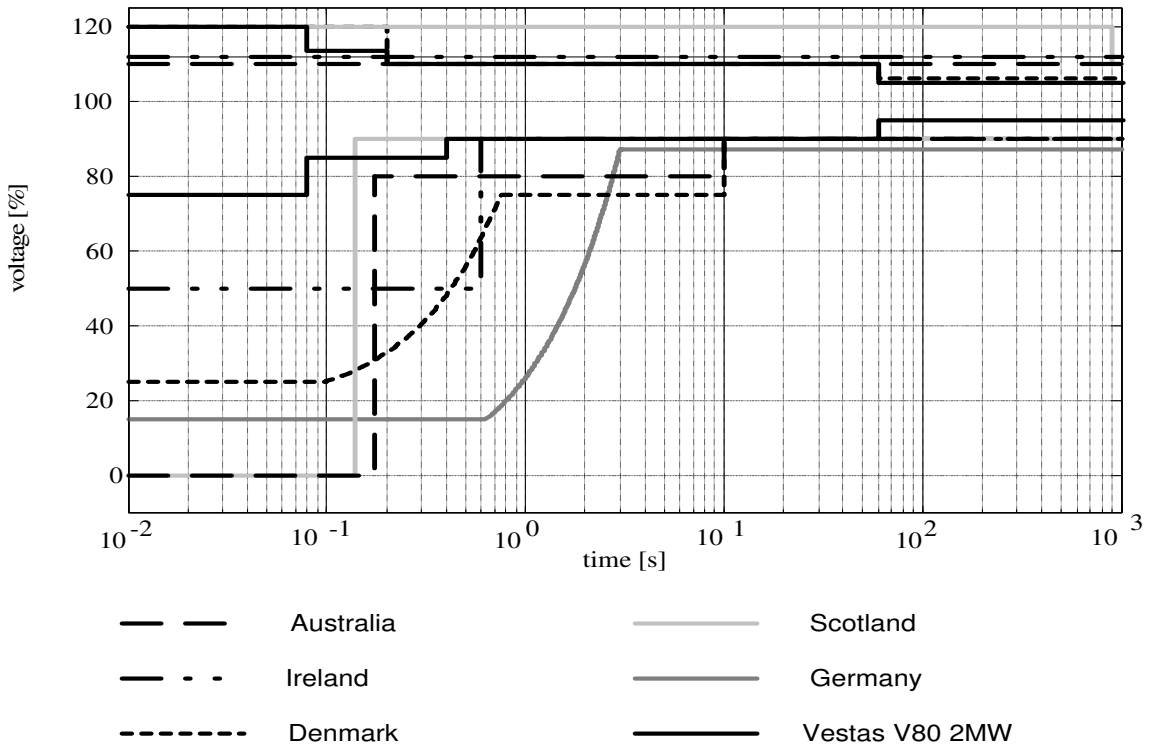

Figure 8 Voltage tolerance requirements in different countries and Vestas V80 capability

As shown in Figure 8 the demands between the countries are very different. In Australia the grid connected unit has to sustain 0% voltage for 175 ms, while in Denmark it is only 25% voltage for 100 ms without disconnecting from the grid. The Vestas standard V80 2 MW can satisfy these requirements using additional options, which expand the usual voltage tolerance of the wind turbine. In practice there is a major difference to develop a solution for no rest voltage or some rest voltage during a voltage dip. The worst case is zero voltage, what is equivalent to a terminal short circuit. The induction generator will loose all magnetisation and is not able to operate further on. A possible way of handling such a case is described in /12/. The DFIG is not able to support the voltage and build up the grid again as a synchronous machine would be able to do. Another case is a major voltage dip e.g. 15% voltage demanded in Germany or 25% voltage in Denmark. During a voltage drop the currents in the wind turbine increases. To avoid a disconnection of the turbine due to high currents, solutions for limiting these currents have to be developed. However, handling a voltage to a certain rest voltage is less complicated than the handling of no voltage. Several solutions for fault ride through are already presented /25/, /61/. Though there are good solutions for the grid, all the methods introduce high mechanical stress in the wind turbine.

2.3.2 Frequency requirement

Historically power plants use big synchronous generators. Direct grid connected synchronous machines have stability problems due to load changes and frequency changes. In the case of a machine overload, the synchronous machines will drop in speed, which means either they decrease the grid frequency as well or become unstable and drop out. The frequency change in a grid can be caused by loss of transmission, sudden demand changes or some problems of bigger power plants (loss of generation), which would normally stabilise the grid frequency. A change in grid frequency will affect all other

machines connected to it. Therefore an important issue is to operate in a wide range of frequencies (see Figure 9). Wind turbines with induction generators have no problem with asynchronous operation. The frequency operation range is more an issue of control strategy. A high frequency operation range for wind turbines and frequency control is therefore only interesting, if the power system operator uses the wind farm for stabilising the grid frequency. Although wind turbines are able to tolerate major frequency changes they have difficulties to support the frequency control operation in a wide range, hence the inertia in the system is very small. It is possible to initiate a sudden supply or reduction of power, which will actively help to stabilise the grid again. However, it has to be mentioned, that a supply of power into the grid is only possible, if the wind turbine is using an advanced operation at reduced power and thereby has enough power reserve or using another new control strategy. An example is given in the operation of the “Horns Reef” wind farm /14/

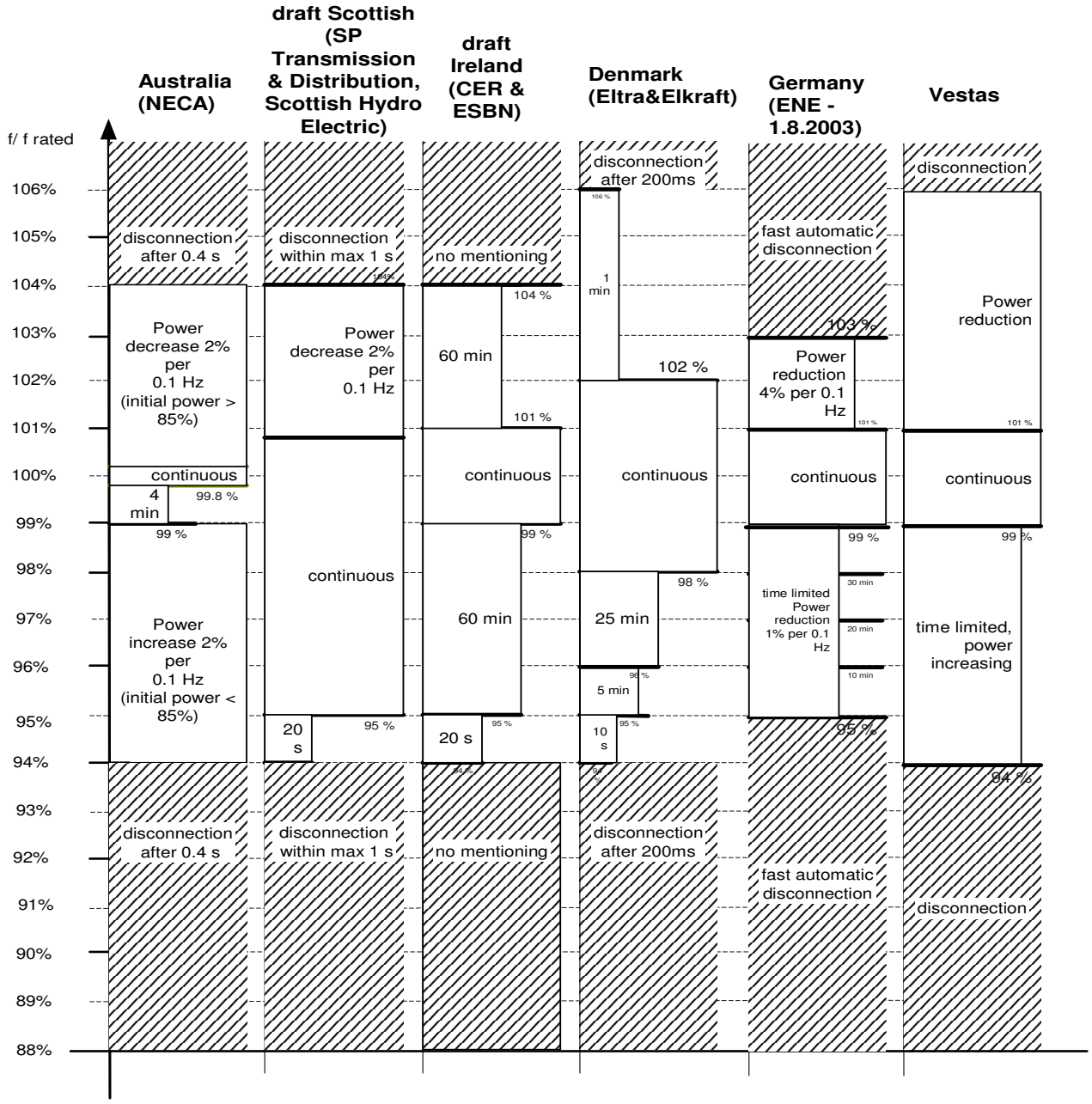

Figure 9 Frequency requirements in different countries compared to the performance of a Vestas V80 2 MW wind turbine

2.3.3 Active – and Reactive power requirement

The reactive power supply and absorption is important to control the voltage of the power system. No absorption or supply of reactive power from the wind turbine to the grid would mean only negligible influence of the wind turbine on the system voltage. However, a control to a power factor of one (only active power) is naturally compensates smaller reactive power changes in the system and therewith supports the grid. In this way wind turbines with DFIG have a positive effect on the grid. Usually the power factor capabilities are described in one point, as the static reactive power exchange with the grid during 100% power production from the turbine. Therefore the focus is on reactive power exchange with the power system, without loss of power production. But does this requirement make any sense for wind turbines? No, this one operation point consideration does validate the wind turbine without seeing the possibilities a wind turbine offers in its other operation points.
The connection demands, which are also the base for draft versions of wind turbine connection requirements, are primarily made for integration of “generating units” into the grid. These “generating units” usually produce full power after connection on to the grid and are slow in decreasing or increasing the power. The power production of a wind farm can vary between 0 and 100%, depending on the wind reserve and type. Because of the nature of wind power production from fluctuating wind, wind turbines have a fast power control. Wind farms are therefore capable in a short time to adjust power production.
On the other hand this gives the possibility to use the wind turbines reactive power capability for compensation or support of the grid in a situation, where no active power is needed. Figure 10 shows the possibility of the V80 2 MW to supply reactive power shown, and in Table 2-1 the specific numbers are collected. Hence Vestas V80 is changing to star connection at small power ranges the reactive power capability is small as well. But it is possible to stay in delta connection with a loss of some efficiency. Even though the wind turbine in smaller power is capable of an excellent power factor control it will cost extra money to expand the reactive power capability at rated power.

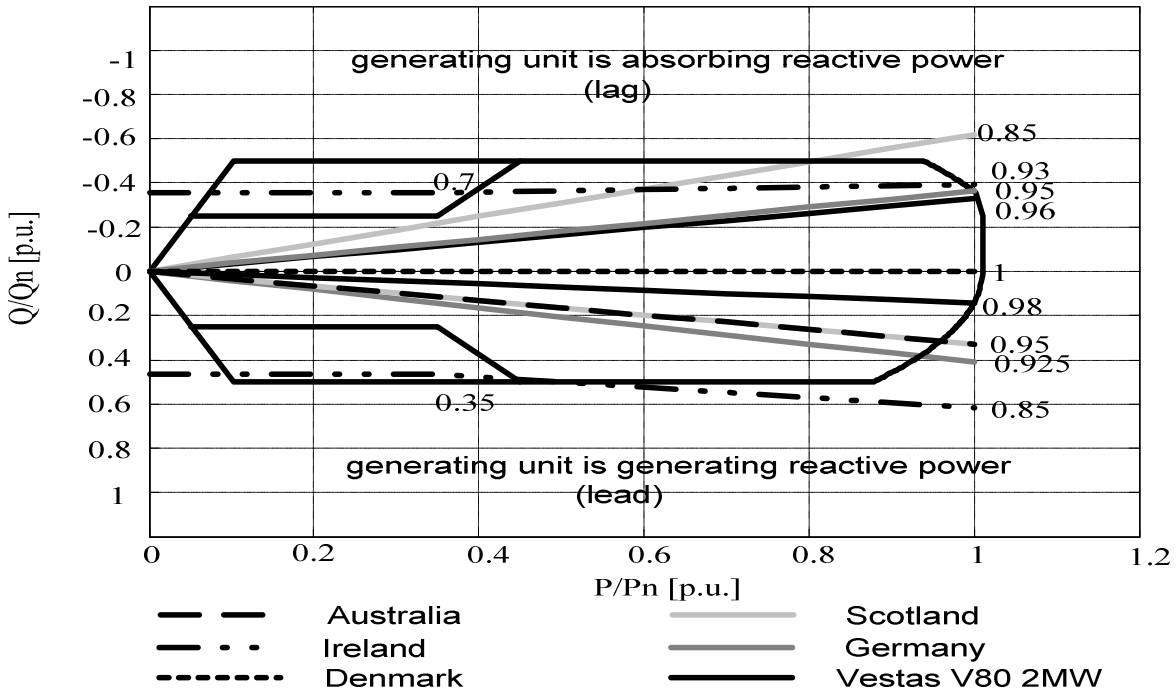

Figure 10 Requirements regarding reactive power in different countries and the technical capability of a Vestas V80 2 MW turbine (per unit of rated active power)

Table 2-1 Specific values for active- and reactive power requirements

Country	P-Q demand
Scotland	0.95 lead to 0.85 lag
Denmark	1 ± 10%P
Ireland	0.93 lead to 0.85 lag (100% power) 0.7 lead to 0.4 lag (35% power)
Germany (E.ON) E.ON additional WT - rules	0.95 lead 0.95 lag (<100MW) 0.925 unit generating reactive power (>=100 MW dependant on voltage range) 0.975 lead to 0,975 lag (P generating) 1 lead to 0.95 lag (P consumption) Q step: <= 0.5% , >= 25 kVar
Australia (NECA)	0.93 lead to 0.9 lag synchronous generator unity to 0.95 lagging asynchronous generator
Vestas (V80 2MW)	unity to 0.98 cap (high voltage side transformer) + at low voltage side transformer 0.98 cap 0.96 ind. (100% power) limited constant reactive power (0 - 100% active power) 0.2 cap. 0.2 ind. (power -> 0) + control power factor adjustments due to voltage, power control, power factor control, customer demands

2.3.4 Discussing the requirements

The specifications given in the above chapter to voltage, frequency and active-reactive power requirements show clearly the discrepancy and the variety in the grid codes. It also has to be mentioned that all requirements are in a rapid development, and these are changing at this moment. One of the tendencies is to follow the E.ON in Germany /23/ established requirements for grid connection of wind turbines. However, every grid is different and it might not be a good idea just copying the requirements. Although it is a good example for the German grid, a more practical solution could be a separation into two groups – wind turbines connected to strong grids, wind turbines connected to weak grids and the introduction of special requirements depend on the case. Grid codes should not have the purpose to avoid the connection of wind turbines to the grid. They should be open enough for discussion project specific issues.

The following points should be treated.

- Turbine should start automatically with a pre-defined time delay and power ramp
- Turbine should stop automatically with a pre-defined disconnection procedure (high wind or fault) and power ramp
- The continuous frequency range should be defined.
- A distinction between synchronous and asynchronous generator should be made.
- A dynamical description during rated operation and fault situations regarding voltage, active power and reactive power should be made.
- Considering the possible power production dependent on the wind input

The problem however stays. Wind turbine producers have a numbered product range, which should be able to fulfil as many grid requirements as possible. With the lack of conformability wind turbines will be designed for the codes for the biggest market and the outer limits. This consequently limits the price reduction of wind turbine technology. Therefore a continuous positive discussion between all grid operators, customers and wind turbine producers is required to find acceptable demands and solutions in the future.
One step forward is to gain knowledge of the behaviour of wind turbines with induction machines during situations such as voltage dips. In a test bench it is hard to produce the necessary operation modes. Therefore the development of wind turbine models as presented in this thesis is a necessary step on the way to define grid codes and design wind turbines.

Chapter 3

3. Induction Machine Models

As mentioned in the chapters above, one main interest of wind turbine manufacturers is the precise knowledge about the influence of certain grid conditions to the wind turbine itself. Detailed knowledge about e.g. the torque on the wind turbine shaft caused by faults in the grid or transient current rises is important for the estimation of the load on the wind turbines. Accurate knowledge of these effects ensures low costs and the availability for the estimated life time of the wind turbine. Therewith the generator as connection point between the electrical grid and the mechanical wind turbine plays a central role. Though for understanding and calculation of the dynamic behaviour in a wind turbine, the realistic representation of the generator is important.
However wind turbine producers face several problems which are limiting the information gained from a machine model. Because most wind turbine manufacturers don't produce their own generators, there is only a minimum access to data. Representing a range of generators in a model, facing the additional variation in each generators dimension and material, detailed FEM studies of the generator are not sufficient.
Therefore the purpose of the presented work is to find an analytical generator model for the simulation of fault conditions on variable speed Wind Turbines e.g. asymmetrical voltage supply or 1- ,2- , 3-phase short circuit using the program Matlab/ Simulink®.

3.1 General equations in ABC/abc Reference Frame

In order to make a mathematical description of the double fed induction machine it will be assumed that a uniform air gap machine can be modelled initially as two concentric cylinders with an air gap of constant radial length /68/. The stator and rotor have wounded three phase windings. Furthermore iron losses, and changing of parameters with temperature, are not considered.
A balanced three-phase machine is expressed in Figure 11. The conceptual windings are placed along the magnetic axes of the windings. The subscript 's' indicates the stator windings with effective number of turns $N_s\xi_s$ and 'r' the rotor windings with effective number of turns $N_r\xi_r$. The couplings between the phases are depending from the electrical angle between the phases θ. If the three windings subscripted with 'a, b, c' are displaced by ±120° the angle θ is only dependent from the rotor displacement angle ρ.
The basic equations for developing a three phase model can be found in various books about electrical machines and drives /50/, /52/. The variables of the machine are defined in vectors, where each element is represented per phase:
The equation for stator and rotor voltages can be written as:

$$\vec{u}_s^{\,s} = R_s \cdot \vec{i}_s^{\,s} + \frac{d\vec{\Psi}_s^{\,s}}{dt} \quad (1)$$

$$\vec{u}_r^{\,r} = R_r \cdot \vec{i}_r^{\,r} + \frac{d\vec{\Psi}_r^{\,r}}{dt} \quad (2)$$

Where the voltages u, the currents i and Flux Ψ are vectors exemplified for stator values defined by (3). A similar definition can be written for rotor values.

$$\vec{u}_s = \begin{pmatrix} u_{as} \\ u_{bs} \\ u_{cs} \end{pmatrix}, \vec{i}_s = \begin{pmatrix} i_{as} \\ i_{bs} \\ i_{cs} \end{pmatrix}, \vec{\Psi}_s = \begin{pmatrix} \Psi_{as} \\ \Psi_{bs} \\ \Psi_{cs} \end{pmatrix} \quad (3)$$

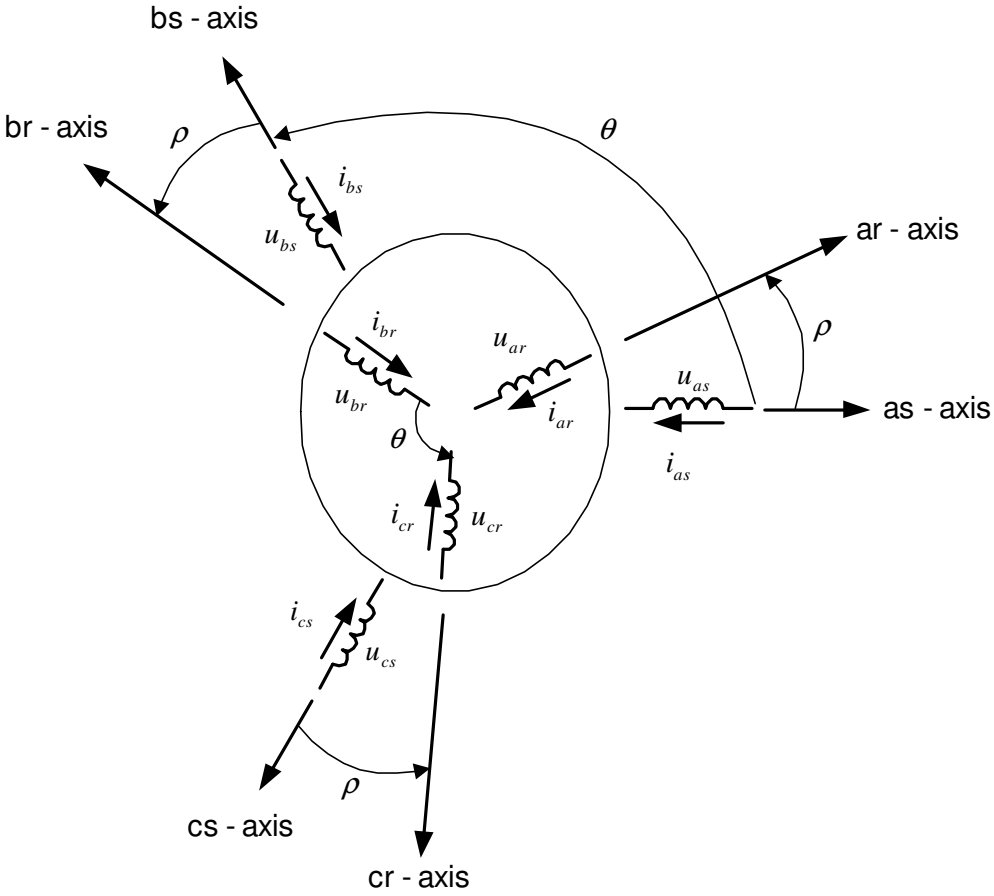

Figure 11 Magnetic axes, concentric stator and rotor windings, currents and voltages and angle dependencies of a three phase induction machine /67/

The flux in stator of the machine can be expressed with the flux created by the stator phases itself and the flux part influencing the stator originated from the rotor phases. In the same way the rotor flux can be separated into the flux belonging to the rotor and a part penetrating the rotor windings originating from the stator phases.

$$\vec{\Psi}_s = \vec{\Psi}_{s(s)} + \vec{\Psi}_{s(r)} \quad (4)$$

$$\vec{\Psi}_r = \vec{\Psi}_{r(r)} + \vec{\Psi}_{r(s)} \quad (5)$$

The flux can be expressed as a product of an inductance matrix and the current vector $\vec{i}$. The flux created from the stator windings is expressed in equation (6).

$$\vec{\Psi}_{s(s)} = \begin{pmatrix} L_{\sigma s}+L_{ms} & -\frac{L_{ms}}{2} & -\frac{L_{ms}}{2} \\ -\frac{L_{ms}}{2} & L_{\sigma s}+L_{ms} & -\frac{L_{ms}}{2} \\ -\frac{L_{ms}}{2} & -\frac{L_{ms}}{2} & L_{\sigma s}+L_{ms} \end{pmatrix} \cdot \vec{i}_s \quad (6)$$

In the same way the flux created from the rotor windings can be expressed in equation (7).

$$\vec{\Psi}_{r(r)} = \begin{pmatrix} L_{\sigma r}+\left(\frac{N_r\xi_r}{N_s\xi_s}\right)^2 \cdot L_{ms} & -\frac{L_{ms}}{2}\cdot\left(\frac{N_r\xi_r}{N_s\xi_s}\right)^2 & -\frac{L_{ms}}{2}\cdot\left(\frac{N_r\xi_r}{N_s\xi_s}\right)^2 \\ -\frac{L_{ms}}{2}\cdot\left(\frac{N_r\xi_r}{N_s\xi_s}\right)^2 & L_{\sigma r}+\left(\frac{N_r\xi_r}{N_s\xi_s}\right)^2 \cdot L_{ms} & -\frac{L_{ms}}{2}\cdot\left(\frac{N_r\xi_r}{N_s\xi_s}\right)^2 \\ -\frac{L_{ms}}{2}\cdot\left(\frac{N_r\xi_r}{N_s\xi_s}\right)^2 & -\frac{L_{ms}}{2}\cdot\left(\frac{N_r\xi_r}{N_s\xi_s}\right)^2 & L_{\sigma r}+\left(\frac{N_r\xi_r}{N_s\xi_s}\right)^2 \cdot L_{ms} \end{pmatrix} \cdot \vec{i}_r \quad (7)$$

The coupling between the rotor and stator is depending from the rotor displacement angle. The flux penetrating the stator initiated in the rotor is shown in equation (8) and the stator flux penetrating the rotor is shown in equation (9)

$$\vec{\Psi}_{s(r)} = \left(\frac{N_r\xi_r}{N_s\xi_s}\right)\cdot L_{ms}\cdot\begin{pmatrix} \cos\rho & \cos(\rho+2\pi/3) & \cos(\rho-2\pi/3) \\ \cos(\rho-2\pi/3) & \cos\rho & \cos(\rho+2\pi/3) \\ \cos(\rho+2\pi/3) & \cos(\rho-2\pi/3) & \cos\rho \end{pmatrix}\cdot\vec{i}_r \quad (8)$$

$$\vec{\Psi}_{r(s)} = \left(\frac{N_r\xi_r}{N_s\xi_s}\right)\cdot L_{ms}\cdot\begin{pmatrix} \cos\rho & \cos(\rho-2\pi/3) & \cos(\rho+2\pi/3) \\ \cos(\rho+2\pi/3) & \cos\rho & \cos(\rho-2\pi/3) \\ \cos(\rho-2\pi/3) & \cos(\rho+2\pi/3) & \cos\rho \end{pmatrix}\cdot\vec{i}_s \quad (9)$$

The winding turns in stator and rotor are in most cases different. For expression of the stator and rotor system in an equivalent coupled system the ratio *ue* is introduced in (10). This ratio is already implied in the flux equations.

$$ue = \left(\frac{N_s\xi_s}{N_r\xi_r}\right) \quad (10)$$

$$ue\cdot\underline{u}_r = \underline{u}_r' \quad (11) \qquad ue\cdot\underline{\Psi}_r = \underline{\Psi}_r' \quad (12)$$

$$\frac{\underline{i}_r}{ue} = \underline{i}_r' \quad (13) \qquad ue^2\cdot L_{mr} = L_{ms} = ue\cdot L_{msr} \quad (14)$$

$$\text{with: } L_{msr} = \sqrt{L_{ms}\cdot L_{mr}}$$

$$ue^2\cdot R_r = R_r' \quad (15) \qquad ue^2\cdot L_{\sigma r} = L_{\sigma r}' \quad (16)$$

When using the ratio *ue* the flux equations are simplified to:

$$\vec{\Psi}_s = \begin{pmatrix} L_{\sigma s}+L_{ms} & -\frac{L_{ms}}{2} & -\frac{L_{ms}}{2} \\ -\frac{L_{ms}}{2} & L_{\sigma s}+L_{ms} & -\frac{L_{ms}}{2} \\ -\frac{L_{ms}}{2} & -\frac{L_{ms}}{2} & L_{\sigma s}+L_{ms} \end{pmatrix} \cdot \vec{i}_s + L_{msr} \cdot \begin{pmatrix} \cos\rho & \cos(\rho+2\pi/3) & \cos(\rho-2\pi/3) \\ \cos(\rho-2\pi/3) & \cos\rho & \cos(\rho+2\pi/3) \\ \cos(\rho+2\pi/3) & \cos(\rho-2\pi/3) & \cos\rho \end{pmatrix} \cdot \vec{i}_r' \qquad (17)$$

$$\vec{\Psi}_r' = \begin{pmatrix} L_{\sigma r}'+L_{mr} & -\frac{L_{mr}}{2} & -\frac{L_{mr}}{2} \\ -\frac{L_{mr}}{2} & L_{\sigma r}'+L_{mr} & -\frac{L_{mr}}{2} \\ -\frac{L_{mr}}{2} & -\frac{L_{mr}}{2} & L_{\sigma r}'+L_{mr} \end{pmatrix} \cdot \vec{i}_r' + L_{msr} \cdot \begin{pmatrix} \cos\rho & \cos(\rho-2\pi/3) & \cos(\rho+2\pi/3) \\ \cos(\rho+2\pi/3) & \cos\rho & \cos(\rho-2\pi/3) \\ \cos(\rho-2\pi/3) & \cos(\rho+2\pi/3) & \cos\rho \end{pmatrix} \cdot \vec{i}_s \qquad (18)$$

Often the expression in one matrix is used /10/, /29/ expressing the angle dependency in a function:

$$f_1 = \cos\rho \qquad (19)$$

$$f_2 = \cos(\rho + 2\pi/3) \qquad (20)$$

$$f_3 = \cos(\rho - 2\pi/3) \qquad (21)$$

$$\begin{pmatrix} \Psi_{as} \\ \Psi_{bs} \\ \Psi_{cs} \\ \Psi_{ar}' \\ \Psi_{br}' \\ \Psi_{cr}' \end{pmatrix} = \begin{pmatrix} L_{\sigma s}+L_{ms} & -\frac{L_{ms}}{2} & -\frac{L_{ms}}{2} & L_{msr}\cdot f_1 & L_{msr}\cdot f_2 & L_{msr}\cdot f_3 \\ -\frac{L_{ms}}{2} & L_{\sigma s}+L_{ms} & -\frac{L_{ms}}{2} & L_{msr}\cdot f_3 & L_{msr}\cdot f_1 & L_{msr}\cdot f_2 \\ -\frac{L_{ms}}{2} & -\frac{L_{ms}}{2} & L_{\sigma s}+L_{ms} & L_{msr}\cdot f_2 & L_{msr}\cdot f_3 & L_{msr}\cdot f_1 \\ L_{msr}\cdot f_1 & L_{msr}\cdot f_3 & L_{msr}\cdot f_2 & L_{\sigma r}'+L_{mr} & -\frac{L_{mr}}{2} & -\frac{L_{mr}}{2} \\ L_{msr}\cdot f_2 & L_{msr}\cdot f_1 & L_{msr}\cdot f_3 & -\frac{L_{mr}}{2} & L_{\sigma r}'+L_{mr} & -\frac{L_{mr}}{2} \\ L_{msr}\cdot f_3 & L_{msr}\cdot f_3 & L_{msr}\cdot f_1 & -\frac{L_{mr}}{2} & -\frac{L_{mr}}{2} & L_{\sigma r}'+L_{mr} \end{pmatrix} \cdot \begin{pmatrix} i_{as} \\ i_{bs} \\ i_{cs} \\ i_{ar}' \\ i_{br}' \\ i_{cr}' \end{pmatrix} \qquad (22)$$

The inductance matrix is expressing the coupling of the flux in the stator and rotor windings. It takes a central position in the machine modelling. Depending on the form of the inductance matrix, the machine model is more or less detailed. In progress of this chapter, consideration of saturation effects will change the constant inductances in this matrix to time dependent functions.

3.1.1 Complex space Vector representation

A lot of authors /50/, /55/, /67/ introduce the method of complex space vector for a more convenient mathematical description of the machine variables. It is widely used in the field of machine modelling and machine control.
The phase currents of the three machine windings displaced by ±120° as already shown in Figure 11 can be described as complex vectors. With the help of the complex versor $\underline{a}$ (23) this complex vectors can be expressed by (24). For convenience the real part of the

complex space vector is aligned to phase a of the 3 phase stator system or 3 phase rotor system.

$$\underline{a} = 1\angle 120^o = -\frac{1}{2} + \frac{\sqrt{3}}{2}\cdot j = e^{j\cdot\frac{2}{3}\cdot\pi} \quad (23)$$

$$\underline{i}_a = i_a, \quad \underline{i}_b = \underline{a}\cdot i_b, \quad \underline{i}_c = \underline{a}^2\cdot i_c \quad (24)$$

Where i_a, i_b, i_c are the absolute values of the current time vector. A resulting current vector can be achieved through an addition of the three phase current vectors (25).

$$\underline{i} = \underline{i}_a + \underline{i}_b + \underline{i}_c = i_a + \underline{a}\cdot i_b + \underline{a}^2\cdot i_c \quad (25)$$

Some authors /3/, /56/ interpret this equation as a definition for the complex space vector. In interpretation as complex space vector the time vectors itself can be complex vectors. Instead of the definition (25) a more common definition is achieved through multiplying (25) by the factor 2/3 (26).

$$\underline{i}_s = \frac{2}{3}\cdot\left(i_{as} + \underline{a}\cdot i_{bs} + \underline{a}^2\cdot i_{cs}\right) \quad (26)$$

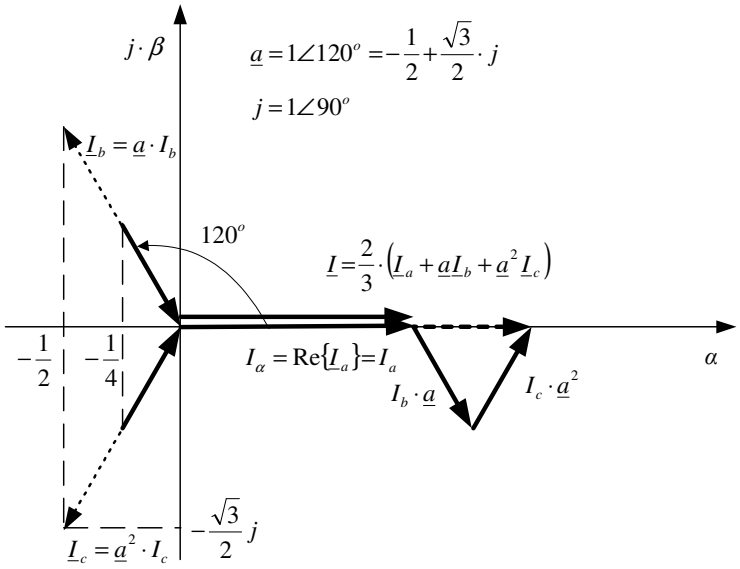

Figure 12 Space vector constructed from a three phase system

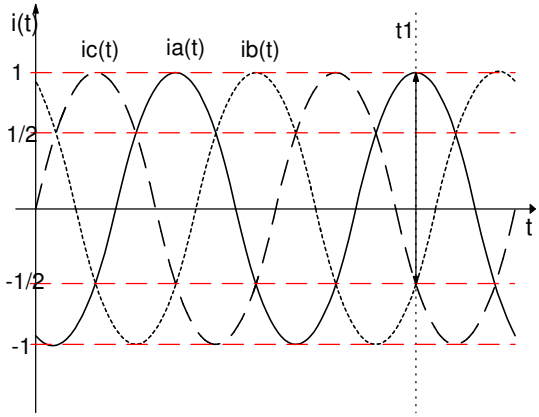

Figure 13 Phase currents in a time based system

The advantages of using definition (26) are that the projections from the space vector $\underline{i}_s$ to the magnetic axes achieve the absolute time values of the existing axes-currents (27). The vector changes its length and position with the phase currents (Figure 12, Figure 13). Furthermore the space vector can be used for voltages and fluxes in the same way as for the currents (28), (29). The calculated power using the vectors defined as in (26), (28) is invariant. The calculation of power and torque (see equations (32), (33), (34)) gives the same expressions like the general equations of symmetrical three phase systems /55/. Therefore this definition is often called the real or correct power definition.

$$i_{as} = \mathrm{Re}\{\underline{i}_s\}, \quad i_{bs} = \mathrm{Re}\{\underline{a}^2 \cdot \underline{i}_s\}, \quad i_{cs} = \mathrm{Re}\{\underline{a} \cdot \underline{i}_s\} \tag{27}$$

$$\underline{u}_s = \frac{2}{3} \cdot \left(u_{as} + \underline{a} \cdot u_{bs} + \underline{a}^2 \cdot u_{cs}\right) \tag{28}$$

$$\underline{\Psi}_s = \frac{2}{3} \cdot \left(\Psi_{as} + \underline{a} \cdot \Psi_{bs} + \underline{a}^2 \cdot \Psi_{cs}\right) \tag{29}$$

The power calculated using the method of complex space vector is shown in equation (30)

$$\begin{aligned} S_s &= \frac{3}{2} \cdot \left\{\underline{u}_s \cdot \underline{i}_s^*\right\} = \frac{3}{2} \cdot \left\{\frac{2}{3} \cdot \left(u_{as} + \underline{a} \cdot u_{bs} + \underline{a}^2 \cdot u_{cs}\right) \cdot \frac{2}{3} \cdot \left(i_{as} + \underline{a}^2 \cdot i_{bs} + \underline{a} \cdot i_{cs}\right)\right\} \\ &= \frac{3}{2} \cdot \left\{\begin{array}{l} \frac{4}{9} \cdot \left\{\left(u_{as} \cdot i_{as} + u_{bs} \cdot i_{bs} + u_{cs} \cdot i_{cs}\right) - \frac{1}{2}\left(u_{as} \cdot (i_{bs} + i_{cs}) + u_{bs} \cdot (i_{as} + i_{cs}) + u_{cs} \cdot (i_{as} + i_{bs})\right)\right\} \\ + \frac{4}{9} \cdot \frac{\sqrt{3}}{2} j \cdot \left(i_{as} \cdot (u_{bs} - u_{cs}) + i_{bs} \cdot (u_{cs} - u_{as}) + i_{cs} \cdot (u_{as} - u_{bs})\right) \end{array}\right\} \end{aligned} \tag{30}$$

Assuming the phase currents can be added to zero, as shown in equation (31). The active stator power in equation (32) and reactive stator power equation (33) can be achieved as real and imaginary part of the total power shown in equation (30). The assumption of equation (31) means there is no zero component existing, or the zero component is not considered in the calculation. It can be easily considered separately on a later (see chapter 3.2).

$$i_a + i_b + i_c = 0 \tag{31}$$

$$P_s = \frac{3}{2} \cdot \mathrm{Re}\left\{\underline{u}_s \cdot \underline{i}_s^*\right\} = u_{as} \cdot i_{as} + u_{bs} \cdot i_{bs} + u_{cs} \cdot i_{cs} \tag{32}$$

$$Q_s = \frac{3}{2} \cdot \mathrm{Im}\left\{\underline{u}_s \cdot \underline{i}_s^*\right\} = \frac{1}{\sqrt{3}} \cdot \left(i_{as} \cdot (u_{cs} - u_{bs}) + i_{bs} \cdot (u_{as} - u_{cs}) + i_{cs} \cdot (u_{bs} - u_{as})\right) \tag{33}$$

and the torque in an analogous manner (damping due to friction and windage is not included):

$$\begin{aligned} T_e &= \frac{3}{2} \cdot p_p \cdot \mathrm{Im}\left\{\underline{\Psi}_s^{s^*} \cdot \underline{i}_s^s\right\} \\ &= \frac{p_p}{\sqrt{3}} \cdot \left(i_{as}\left(\Psi_{cs} - \Psi_{bs}\right) + i_{bs}\left(\Psi_{as} - \Psi_{cs}\right) + i_{cs}\left(\Psi_{bs} - \Psi_{as}\right)\right) \end{aligned} \tag{34}$$

3.1.2 Using space vector for the general machine equations

Using the above introduced complex space vector, the general machine equation can be expressed more conveniently compared to the vector presentation for the per phase presentation. The voltage equations (35), (36) using the complex space vector representation for the stator and rotor can be expressed through the stator flux $\underline{\Psi}_s^s$ and rotor flux $\underline{\Psi}_r^r$ transient and winding losses:

$$\underline{u}_s^s = R_s \cdot \underline{i}_s^s + \frac{d\underline{\Psi}_s^s}{dt} \quad (35)$$

$$\underline{u}_r^r = R_r \cdot \underline{i}_r^r + \frac{d\underline{\Psi}_r^r}{dt} \quad (36)$$

The flux is defined with the following equations /67/

$$\underline{\Psi}_s^s = \underline{\Psi}_{s(s)} + \underline{\Psi}_{s(r)} \quad (37)$$

$$\underline{\Psi}_r^r = \underline{\Psi}_{r(r)} + \underline{\Psi}_{r(s)} \quad (38)$$

Where the flux components are expressed as:

$$\underline{\Psi}_{s(s)} = (L_{\sigma s} + \frac{3}{2} \cdot L_{ms}) \cdot \underline{i}_s \quad (39)$$

$$\underline{\Psi}_{r(r)} = (L_{\sigma r} + \frac{3}{2} \cdot L_{mr}) \cdot \underline{i}_r \quad (40)$$

$$\underline{\Psi}_{r(s)} = \frac{3}{2} \cdot L_{msr} \cdot \underline{i}_s \cdot e^{-j\rho} \quad (41)$$

$$\underline{\Psi}_{s(r)} = \frac{3}{2} \cdot L_{msr} \cdot \underline{i}_r \cdot e^{j\rho} \quad (42)$$

If the mutual inductances and couple inductances are equal as assumed in a one phase equivalent diagram, then the magnetizing inductance can be written as:

$$L_m = \frac{3}{2} \cdot L_{ms} = \frac{3}{2} \cdot L_{mr}' = \frac{3}{2} \cdot L_{msr} \quad (43)$$

The flux equations become:

$$\underline{\Psi}_s = (L_{\sigma s} + L_m) \cdot \underline{i}_s + L_m \cdot \underline{i}_r' \cdot e^{j\rho} \quad (44)$$

$$\underline{\Psi}_r' = (L_{\sigma r}' + L_m) \cdot \underline{i}_r' + L_m \cdot \underline{i}_s \cdot e^{-j\rho} \quad (45)$$

The rotor voltage equation related to the stator become:

$$\underline{u}_r^{r'} = R_r' \cdot \underline{i}_r^{r'} + \frac{d\underline{\Psi}_r^{r'}}{dt} \quad (46)$$

The vectors expressing the rotor current, voltage and flux are still related to their own reference frame, marked by the upper index ‘r’, while the stator vectors are related to the stator reference frame, marked by the upper index ‘s’. This difference of the two coordinate systems is expressed with the rotor angle ρ (Figure 11). With using vector transformation (Chapter 11 Appendix) and this angle, the rotor voltage equation can be written as:

$$\underline{u}_r^{s'} = R_r' \cdot \underline{i}_r^{s'} + \frac{d\underline{\Psi}_r^{s'}}{dt} - j \cdot \dot{\rho} \cdot \underline{\Psi}_r^{s'} \quad (47)$$

Finally all general equations for modelling an induction machine using the representation of complex space vectors are:

$$\underline{u}_s^s = R_s \cdot \underline{i}_s^s + \frac{d\underline{\Psi}_s^s}{dt} \quad (48)$$

$$\underline{u}_r^{s'} = R_r^{'} \cdot \underline{i}_r^{s'} + \frac{d\underline{\Psi}_r^{s'}}{dt} - j \cdot \dot{\rho} \cdot \underline{\Psi}_r^{s'} \quad (49)$$

$$\underline{\Psi}_s = (L_{\sigma s} + L_m) \cdot \underline{i}_s + L_m \cdot \underline{i}_r^{'} \cdot e^{j\rho} \quad (50)$$

$$\underline{\Psi}_r^{'} = (L_{\sigma r}^{'} + L_m) \cdot \underline{i}_r^{'} + L_m \cdot \underline{i}_s \cdot e^{-j\rho} \quad (51)$$

$$T_e = \frac{3}{2} \cdot p_p \cdot \mathrm{Im}\left\{ \underline{\Psi}_s^{s^*} \cdot \underline{i}_s^s \right\} \quad (52)$$

$$T_e - T_m = J \frac{d\omega_r}{dt} + D\omega_r \text{ (/98/ page 56)} \quad (53)$$

$$\ddot{\rho} = \frac{d\omega_e}{dt} = \frac{d\omega_r \cdot p_p}{dt} = \frac{p_p}{J} \cdot \left(T_e - T_m - D\omega_r\right) \quad (54)$$

The achieved equations and parameters can be visualized in the dynamical one phase equivalent diagram seen in Figure 14.

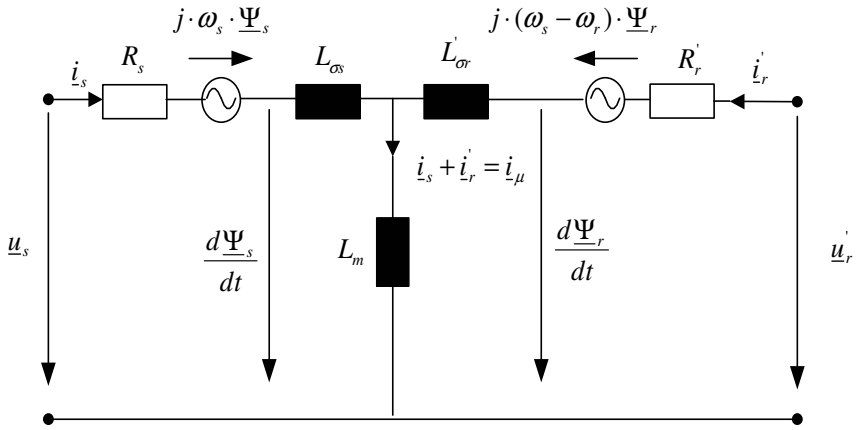

Figure 14 Dynamical per phase equivalent diagram for induction machine

3.2 The Clark Transformation (α, β, 0 equivalent frame)

The complex space vector representation is the base for several different description of an electrical machine. One of the possible interpretations of the with the complex space vector deduced machine equations are the so called α, β - components[1]. The α, β - components, also known as Clark Transformation are deduced by separating the complex space vectors of the machine into their real and imaginary part and referring them to a stationary reference system. The so achieved components can be physically imagined as two fields in normative direction to each other, meaning the three-phase machine has been deduced to an equivalent two-phase machine see Figure 15.

[1] Equivalent to the used x, y – components in some literature

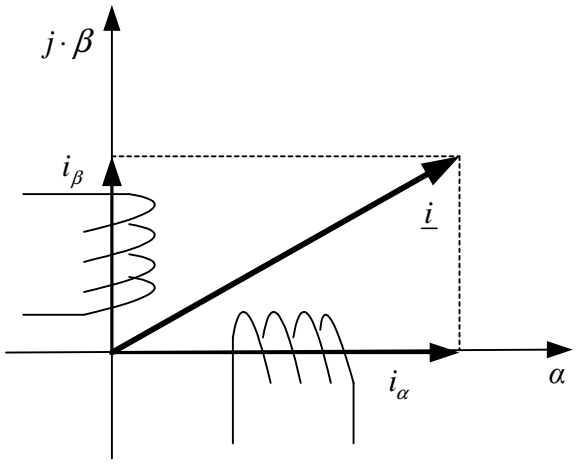

Figure 15 Equivalent two-phase machine showing Clark-Transformation

The real component is calculated as shown in equation (55) and the imaginary part equation (56).

$$i_\alpha = \mathrm{Re}\{\underline{i}\} = \mathrm{Re}\left\{\frac{2}{3}\left(i_a + \underline{a}\, i_b + \underline{a}^2 i_c\right)\right\} = \frac{2}{3}\left(i_a - \frac{i_b + i_c}{2}\right) \tag{55}$$

$$i_\beta = \mathrm{Im}\{\underline{i}\} = \mathrm{Im}\left\{\frac{2}{3}\left(i_a + \underline{a}\, i_b + \underline{a}^2 i_c\right)\right\} = \frac{1}{\sqrt{3}}\left(i_b - i_c\right) \tag{56}$$

The complex space vector can be written as:

$$\underline{i} = i_\alpha + j \cdot i_\beta \tag{57}$$

If the addition of the three phases does not equate to zero an additional component the so called zero component has to be used as well.

$$i_0 \quad = \quad \frac{i_a + i_b + i_c}{3} \tag{58}$$

Very positive is the fact, that in case of no existing zero component the real part is identical to the phase a of the 3-phase system.

$$i_\alpha = \mathrm{Re}\{\underline{i}\} = \frac{2}{3}\left(i_a - \frac{i_b + i_c}{2}\right) = \frac{2}{3}\left(i_a - \frac{i_a + i_c - i_c}{2}\right)\Bigg|_{i_a + i_b + i_c = 0} = i_a \tag{59}$$

In the following matrices the complete transformation (including zero component) is shown.

$$\begin{pmatrix} i_\alpha \\ i_\beta \\ i_0 \end{pmatrix} = \frac{1}{3} \cdot \begin{pmatrix} 2 & -1 & -1 \\ 0 & \sqrt{3} & -\sqrt{3} \\ 1 & 1 & 1 \end{pmatrix} \cdot \begin{pmatrix} i_a \\ i_b \\ i_c \end{pmatrix} \tag{60}$$

$$\begin{pmatrix} i_a \\ i_b \\ i_c \end{pmatrix} = \frac{1}{2} \cdot \begin{pmatrix} 2 & 0 & 2 \\ -1 & \sqrt{3} & 2 \\ -1 & -\sqrt{3} & 2 \end{pmatrix} \cdot \begin{pmatrix} i_\alpha \\ i_\beta \\ i_0 \end{pmatrix} \tag{61}$$

Where equation (60) is used for the transformation of the three-phase system into the α, β - components the equation (61) is used for the back transformation. The equivalent diagrams for the machine representation can be seen in Figure 16 and Figure 17.

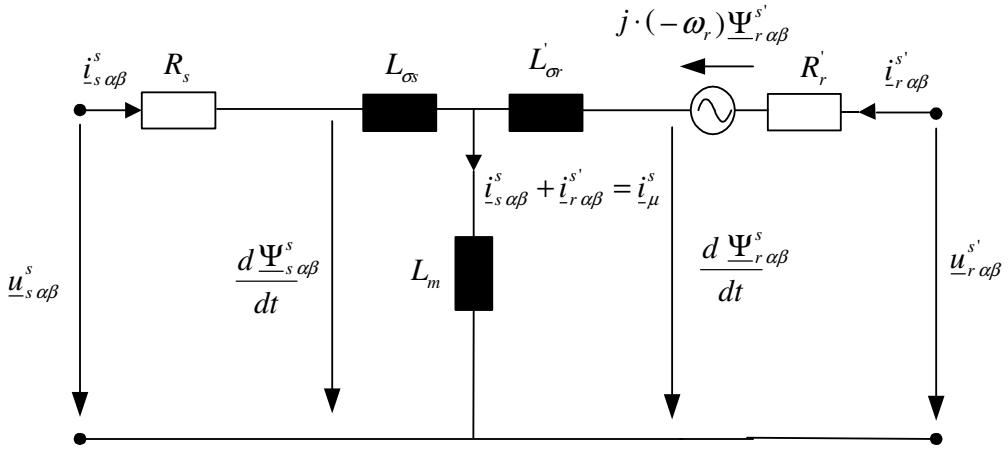

Figure 16 Equivalent circuit diagram for α and β - components

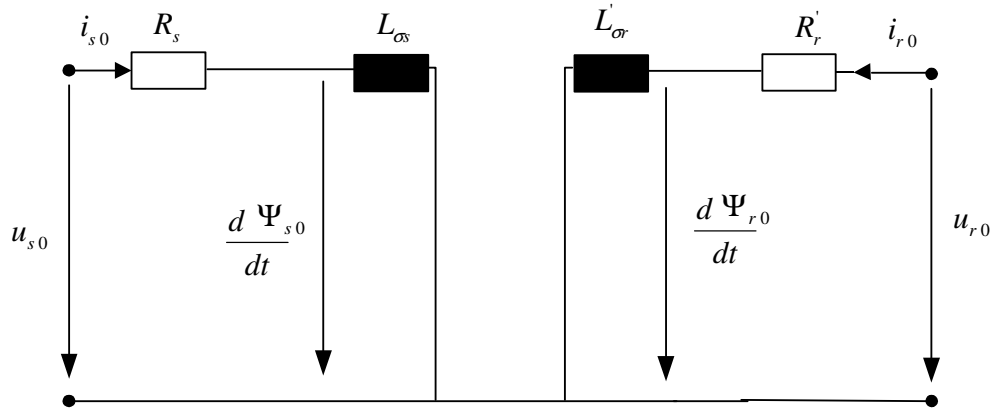

Figure 17 Equivalent circuit diagram for the zero component

The equations for description of the machine are concluded in equation (62) to (72). The zero components are assumed to be only linked via the leakage field.

$$\underline{u}_s^s = R_s \cdot \underline{i}_s^s + \frac{d\underline{\Psi}_s^s}{dt} \quad (62)$$

$$u_{s0} = R_s \cdot i_{s0} + \frac{d\Psi_{s0}}{dt} \quad (63)$$

$$\underline{u}_r^{s'} = R_r' \cdot \underline{i}_r^{s'} + \frac{d\underline{\Psi}_r^{s'}}{dt} - j \cdot \dot{\rho} \cdot \underline{\Psi}_r^{s'} \quad (64)$$

$$u_{r0} = R_r \cdot i_{r0} + \frac{d\Psi_{r0}}{dt} \quad (65)$$

$$\underline{\Psi}_s = (L_{\sigma s} + L_m) \cdot \underline{i}_s + L_m \cdot \underline{i}_r' \cdot e^{j\rho} \quad (66)$$

$$\Psi_{s0} = L_{\sigma s} \cdot i_{s0} \quad (67)$$

$$\underline{\Psi}_r' = (L_{\sigma r}' + L_m) \cdot \underline{i}_r' + L_m \cdot \underline{i}_s \cdot e^{-j\rho} \quad (68)$$

$$\Psi_{r0} = L_{\sigma r} \cdot i_{r0} \quad (69)$$

$$T_e = \frac{3}{2} \cdot p_p \cdot \mathrm{Im}\left\{ \underline{\Psi}_s^{s^*} \cdot \underline{i}_s^s \right\} = \frac{3}{2} \cdot p_p \cdot \left(\Psi_{s\alpha} \cdot i_{s\beta} - \Psi_{s\beta} \cdot i_{s\alpha} \right) \quad (70)$$

$$T_e - T_m = J \frac{d\omega_r}{dt} + D\omega_r \text{ (/98/ page 56)} \quad (71)$$

$$\ddot{\rho} = \frac{d\omega_e}{dt} = \frac{d\omega_r \cdot p_p}{dt} = \frac{p_p}{J} \cdot (T_e - T_m - D\omega_r) \quad (72)$$

The power is calculated as shown in equation (73) and equation (75).

$$P_s = \frac{3}{2} \cdot \mathrm{Re}\left\{ \underline{u}_s \cdot \underline{i}_s^* \right\} = \frac{3}{2} \cdot \mathrm{Re}\left\{ \left(u_{s\alpha} + j u_{s\beta} \right) \cdot \left(i_{s\alpha} - j\, i_{s\beta} \right) \right\} = \frac{3}{2} \left(u_{s\alpha} i_{s\alpha} + u_{s\beta} i_{s\beta} \right) \quad (73)$$

$$P_0 = 3 \cdot u_0 \cdot i_0 \quad (74)$$

$$Q_s = \frac{3}{2} \cdot \mathrm{Im}\left\{ \underline{u}_s \cdot \underline{i}_s^* \right\} = \frac{3}{2} \cdot \mathrm{Im}\left\{ \left(u_{s\alpha} + j u_{s\beta} \right) \cdot \left(i_{s\alpha} - j\, i_{s\beta} \right) \right\} = \frac{3}{2} \left(u_{s\beta} i_{s\alpha} - u_{s\alpha} i_{s\beta} \right) \quad (75)$$

3.3 The Park Transformation (d, q, 0 equivalent frame)

In the same way as in the α, β - components, shown in the chapter 3.2, the d, q – components are a separation of the complex space vector in real and imaginary part.

$$\underline{i} = i_d + j \cdot i_q = \frac{2}{3} \left(i_a + \underline{a} i_b + \underline{a}^2 i_c \right) \cdot e^{-j\gamma} \quad (76)$$

In opposite to referring the space vector to a stationary reference frame as done in the Clark's components, in the so called Park's transformation the complex space vector is expressed in the rotating orthogonal system linked with the rotor of the machine. The method is however used to express the complex space vector in any rotating reference frame. The advantage by doing so rotating space vectors change to appear stationary in a rotating reference frame, which means alternating traces of the space vector are steady and the changes in absolute value of the vector is depicted clearly. This is beneficially

[2] Be aware - Definition is varying in the literature

used for fast control of electrical machines.

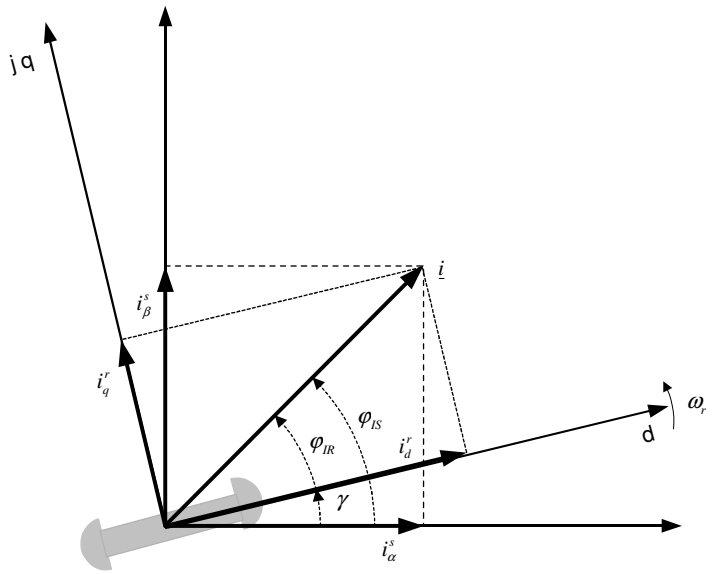

Figure 18 Park's - transformation

In Figure 18 the Parks transformation in relation to the α, β - components are shown. The transformation between these components and an arbitrary rotating frame is:

$$i_d + j \cdot i_q = \left(i_\alpha + j \cdot i_\beta\right) \cdot e^{-j \cdot \varphi} \tag{77}$$

and for return to the α, β - components

$$i_\alpha + j \cdot i_\beta = \left(i_d + j \cdot i_q\right) \cdot e^{j \cdot \varphi} \tag{78}$$

The zero – component is equal for both transformations, hence it formed during expressing the 3-phase machine into a two-phase equivalent machine.

$$i_{0\,dq} = i_{0\,\alpha\beta} \tag{79}$$

Expressing the transformation in Matrices, the following Matrices for forward and back transformation can be written.

$$\begin{pmatrix} i_\alpha \\ i_\beta \\ i_{0\alpha\beta} \end{pmatrix} = \begin{pmatrix} \cos(\varphi) & -\sin(\varphi) & 0 \\ \sin(\varphi) & \cos(\varphi) & 0 \\ 0 & 0 & 1 \end{pmatrix} \cdot \begin{pmatrix} i_d \\ i_q \\ i_{0dq} \end{pmatrix} \tag{80}$$

$$\begin{pmatrix} i_d \\ i_q \\ i_{0dq} \end{pmatrix} = \begin{pmatrix} \cos(\varphi) & \sin(\varphi) & 0 \\ -\sin(\varphi) & \cos(\varphi) & 0 \\ 0 & 0 & 1 \end{pmatrix} \cdot \begin{pmatrix} i_\alpha \\ i_\beta \\ i_{0\alpha\beta} \end{pmatrix} \tag{81}$$

Transformation from a 3-phase system direct to an arbitrary rotating system can be done in the following way:

$$\begin{pmatrix} i_d \\ i_q \\ i_0 \end{pmatrix} = \frac{2}{3} \cdot \begin{pmatrix} \cos\ \gamma & \cos\left(\gamma - \frac{2}{3}\pi\right) & \cos\left(\gamma + \frac{2}{3}\pi\right) \\ \sin\ \gamma & \sin\left(\gamma - \frac{2}{3}\pi\right) & \sin\left(\gamma + \frac{2}{3}\pi\right) \\ \frac{1}{2} & \frac{1}{2} & \frac{1}{2} \end{pmatrix} \cdot \begin{pmatrix} i_a \\ i_b \\ i_c \end{pmatrix} \tag{82}$$

$$\begin{pmatrix} i_a \\ i_b \\ i_c \end{pmatrix} = \begin{pmatrix} \cos\ \gamma & \sin\ \gamma & 1 \\ \cos\left(\gamma - \frac{2}{3}\pi\right) & \sin\left(\gamma - \frac{2}{3}\pi\right) & 1 \\ \cos\left(\gamma + \frac{2}{3}\pi\right) & \sin\left(\gamma + \frac{2}{3}\pi\right) & 1 \end{pmatrix} \cdot \begin{pmatrix} i_d \\ i_q \\ i_0 \end{pmatrix} \tag{83}$$

The equivalent diagram for a machine in Park's transformation is shown in Figure 19. The equivalent for the zero components is equal as shown in Figure 17 in chapter 3.2. Since all machine equations are very similar to the description of the machine in Clark components it is not necessary to show them again. Just the torque and power equations are shown in equation (84), (85) and (86).

$$T_e = \frac{3}{2} \cdot p_p \cdot \mathrm{Im}\left\{ \underline{\Psi}_s^{s^*} \cdot \underline{i}_s^s \right\} = \frac{3}{2} \cdot p_p \left(i_{qs} \cdot \Psi_{ds} - \underbrace{\Psi_{qs} \cdot i_{ds}}_{\approx 0} \right) \tag{84}$$

$$P_s = \frac{3}{2} \cdot \mathrm{Re}\left\{ \underline{u}_s \cdot \underline{i}_s^{\,*} \right\} = \frac{3}{2} \left(u_d i_d + u_q i_q \right) \tag{85}$$

$$Q_s = \frac{3}{2} \cdot \mathrm{Im}\left\{ \underline{u}_s \cdot \underline{i}_s^{\,*} \right\} = \frac{3}{2} \left(u_q i_d - u_d i_q \right) \tag{86}$$

The equivalent diagram for the d,q – components is shown in Figure 19. The equivalent diagram for the zero component is identical to the diagram shown in Figure 17.

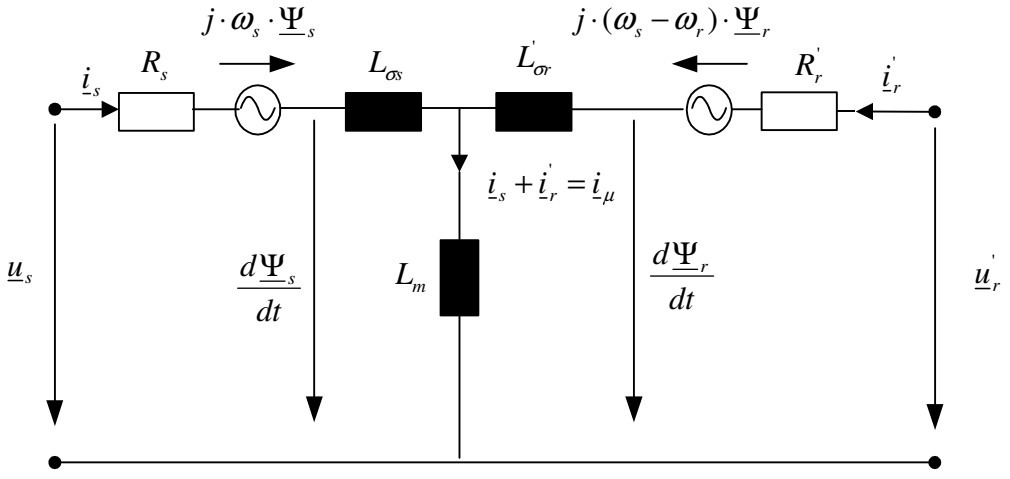

Figure 19 Equivalent circuit diagram for d, q - components

3.4 Saturation effects

In the ideal machine it is assumed, that the leakage reactance and magnetizing reactance are independent of the current and the voltage. In a real machine the magnetic voltage through the iron is not directly proportional to the current and therefore this assumption is not valid. For taking a closer look at the phenomena, the influence of saturation of the leakage reactances and the magnetizing reactance should be taken into account. /81/

3.4.1 Saturation of main reactance

The main reactance or magnetizing reactance X_m is mainly defined through the stator induced electromotive force (EMF/ EMK). The reactance would not be changing, if the characteristic of $E_s(I_\mu)$ would be a straight line. In reality the curve is bending in the upper part as shown in Figure 20.

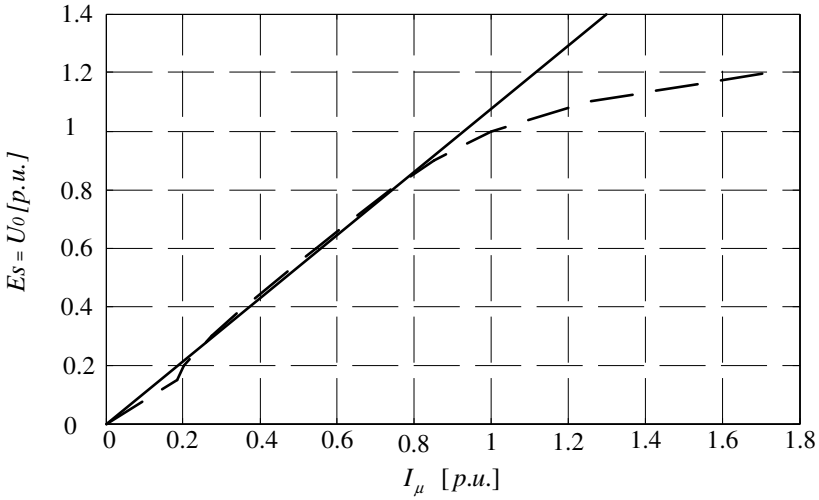

Figure 20 Example of a measured no load (magnetizing) curve – dashed line and the theoretical not saturating curve – solid line of an induction machine

When increasing the induced voltage (E_s) the magnetizing reactance slightly decreases. The consequence is a faster decrease of the magnetizing current as the decrease of the induced rotor EMF. The effect of main reactance saturation on the stator currents is most noticeable during no load operation. In Figure 21 this influence of magnetizing reactance is visualized.

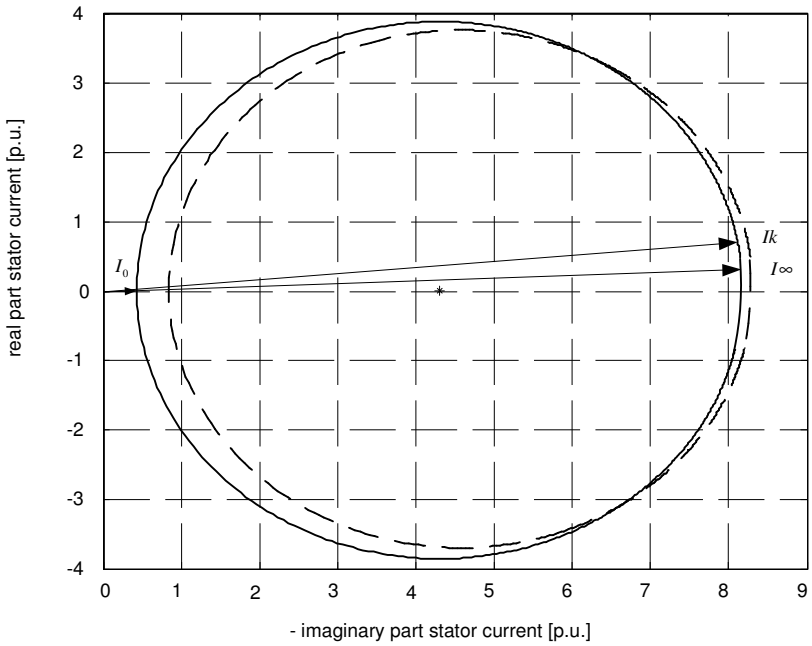

Figure 21 Current circle diagram showing the effect of main inductance saturation; rated-solid line, halve *Xm* (saturated)– dashed line, I_k-short circuit current at slip=1 and I∞ - current at infinite slip

To find the dependency it is therefore best to measure the no load curve. There are two possibilities of measuring the curve. If a slip-ring machine is used it is possible to measure directly the rotor current and stator currents. This simplifies the machines complexity, the machine is at stand still and the rotor windings are open and voltage and currents on both terminals can be measured (direct measurement of magnetizing curve). However more common is the measurement at nearly synchronous speed (used for squirrel cage motors), the so called no load curve.

In no load operation at synchronous speed or at standstill the rotor current can be assumed to zero. Therefore it can be assumed that the current of the stator windings and the magnetizing current are equal. The voltage drop is now only over the stator resistance, stator leakage reactance, iron loss resistance and the magnetizing reactance. The magnetizing inductance dependent at the current can be achieved with the following equations. It is assumed that the resistances and the stator leakage inductance are not changing with the current. The so deduced function of the main inductance from the magnetizing current is a common way to include saturation effects into a machine model (87).

$$X_m\left(I_\mu\right) = L_m\left(I_\mu\right)\cdot\omega_0 = \sqrt{\frac{U_0^{\,2}}{3\cdot I_\mu^{\,2}} - (R_s + R_m)^2} - L_{\sigma s}\cdot\omega_0 \tag{87}$$

In Figure 22 the main inductance dependency from the magnetizing current, which was achieved through the no load curve measurements and then calculated with equation (87) is shown. Very often rated inductance is assumed at low currents. In reality there is not enough flux in the machine because of the low voltage and the inductance is decreasing again towards low currents.

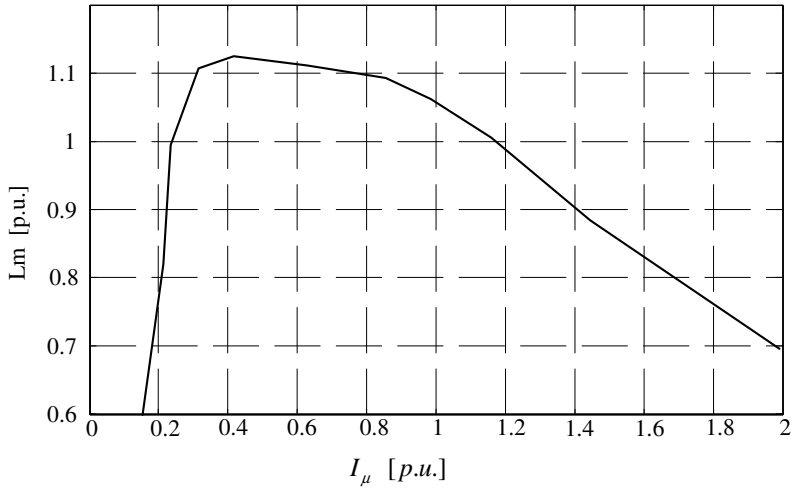

Figure 22 Main inductance dependency of the magnetizing current $L_m(I_\mu)$

3.4.2 Saturation of leakage reactance

For the research in fault situations like short circuit the operation with high currents is far more important than no load operation. Therefore a larger importance is the consideration of the dependency of leakage reactances $X_{\sigma s}$ and $X'_{\sigma r}$ on the current. With increasing current the leakage reactances will decrease as well as the magnetizing reactance. In Figure 21 and Figure 23 the current circle diagram is calculated for a machine with half of the rated magnetizing reactance or leakage reactances and compared to a machine with rated values. While in rated operation range, which is around 1 p.u., the influence of the magnetizing inductance is dominating, the changes during fault operations with high currents are clearly dominated by the leakage reactances. The current considering a change of leakage reactances is essentially larger than without this consideration.

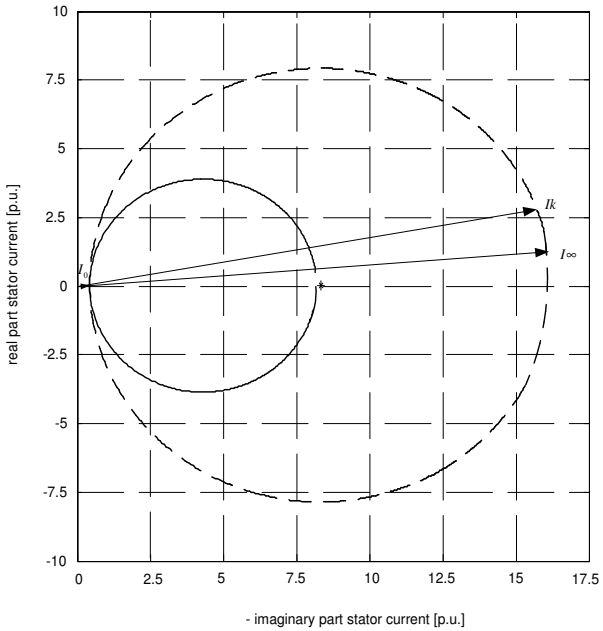

Figure 23 Current circle diagram showing the effect of leakage reactance saturation; rated value-solid line, halve $X_{\sigma s}$ and $X'_{\sigma r}$ (saturated) – dashed line

The leakage reactances can be achieved from the blocked rotor test. In this test with short circuit rotor coils the magnetizing current is very small and can be neglected. With measurement of the voltage and current and the power factor cos φ the total leakage reactance can be calculated as:

$$X_\sigma = \frac{U \cdot \sin\varphi_k}{I} \tag{88}$$

To separate the leakage reactance X_σ into the stator leakage reactance $X_{\sigma s}$ and the rotor leakage reactance $X'_{\sigma r}$ the no load measurement can be used again. In the no load measurement the reactances $X_m + X_{\sigma s}$ are measured and therewith the part of the rotor leakage reactance can be estimated. Another factor helping the more exact separation between the stator and rotor leakage reactances is the measurement of the leakage factor σ.

$$\sigma = 1 - \frac{X_m^{\,2}}{X_s \cdot X'_r} \tag{89}$$

where $X_s = X_{ms} + X_{\sigma s}$ and $X'_r = X_{mr} + X'_{\sigma r}$

However, the methods are detailed discussed in book /81/ and other machine books and therefore will not further deepened in this thesis.

3.5 Windage losses and Friction losses

Windage and frictional losses of a machine can be divided into two parts, which have a different proportion to the rotational speed ω

- Ventilation losses are proportional to ω^3. This includes all ventilation losses (end winding ventilation loss, rotor cooling ducts ventilation loss etc.)
- Frictional losses are proportional to *less than* ω^3 ($P \sim \omega^{7/3}$). These losses include frictional losses in bearings. The correct proportional ratio is quite hard to estimate, since it may fluctuate. e.g. temperature of the grease has some influence into frictional losses. This means that in different service conditions the proportional ratio may be different.

When combining the above components total windage and frictional losses are achieved. Total losses can be approximated to a proportion between $\omega^{2.5}$ ... $\omega^{2.7}$. Unfortunately it is very hard to include such non integer potential dependency into the model. Since the difference between the different potential dependencies is very small in the operating area it is chosen to use a dependency in the second order. A second order dependency due to power losses leads to a simple dependency of the torque, which can be found in various books.

The damping factor can be from the no load losses:

$$D = \frac{P_{0\,fw}}{\omega_0^2} \tag{90}$$

The windage and friction losses depending on the speed will be calculated using the constant damping factor achieved above.

$$P_{fw}(\omega) = D \cdot \omega^2 \tag{91}$$

Though the damping factor is only an equivalent there are a range of possible methods considering the leakage and windage losses. In Figure 24 and Figure 25 the influence of the different exponential dependencies is shown. The damping factor D is determined by measuring the rotational losses at synchronous speed and dividing it by the exponents chosen.

$$D = \frac{P_{0\,fw}}{\omega^{2...2,5...2,7...3}} \tag{92}$$

The windage and friction losses in the model would accordingly be calculated in the following way.

$$P_{fw}(\omega) = D \cdot \omega^{2...2,5...2,7...3} \tag{93}$$

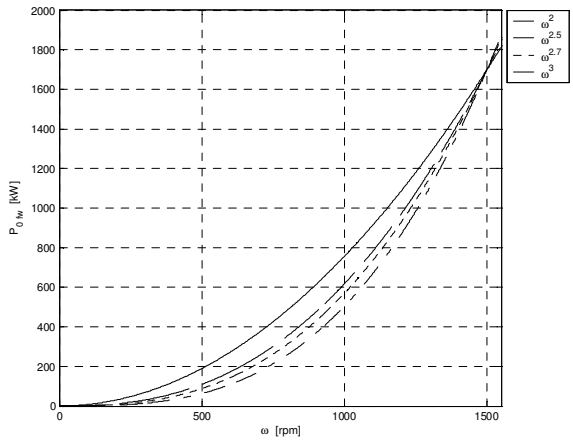

Figure 24 Different exponential dependencies of D between 0…1500 rpm

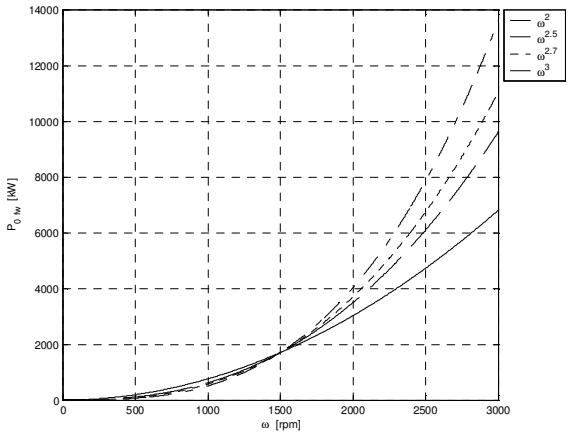

Figure 25 Different exponential dependencies of D at over speed

In the operation range from approx. 500 rpm up to 1700 rpm the difference in the calculation of the potential dependencies is very small. If used for the purpose of modelling at over speed situations, a change from the chosen dependency of second order might be reconsidered, and instead the use of a model with a dependency of third order is more appropriate.

3.6 The Three Phase – Model in Matlab®/ Simulink®

The machine model is based on the equations (1), (2), (22), (34), (54) and implemented in Matlab/ Simulink as shown in Figure 25.

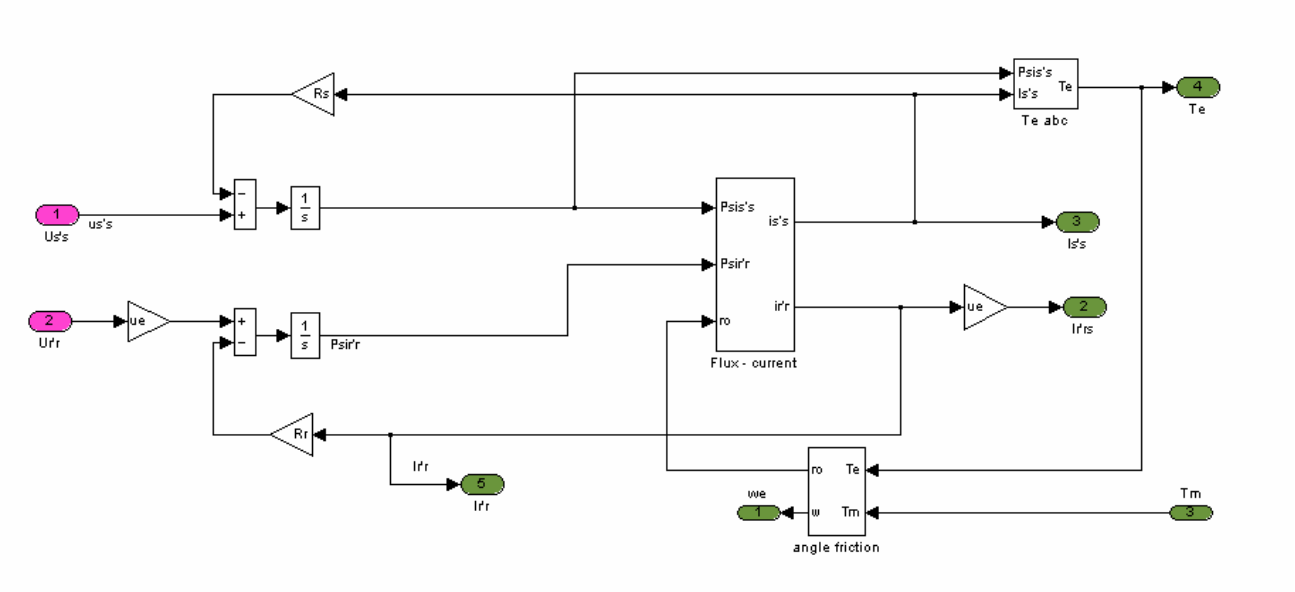

Figure 26 The unmasked Machine model in Matlab/ Simulink

The inputs of the machine model are the three phase voltages of stator and rotor and the mechanical load torque T_m of the generator axis/shaft. Outputs are the three phase stator and rotor currents, the speed of the machine expressed as electrical angular speed of the rotor or mechanical speed and the electric magnetic air gap torque T_e of the machine. The power of the machine is calculated from the voltages and currents of stator and rotor as described in the chapter above. The model is independent of the usage as generator or motor. The mechanical load torque is defined negative for generator operation. The power is negative for power production and positive for power consumption. For rotor power calculation as already for the stator deduced equations (32), (33) are equivalently used.

$$P_r = u_{ar} \cdot i_{ar} + u_{br} \cdot i_{br} + u_{cs} \cdot i_{cr} \quad (94)$$

$$Q_r = \frac{1}{\sqrt{3}} \cdot \left(i_{ar} \cdot (u_{cr} - u_{br}) + i_{br} \cdot (u_{ar} - u_{cr}) + i_{cr} \cdot (u_{br} - u_{ar}) \right) \quad (95)$$

The block called “angle – friction” expresses the equations of motion. With this equation the generator speed and the necessary rotor displacement angle ρ is achieved. Furthermore the friction losses are implemented with using the damping factor D as shown in Figure 27.

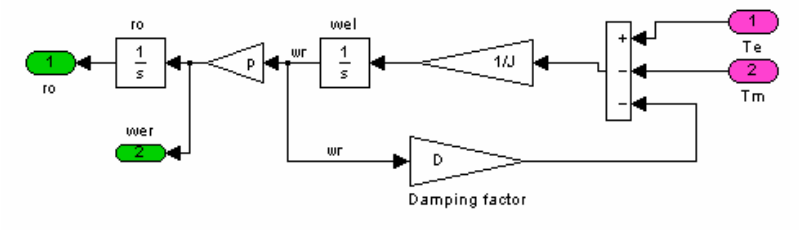

Figure 27 Block angle - friction

The machine block called “flux – current” is expressing the flux equations to calculate the currents with help of the inductance matrix. The saturation effect is taken into account as variable inductances in the inductance matrix.

$$L = \begin{pmatrix} L_{\sigma s} + L_{msA} & -0.5L_{mA} & -0.5L_{mA} & L_{msrAa} \cdot f_1 & L_{msrAb} \cdot f_2 & L_{msrAc} \cdot f_3 \\ -0.5L_{msB} & L_{\sigma s} + L_{msB} & -0.5L_{msB} & L_{msrBa} \cdot f_3 & L_{msrBb} \cdot f_1 & L_{msrBc} \cdot f_2 \\ -0.5L_{msC} & -0.5L_{msC} & L_{\sigma s} + L_{msC} & L_{msrCa} \cdot f_2 & L_{msrCb} \cdot f_3 & L_{msrCc} \cdot f_1 \\ L_{msraA} \cdot f_1 & L_{msraB} \cdot f_3 & L_{msraC} \cdot f_2 & L'_{\sigma r} + L_{mra} & -0.5L_{mra} & -0.5L_{mra} \\ L_{msrbA} \cdot f_2 & L_{msrbB} \cdot f_1 & L_{msrbC} \cdot f_3 & -0.5L_{mrb} & L'_{\sigma r} + L_{mrb} & -0.5L_{mrb} \\ L_{msrcA} \cdot f_3 & L_{msrcB} \cdot f_2 & L_{msrcC} \cdot f_1 & -0.5L_{mrc} & -0.5L_{mrc} & L'_{\sigma r} + L_{mrc} \end{pmatrix} \quad (96)$$

In chapter 3.4 the influence of the saturation on the machine is described. For the variable main inductance the magnetizing current is determined in the following way.

$$\vec{i}_\mu = \vec{i}_s + \vec{i}_r' \quad (97)$$

Using (97) in the stator flux equation (98):

$$\vec{\Psi}_s^s = (L_{\sigma s} + L_m) \cdot \vec{i}_s^{\,s} + L_m \cdot \vec{i}_r^{\,s'} \quad (98)$$

$$\vec{\Psi}_s^s = (L_{\sigma s} + L_m) \cdot \vec{i}_s^{\,s} + L_m \cdot (\vec{i}_\mu - \vec{i}_s^{\,s}) \quad (99)$$

the magnetizing current can be calculated with the stator flux and stator current to:

$$\vec{i}_\mu = \frac{\vec{\Psi}_s^s - L_{\sigma s} \cdot \vec{i}_s^{\,s}}{L_m} \quad (100)$$

Because the magnetizing curve is based on rms values, the rms value of the magnetizing current is calculated as well. This magnetizing current is used with magnetizing curve to achieve the $L_m(I_\mu)$. To secure a stable functioning of the model the current and therewith the main inductance are limited to the known values. Figure 28 show the implementation in Matlab/ Simulink.

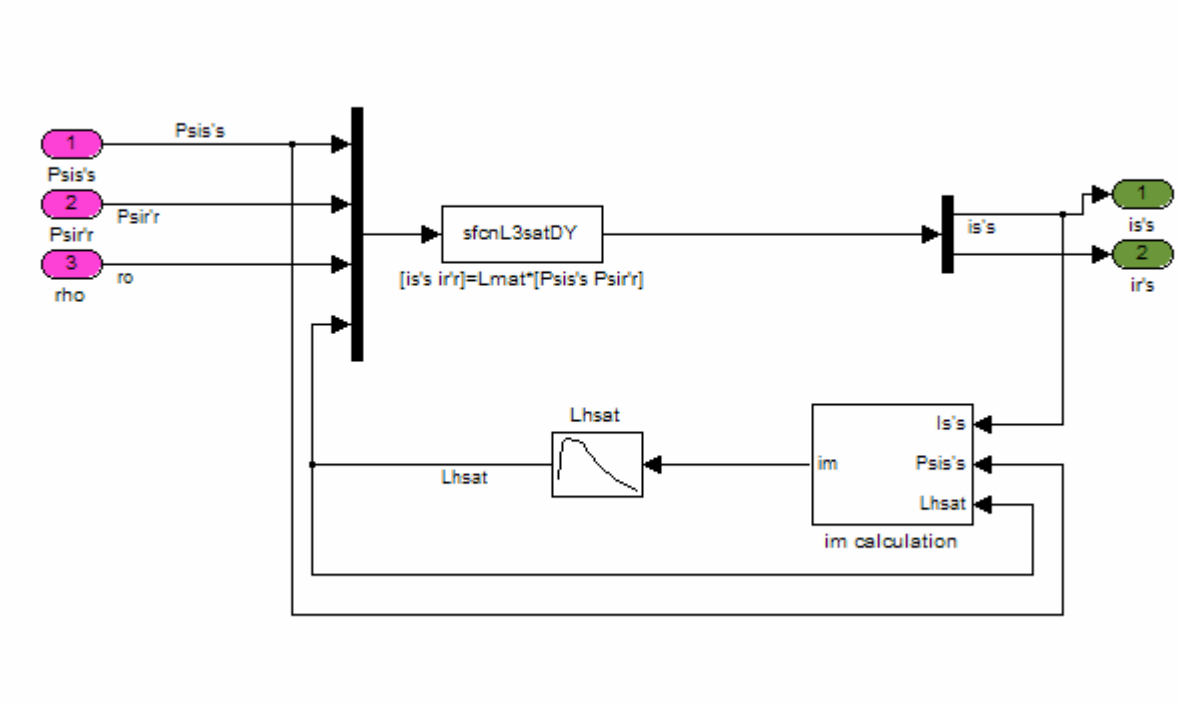

Figure 28 Block flux – current used in the machine model (**Figure 26**)

3.6.1 Steady state validation of the different detailed ABC/abc models

In this chapter a comparison between the machine models including different features are made. At first three different models during rated conditions are chosen. One model shows the ideal machine, without friction losses or saturation effects of the reactances; the second model is a model considering friction losses and the third model is a model including friction losses and saturation of main magnetizing reactance.
The input parameters for the three-phase model are deduced from the one phase equivalent supplied by the machine manufacturer, which are exemplary data of a 1.8 MW machine (Figure 14).
During the simulation the rotor of the induction machine is short circuit, which is modelled with setting the input rotor voltages to zero. The input stator voltages are rated. Therewith a start of the machine, three load changes and a three phase short circuit are simulated. The three different operation points during the load changes are then compared by the manufacturer supplied measured operation points of the machine. The machine starts up in motor mode and then settles into generator mode producing electrical power according to the load torque on the axis of the machine.
In Figure 29 and Figure 30 the torque and the active power over the whole simulation period from the model with saturation are shown.

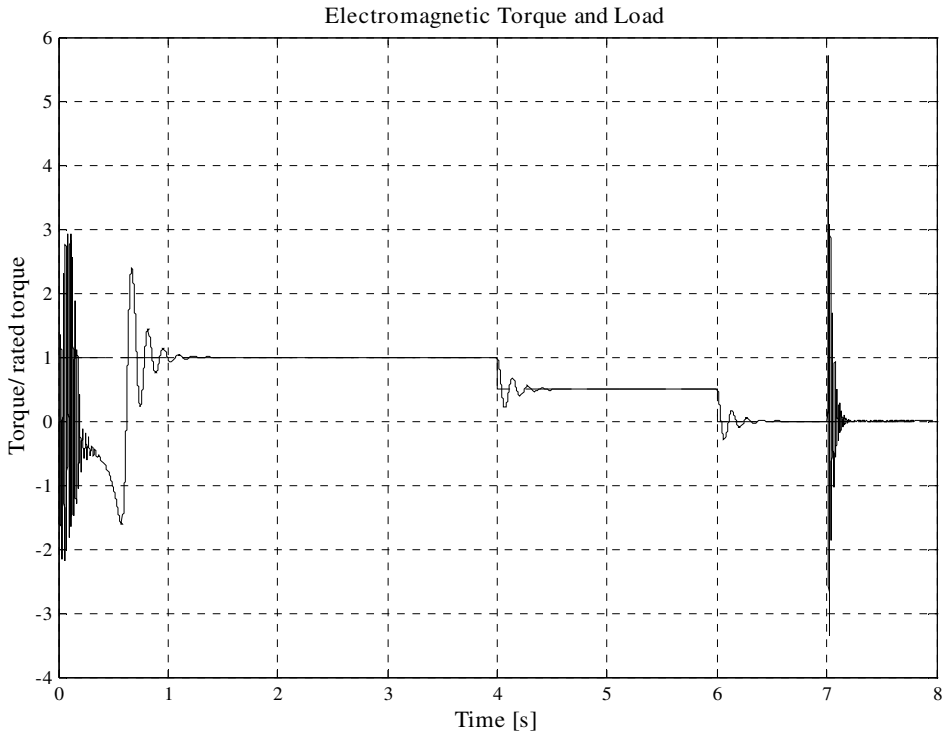

Figure 29 Simulated generator electromagnetic reaction torque and input shaft torque in operation machine start; stepping from rated load torque decreasing to no load torque to 3-phase short circuit in [p.u.]

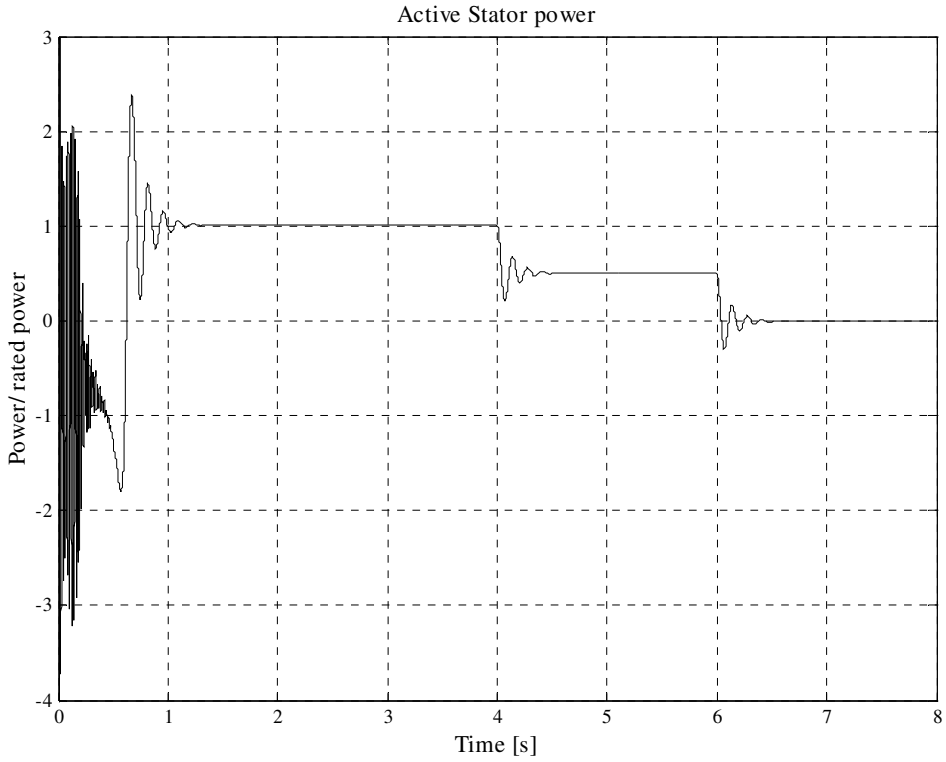

Figure 30 Simulated active stator power [p.u.] corresponding to the input torque

In Figure 31 and Figure 32 the stator current for all three models are shown in comparison to the measured rms value taken from manufacturer supplied data. The peaks of the time

values should theoretically touch the line of the stator peak value ($rms \cdot \sqrt{2}$).
Figure 31 compares the ideal model and the model with implemented damping. The model with damping (friction and windage losses) shows a smaller stator current output with the same load, which is easy to explain. Since the friction losses are depending on the speed and the speed is increasing with the load, this consequently means higher losses and therewith a smaller stator current. At no load operation the friction losses are smaller than at rated load and therewith hard to notice in the simulation.

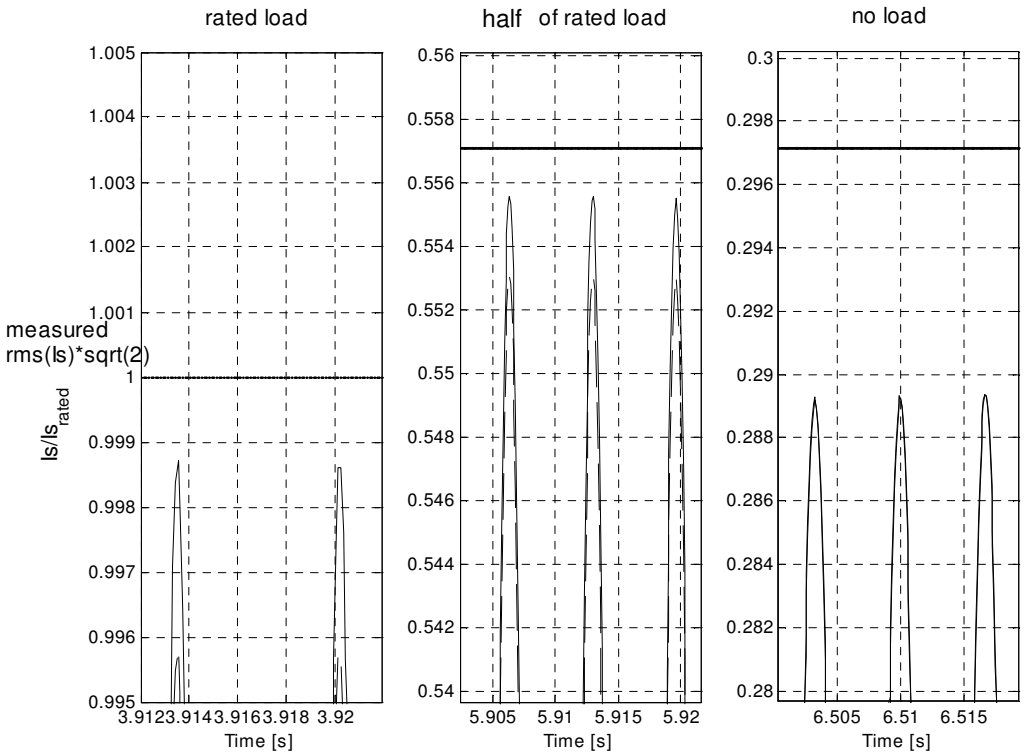

Figure 31 Stator current related to rated stator current; solid line – ideal model, dashed line – model with friction

Figure 32 compares the model with saturation and damping to the model without saturation though with included damping. During the operation with rated load it is hard to see a difference in the simulated stator currents. As it is explained in chapter 3.4, the saturation of main inductance has only an insignificant influence in the area of rated operation up to the maximal operation point. With including leakage saturation a higher current would appear. The influence of main flux saturation is clearly seen in half of rated load operation and no load. As expected due to the theory leads the consideration of main magnetizing saturation to an improvement of the model and the simulated results.

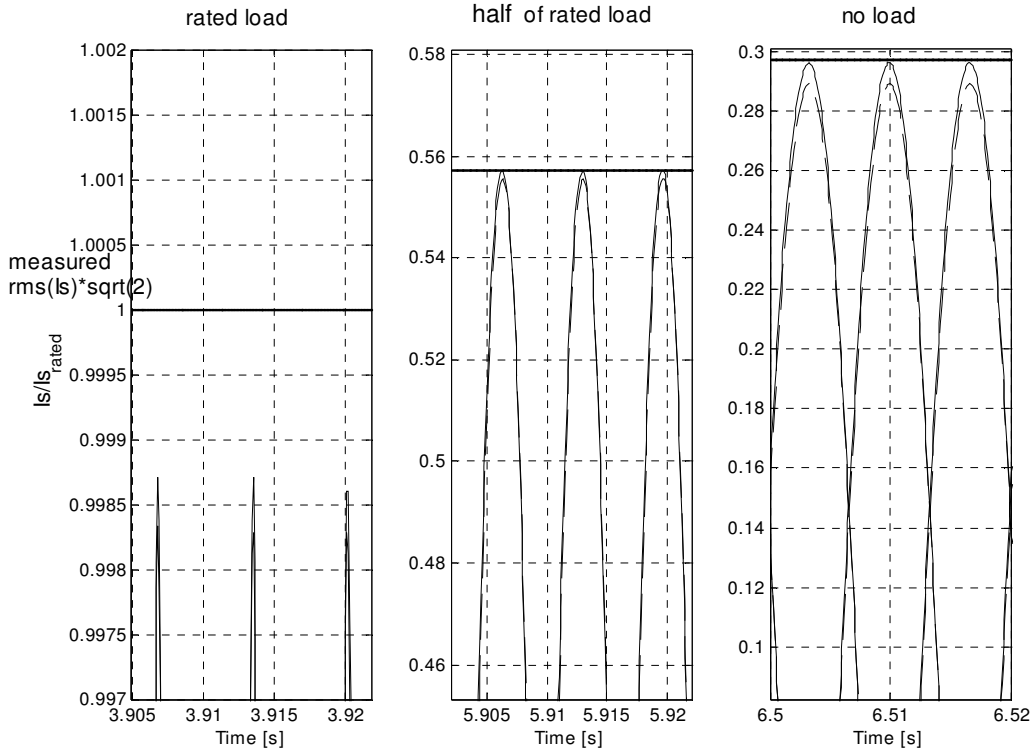

Figure 32 Stator current related to rated stator current; solid line – model with saturation, dashed line –model with friction and windage losses

A further criterion for improvement of the model is shown in the evaluation of the power factor or the reactive power. The power is generally more precisely measurable than the current. Here the model with included saturation and damping shows again the improvement compared to the ideal model.
Calculation of the power factor also approves this result.

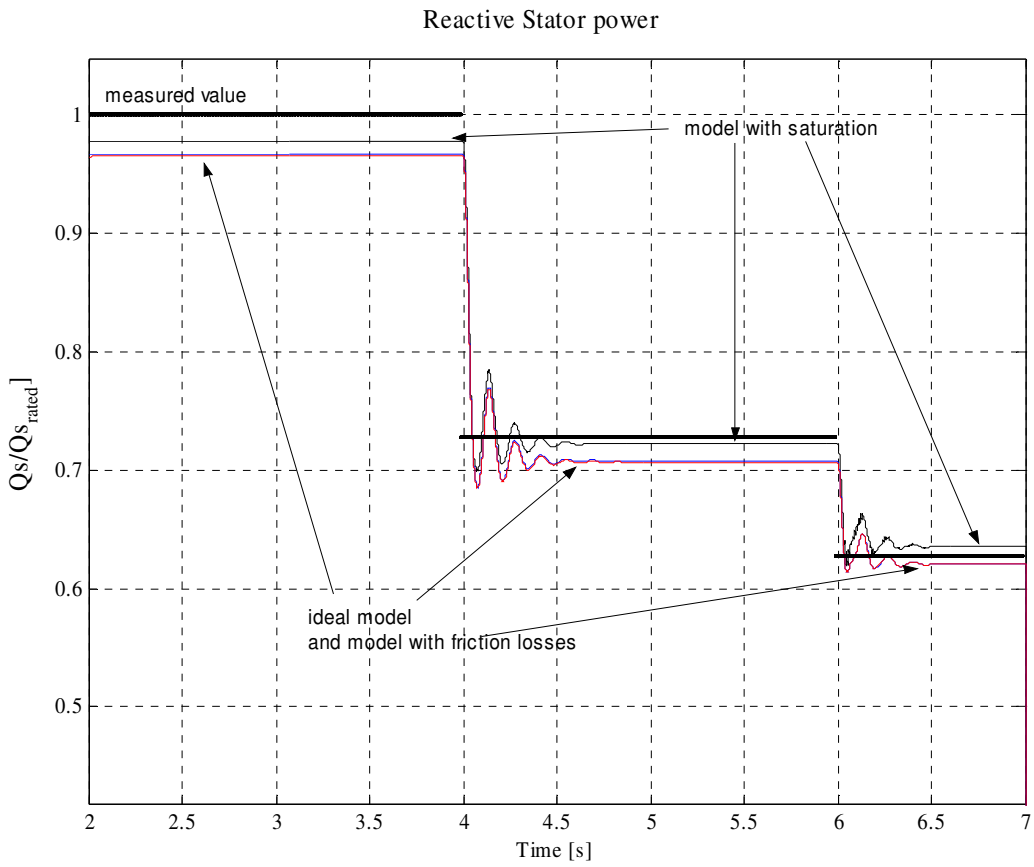

Figure 33 Stator reactive power related to rated reactive stator power [p.u.]; model with saturation – upper line, on top of each other – model with friction losses and ideal model – lower line

The simulations results made with the 1.8 MW machines show only small differences between the different machine models. This is due to the fact that the data used as input for the model is given to meet the expected operation area requirements. Saturation has in this area only minimal influence. Machines with stronger saturation effect will show a more significant difference. For using the model for short circuit simulations, the leakage field saturation should be included as well.

3.6.2 Dynamical validation of the ABC/abc model

The aimed use of the developed model is for simulation of dynamical situations including fault situations. The above steady state validations though are not sufficient enough to verify the use for this kind of simulations. Therefore a Direct On Line (DOL) start of a 850/ 800 kW machine is initiated in a laboratory test set-up. The DOL start has been chosen to produce high currents and achieve saturation effects in the machine, since real short circuits for validation of the machine model are not feasible in the researched machine size of 850kW to 3MW. During the test speed, three-phase stator currents, three phase rotor currents and three phase stator voltages have been measured. The measured voltage is later on used as input for the machine model.
At first the model considering main magnetizing reactance saturation and friction losses will be compared to the measurements. The machine is connected star/ star and the rotor windings are short circuited. Due to the impedance in the grid the stator voltage drops with connection the machine direct to the grid. The stator voltage keeps the decreased voltage amplitude until the machine has started up. With finishing the start up the voltage rise to the rated value again (Figure 34). The experienced long starting sequence is rather unusual for induction machines. The machine is designed for generator operation and not for motor operation and therefore develops very little starting torque. The long starting period gives the possibility to use it for validation. There exist an asymmetrical transient and a quasi stationary part during the DOL start of the machine.

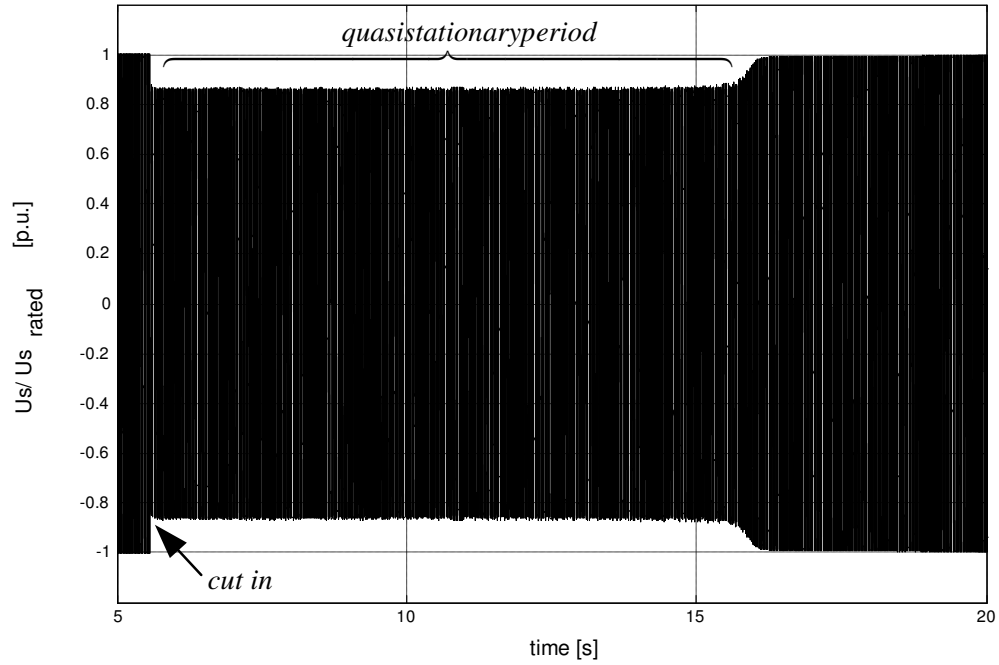

Figure 34 Measured Grid voltages/Stator voltages during the DOL of a 850/800 kW generator

In Figure 35 the speed during the DOL start is shown. There are only small differences between the simulated speed and the measured speed. In the last phase of the start, before reaching the final steady speed the model shows a small overshoot. There are

many different possibilities casing this overshoot /95/.

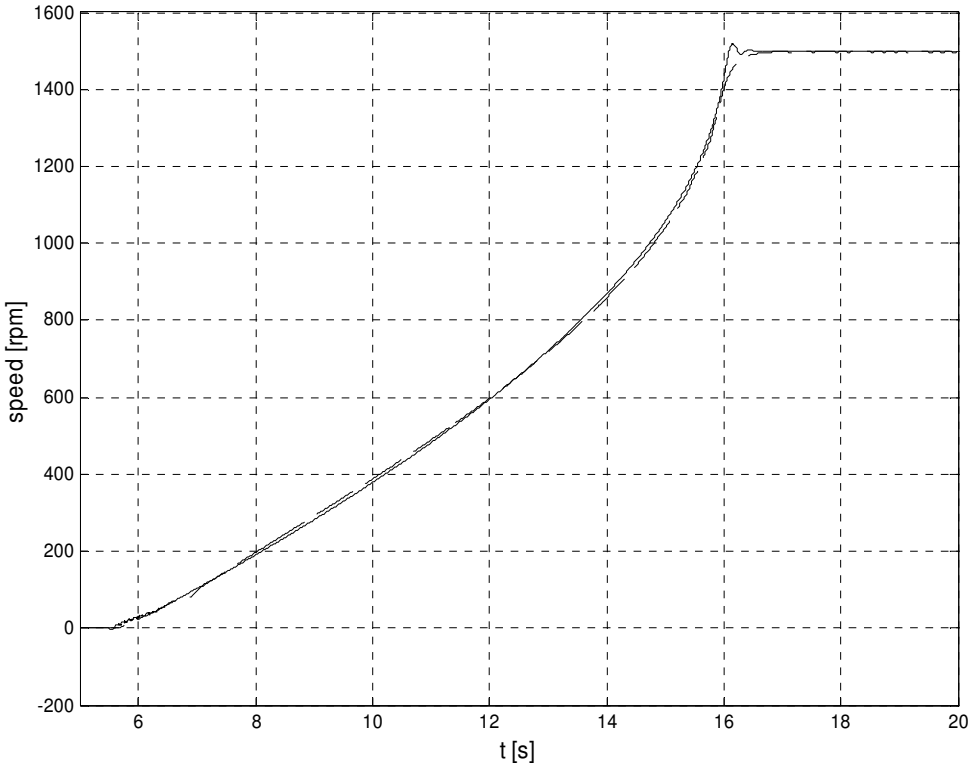

Figure 35 Speed during DOL start of a 850/800 kW generator; model with main saturation and friction losses – solid line, measurement speed – dashed line

Figure 36 and Figure 37 show a window of the simulated and measured stator currents. The measured stator currents are bigger than the simulated values. This is not surprising, since different effects are not included in the model e.g. the saturation of leakage reactances. The biggest difference though can be seen in the transient situation as in Figure 36, during the first seconds after connecting the machine to the grid. The biggest difference between the simulated values and the measurements are at the highest peak value, which is 38% smaller than the measured value. The smallest difference can be seen at the first peak, which is the smallest of all, with 11% difference referred to the measured peak value. During the quasi stationary period while running up of the machine, the current is quasi stationary as well. The average difference between the peak values of the stator currents is now 10% (Figure 37).

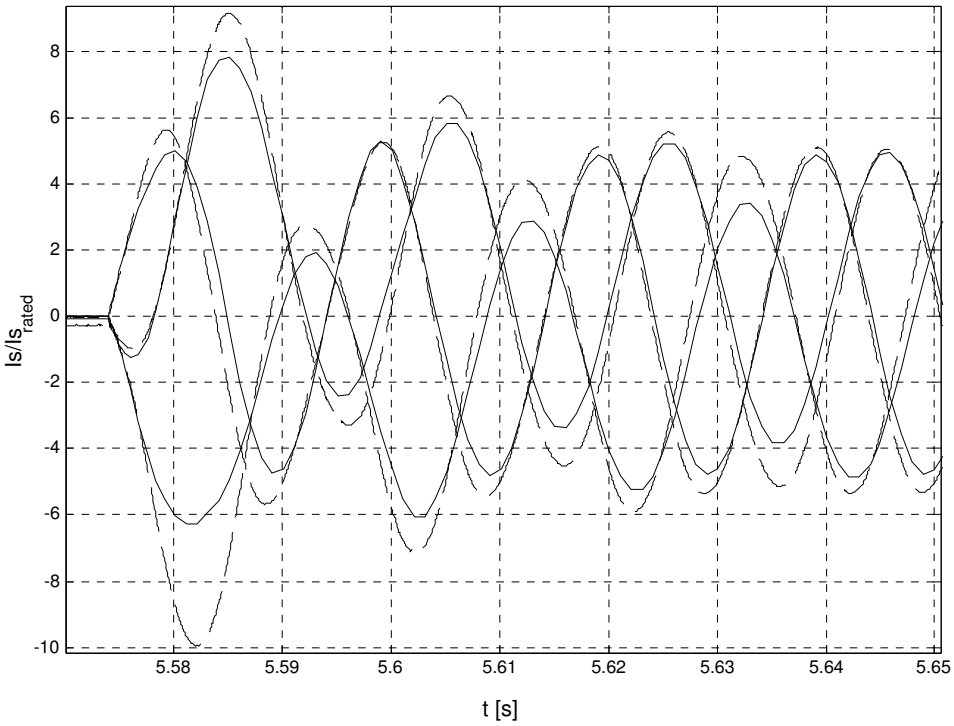

Figure 36 Zoom into the stator currents at start of the DOL-start (solid- model including main saturation and friction losses, dashed - measured)

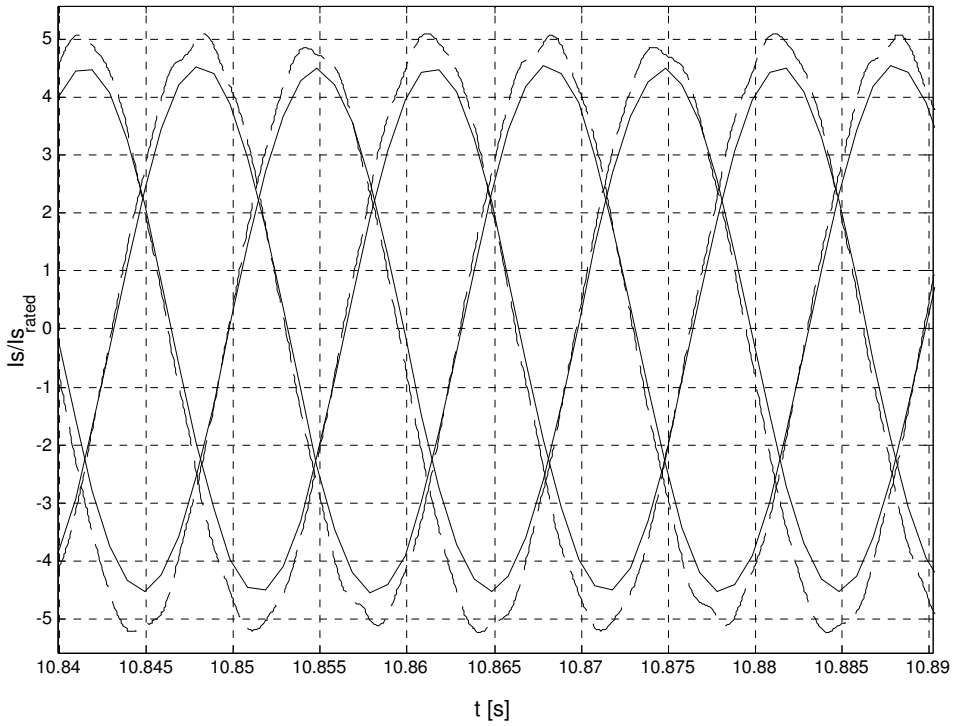

Figure 37 Window of the stator currents in the middle of the DOL-start (solid- model including main saturation and friction losses, dashed - measured)

After the start up the machine it is running in no load operation and consumes only the power for covering the own losses. Figure 38 shows the current during this no load

conditions. The simulated current is insignificantly bigger than the measured, which verifies the correct implementation of the main magnetizing reactance saturation. The noticeable asymmetric between the phase currents is due to the slightly asymmetrical real voltage input.

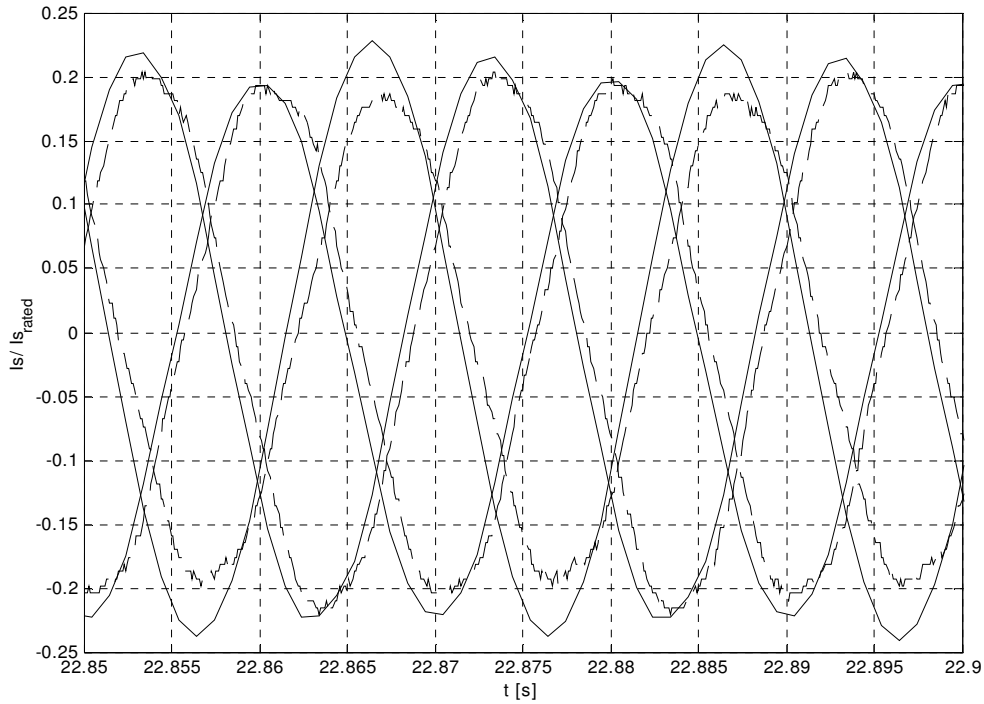

Figure 38 Window of stator currents at no load operation after DOL- start

3.6.3 Implementation and validation of leakage reactance saturation

It is highly desirable to minimise the differences between the simulated and experimental values in Figure 36 and Figure 38. The exact knowledge of the current peaks enables a better design of protection systems or the components withstanding the dynamical load. As already implied in the chapter about saturation effects an implementation of leakage reactance saturation could improve the model especially during situations with high currents e.g. short circuits.
Unfortunately, there is a lack of data to have a detailed implementation of the nonlinearity of the leakage reactances. However the saturated leakage reactance of stator and rotor are estimated from the blocked rotor measurements with smaller voltage and available in the data sheet supplied by the manufacturer. Also known are the saturated stator currents or blocked rotor stator current. Using the two described points of rated and saturated operation a linear approximation has been chosen to express change in the leakage inductances.

Stator current	Leakage inductance
0	rated
rated value	rated
Blocked rotor stator current	saturated value at slip=1
10x rated current value	saturated value at slip=1

Table 3-1 Leakage inductance saturation reference

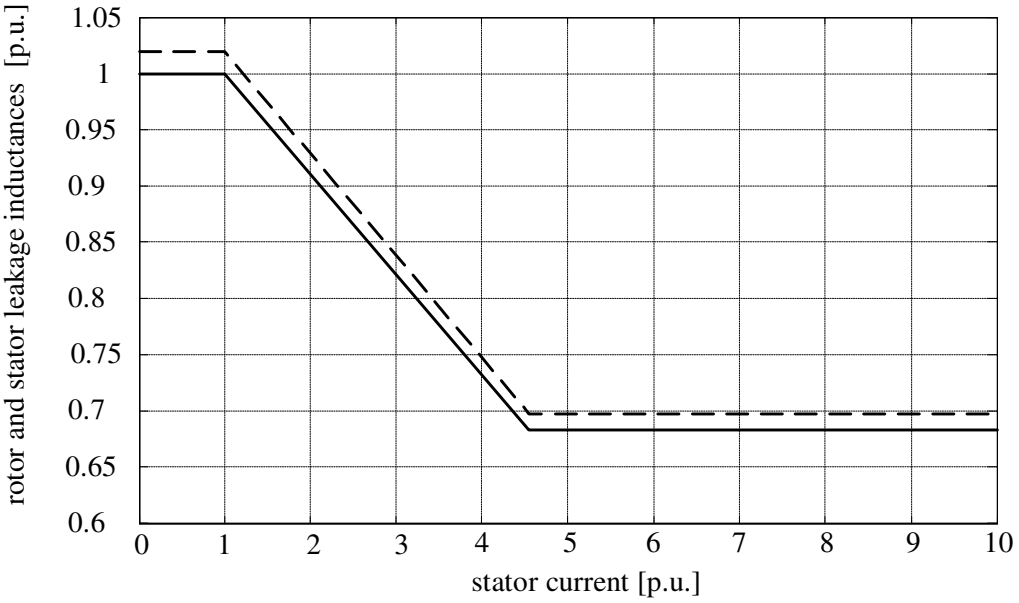

Figure 39 Example for stator (solid line) and rotor (dashed line) leakage inductance

Changing the leakage inductance in the presented manner might seem odd, since commonly the changes in inductances are made depending on the slip of the machine /86/. Dependency from the slip though has the disadvantage that all 3-phase values are changed simultaneously. The dependency on the current gives the possibility of changing the phase inductances separately due to the phase instantaneous current.

Figure 40 shows the implementation of main and leakage saturation in the machine model in Matlab/ Simulink. The rest of the machine model is the same as already described above.

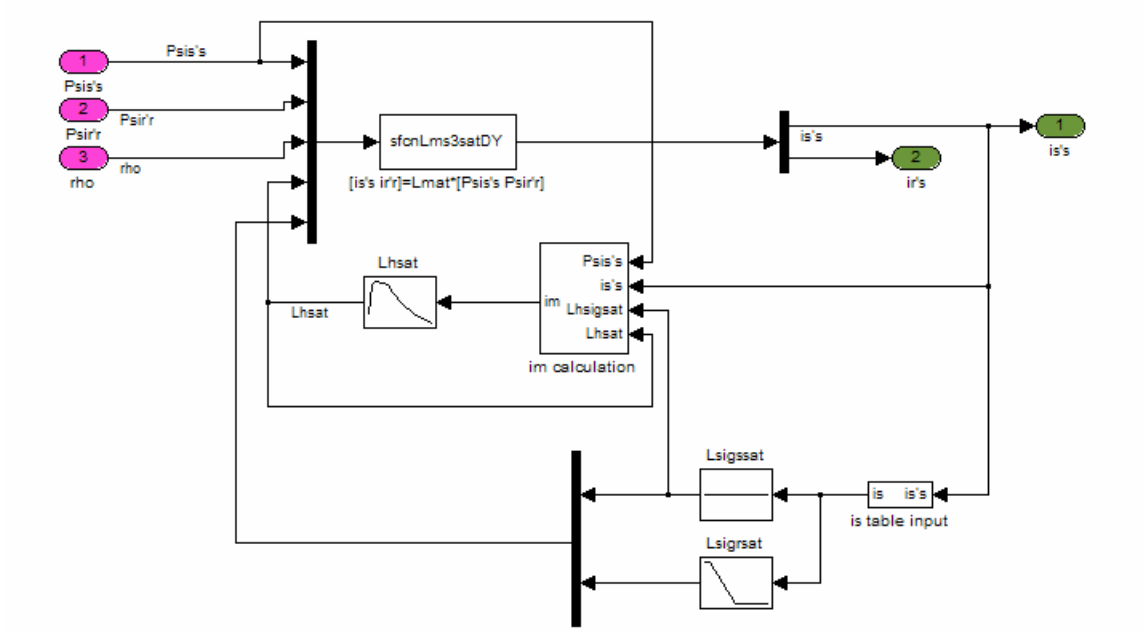

Figure 40 Modified Matlab/ Simulink block “flux – current” including leakage inductance saturation

The same simulation has been performed as already done with the model considering only the main magnetizing inductance saturation. There is not a noticeable change in the speed characteristic compared to the model including only main saturation. Figure 41 shows the model with the implementation of the leakage inductance saturation compared to the measurement of the test bench.

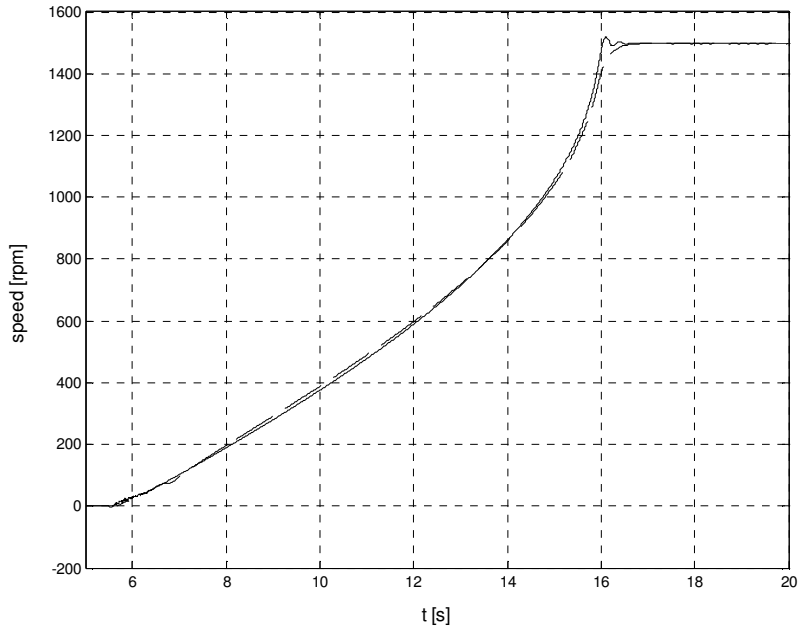

Figure 41 Speed during DOL start (solid line – model including main and leakage inductance saturation, dashed - measurement)

In Figure 42 and Figure 43 the stator current windows from the cut in of the machine and from the quasi stationary situation are shown. Implementation shows a large improvement in the stator current simulation compared to the simulations with the models not considering leakage saturation. The difference in the maximum peak values during the DOL start have been decreased from 38% to 21%. In the quasi stationary state after the start up the average difference between the peak values of the stator current is decreased from 10% to 2% (Figure 43).

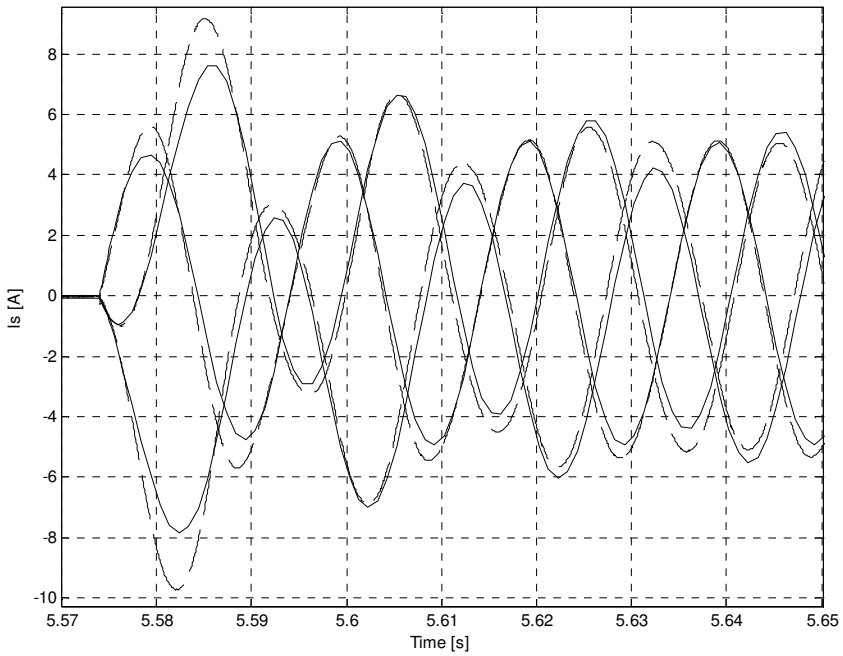

Figure 42 Zoom into stator currents simulation at start of the DOL start (solid- model including main and leakage saturation, dashed - measured)

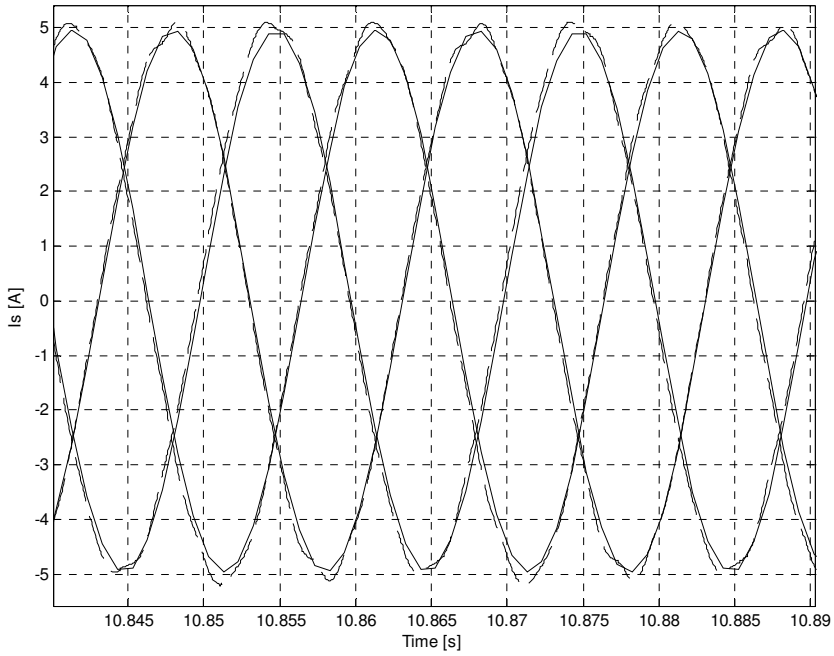

Figure 43 Window of Stator currents in the quasi stationary state of the DOL-start (solid-model including main and leakage saturation, dashed - measured)

Hence the influence of the saturation of main and leakage inductances could be clearly shown, the influence during no load operation is insignificant. Figure 44 shows the currents during the no load state after the DOL start. The missing behaviour during no load operation is easily explained with the used implementation method. While the main inductance is more correctly changing accordingly the available points from the no-load curve, the leakage inductances are assumed constant to their rated values and do not change dependant from the current between zero and rated current. The Figure 44 gives also only information about the functionality of the model even with very small currents.

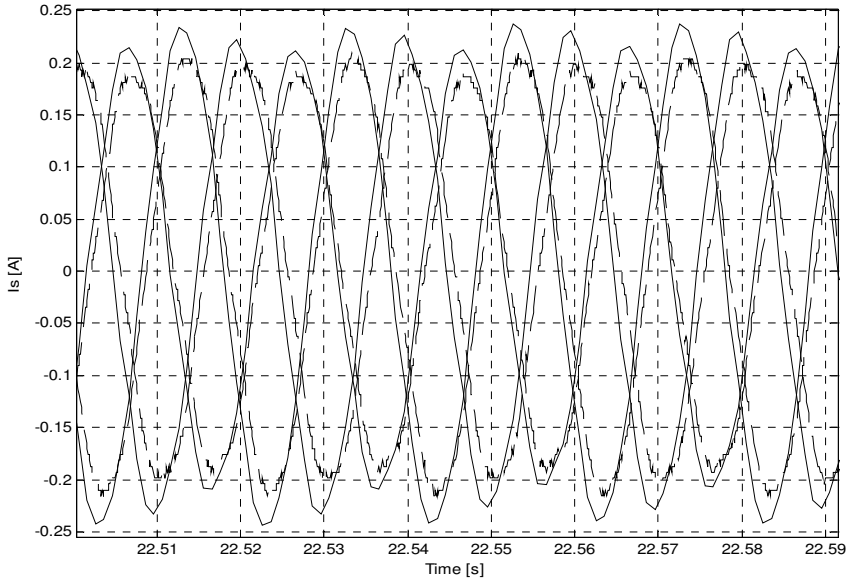

Figure 44 Zoom into stator currents at no load operation after DOL- start; solid line – model including main and leakage inductance saturation, dashed line - measured

3.6.4 Influence of the machines coupling

In the above chapters the influences of saturation effects and friction losses have been discussed. The discussed dependencies are in principle the same independence of the use of a three phase model or made with Clark or Park transformation. In the following the influences of the machine coupling will be discussed. Unfortunately it is not only secondary discussed, though found important during the consideration of choosing the method of machine modelling for the purpose of simulating non rated conditions. Therefore some presumption done during developing the analytical model will be paid attention.
The general ABC/abc generator modelling has been described. Gaining the input for this model is very challenging under the given circumstances. Though it is worth the effort, since a three-phase ABC/abc generator model gives the possibility to look at each phase separately as well as the coupling between the phases /104/ Thereby the ABC/abc model is not limited by conditions of symmetry of either supply voltages or phase impedances /68/. The three-phase analytical model can be easily improved with accessibility of more input parameters, without complete model changes. All these advantages are improving the simulation result.
Another possible presentation of the ABC/abc per phase machine model, point out the field coupling between stator and rotor and the correlation to the voltage equation is given in Figure 45.

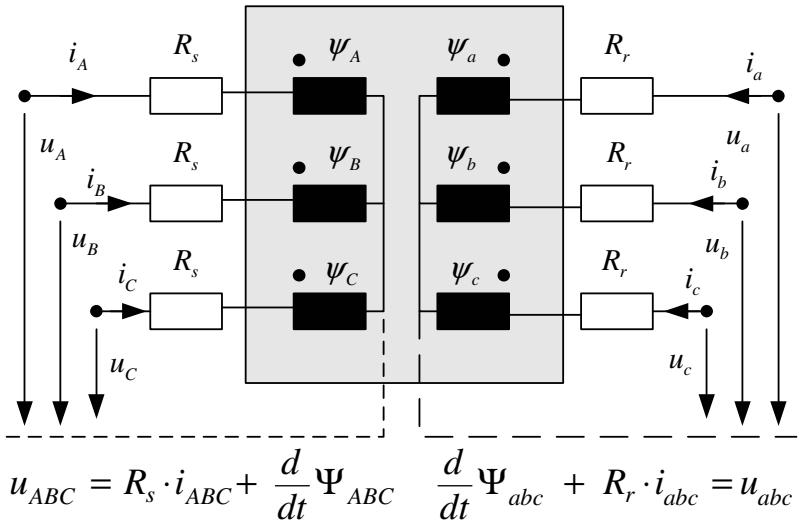

Figure 45 Three phase equivalent ABC/abc circuit diagram of a doubly fed induction machine

The coupling is derived to be expressed as a product of the inductance matrix L /79/ and the current vector i. The inductance matrix of the machine model takes a central position. During the computing of the machine model the inverse of the inductance matrix has to be calculated. This introduces a rather difficult task and is slowing down the simulation process. Including saturation effects improves the realistic presentation of the machine but also complicates the model even more, since the inverse of the matrix has to be computed every time step. Taking the electrical coupling in the induction matrix into account give a possibility to relax the complexity of the model it self and therewith simplify the computing of the inverse matrix as proposed by Pillay /79/ and Goldemberg /30/. The inductance matrix of the induction machine including saturation of the inductances has been previously determined to:

$$L=\begin{pmatrix} L_{\sigma sA}+L_{msA} & -0.5L_{msA} & -0.5L_{msA} & L_{msrAa}\cdot f_1 & L_{msrAb}\cdot f_2 & L_{msrAc}\cdot f_3 \\ -0.5L_{msB} & L_{\sigma sB}+L_{msB} & -0.5L_{msB} & L_{msrBa}\cdot f_3 & L_{msrBb}\cdot f_1 & L_{msrBc}\cdot f_2 \\ -0.5L_{msC} & -0.5L_{msC} & L_{\sigma sC}+L_{msC} & L_{msrCa}\cdot f_2 & L_{msrCb}\cdot f_3 & L_{msrCc}\cdot f_1 \\ L_{msraA}\cdot f_1 & L_{msraB}\cdot f_3 & L_{msraC}\cdot f_2 & L'_{\sigma ra}+L_{mra} & -0.5L_{mra} & -0.5L_{mra} \\ L_{msrbA}\cdot f_2 & L_{msrbB}\cdot f_1 & L_{msrbC}\cdot f_3 & -0.5L_{mrb} & L'_{\sigma rb}+L_{mrb} & -0.5L_{mrb} \\ L_{msrcA}\cdot f_3 & L_{msrcB}\cdot f_2 & L_{msrcC}\cdot f_1 & -0.5L_{mrc} & -0.5L_{mrc} & L'_{\sigma r}+L_{mrc} \end{pmatrix} \tag{101}$$

Assuming a star/star (YY) connected machine with no external accessible star point, the addition of the rotor currents per phase and stator currents per phase is zero in the star point as shown in equation (102).

$$i_A+i_B+i_C=0\,,\; i_a+i_b+i_c=0 \tag{102}$$

Taking this into account, the induction matrix takes the following form (13).

$$L=\begin{pmatrix} L_{\sigma sA}+1.5L_{msA} & 0 & 0 & L_{msrAa}\cdot f_1 & L_{msrAb}\cdot f_2 & L_{msrAc}\cdot f_3 \\ 0 & L_{\sigma sB}+1.5L_{msB} & 0 & L_{msrBa}\cdot f_3 & L_{msrBb}\cdot f_1 & L_{msrBc}\cdot f_2 \\ 0 & 0 & L_{\sigma sC}+1.5L_{msC} & L_{msrCa}\cdot f_2 & L_{msrCb}\cdot f_3 & L_{msrCc}\cdot f_1 \\ L_{msraA}\cdot f_1 & L_{msraB}\cdot f_3 & L_{msraC}\cdot f_2 & L'_{\sigma ra}+1.5L_{mra} & 0 & 0 \\ L_{msrbA}\cdot f_2 & L_{msrbB}\cdot f_1 & L_{msrbC}\cdot f_3 & 0 & L'_{\sigma rb}+1.5L_{mrb} & 0 \\ L_{msrcA}\cdot f_3 & L_{msrcB}\cdot f_2 & L_{msrcC}\cdot f_1 & 0 & 0 & L'_{\sigma r}+1.5L_{mrc} \end{pmatrix} \tag{103}$$

Notice, the stator and rotor mutual inductances L_{ms} , L_{mr} are of *2/3* L_m the one phase equivalent diagram.

For models represented in Clark or Park transformation the YY coupling of the machine is assumed in the most cases and the experiences made with the three phase model are exemplary for the models made with a transformation as well.
In case of a ΔY connected machine the coupling of the rotor phases can be simplified as shown above in the YY example, while leaving the stator phases untouched. The inductance matrix for a ΔY connected machine takes the form shown in (104).

$$L=\begin{pmatrix} L_{\sigma sA}+L_{msA} & -0.5L_{msA} & -0.5L_{msA} & L_{msrAa}\cdot f_1 & L_{msrAb}\cdot f_2 & L_{msrAc}\cdot f_3 \\ -0.5L_{msB} & L_{\sigma sB}+L_{msB} & -0.5L_{msB} & L_{msrBa}\cdot f_3 & L_{msrBb}\cdot f_1 & L_{msrBc}\cdot f_2 \\ -0.5L_{msC} & -0.5L_{msC} & L_{\sigma sC}+L_{msC} & L_{msrCa}\cdot f_2 & L_{msrCb}\cdot f_3 & L_{msrCc}\cdot f_1 \\ L_{msraA}\cdot f_1 & L_{msraB}\cdot f_3 & L_{msraC}\cdot f_2 & L'_{\sigma ra}+1.5L_{mra} & 0 & 0 \\ L_{msrbA}\cdot f_2 & L_{msrbB}\cdot f_1 & L_{msrbC}\cdot f_3 & 0 & L'_{\sigma rb}+1.5L_{mrb} & 0 \\ L_{msrcA}\cdot f_3 & L_{msrcB}\cdot f_2 & L_{msrcC}\cdot f_1 & 0 & 0 & L'_{\sigma r}+1.5L_{mrc} \end{pmatrix} \tag{104}$$

Leaving the magnetic coupling of the stator phases in the original allows the stator currents to flow in a circle. This gives a more realistic result than the usually used method of assuming a magnetically YY connected machine and afterwards calculation of the electrical delta coupling of the stator windings, which is shown in the following example. A delta coupled generator experiences a 2-phase line to line short circuit at the terminals.

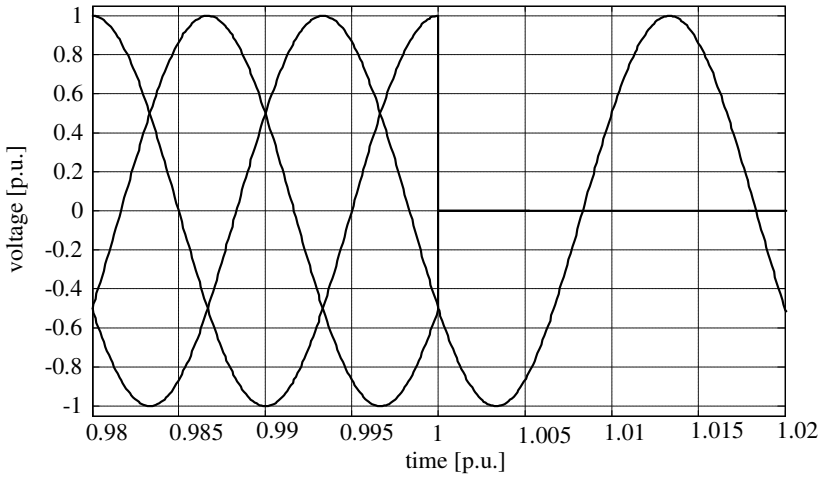

Figure 46 Voltage at generator stator terminal during a two-phase short circuit

While there is no difference between the simulated stator current under symmetrical conditions before the short circuit, the difference between the models can be seen in the asymmetrical condition Figure 47. The current modelled with the star connected machine model and a calculated delta coupling shows difference in phase and amplitude to the current simulated with the delta connected machine model.

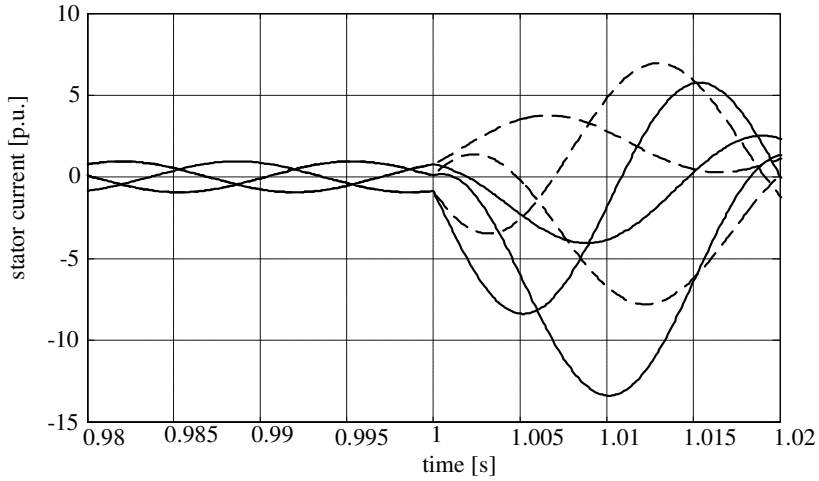

Figure 47 Stator currents of the generator dashed line – star modelled machine with calculated delta coupling and solid lines – delta modelled machine

They are many different ways of machine modelling, but as the machines are designed for their application, the model has to be developed for the expected use and the reality. The modelling in this thesis uses a three-phase model because it has the purpose of accurately fault simulation in Vestas variable speed wind turbines. Thereby it has been shown, that different analytical description of the e.g. connection of the machine phases have an increased importance, while looking at asymmetrical conditions. Leakage saturation has an important influence, while looking at short circuit contribution to the grid, which plays an important role for grid connection of the turbine. Not all influences have been studied in this presented work. The influence of iron losses and skin effect as well as the changes due to temperature changes are open for future research activities. The ABC/abc machine model is beneficial to use, because it does not only simplify the inclusion of connection

condition influence and per phase variability of saturation. The three-phase model can be easily expanded for other simulation purposes e.g. asymmetry in the machine parameters or harmonics.

Chapter 4

4. Modelling of Transformers

The Transformer is an important part to connect the wind turbine to the grid. However, it is very common to neglect the dynamic behaviour of the transformer and only consider a very simple ideal model or the use of equivalent impedances for calculations. In this thesis it is very important to consider the dynamic behaviour of the wind turbine transformer. The content of this chapter are the development of the 2-windings 3-phase transformer model and the 3-winding 3-phase transformer model. In the end the 2-winding 3-phase Autotransformer model is derived.

4.1 The 2-windings 3-phase transformer model

The 2-windings 3-phase transformer (2w 3ph transformer) connects a three phase system with two different voltage levels. The transformer consists of 2 windings, which are connected through a magnetic circuit in the core. The two different voltage levels on the transformer are called high- and low-voltage side or commonly also known as primary and secondary side, because the high voltage side is usual connected to the 1st winding and the low voltage side is connected to the 2nd winding.
Assuming there is no air gap in the core, no voltage drop in the magnetic circle (infinite core permeability), and no hysteresis losses, the resistances of the windings are negligible. The result of all assumptions together is a loss-less (ideal) transformer, which is only representing a simple relationship between the two voltages and currents.

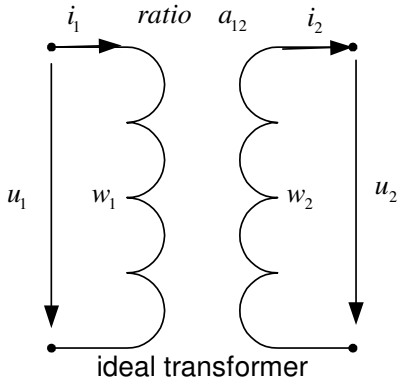

The voltage equations for the two windings of such an ideal transformer is:

$$\underline{u}_1 = -\underline{e}_1 = \frac{d\underline{\Psi}_1}{dt} \qquad \underline{u}_2 = -\underline{e}_2 = \frac{d\underline{\Psi}_2}{dt}$$

Hence the whole flux is closing inside the core the flux in winding 1 and winding 2 are identical and therewith the flux linkages can be expressed as:

$$\underline{\Psi}_1 = w_1 \cdot \underline{\Phi} \qquad \underline{\Psi}_2 = w_2 \cdot \underline{\Phi}$$

In this loss-less transformer the summation of the currents considering the number of windings is $w_1 \cdot \underline{i}_1 + \underline{i}_2 \cdot w_2 = 0$. Using the current correlation in combination with the voltage equation the relationship between primary and secondary voltage can be easily expressed with the winding ratio a_{12}.

$$\frac{\underline{u}_1}{\underline{u}_2} = \frac{w_1}{w_2} \qquad a_{12} = \frac{w_1}{w_2} \qquad \underline{u}_1 = a_{12} \cdot \underline{u}_2 = \underline{u}_2'$$

The secondary voltage transformed with the winding ratio is equivalent to the primary voltage. Similarly the currents can be expressed with the winding ratio to:

$$\underline{i}_1 = \frac{1}{a_{12}} \cdot \underline{i}_2 = \underline{i}_2'$$

These with the ideal model achieved simple correlation are the most basic equations for transformer consideration. In a realistic transformer a part of the magnetic field will close via the air and therefore only a part of the magnetic field is linked to both windings. The part of the flux, which is not linked through the core, is called the leakage flux, which only links to either primary or secondary winding. The losses in the windings of the transformer are expressed with an electrical resistance.

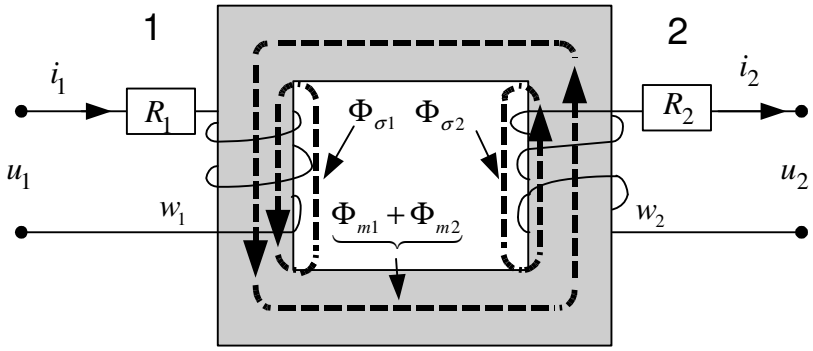

Figure 48 2-windings 2-phase Transformer

The definition of the flux is very similar as in an electrical machine, divided into main flux in the core and the leakage flux.

$$\Psi_1 = w_1 \cdot \Phi_{\sigma 1} + w_1 \cdot \Phi_{m1} + w_1 \cdot \Phi_{m2} \quad (105)$$

$$\Psi_2 = w_2 \cdot \Phi_{\sigma 2} + w_2 \cdot \Phi_{m2} + w_2 \cdot \Phi_{m1} \quad (106)$$

As in the electrical machine theory the transformer is often expressed in a one phase equivalent. The inductances are achieved as:

$$L_{11} = L_{\sigma 1} + L_{m1} = \frac{w_1(\Phi_{\sigma 1} + \Phi_{m1})}{i_1} \qquad L_{m1} = \frac{w_1 \Phi_{m1}}{i_1} \quad (107)$$

$$L_{22} = L_{\sigma 2} + L_{m2} = \frac{w_2(\Phi_{\sigma 2} + \Phi_{m2})}{i_2} \qquad L_{m2} = \frac{w_2 \Phi_{m2}}{i_2} \quad (108)$$

$$L_{12} = \frac{w_1 \Phi_{m2}}{i_2} \qquad L_{12} = \frac{w_2}{w_1} L_{m1} \quad (109)$$

$$L_{21} = \frac{w_2 \Phi_{m1}}{i_1} \qquad L_{21} = \frac{w_1}{w_2} L_{m2} \quad (110)$$

$$L_{21} = L_{12} \qquad L_{m1} = \left(\frac{w_1}{w_2}\right)^2 L_{m2} \quad (111)$$

L_{21} and L_{12} describe the mutual inductances between the two windings and L_{11}, L_{22} the self-induction of the windings. The flux coupling between winding 1 and 2 can be written as:

$$\begin{bmatrix}\Psi_1\\ \Psi_2\end{bmatrix}=\begin{bmatrix}L_{11} & L_{12}\\ L_{21} & L_{22}\end{bmatrix}\times\begin{bmatrix}i_1\\ i_2\end{bmatrix} \tag{112}$$

The voltage equations therewith become:

$$[u]=[R]\times[i]+\frac{d}{dt}\left([L]\times[i]\right)$$

$$\begin{bmatrix}u_1\\ u_2\end{bmatrix}=\begin{bmatrix}R_1 & R_2\end{bmatrix}\times\begin{bmatrix}i_1\\ i_2\end{bmatrix}+\frac{d}{dt}\left(\begin{bmatrix}L_{11} & L_{12}\\ L_{21} & L_{22}\end{bmatrix}\times\begin{bmatrix}i_1\\ i_2\end{bmatrix}\right) \tag{113}$$

This one phase equivalent system can be depicted in the well-known equivalent T circuit of two magnetically coupled coils. Preferred is to relate the parameters and variables to one side of the transformer and using the ideal transformer to express the transformation. The parameters are transformed using the introduced ratio a_{12}. The transformation from all value to the primary side can be made in the following way:

$$u_2^{'}=a_{12}\cdot u_2 \qquad i_2^{'}=\frac{1}{a_{12}}\cdot i_2 \qquad \Psi_2^{'}=a_{12}\cdot\Psi_2$$

$$L_{12}^{'}=a_{12}^2\cdot L_{12} \qquad L_{22}^{'}=a_{12}^2\cdot L_{22} \qquad R_2^{'}=a_{12}^2\cdot R_2 \tag{114}$$
$$L_{21}^{'}=a_{12}^2\cdot L_{21}$$

The calculation of the values to the secondary side can be made in the same way. The parameters itself can be determined with a no load and a short circuit test /25/, /61/, /67/, /75/, /81/.

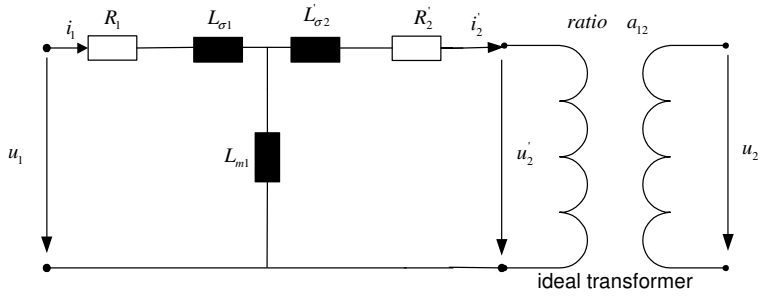

Figure 49 Equivalent circuit of a transformer referred to primary side

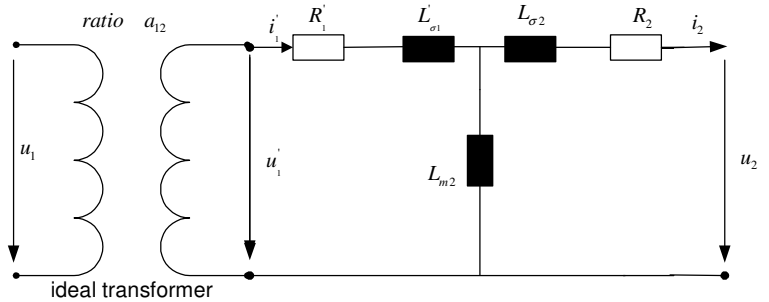

Figure 50 Equivalent circuit of a transformer referred to secondary side

For asymmetrical dynamic simulations of the 2w3ph transformer the equivalent one phase equation developed above are not sufficient enough. The coupling between the phases has to be considered as well. The general voltage equations for a two windings 2w3ph transformer considering all phases can now be written as:

$$[u] = [R] \times [i] + \frac{d}{dt}\left([L] \times [i] \right)$$

$$\begin{bmatrix} u_{1a} \\ u_{1b} \\ u_{1c} \\ u_{2a} \\ u_{2b} \\ u_{2c} \end{bmatrix} = \begin{bmatrix} R_{1a} & R_{1b} & R_{1c} & R_{2a} & R_{2b} & R_{2c} \end{bmatrix} \times \begin{bmatrix} i_{1a} \\ i_{1b} \\ i_{1c} \\ i_{2a} \\ i_{2b} \\ i_{2c} \end{bmatrix} + \cdots$$

$$+ \frac{d}{dt}\left(\begin{bmatrix} L_{11a} & L_{1ab} & L_{1ac} & L_{12a} \cdot f_1 & L_{12ab} \cdot f_2 & L_{12ac} \cdot f_3 \\ L_{1ba} & L_{11b} & L_{1bc} & L_{12ba} \cdot f_3 & L_{12b} \cdot f_1 & L_{12bc} \cdot f_2 \\ L_{1ca} & L_{1cb} & L_{11c} & L_{12ca} \cdot f_2 & L_{12cb} \cdot f_3 & L_{12c} \cdot f_1 \\ L_{21a} \cdot f_1 & L_{21ab} \cdot f_3 & L_{21ac} \cdot f_2 & L_{22a} & L_{2ab} & L_{2ac} \\ L_{21ba} \cdot f_2 & L_{21b} \cdot f_1 & L_{21bc} \cdot f_3 & L_{2ba} & L_{22b} & L_{2bc} \\ L_{21ca} \cdot f_3 & L_{21cb} \cdot f_2 & L_{21c} \cdot f_1 & L_{2ca} & L_{2cb} & L_{22c} \end{bmatrix} \times \begin{bmatrix} i_{1a} \\ i_{1b} \\ i_{1c} \\ i_{2a} \\ i_{2b} \\ i_{2c} \end{bmatrix} \right) \tag{115}$$

$$f_1 = \cos(\vartheta) \qquad f_2 = \cos(\vartheta + \frac{2}{3}\pi) \qquad f_3 = \cos(\vartheta - \frac{2}{3}\pi)$$

In the inductance matrix equation (115) new factors $f_1, f_{2,} f_3$ are introduced. The factors consider the external connection of the windings and the related turn in the phases. The factor is easy explained with an example:

A very common coupling of the windings of a three-phase transformer is DYN5. The expected phase difference between the voltage in phase a of the primary winding compared to the voltage in phase a of the secondary winding is $5 \cdot 30 grad = 150 grad$. To achieve this phase difference with the model the angle theta should be set to $\vartheta = -2.618 rad$.

4.2 The 3-windings 3-phase transformer model

The three-winding three-phase (3w3ph) transformer is modelled in the same way as the 2w3ph transformer. The general equations simply get expanded with a third system representing the additional three phases in the third winding:

$$[u] = [R] \times [i] + \frac{d}{dt}\left([L] \times [i] \right)$$

$$\begin{bmatrix} u_{1a} \\ u_{1b} \\ u_{1c} \\ u_{2a} \\ u_{2b} \\ u_{2c} \\ u_{3a} \\ u_{3b} \\ u_{3c} \end{bmatrix} = \begin{bmatrix} R_{1a} & R_{1b} & R_{1c} & R_{2a} & R_{2b} & R_{2c} & R_{3a} & R_{3b} & R_{3c} \end{bmatrix} \times \begin{bmatrix} i_{1a} \\ i_{1b} \\ i_{1c} \\ i_{2a} \\ i_{2b} \\ i_{2c} \\ i_{3a} \\ i_{3b} \\ i_{3c} \end{bmatrix} + \frac{d}{dt} \begin{bmatrix} \Psi_{1a} \\ \Psi_{1b} \\ \Psi_{1c} \\ \Psi_{2a} \\ \Psi_{2b} \\ \Psi_{2c} \\ \Psi_{3a} \\ \Psi_{3b} \\ \Psi_{3c} \end{bmatrix} \tag{116}$$

$$\begin{bmatrix} \Psi_{1a} \\ \Psi_{1b} \\ \Psi_{1c} \\ \Psi_{2a} \\ \Psi_{2b} \\ \Psi_{2c} \\ \Psi_{3a} \\ \Psi_{3b} \\ \Psi_{3c} \end{bmatrix} = \begin{bmatrix} L_{1a} & L_{1ab} & L_{1ac} & L_{12a} \cdot f_1 & L_{12ab} \cdot f_2 & L_{12ac} \cdot f_3 & L_{13a} \cdot f_1 & L_{13ab} \cdot f_2 & L_{13ac} \cdot f_3 \\ L_{1ba} & L_{1b} & L_{1bc} & L_{12ba} \cdot f_3 & L_{12b} \cdot f_1 & L_{12bc} \cdot f_2 & L_{13ba} \cdot f_3 & L_{13b} \cdot f_1 & L_{13bc} \cdot f_2 \\ L_{1ca} & L_{1cb} & L_{1c} & L_{12ca} \cdot f_2 & L_{12cb} \cdot f_3 & L_{12c} \cdot f_1 & L_{13ca} \cdot f_2 & L_{13cb} \cdot f_3 & L_{13c} \cdot f_1 \\ L_{21a} \cdot f_1 & L_{21ab} \cdot f_3 & L_{21ac} \cdot f_2 & L_{22a} & L_{2ab} & L_{2ac} & L_{23a} \cdot f_4 & L_{23ab} \cdot f_5 & L_{23ac} \cdot f_6 \\ L_{21ba} \cdot f_2 & L_{21b} \cdot f_1 & L_{21bc} \cdot f_3 & L_{2ba} & L_{22b} & L_{2bc} & L_{23ba} \cdot f_6 & L_{23b} \cdot f_4 & L_{23bc} \cdot f_5 \\ L_{21ca} \cdot f_3 & L_{21cb} \cdot f_2 & L_{21c} \cdot f_1 & L_{2ca} & L_{2cb} & L_{22c} & L_{23ca} \cdot f_5 & L_{23cb} \cdot f_6 & L_{23c} \cdot f_4 \\ L_{31a} \cdot f_1 & L_{31ab} \cdot f_3 & L_{31ac} \cdot f_2 & L_{32a} \cdot f_4 & L_{32ab} \cdot f_6 & L_{32ac} \cdot f_5 & L_{33a} & L_{3ab} & L_{3ac} \\ L_{31ba} \cdot f_2 & L_{31b} \cdot f_1 & L_{31bc} \cdot f_3 & L_{32ba} \cdot f_5 & L_{32b} \cdot f_4 & L_{32bc} \cdot f_6 & L_{3ba} & L_{33b} & L_{3bc} \\ L_{31ca} \cdot f_3 & L_{31cb} \cdot f_2 & L_{31c} \cdot f_1 & L_{32ca} \cdot f_6 & L_{32cb} \cdot f_5 & L_{32c} \cdot f_4 & L_{3ca} & L_{3cb} & L_{33c} \end{bmatrix} \begin{bmatrix} i_{1a} \\ i_{1b} \\ i_{1c} \\ i_{2a} \\ i_{2b} \\ i_{2c} \\ i_{3a} \\ i_{3b} \\ i_{3c} \end{bmatrix}$$

$$f_1 = \cos(\vartheta) \qquad f_2 = \cos(\vartheta + \frac{2}{3}\pi) \qquad f_3 = \cos(\vartheta - \frac{2}{3}\pi)$$

$$f_4 = \cos(\vartheta 1) \qquad f_5 = \cos(\vartheta 1 + \frac{2}{3}\pi) \qquad f_6 = \cos(\vartheta 1 - \frac{2}{3}\pi)$$

In the same way multiphase and multi-winding systems can be modelled.

One problem for modelling such a transformer is the determination of the input parameter for the model. A possible way is to determine the parameters of the 3w3ph transformer from the data sheet of the transformer, which are usually given in the following form.

Typical data	Voltages	Un1, Un2, Un3
	Apparent power	S_n, S_{12}, S_{13}, S_{23}
	Vector group	e.g. DY5
	Short circuit voltages	u_{k12}, u_{k13}, u_{k23}
	Short circuit voltages (resistive)	u_{r12}, u_{r13}, u_{r23}
	No load excitation losses	I_0 [%]
	Iron losses	P_0 [W]

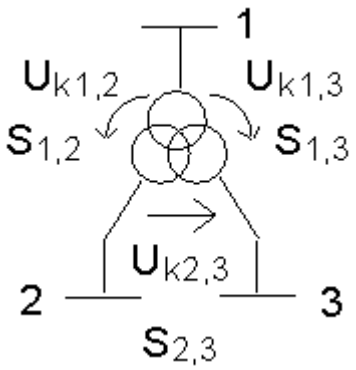

Figure 51 Simplification of 3w3ph transformer

The coupling between the 3 windings of the 3w3ph transformer shown in Figure 51 is separated into three single equivalent diagrams Figure 52 in order to understand the interpretation of the typical data set. The typical data describe usually the coupling between the different windings and therefore the derived parameters are always a mixture of both windings. For the 3w3ph dynamical transformer model the individual parameters per winding have to be achieved. However, it is not exactly possible, but they can be estimated with assuming a star connection of the windings. The parameters though can be used later on in the general model as described above.

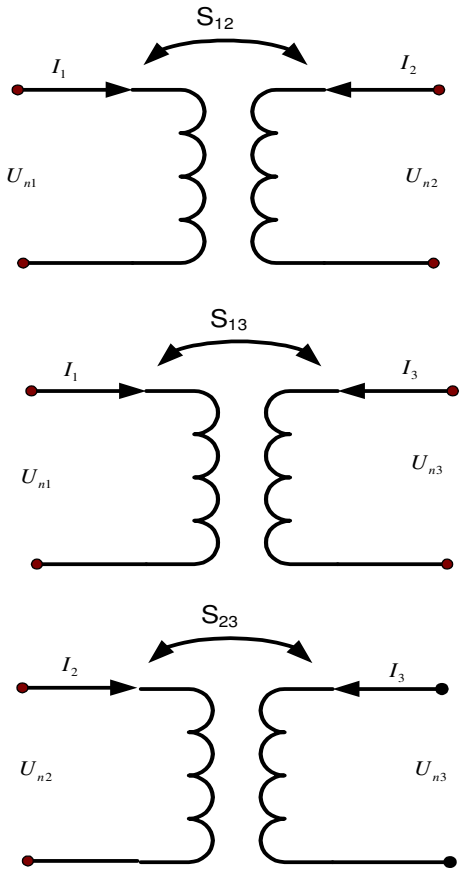

Figure 52 Simple equivalent circuit of a 3w3ph transformer

The parameters related to the primary side can be calculated as followed:

$$Z_{k12} = \frac{u_{k12}}{100\%} \cdot \frac{U_1^{\,2}}{S_{12}} \quad [\Omega] \qquad Z_{k12} = Z_{k1} + Z_{k2}$$

$$Z_{k13} = \frac{u_{k13}}{100\%} \cdot \frac{U_1^{\,2}}{S_{13}} \quad [\Omega] \qquad Z_{k13} = Z_{k1} + Z_{k3}$$

$$Z_{k23} = \frac{u_{k23}}{100\%} \cdot \frac{U_1^{\,2}}{S_{23}} \quad [\Omega] \qquad Z_{k23} = Z_{k2} + Z_{k3}$$

$$R_{13} = \frac{u_{kr13}}{100\%} \cdot \frac{U_1^{\,2}}{S_{13}} \quad [\Omega] \qquad R_{13} = R_1 + R_3$$

$$R_{12} = \frac{u_{kr12}}{100\%} \cdot \frac{U_1^{\,2}}{S_{12}} \quad [\Omega] \qquad R_{12} = R_1 + R_2 \qquad (117)$$

$$R_{23} = \frac{u_{kr23}}{100\%} \cdot \frac{U_1^{\,2}}{S_{23}} \quad [\Omega] \qquad R_{23} = R_2 + R_3$$

$$X_{k12} = \sqrt{Z_{k12}^{\,2} - R_{12}^{\,2}} \quad [\Omega] \qquad X_{k12} = X_{\sigma 1} + X'_{\sigma 2}$$

$$X_{k13} = \sqrt{Z_{k13}^{\,2} - R_{13}^{\,2}} \quad [\Omega] \qquad X_{k13} = X_{\sigma 1} + X'_{\sigma 3}$$

$$X_{k23} = \sqrt{Z_{k23}^{\,2} - R_{23}^{\,2}} \quad [\Omega] \qquad X_{k23} = X'_{\sigma 2} + X'_{\sigma 3}$$

$$Z_{k1} = \frac{Z_{k13} + Z_{k12} - Z_{k23}}{2} \quad [\Omega]$$

$$Z_{k2} = \frac{Z_{k12} + Z_{k23} - Z_{k13}}{2} \quad [\Omega] \qquad (118)$$

$$Z_{k3} = \frac{Z_{k23} + Z_{k13} - Z_{k12}}{2} \quad [\Omega]$$

The resistance and the leakage reactance can be found equivalent to the impedance calculation. Notice though that resistances and impedances, which are calculated in this way, are only estimated artificial values and are not directly related to the real parameters. In some cases the calculated values become negative, especially if using the technique for an autotransformer /39/.

The main flux inductance can be calculated from the no load measurement.

$$X_m = \frac{1}{I_0\%} \cdot \frac{U_1^{\,2}}{S_{12}} \quad [\Omega] \qquad R_{fe} = \frac{U_1^{\,2}}{P_0} \quad [\Omega] \qquad (119)$$

The Matrix parameter can now be determined for e.g. symmetrical geometry to:

$$
\begin{array}{lll}
R_1 = R_1 & R_2 = \dfrac{R_2^{'}}{a_{12}^{\ 2}} & R_3 = \dfrac{R_3^{'}}{a_{13}^{\ 2}} \\
L_{\sigma 1} = \dfrac{X_{\sigma 1}}{\omega} & L_{\sigma 2} = \dfrac{X_{\sigma 2}^{'}}{\omega \cdot a_{12}^{\ 2}} & L_{\sigma 3} = \dfrac{X_{\sigma 3}^{'}}{\omega \cdot a_{13}^{\ 2}} \\
L_{m1} = \dfrac{X_m}{\omega} & L_{m2} = \dfrac{X_m}{\omega \cdot a_{12}^{\ 2}} & L_{m3} = \dfrac{X_m}{\omega \cdot a_{13}^{\ 2}} \\
L_{12} = L_{21} = \dfrac{X_m}{\omega \cdot a_{12}} & L_{13} = L_{31} = \dfrac{X_m}{\omega \cdot a_{13}} & L_{23} = L_{32} = L_{m3} \cdot a_{23}
\end{array}
\qquad (120)
$$

4.3 The 2-windings 3-phase autotransformer

Using the same approach as described in the chapter 4.2, the three-phase Autotransformer can be seen as a modification of the 3w3ph transformer; even it belongs to the group of 2w3ph transformers. While a 3w3ph transformer has three separated three-phase windings, the Auto transformer has a galvanic connection between the second and third winding. This can be expressed in the equivalent diagram as shown in Figure 53.

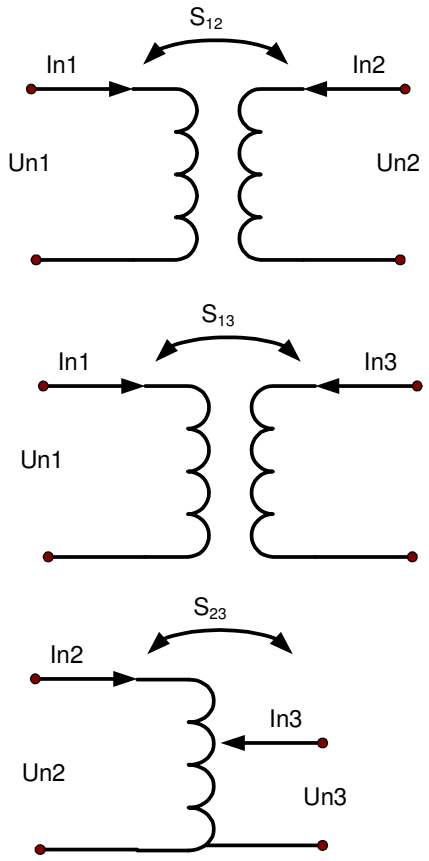

Figure 53 Simple equivalent diagram of the three-phase three-windings autotransformer

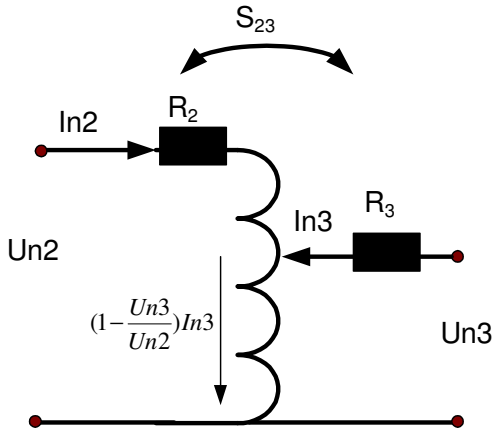

Figure 54 Coupling of the second and third winding in an autotransformer

The simple equivalent diagram of the 3w3ph transformer shown in Figure 52 has only changed the coupling between the second and third winding. In Figure 54 is the coupling between the second and third winding is shown separately to visualise the determination of the resistance parameters.

$$R_{13} = R_1 + R_3 \qquad R_{12} = R_1 + R_2 \qquad R_{23} = R_2 + R_3 \tag{121}$$

If the definition of the resistances between the windings is still valid as shown in equation (121) and current between ground and the shared winding is:

$$I_{n23} = (\frac{U_3^2}{U_2^2} - 1) \cdot I_{n3} \tag{122}$$

The couplings resistances between the primary and tertiary winding can be calculated to:

$$R_{13} = (\frac{U_3^2}{U_2^2} - 1) \cdot R_2 + R_{12} \tag{123}$$

While the resistance of the tertiary winding is:

$$R_3 = \left(\frac{U_3}{U_2}\right)^2 \cdot R_2 \tag{124}$$

Following this path the same equation set as shown for the 3w3ph transformer is deduced. The model for the 3w3ph transformer can also be used for describing the autotransformer. The only difference is the calculation of the parameter inputs, since the parameters of winding three is dependent on the parameters from winding two.

4.4 The transformer models implemented in Matlab/ Simulink

The 2w3ph transformer model as developed with the equation (115) is implemented in Matlab/ Simulink as depicted in Figure 55. In the block “Flux - current” is the 6x6 inductance matrix is programmed. The input values are the three-phase voltages of winding 1 and winding 2. The outputs are the three-phase currents of both windings.

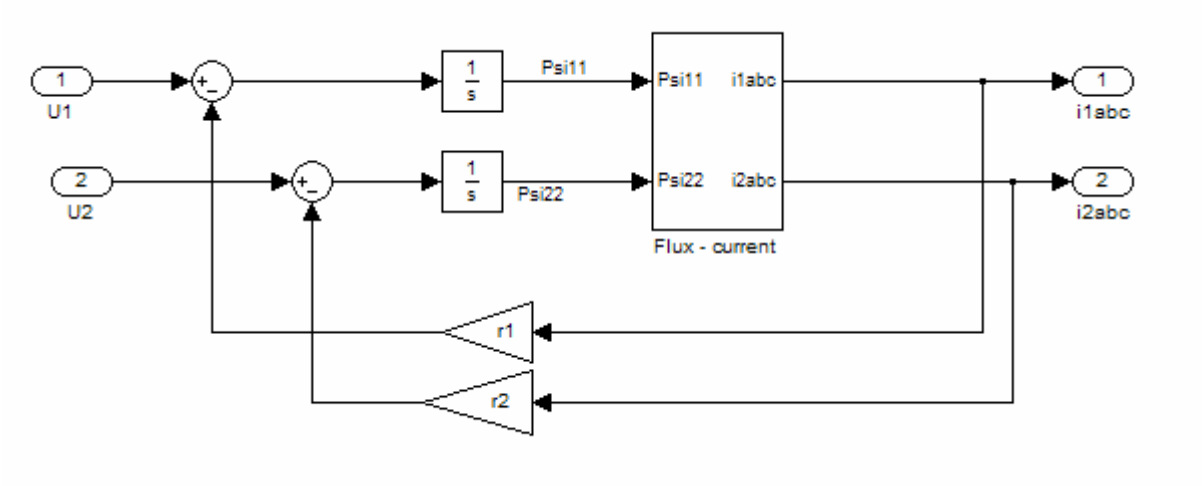

Figure 55 The 2w3ph transformer model in Matlab/ Simulink

Included in the model is the phase difference due to the coupling. In Figure 56 a simulation of a DY5 (delta-star) transformer coupling is demonstrated. The primary and secondary voltage refer to their rated values at a no load simulation is shown. The 150-degree phase difference for the 50 Hz signals is clearly visible.

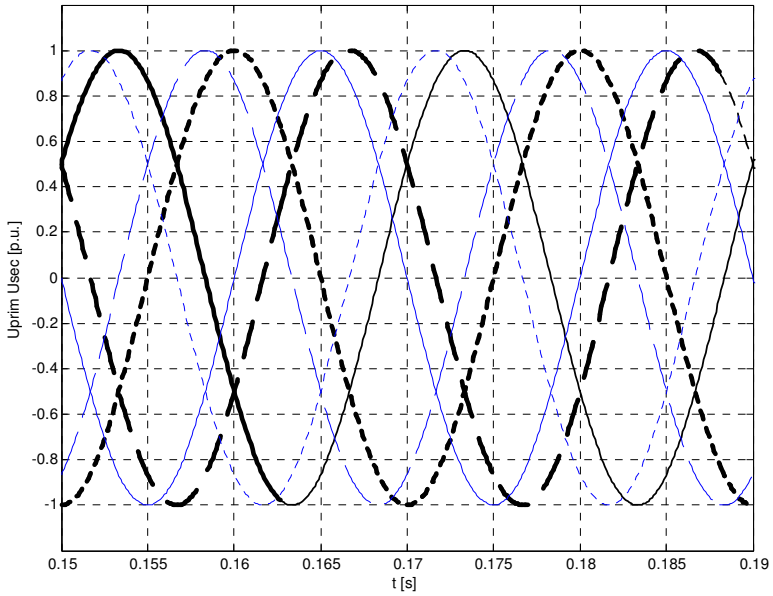

Figure 56 Phase difference primary (thick line) and secondary (thin line) voltage simulating a DY5 2w3ph transformer

In Figure 57 and Figure 58 the transformer is shown at no load and loaded operation. At no load there the no load losses can be measured. The voltage is not ideal and a no load current is existing. During load the transformer voltage is decreasing at the same time the current rises.

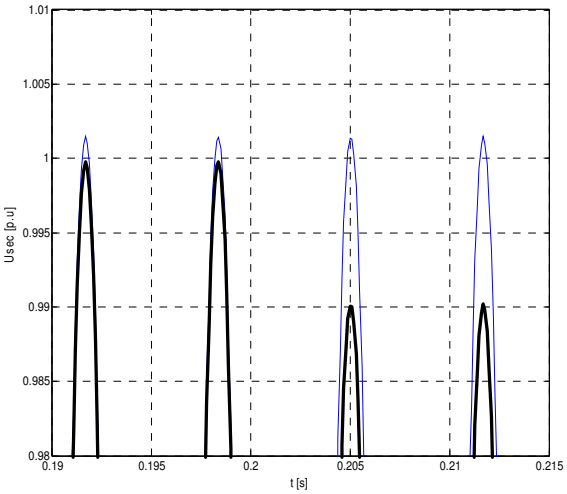

Figure 57 Ideal (thin line) and real secondary voltage (thick line) at no load and full loaded

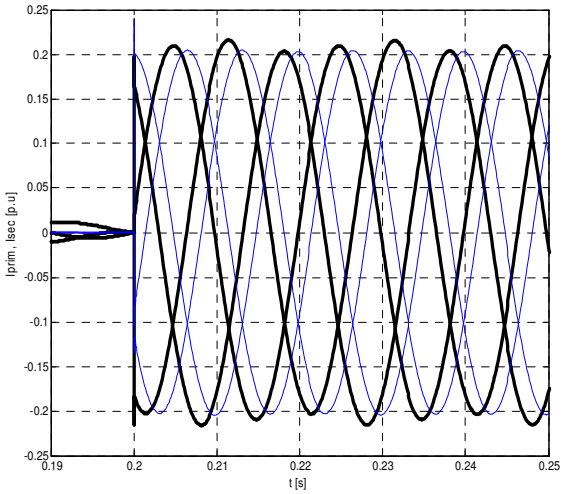

Figure 58 Primary (thick line) and secondary current (thin line) at no load and loaded

Typically the transformer is grounded at the star coupling of the secondary side. This grounding can be implemented in the transformer model. The ground current can be calculated as a difference between the load current and the current output of the transformer and initiate a voltage drop to ground. This potential difference is considered at the secondary voltage of the transformer. The 2w3ph transformer model inclusive with a resistive grounding is shown in Figure 59. The input and outputs of the model change due to the implementation. The input is now the 3-phase primary voltage and the secondary side 3-phase current. The output of the model is now the secondary 3-phase voltage and the 3-phase primary current.

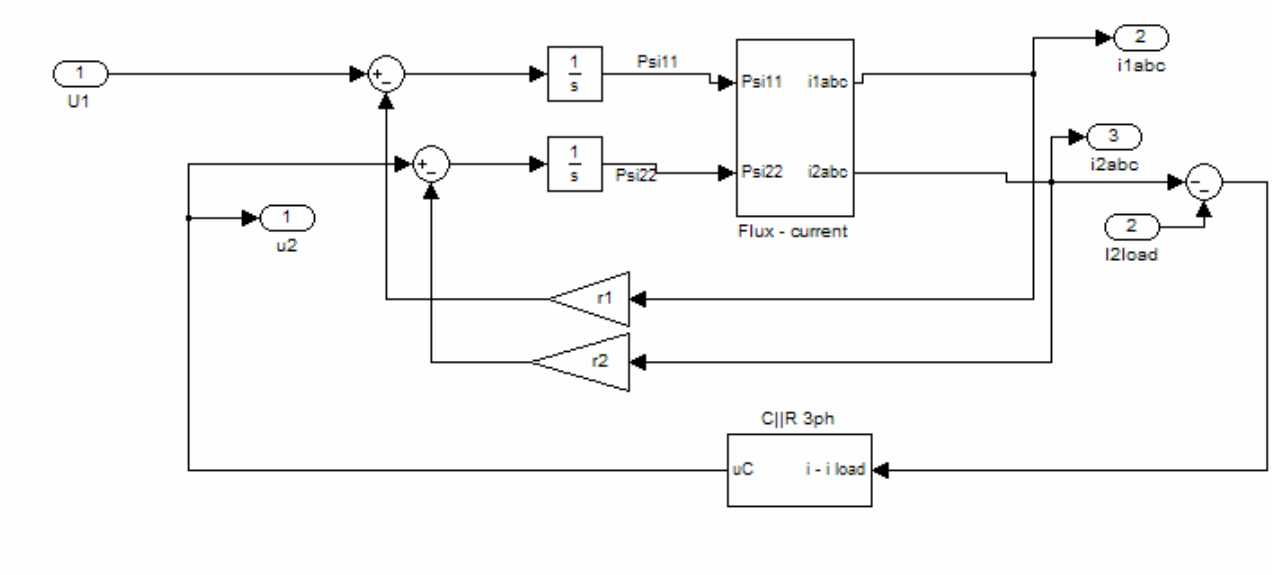

Figure 59 The 2w3ph transformer inclusive grounding system

The 3w3ph transformer model or the 2w3ph autotransformer model is equivalent to the 2w2ph model. The only change is the additional third input vector of the voltage and the third output representing the tertiary current. The block Flux – current now includes a 9x9 inductance matrix.

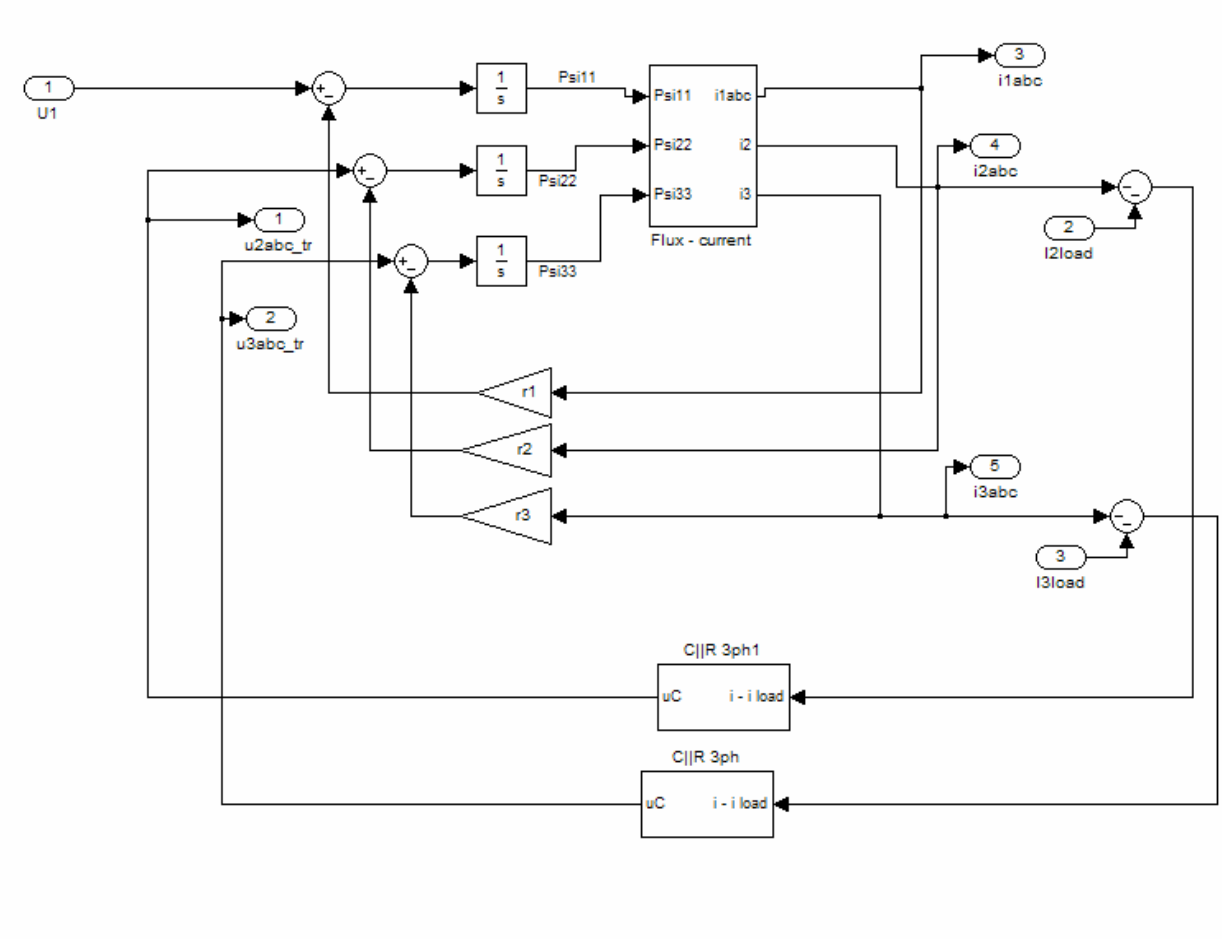

Figure 60 The 3w3ph transformer model in Matlab/ Simulink including star point grounding

In the same way as applied in the induction machine model the main saturation can be implemented as a variable induction dependent upon from the magnetizing current. The change in the main inductance due to saturation is more than in an induction machine, related to the different flux path in transformer and induction machine. The beginning of the magnetizing curve characterizes the inductance of the flux through the air, while the second part of the curve characterizes the inductance influenced from the magnetizing material. Because in the transformer a huge part of the flux is coupled over the air, where contrary to the induction machine which has only a minimal air gap, the curve is rising very fast in the beginning (Figure 61).

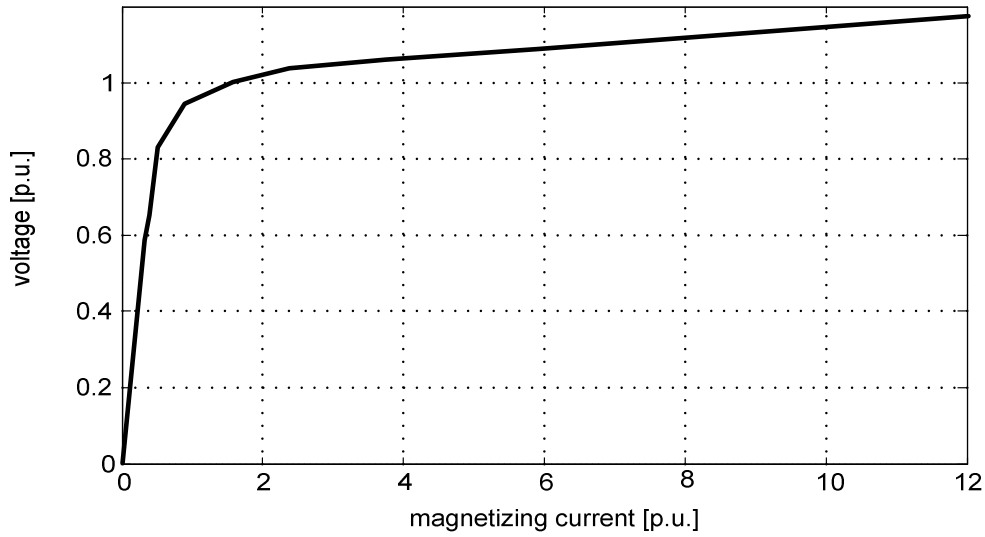

Figure 61 Magnetizing curve of a 2.1 MVA 3w3ph transformer related to the rated current

The magnetizing impedance can be calculated from the no load measurements. The value of the magnetizing impedance consists of an iron losses resistance in parallel to the main inductance. The magnetizing inductance can be calculated with equation (125).

$$Z_m = \frac{\left(\frac{U_0}{\sqrt{3}} - I_0 \cdot Z_{12}\right)}{I_0} \qquad Z_m = \frac{R_m \cdot \omega_0 L_m}{\sqrt{R_m^2 + \omega_0{}^2 L_m^2}} \qquad L_m = \frac{1}{\omega_0} \frac{R_m \cdot Z_m}{\sqrt{R_m{}^2 - Z_m{}^2}} \tag{125}$$

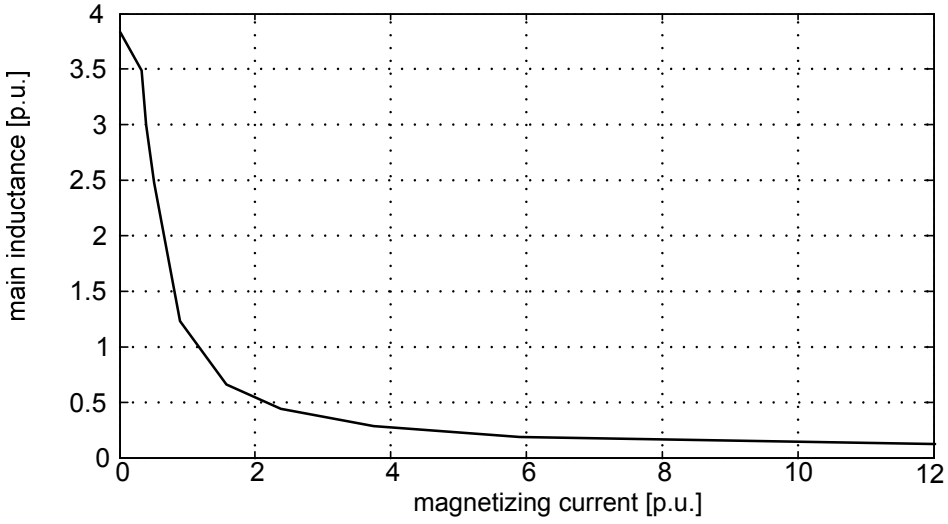

Figure 62 Main inductance saturation curve of a 2.1 MVA 3w3ph transformer

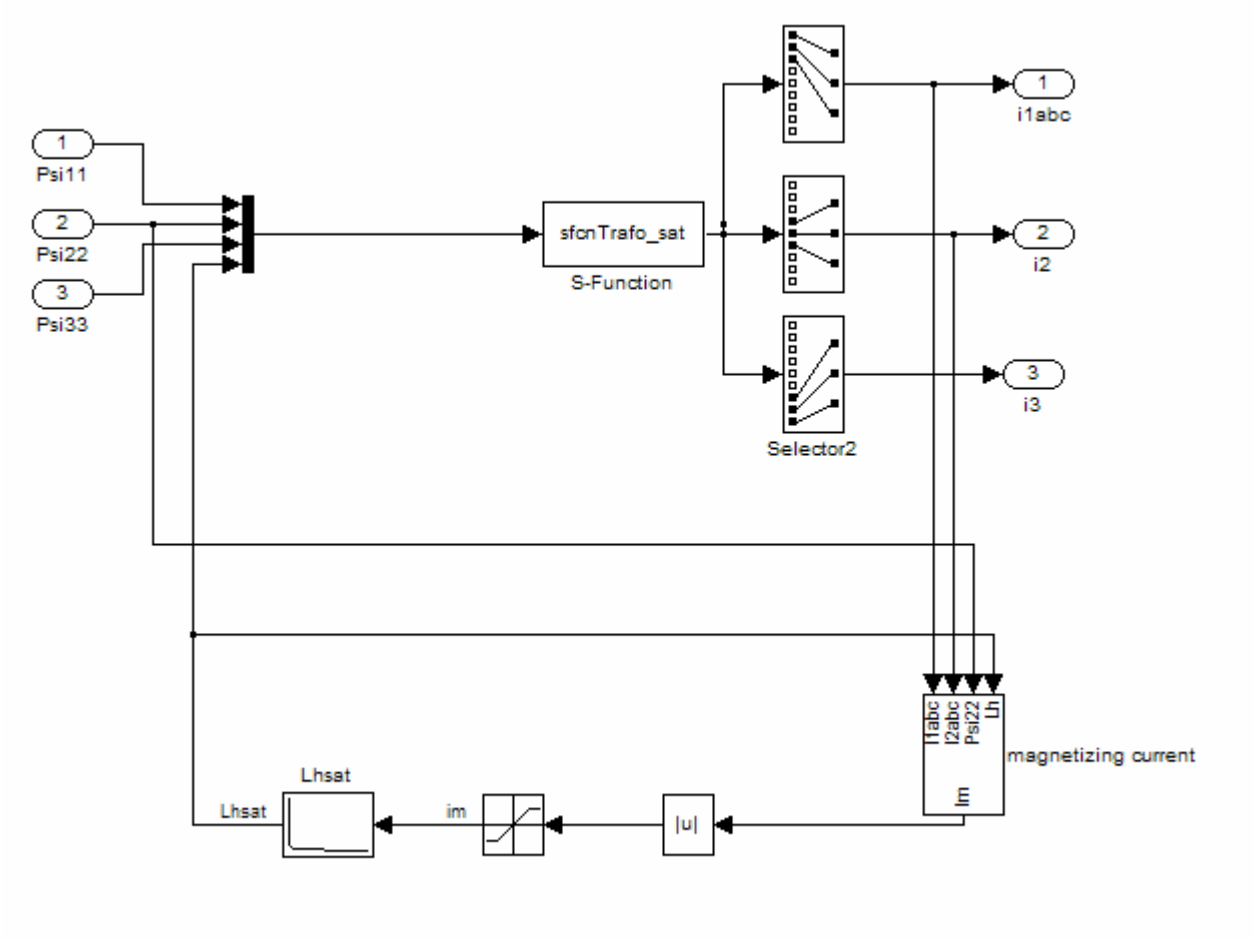

Figure 63 Block flux – current of a 3w3ph transformer with main saturation

4.5 Geometry Development of three-phase Transformers

The three phase model has beside the non-linearity caused by the saturation another natural asymmetry caused by the geometrical construction of the three-phase Transformer. This fact is usually neglected, though plays an important part if the purpose is three phase simulation of symmetrical and asymmetrical conditions.
Generally a three phase transformer can be achieved by connecting three one-phase transformer units.

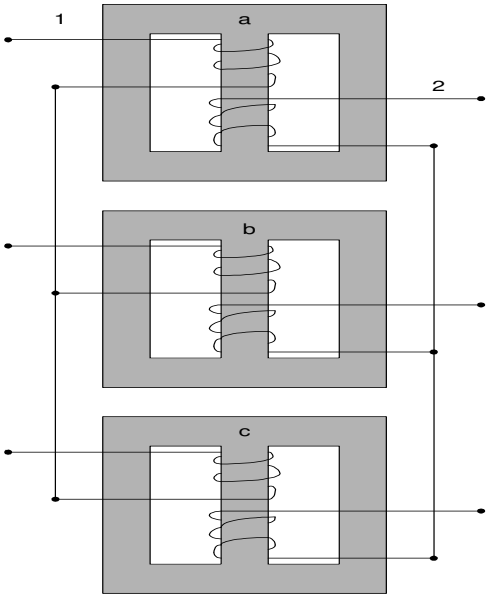

Figure 64 Three one-phase E-core transformer in star connection

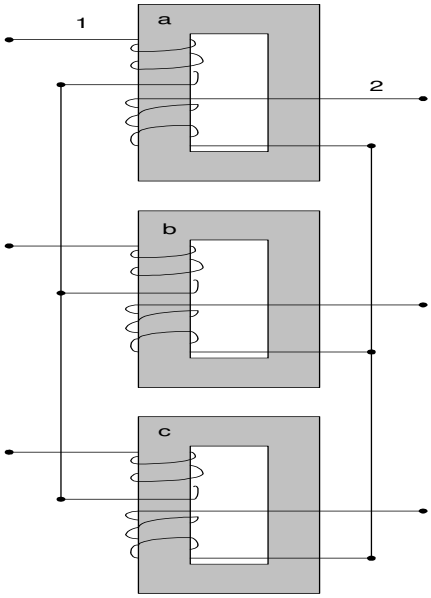

Figure 65 Three one-phase U-core transformer in star connection

The difference between the two different transformer core shapes is the distribution of the flux. In comparison to the assembly in Figure 65, the flux in Figure 64 is separating and closing over the outer core, which causes a bigger size of the transformer unit. The connection of 3 one-phase transformer is not the most used solution for a three-phase system. Rather than this assembly a combination from the 3 transformer to one three-phase transformer is used. In Figure 67 one step for the development of such an arrangement is shown.

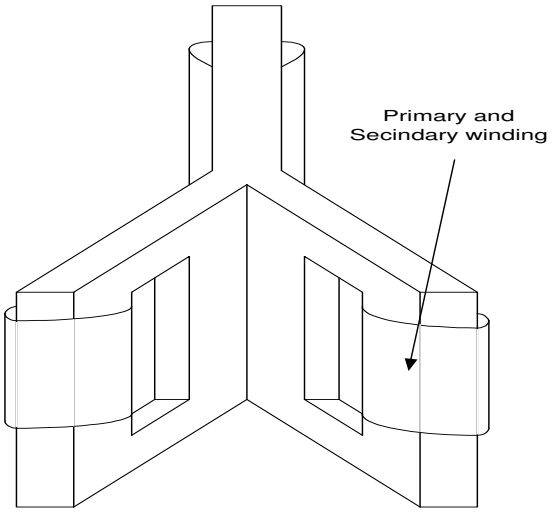

Figure 66 Magnetic connection of 3 one phase transformer to a three phase transformer arrangement

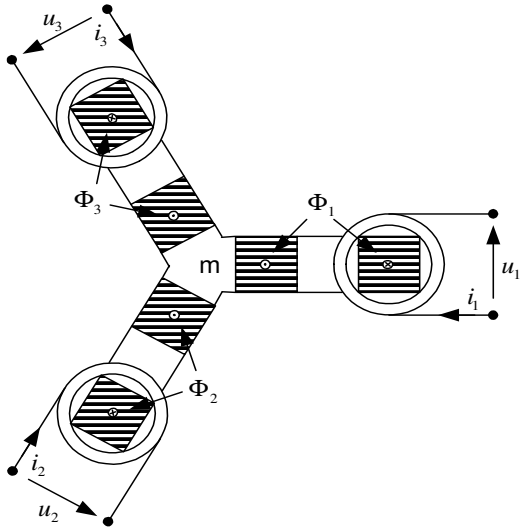

Figure 67 Slice of the three-phase transformer arrangement

The flux in the middle core m is the addition of the flux from the three phases.

$$\Phi_m = \Phi_1 + \Phi_2 + \Phi_3$$

In the case of symmetrical construction and excitation the flux in the common core adds by superposed to zero, that means no flux is present in the common leg.

$$\Phi_m = \Phi_1 + \Phi_2 + \Phi_3 = 0$$

Therefore the common leg can be cut out of the construction.

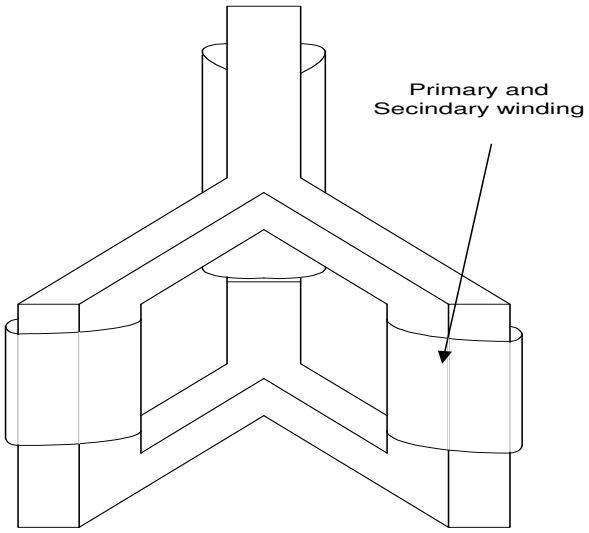

Figure 68 Symmetrical three-phase transformer

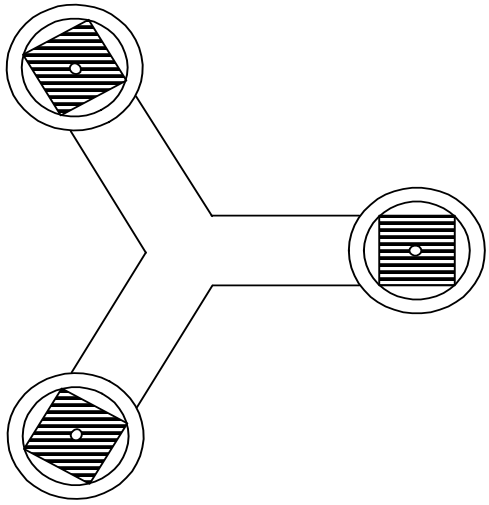

Figure 69 Symmetrical three-phase transformer

However, this symmetrical arrangement uses too much space and therefore it is widely used to arrange the three legs of the transformer in one plan. However this is changing the flux path and a part of the now asymmetrical flux has to close over the air outside of the transformers core $\Phi_1 + \Phi_2 + \Phi_3 = \Phi_{air}$.

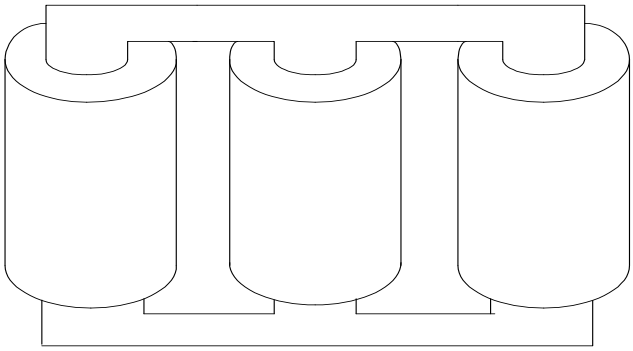

Figure 70 Unsymmetrical three-phase transformer

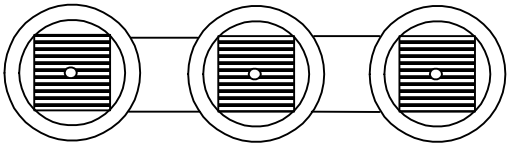

Figure 71 Unsymmetrical three-phase transformer

If it is assumed the flux in the air is minimised, the flux coupling from the middle leg is shorter that from the outer legs and causes an unsymmetrical flux contribution. This causes a smaller magnetising current in the middle leg and also a smaller phase current /61/, /81/. This unbalance can also be observed during operation on a symmetrical grid and in no load operation.

Chapter 5

5. Power system modelling in Matlab/ Simulink

The achieved generator and machine model are parts of the electrical system in wind turbine simulation. Beside these two shown components, other elements are necessary in order to study the wind turbine's behaviour during short circuits. Any small network consists of a source, line and a load. In the present case the wind turbine is the load of the network, connected to a voltage source and a transmission line or cable, which represent network dynamics. The wind turbine itself consists of different electrical elements. The in Chapter 3 developed machine model and the in Chapter 4 developed transformer model are two main parts of the wind turbine model. In this chapter the other electrical elements will be modelled. In the beginning the dynamic node technique will be introduced, followed by the source modelling and finally a transmission line model is deduced.

5.1 Dynamic node technique

In the case of connecting the different electrical elements like generator transformer, cable, loads, sources etc. to a smaller electrical network in Matlab/ Simulink a modelling method has to be found. A usable method is the "Dynamic node technique" from F. Flinders and W. Oghanna in /25/, /27/ which is developed for power converter simulation. This method can be used for any electrical circuit simulation in Matlab/ Simulink. The most difficulties with modelling electrical networks in Simulink are given due to simulation stability. Complicated mathematical structures with differential equations and nonlinear behaviour often lead to unstable simulations and algebraic loops. The most efficient way is to model electrical machines and transformers due to the current, which means with voltage as input variable and current as output variable. If it is desired to connect a transformer and machine the voltage need to be a function of the current. The problem is drafted in Figure 72.

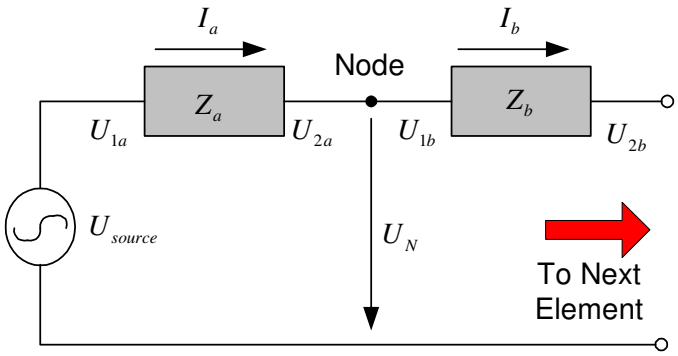

Figure 72 Electrical network draft for simulation of the power system

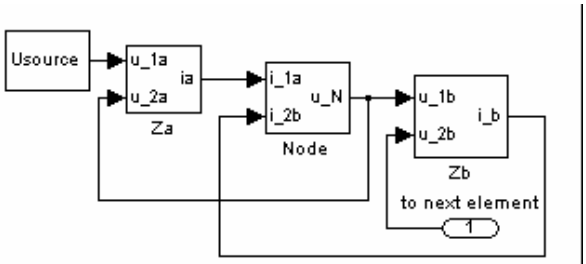

Figure 73 Block diagram expressing the theory in Matlab/ Simulink

The problem can be solved by considering the parasitic capacitances between the elements, which are desired to connect. The capacitance can be assumed as lumped at the circuit node. The voltage over the capacitor can be calculated with the summation of the current connected trough this node.

$$u_{node} = \frac{1}{C_{node}} \int \sum i_n dt \tag{126}$$

During steady state the node voltage is constant and has no influence on the simulation. Kirchhoff's current law would be satisfied for every node within the circuit.

$$\sum i_{n\ (steady\ state)} = 0 \tag{127}$$

The proper function of this method during dynamical simulations, without influencing the simulation result, is ensured by the choice of a very small nodal capacitance (less than 1 nF).
The integral nature of the node decouples the mathematical loop system and therewith shows the additional advantage of counteract algebraic loops.
With this technique different devices can easily be modelled. In Table 5-1 a few examples are given.

Table 5-1 Different electrical element modelled with the dynamic node technique in Matlab/ Simulink

Device	Circuit	Block (current -> voltage)
node	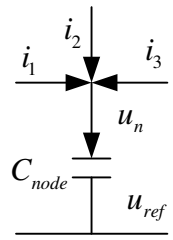	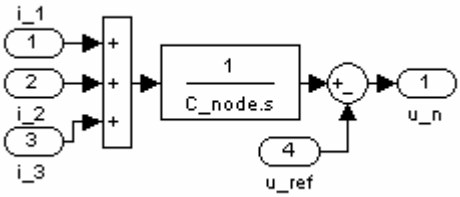
Resistor	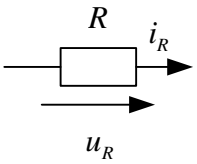	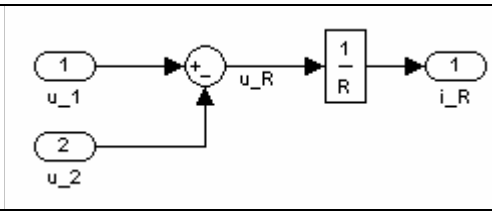
Parallel inductance/ resistance	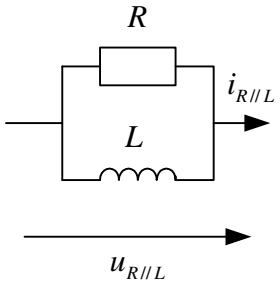	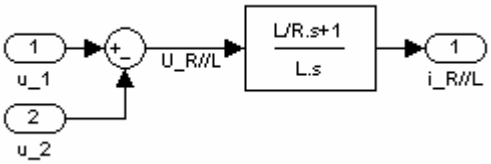
serial inductance/ resistance	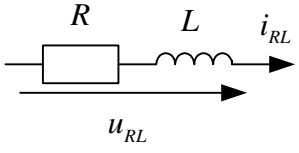	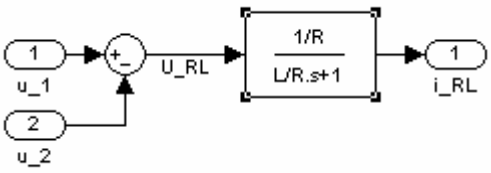

parallel capacitor/ resistance	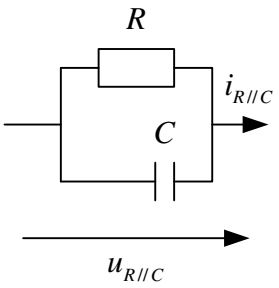	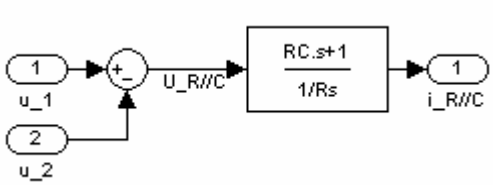
serial capacitor/ resistance	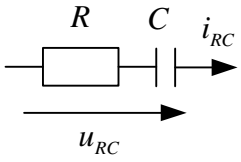	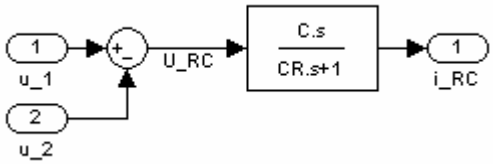

5.2 Power system elements

5.2.1 General modelling

The voltage source used for the simulation is an ideal voltage source, with different simulation options. The model implemented in Matlab/ Simulink can be derived from the equations (128)

$$\begin{aligned} u_a &= \hat{U}_a \sin\left(2\pi f_1 \cdot t + \varphi_a\right) \\ u_b &= \hat{U}_b \sin\left(2\pi f_1 \cdot t + \varphi_b\right) \\ u_c &= \hat{U}_c \sin\left(2\pi f_1 \cdot t + \varphi_c\right) \end{aligned} \tag{128}$$

Thereby the basic frequency f_1 is assumed as equal in all three phases and has the 50 Hz for a 50 Hz system. The phase angle φ and voltage amplitude $\hat{U}$ can be changed independently for each phase. In case of a symmetrical three phase system the phase angle between the phases can be assumed constant as a phase difference of *120 °* or *2/3π*. Figure 74 shows the implementation in Matlab/ Simulink for such a system.

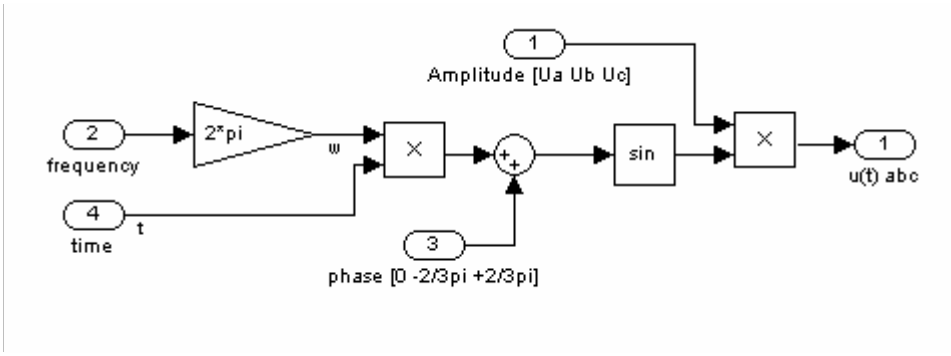

Figure 74 Three-phase ideal voltage source in Matlab/ Simulink

This basic principle was expanded with several functions to simulate short circuits, voltage drops and frequency changes in the system voltage. The input masked for the Matlab/ Simulink block is shown in Figure 75. The model is in an advanced model further

expanded with the superposition of harmonics to the described fundamental function.

$$u = \hat{U}_1 \sin\left(2\pi f_1 \cdot t + \varphi_1\right) + \sum \hat{U}_\upsilon \left(2\pi f_\upsilon \cdot t + \varphi_1\right) \tag{129}$$

The index υ thereby describes the number of the harmonic.

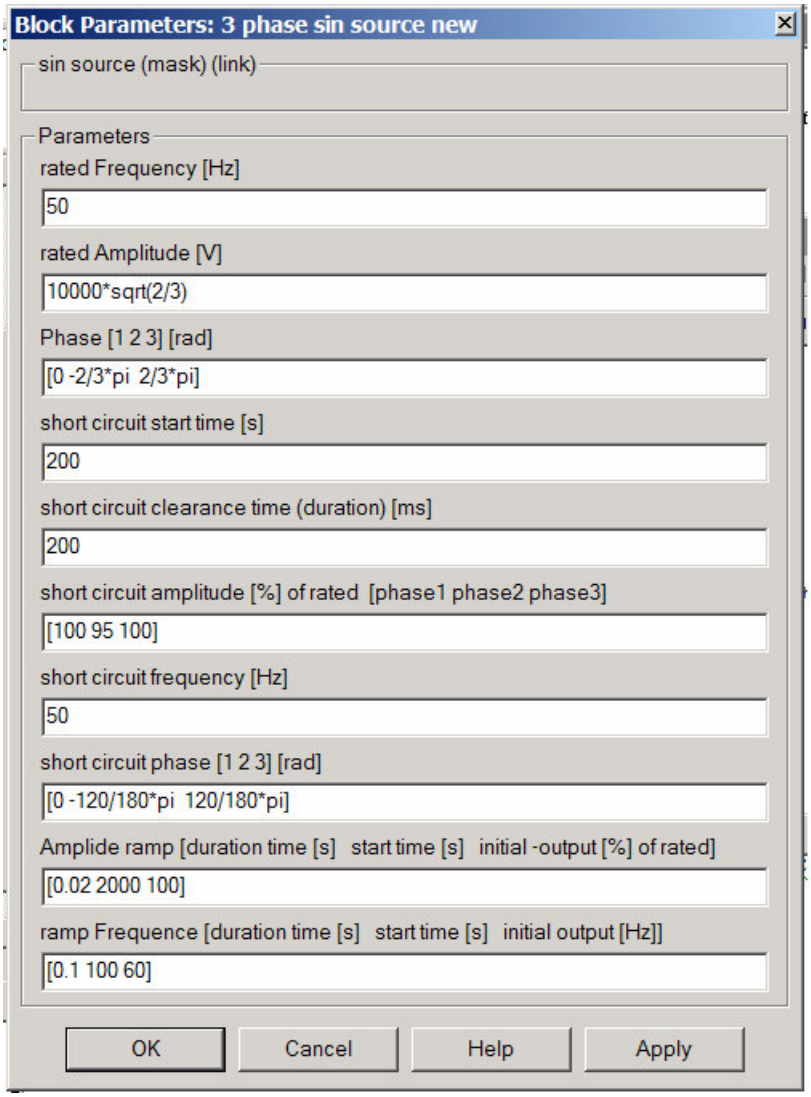

Figure 75 Input mask for the simple Matlab/ Simulink block 3 phase voltage source

To achieve a more realistic behaviour a serial resistance and inductance can be added to the source. Using the dynamic node technique this is implemented as shown in Figure 76 and Figure 77.

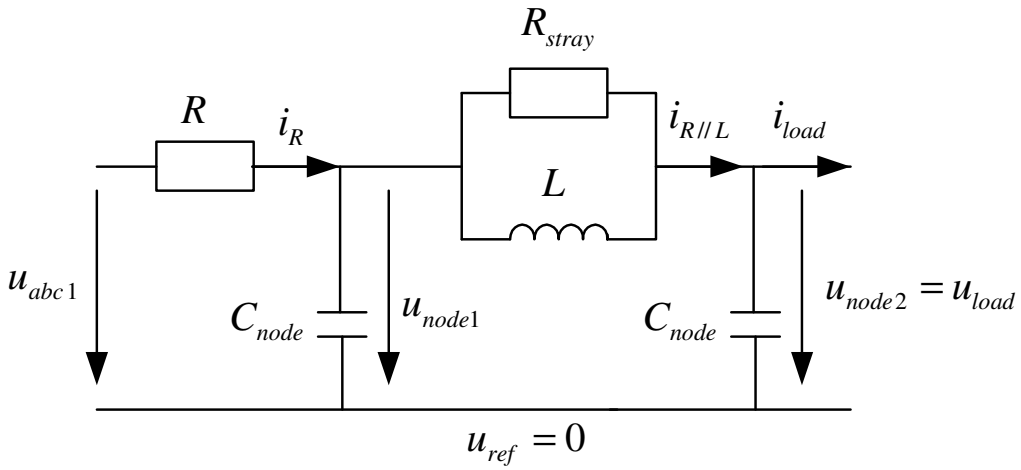

Figure 76 possible RL equivalent network

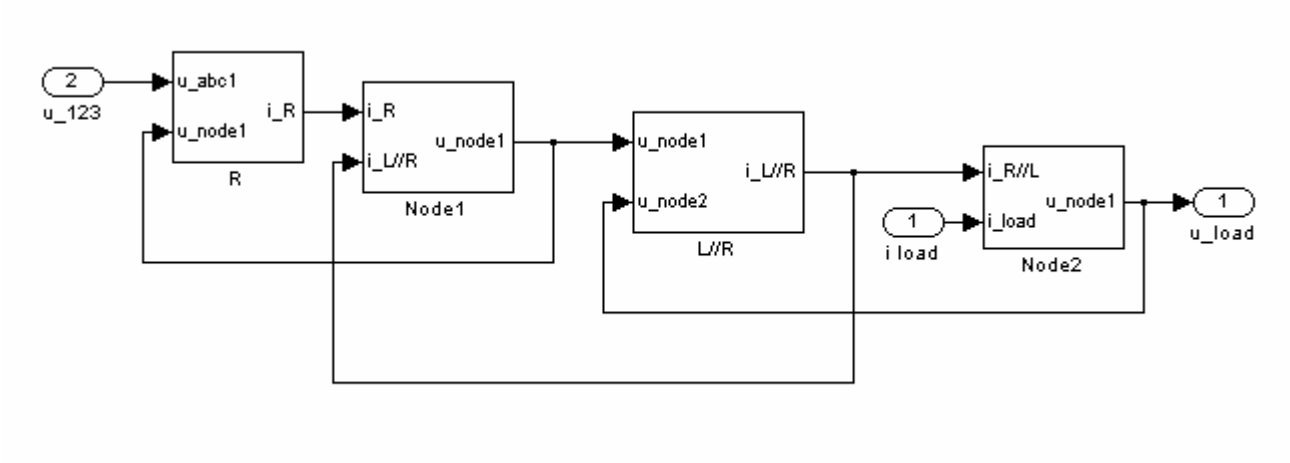

Figure 77 Possible RL equivalent network in Matlab/ Simulink

As probably noticed there is a parallel resistance added to the inductance. This resistance introduces a damping of the inductance. The usual value for this resistance is very large as e.g. $R_{stray} = 1\,M\Omega$.

In Figure 78 the entire system source with a serial RL transmission is shown.

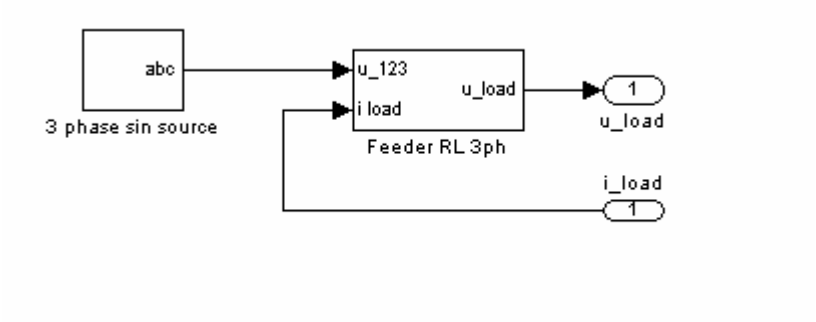

Figure 78 Source and RL transmission part in Matlab/ Simulink

The same strategy can be used for connecting arbitrary two devices.

5.2.2 Transmission line modelling

The common π model of transmission lines is easily modelled and implemented in the same way as described for the connection of two elements. For the purpose of dynamical simulation a higher order transmission line model including the coupling between the phases is derived. In order to clarify the input parameters for this dynamical model basic correlations are described again. The overall model is shown in Figure 79.

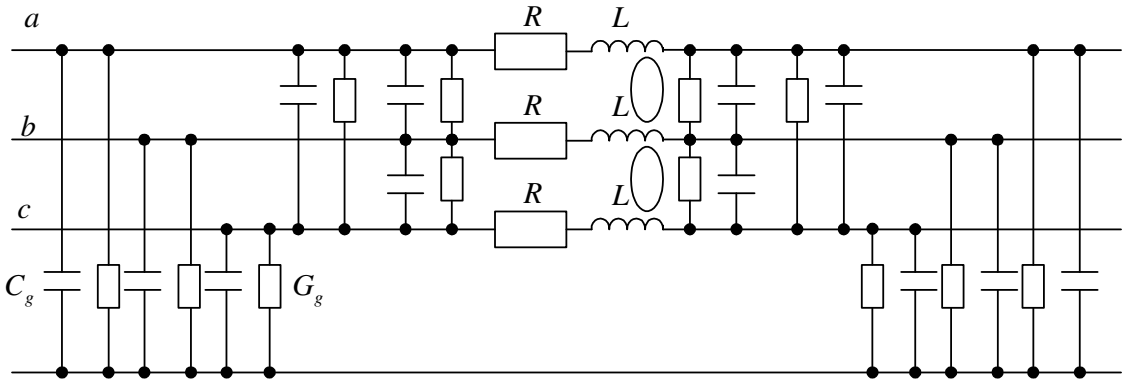

Figure 79 Dynamical transmission line model

However, the task of modelling a higher order transmission line or cable is not as easy a task as it seems. Partly this is because there are many different types of lines, which complicates the task of finding a general model. In order to give a proper introduction in this field, the background of transmission line modelling is explained in more depth than the previous developed modelled components.

Line Impedance

It is assumed that an overhead line should be modelled, which is simplified to an infinite long, parallel and straight line. These assumptions give the possibility to derive the necessary equations, which describe sufficiently the behaviour of a realistic system as well /61/, /94/.
The magnetic field strength outside and inside a line, which is carrying a current, can be calculated with the help of Maxwell's equations to:

$$H(r) = \frac{I}{2\pi \cdot r_P} \qquad r_P > r \text{ (outside line)} \tag{130}$$

$$H(r) = \frac{I \cdot r_P}{2\pi \cdot r^2} \qquad r_P < r \text{ (inside line)} \tag{131}$$

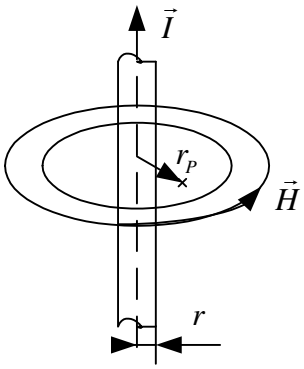

Figure 80 Magnetic field strength of a line

The inductive coupling between the two lines can be derived from the superposition from the fields of the lines. If two parallel lines 1, 2 are studied which have the distance D and a radius r (Figure 81), the electromagnetic field is defined through the magnetic field force B and electrical field force H.

$$B = \mu \cdot H \qquad \mu = \mu_0 \cdot \mu_r \tag{132}$$

$$\Phi = \int B \cdot dA \tag{133}$$

$$B_{12} = B_1 + B_2 \tag{134}$$

$$\Phi_{12} = \mu_0 \int (H_1 + H_2) \cdot dA \qquad \mu_0 = 4\pi \cdot 10^{-7} \frac{H}{m} \qquad \mu_r = 1 \quad (air) \tag{135}$$

$$\frac{\Phi_{12}}{l} = \frac{\mu_0 I}{2\pi} \cdot \ln\left(\frac{D}{r}\right) \tag{136}$$

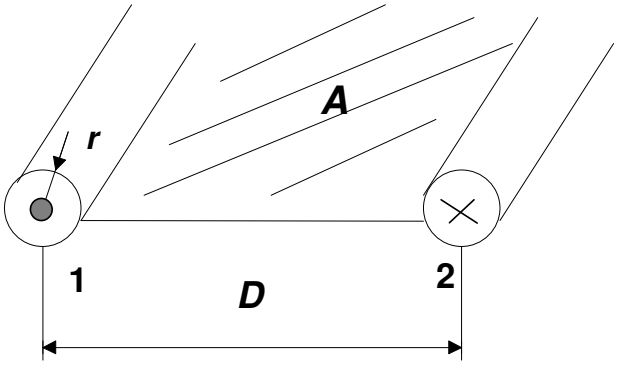

Figure 81 Inductances of two parallel lines

The inductance between the two lines is dependent on the length and calculated from the field:

$$\frac{L_{12}}{l} = L'_{12} = \frac{\Phi \cdot n}{I} = \frac{\mu_0}{2\pi} \cdot \ln\left(\frac{D}{r}\right) \qquad \text{with } n = 1 \tag{137}$$

The internal inductance of the line itself can be calculated like in equation (138). It is noticed that the internal inductance and field is not dependent on the radius. This is caused due to the assumption of homogeneous current density of the conductor.

$$L_i^{'} = \frac{\mu}{8\pi} \tag{138}$$

The total inductance per length of line1 from the two-line system is:

$$L_1^{'} = L_{12}^{'} + L_{i1}^{'} = \frac{\mu}{2\pi}\left(\ln\frac{D}{r} + \frac{1}{4}\right) \tag{139}$$

The equation (139) can also be used to achieve an average inductance per conductor for a three-phase system, as e.g. shown in Figure 82.

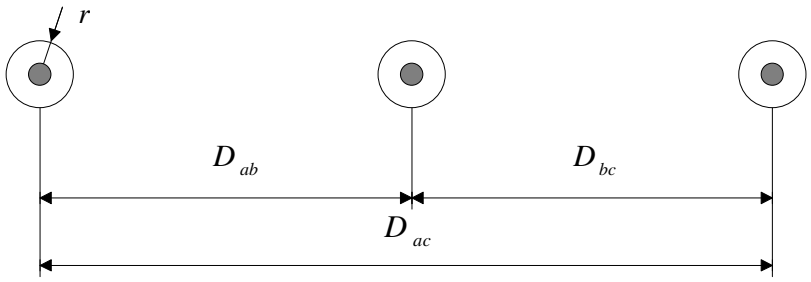

Figure 82 Inductance of a three phase overhead line

The inductance of the three conductors can be different, because of its dependency on the distance between them and the currents in the lines. In most transmission lines the method of transposition is used. The phase-lines change thereby their geometrical place. In this way the geometrical asymmetry gets adjusted to a nearly symmetrical system. If it is furthermore assumed that the currents in the three phases are $I_a + I_b + I_c = 0$ an equivalent average distance (140) and can be used to calculate the average per phase inductance (141):

$$D_{nm} = \sqrt[3]{D_{ab} D_{bc} D_{ac}} \tag{140}$$

$$L^{'} = L_{abc}^{'} + L_{i\,abc}^{'} = \frac{\mu}{2\pi}\left(\ln\frac{D_{nm}}{r_B} + \frac{1}{4}\right) \tag{141}$$

A similar method for the calculation of the average inductances can be used for the n-bundle conductor figurations.

$$r_B = \sqrt[n]{n\, r\, r_T^{n-1}}$$

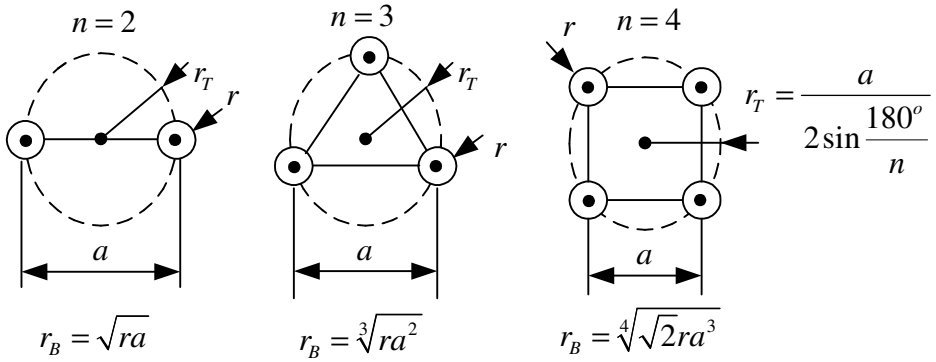

Figure 83 n-bundle conductor lines

Where *n* defines the number of conductors, *r* the radius of the conductor, r_T the equivalent circle radius, *a* is the distance between the conductors and r_B the equivalent radius of the n-bundle conductor. The equivalent radius replaces the radius of one conductor in equation (141).

The resistance of the line can be calculated from the cross section area A of the conductor and the electrical conductivity ρ.

$$R_i = \frac{\rho \cdot l}{A} = \frac{l}{\kappa \cdot A} \tag{142}$$

The electrical conductivity for copper is $\kappa = 56 \ \frac{m \cdot S}{mm^2}$ and for aluminium $\kappa = 35.5 \ \frac{m \cdot S}{mm^2}$. Although it is more appropriate to use reference books for the determination of resistance. Calculation can cause not accurate enough results, because the additional effects such as skin and proximity effect are very difficult to estimate in the cross section area.

The above described inductances are appropriate for the use in an equivalent model such as the common π-line model. In order to achieve a dynamical transmission-line model the influence of the ground has to be considered as well. If an ideal ground is assumed which has an infinite conductivity, the influence can be calculated with using the method of reflected conductor. With this method a second conductor can be imagined in the ground, which is reflected on the ground surface and carries the same amount of current, see Figure 84. The external inductance of a single conductor with ground is calculated to:

$$L_j' = \frac{\mu}{2\pi} \ln \frac{2h_j}{r} \tag{143}$$

In reality the ground does not perfectly conduct. Therefore the equation (143) gives no realistic result. In /44/ two main methods for calculation of the ground impedance are discussed. If it is assumed that the conductor radius is small compared to the distance between conductor and ground, an expression derived from Carlson /44/, /94/ can be used.
The other inductance can now be written as:

$$L_j' = \frac{\mu}{2\pi} \ln \frac{\delta_g}{r} \tag{144}$$

The value δ_g is the equivalent depth for the current penetration in the ground.

$$\delta_g = 660 \sqrt{\frac{\rho_g}{f}} \tag{145}$$

ρ_g is the ground conductivity and its value lies between 10 and 1000 Ωm and f is the frequency. Typical values for the equivalent depth and the ground conductivity are given in /1/. If the ground is not known a conductivity of 100 Ωm can be used, which leads to an equivalent depth of 930 m at 50 Hz.

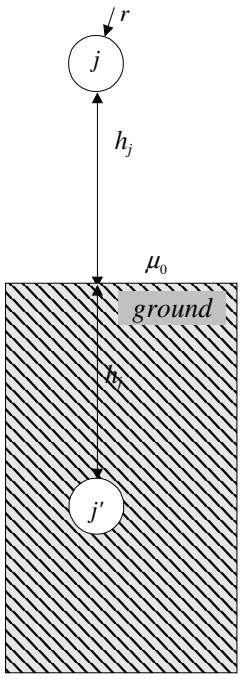

Figure 84 Single Line-ground coupling

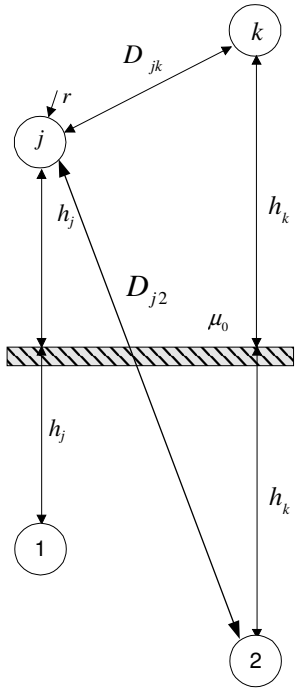

Figure 85 Two line system with ground coupling

The resistance of the ground is

$$R_g^{'} = \pi^2 \cdot f \cdot 10^{-4} \quad \frac{\Omega}{km} \tag{146}$$

It is only dependent of the frequency and independent from the current penetration. This is due to the arbitrary big area for the current flow in the ground.

The impedance of one conductor to ground finally completes to:

$$\underline{Z}_{jg}^{'} = R_j + R_g + j\omega(L_j^{'} + L_i^{'}) \tag{147}$$

A more appropriate equation to include in a modelling program is the equation developed by Wedepohl /44/. By introducing a complex depth of penetration δ_{gw} in the ground:

$$\delta_{gw} = \sqrt{\frac{\rho_g}{j\omega\mu}} \tag{148}$$

The ground impedance can be achieved through:

$$\underline{Z}_g^{'} = R_g^{'} + j\omega L_g^{'} = \frac{j\omega\mu}{2\pi} \cdot \ln\left(\frac{2h + 2\delta_{gw}}{r}\right) \tag{149}$$

If a second conductor is introduced as shown in Figure 85 an additional mutual coupling between the two circuits has to be introduced. The inductance can be calculated to /94/.

$$L'_{jk} = L'_{kj} = \frac{\mu}{2\pi} \cdot \ln\left(\frac{D_{j2}}{D_{jk}}\right) \tag{150}$$

The equation for the mutual inductances found by Wedepohl /44/ is:

$$\underline{Z}'_{jk} = \underline{Z}'_{kj} = R_{kj} + j\omega L_{kj} = \frac{j\omega\mu}{2\pi} \cdot \ln\left(\sqrt{\frac{\left(h_j + h_k + 2\delta_{gw}\right)^2 + D_{jk}^2 - \left(h_k - h_j\right)^2}{D_{jk}^2}}\right) \tag{151}$$

If it is furthermore assumed that the equivalent depth for the current penetration in the ground is much bigger than the distance from the conductor to ground for the mutual inductance from a two-line system to ground which can be simplified to:

$$L'_{jk} = L'_{kj} = \frac{\mu}{2\pi} \cdot \ln\left(\frac{\delta_g}{D_{jk}}\right) \tag{152}$$

Expressing the inductances of the two-line or two conductor system as the length related inductance in matrices we can write:

$$L' = \begin{bmatrix} L'_{11} & L'_{12} \\ L'_{21} & L'_{22} \end{bmatrix} \tag{153}$$

Where the self-inductances L_{11}, L_{22} are the addition of external inductance and internal inductance and L_{12}, L_{21} are the mutual inductances.

$$\begin{aligned} L'_{11} &= L_i + L_j \\ L'_{22} &= L_i + L_k \end{aligned} \qquad L'_{12} = L'_{21} = L'_{jk} \tag{154}$$

Equivalent the resistance matrix can be found.

$$R' = \begin{bmatrix} R'_{11} & R'_{12} \\ R'_{21} & R'_{22} \end{bmatrix} \tag{155}$$

Where R'_{11} and R'_{22} are the total self-resistance including the return path and the mutual resistance R'_{12}, R'_{21} is the value of the return path /44/.

$$\begin{aligned} R'_{11} &= R'_i + R'_g \\ R'_{22} &= R'_j + R'_g \end{aligned} \qquad R'_{12} = R'_{21} = R'_g \tag{156}$$

Line admittance

There is an analogy between the electrical field calculation methods and the magnetical field calculation methods. Therefore the result for the capacitance calculation of a line is quite similar to the inductance calculation.
A cylindrical line is assumed, which has charged particles on the surface. The charge

density of the line is q and Q defines the charge of the line and can be calculated with the flux density $\vec{D}$ from Maxwell's equations and the Gauss's law:

$$\oint \vec{D}\, d\vec{A} \;=\; \int q\, dl \;= Q \qquad \vec{D} \parallel d\vec{A} \tag{157}$$

Because the vector $\vec{D}$ is parallel to the surface area vector, the whole value is in this direction and a scalar description can be used.

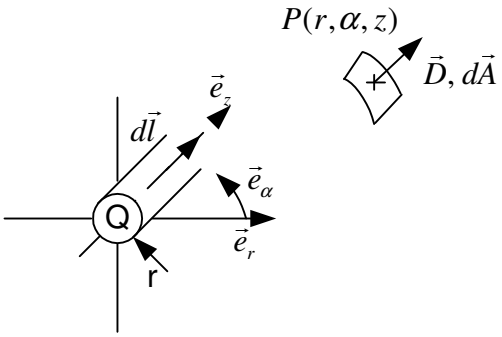

Figure 86 Flux density and electrical field intensity of a line

The electrical field intensity calculates from the flux density to:

$$D = \varepsilon E \qquad\qquad \varepsilon = \varepsilon_0 \cdot \varepsilon_r \tag{158}$$

ε is the material constant describing the permittivity. The permittivity of the free space ε_0 is $8.85 \cdot 10^{-12}$ $[F/m]$. Solving Poisson's differential equation the capacity of the line calculates from the potential different – voltage.

$$U = \Delta\varphi = \int E\, dr \;=\; \int \frac{D}{\varepsilon} dr \tag{159}$$

$$C = \frac{Q}{U} \tag{160}$$

It is common to use the potential coefficient P as the reciprocal value from the capacitance C. The equation (160) is rearranged to:

$$U = P \cdot Q \tag{161}$$

Using the shown equations the field density of the line is

$$D = \frac{q}{2\pi r} \tag{162}$$

Therewith the potential difference between the line and a point outside line is:

$$U = \int_r^{r_P} \frac{1}{\varepsilon} \cdot \frac{q}{2\pi r} dr = \frac{q}{2\pi\varepsilon} \ln\left(\frac{r_P}{r}\right) \tag{163}$$

The capacity is therefore:

$$C = \frac{Q}{\frac{q}{2\pi\varepsilon}\ln\left(\frac{r_P}{r}\right)} = \frac{1}{\frac{1}{2\pi\varepsilon \cdot l}\ln\left(\frac{r_P}{r}\right)} \tag{164}$$

$$C' = \frac{C}{l} = \frac{2\pi\varepsilon}{\ln\left(\frac{r_P}{r}\right)} \quad \left[\frac{F}{m}\right] \tag{165}$$

As shown for the inductances the possibility for a conductor bundle can be used as well. The radius has to be replaced with the radius of the bundle.

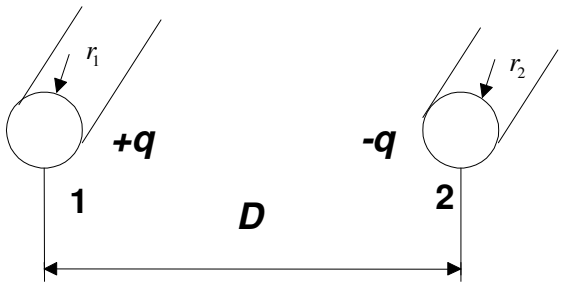

Figure 87 Capacitance of two parallel lines

The mutual capacitance of two-line system can be achieved with superposition of the two fields.

$$U_{12\_1} = \frac{q}{2\pi\varepsilon}\ln\left(\frac{D}{r_1}\right) \tag{166}$$

$$U_{21\_2} = \frac{-q}{2\pi\varepsilon}\ln\left(\frac{r_2}{D}\right) \tag{167}$$

$$U_{12} = \frac{q}{2\pi\varepsilon}\ln\left(\frac{D^2}{r_1 r_2}\right) = \frac{q}{\pi\varepsilon}\ln\left(\frac{D}{\sqrt{r_1 r_2}}\right) \tag{168}$$

$$C'_{12} = \frac{\pi\varepsilon}{\ln\left(\frac{D}{\sqrt{r_1 r_2}}\right)} \tag{169}$$

The Capacitance of one line to ground can be determined with the reflecting method described in Figure 84. The ground is a potential area for zero potential. It is very obvious, that the ground capacitance becomes:

$$C'_g = C'_{jj} = \frac{2\pi\varepsilon_0}{\ln\left(\frac{2h}{r}\right)} \tag{170}$$

The potential coefficient to ground becomes with inserting the permittivity of the free space to:

$$P_g = P_{jj} = \quad 18 \cdot 10^9 \cdot \ln\left(\frac{2h}{r}\right) \quad \left[\frac{m}{F}\right] \tag{171}$$

If there is an arrangement of a two-line system like in Figure 85 the mutual capacitance coupling is.

$$C'_{jk} = C'_{kj} = \quad \frac{2\pi\varepsilon_0}{\ln\left(\frac{D_{j2}}{D_{jk}}\right)} \tag{172}$$

$$P_{jk} = \quad 18 \cdot 10^9 \cdot \ln\left(\frac{D_{j2}}{D_{jk}}\right) \quad \left[\frac{m}{F}\right] \tag{173}$$

It can be concluded that the potential coefficient or the capacitance per line is a superposition from the potential coefficient/ capacitance of the self-charge and the charge from another charge.

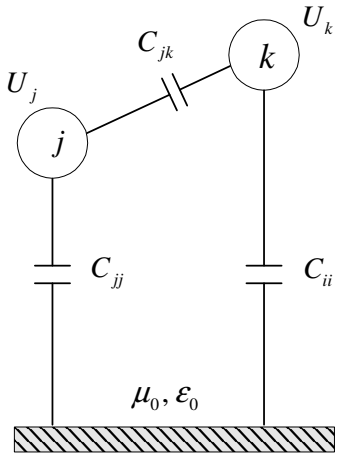

Figure 88 The partial capacity between two lines

Often there is an interest in the individual capacitance values. The correlation between the voltages and charge is given to /61/:

$$\begin{aligned} Q_i &= \quad C_{jj} U_j \qquad\quad + C_{jk}\left(U_j - U_k\right) \\ Q_k &= \quad C_{jk}\left(U_k - U_j\right) + C_{kk} U_k \end{aligned} \tag{174}$$

$$\begin{aligned} Q_i &= \quad \left(C_{jj} + C_{jk}\right) U_j \; - C_{jk} U_k \\ Q_k &= \quad -C_{jk} U_j \qquad\quad + \left(C_{jj} + C_{jk}\right) U_k \end{aligned} \tag{175}$$

Now it is possible to define the coefficients K_{jj}, K_{kk}, K_{jk} and K_{jk}, which have the dimension of a capacitance.

$$\begin{aligned} K_{jj} &= \quad \left(C_{jj} + C_{jk}\right) \qquad K_{jk} = -C_{jk} \\ K_{kj} &= \quad -C_{kj} \qquad\quad\; K_{jj} = \left(C_{jj} + C_{jk}\right) \end{aligned} \tag{176}$$

In general for a system of n lines the following is valid:

$$\begin{aligned} K_{jj} &= C_{jj} + \sum C_{jk} \\ K_{jk} &= -C_{jk} \end{aligned} \tag{177}$$

The capacitance matrix notation can be written:

$$K = \begin{bmatrix} K'_{11} & K'_{12} \\ K'_{21} & K'_{22} \end{bmatrix} \tag{178}$$

According to the equations (177), (178) the capacitance matrix for a three-phase system can be deduced to:

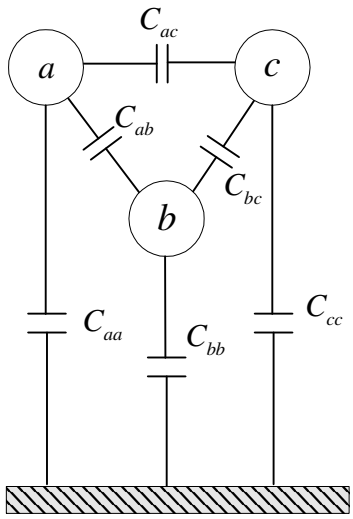

Figure 89 Model capacitances in a three phase overhead line

$$K = \begin{bmatrix} C_{aa} + C_{ab} + C_{ac} & -C_{ab} & -C_{ac} \\ -C_{ba} & C_{bb} + C_{ba} + C_{bc} & -C_{bc} \\ -C_{ca} & -C_{cb} & C_{cc} + C_{ca} + C_{cb} \end{bmatrix} \tag{179}$$

From the Maxwell's equation we can deduce a correlation between the charge and the current can be deduced to:

$$\underline{I} = j\omega \underline{Q} \tag{180}$$

Including the losses of the capacitance the Admittance coefficient to:

$$\underline{A} = G + j\omega K \tag{181}$$

And the complete general description as:

$$i = A\,u \tag{182}$$

5.2.3 Model implementation in Matlab/ Simulink

The basic equations for a dynamic 6th order model of the three phase line shown in Figure 79 are:

$$[u_{abcLR}] = [R_{abc}] \cdot [i_{abc}] + [L_{abc}] \cdot \frac{d}{dt}[i_{abc}] \tag{183}$$

$$[i_{abc}] = [G_{abc}] \cdot [u_{abc}] + [K_{abc}] \cdot \frac{d}{dt}[u_{abc}] \tag{184}$$

In the model the admittance losses G are not neglected. To solve the differential equations (183), (184) in Matlab/ Simulink® equations have to be rewritten.

$$\frac{d}{dt}[i_{abc}] = [L_{abc}]^{-1} \cdot ([u_{abcLR}] - [R_{abc}] \cdot [i_{abc}]) \tag{185}$$

$$\frac{d}{dt}[u_{abc}] = [P_{abc}][i_{abc} - i_{load}] \tag{186}$$

$$[L_{abc}] = \begin{bmatrix} \mathrm{L_{aa}} & \mathrm{L_{ab}} & \mathrm{L_{ac}} \\ \mathrm{L_{ba}} & \mathrm{L_{bb}} & \mathrm{L_{bc}} \\ \mathrm{L_{ca}} & \mathrm{L_{cb}} & \mathrm{L_{cc}} \end{bmatrix} \qquad \mathrm{L_{aa}} = L_i + L_{ag} \qquad \mathrm{L_{ab}} = L_{abg}$$

$$[R_{abc}] = \begin{bmatrix} R_{\mathrm{aa}} & R_{\mathrm{ab}} & R_{\mathrm{ac}} \\ R_{\mathrm{ba}} & R_{\mathrm{bb}} & R_{\mathrm{bc}} \\ R_{\mathrm{ca}} & R_{\mathrm{bc}} & R_{\mathrm{cc}} \end{bmatrix} \qquad R_{\mathrm{aa}} = R_i + R_g \qquad R_{ab} = R_g \tag{187}$$

$$[P] = \begin{bmatrix} C_{aa} + C_{ab} + C_{ac} & -C_{ab} & -C_{ac} \\ -C_{ba} & C_{bb} + C_{ba} + C_{bc} & -C_{bc} \\ -C_{ca} & -C_{cb} & C_{cc} + C_{ca} + C_{cb} \end{bmatrix}^{-1}$$

The model parameters described as matrices are constants, which take the coupling between the 3 phases and ground into account. The line can be modelled with line elements as shown in Figure 90.

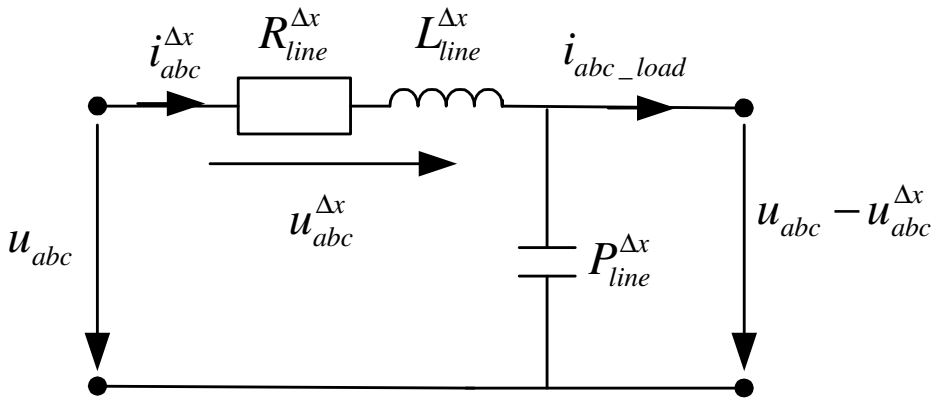

Figure 90 1-phase equivalent for 3-phase model of the line

Dynamical input is the load current at the end of the line and the voltage at the beginning of the line. Output is the current in the line segment and the voltage at the end of the line.

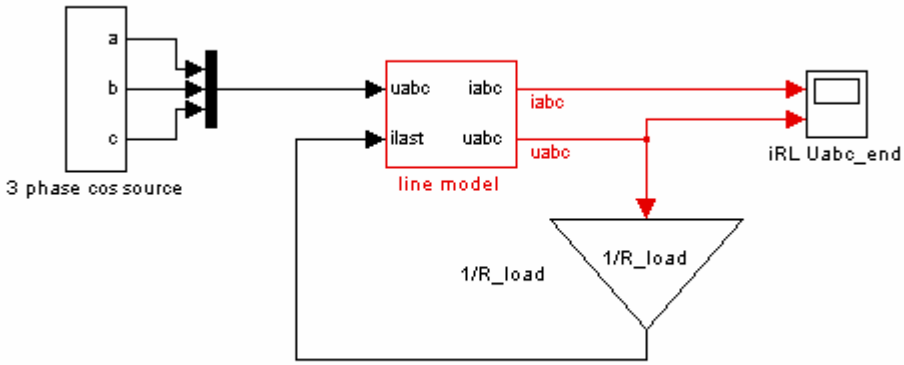

Figure 91 Example for transmission line model implemented in Matlab/ Simulink

The deduced equations can be used for a cable model as well. A cable model differs from the transmission line model in the point, that the single phases are placed close together and therewith skin and proximity effects play an important role. Furthermore there is usually an extra cable for the ground, which so has to be considered in the coupling matrices.

Chapter 6

6. Wind Turbine modelling

In the previous chapters the improved models of the electrical components are described and shown. These advanced electrical models combined with the mechanical model, the aerodynamical model and control system model conclude a complete wind turbine model. In this chapter the aerodynamic and the mechanic model of the wind turbine are described. These models are implemented in Matlab/ Simulink in the block called “mechanical system” as shown in Figure 92.

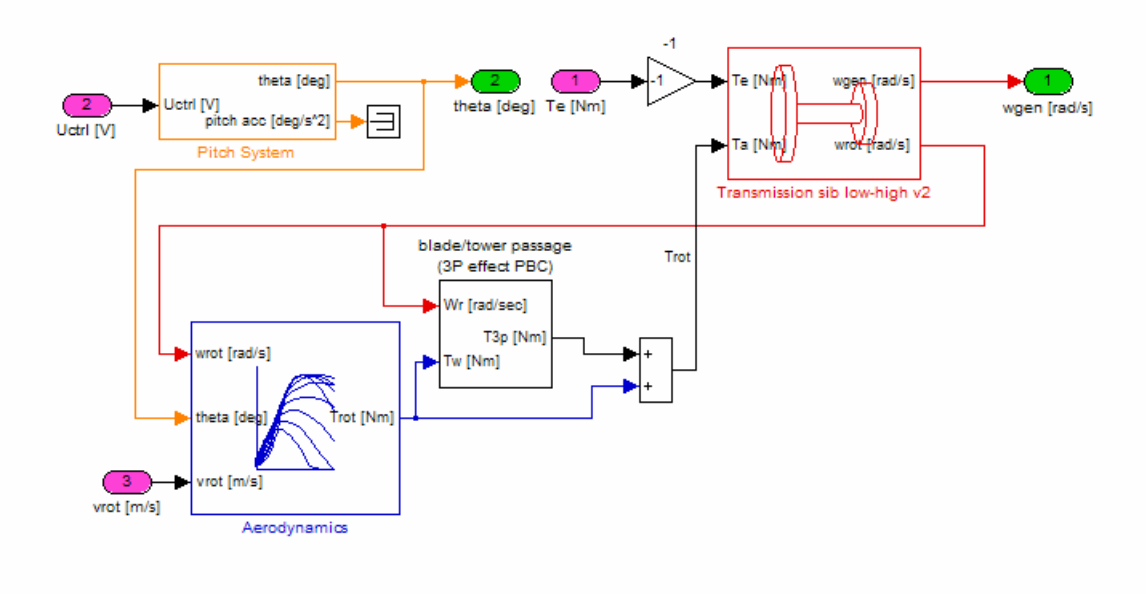

Figure 92 Block “Mechanical System” in Matlab/ Simulink of the Wind Turbine

6.1 Aerodynamic Model

The kinetic energy obtained by the blades from the wind is transformed to mechanical torque on the rotor shaft of the wind turbine. The blades are attached to the rotor shaft and rotate with the tip speed $\omega_{rot} \cdot r$, where r is the length of the blade. The blade profile experiences a relative wind velocity generated by the superposition of the tip speed and the wind velocity v_w. While wind is passing the profile it introduces lift (L) and drag (D) forces on the blade, which results in movement of the blade. From these forces the power obtained from the wind can be calculated as shown in equation (188).

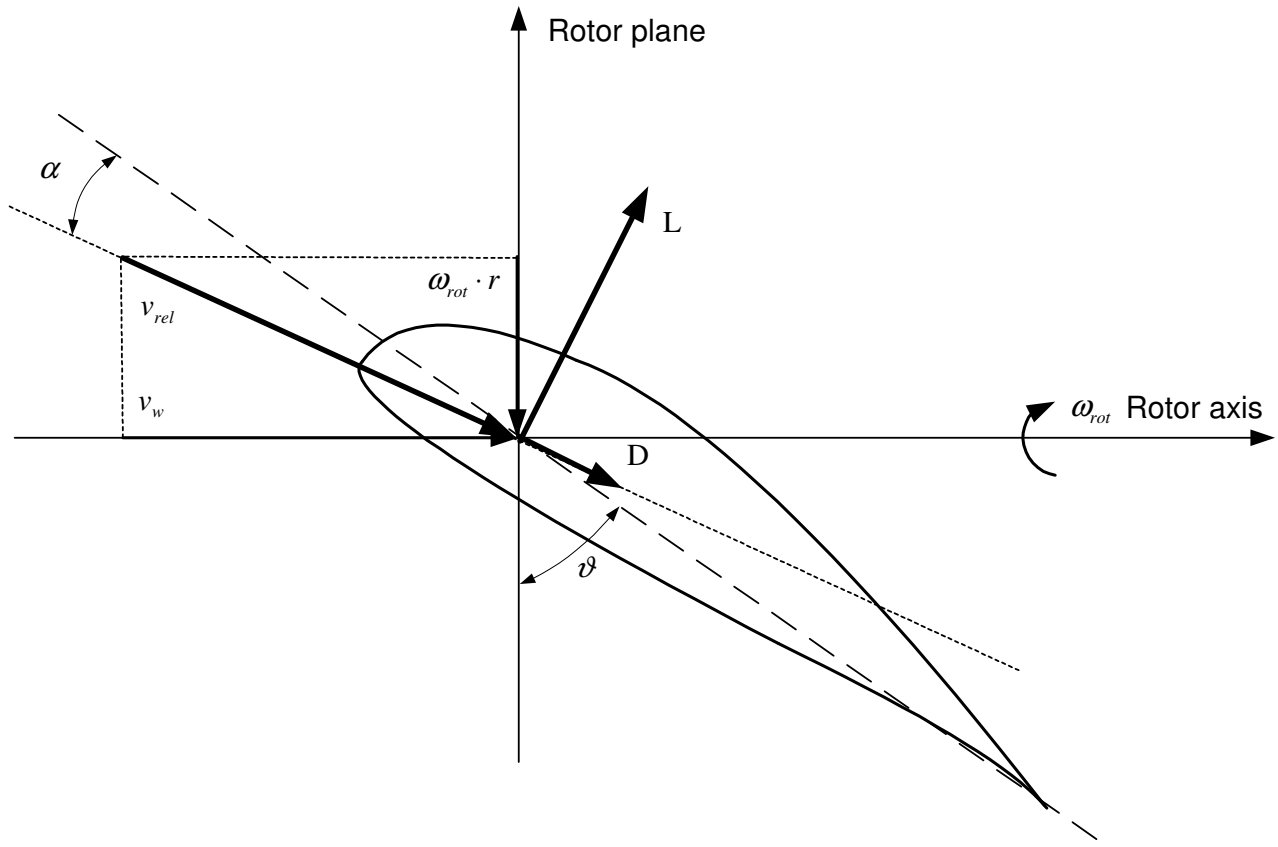

Figure 93 Cross section of a wind turbine blade (α-angle of attack).

$$P_w = \frac{1}{2} \rho_{air} \cdot A_r \cdot c_p(\lambda, \vartheta) \cdot v_w^3 \tag{188}$$

Thereby ρ_{air} is the air density, v_w the free wind speed experienced by the rotor, A_r the swept rotor area and c_p the power coefficient. The power coefficient depends upon the pitch angle ϑ (often denoted as β) and the tip-speed-ratio λ.

$$\lambda = \frac{\omega_{rot} \cdot r}{v_w} \tag{189}$$

The tip-speed ratio is defined by the ratio of the tip speed $\omega_{rot} \cdot r$ and the wind speed v_w. The power coefficient is typically given in a form of a table as shown in Figure 94.

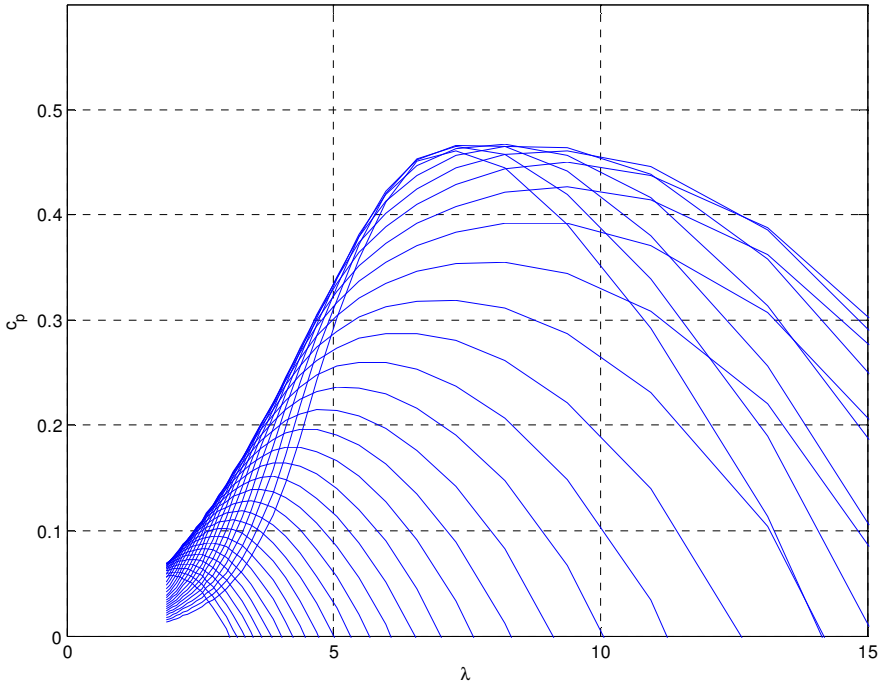

Figure 94 The power coefficient – tip speed ratio curve as a function of the pitch angle

The torque on the rotor shaft, which is important for the shaft model later on (Figure 97), therewith can be calculated from the power with help of the rotational speed.

$$T_A = \frac{P_w}{\omega_r} \tag{190}$$

In Figure 95 the implementation of the aerodynamical model is shown. Notice that the torque calculated with equation (190) is called Trot in the picture. It is the torque, which is obtained by the rotor shaft through the blades related to the low speed side of the turbine shaft.

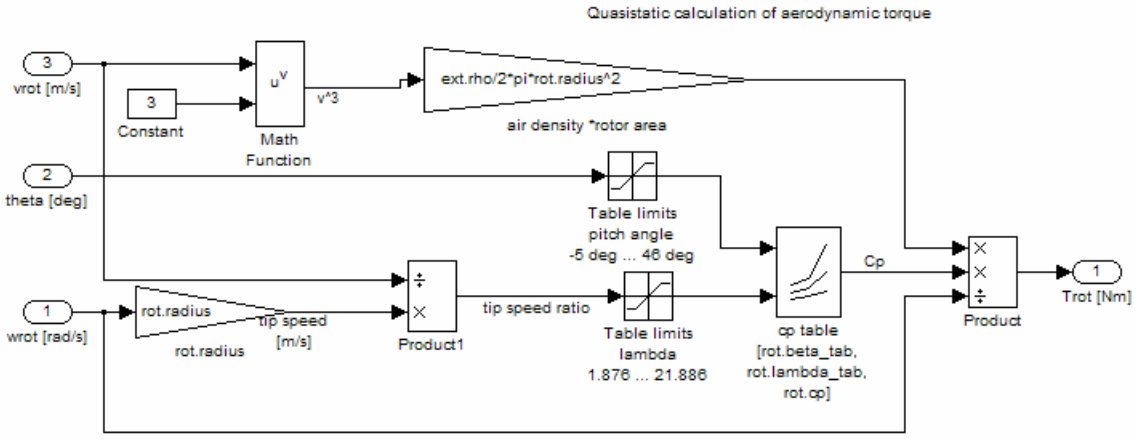

Figure 95 The aerodynamical model implemented in Matlab/ Simulink

6.2 Pitch model

The mechanical arrangement for pitching the blades of the turbine is later found in the Matlab/ Simulink block mechanical systems/pitch system and shown in Figure 96. The pitch model consists of the pitch actuator. The pitch actuator is expressed as a non-linear function between the control voltage signal and the real pitch angle. The characteristic is modelled as a non-linearity with a dead-zone.

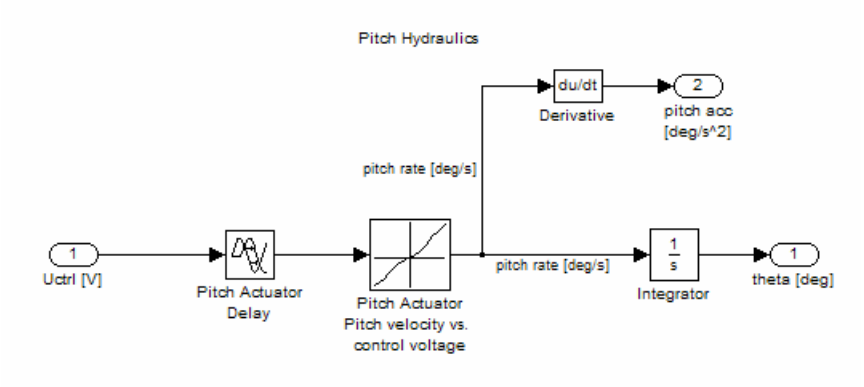

Figure 96 Model of the pitch system implemented in Matlab/ Simulink

6.3 Mechanical Model

In this chapter the simplified mechanical model of the wind turbine will be described. This dynamical model, which can be found in a broad range of literature /56/ - /75/ is widely accepted as expressing the dynamical behaviour of the drive train for the area of research. The simplified model of the drive train is shown in Figure 97. In this model all masses are lumped at the low and high speed shaft. The inertia of the low speed shaft comes mainly from the rotating blades and the inertia of the high speed shaft from the generator. Thus it is more important to include all small masses of the high speed shaft, because they have an important influence on the dynamic system due to the gear ratio transformation. The mass of the gearbox itself is insignificant and neglected. Stiffness and damping of the shaft are combined in one equivalent stiffness and damping placed at the low speed side.

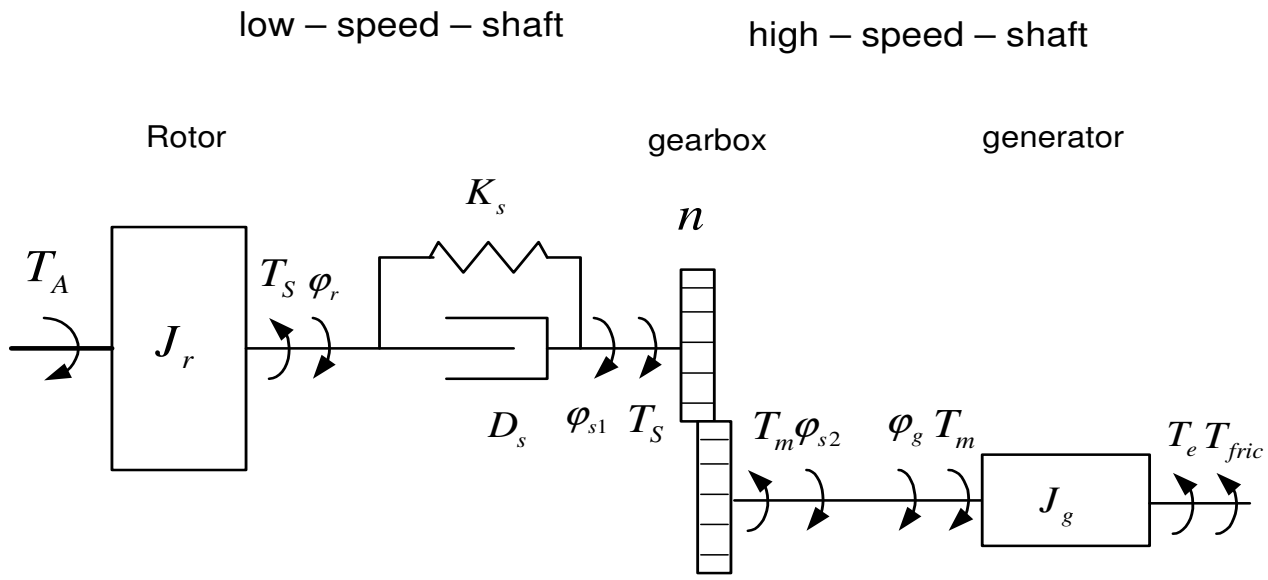

Figure 97 Drive train schematic for modelling of a wind turbine

Input to the model for a two mass system is the torque T_A obtained by the aerodynamic system and the generator reaction torque T_e. Output is the changes in rotor speed ω_r and generator speed ω_g.

The high speed generator dynamics can be expressed as already shown in the description of the machine model. Please notice the sign adjustment due to generator operation. The difference of the mechanical driving torque T_m, the generator reaction torque T_e and the torque due to friction losses T_{fric} result in the change of the generator angular speed $\dot{\omega}_g$.

$$T_m - T_e - T_{fric} = J_g \cdot \dot{\omega}_g \tag{191}$$

$$\dot{\omega}_g = \ddot{\varphi}_g \tag{192}$$

The changes of the angular rotor speed $\dot{\omega}_r$ are caused by the difference of the aerodynamic torque T_A and the shaft torque T_S at the low speed side.

$$T_A - T_S = J_r \cdot \dot{\omega}_r \tag{193}$$

$$\dot{\omega}_r = \ddot{\varphi}_r \tag{194}$$

The mechanical driving torque T_m and the shaft torque T_S are connected by the use of the gear ratio in the following way:

$$T_m = \frac{T_S}{n} \tag{195}$$

The dynamics of the shaft can be described with the equation (196)

$$T_S = K_S \cdot \Delta\varphi + D_S \cdot \Delta\dot{\varphi} \tag{196}$$

$$\Delta\dot{\varphi} = \dot{\varphi}_r - \frac{\dot{\varphi}_g}{n} = \omega_r - \frac{\omega_g}{n} \tag{197}$$

Inserting the equations (196) and (197) into (191) and (193) and using the equations (192), (194) and (195) the equations (198) and (199) will be obtained. The equations are used to describe the drive train dynamics.

$$\dot{\omega}_r = \frac{1}{J_r}\left(T_A - D_S \cdot \omega_r + \frac{D_S}{n} \cdot \omega_g - K_S \int \left(\omega_r - \frac{\omega_g}{n} \right) dt \right) \tag{198}$$

$$\dot{\omega}_g = \frac{1}{J_g}\left(-T_e - \left(D_g + \frac{D_S}{n^2} \right) \omega_g + \frac{D_S}{n} \omega_r + \frac{K_S}{n} \int \left(\omega_r - \frac{\omega_g}{n} \right) dt \right) \tag{199}$$

To obtain the stiffness constant K_S the eigenfrequency of the drive train has to be known. Thinking of a two mass free swinging system the eigenfrequency is defined as:

$$\omega_{0S} = 2\pi f_{0S} = \sqrt{\frac{K_S}{J_{ges}}} \tag{200}$$

The total inertia of the free swinging system on the low speed side can be calculated in the following way:

$$J_{ges} = \frac{J_r \cdot J_g \cdot n^2}{J_r + J_g \cdot n^2} \tag{201}$$

The stiffness constant of the low speed shaft is:

$$K_S = J_{ges} \cdot (2\pi f_{0S})^2 \tag{202}$$

The damping constant of the shaft D_S can be obtained with help of the logarithmic decrement ξ_S. A standard approximation of the logarithmic decrement is 10%. The damping constant can be obtained according to:

$$D_S = 2\xi_s \cdot \sqrt{\frac{K_S \cdot J_{ges}}{\xi_s^2 + 4\pi^2}} \tag{203}$$

Figure 98 shows the drive train as described implemented in Matlab/ Simulink.

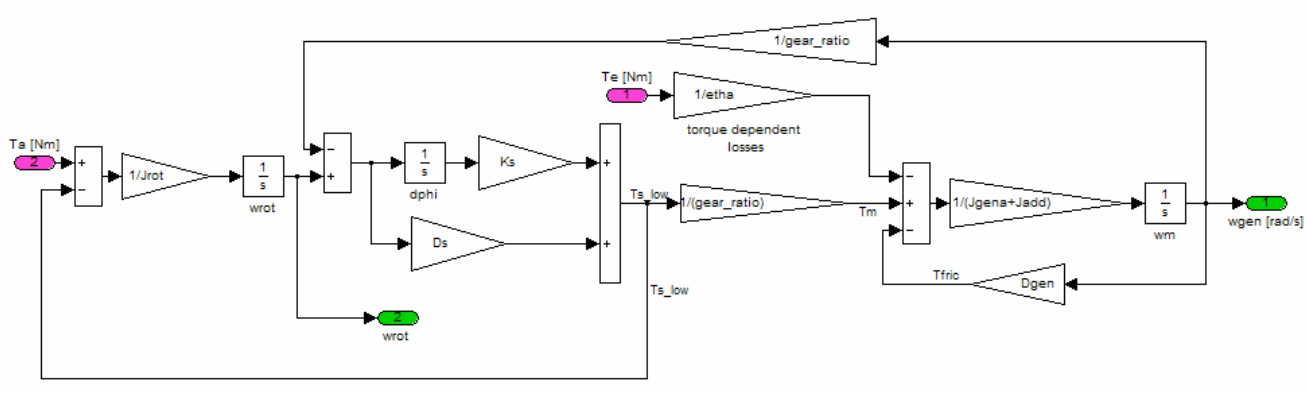

Figure 98 Drive train model implemented in Matlab/ Simulink

6.4 Library for Wind Turbine modelling in Matlab/ Simulink

The electrical and mechanical components modelled in Chapter 3 to Chapter 6 are generally useful for the developments of wind turbine models. In order to make these models accessible for further developments a library in Matlab/ Simulink collects the different models. The library is accessible through the Simulink browser as shown in Figure 99.

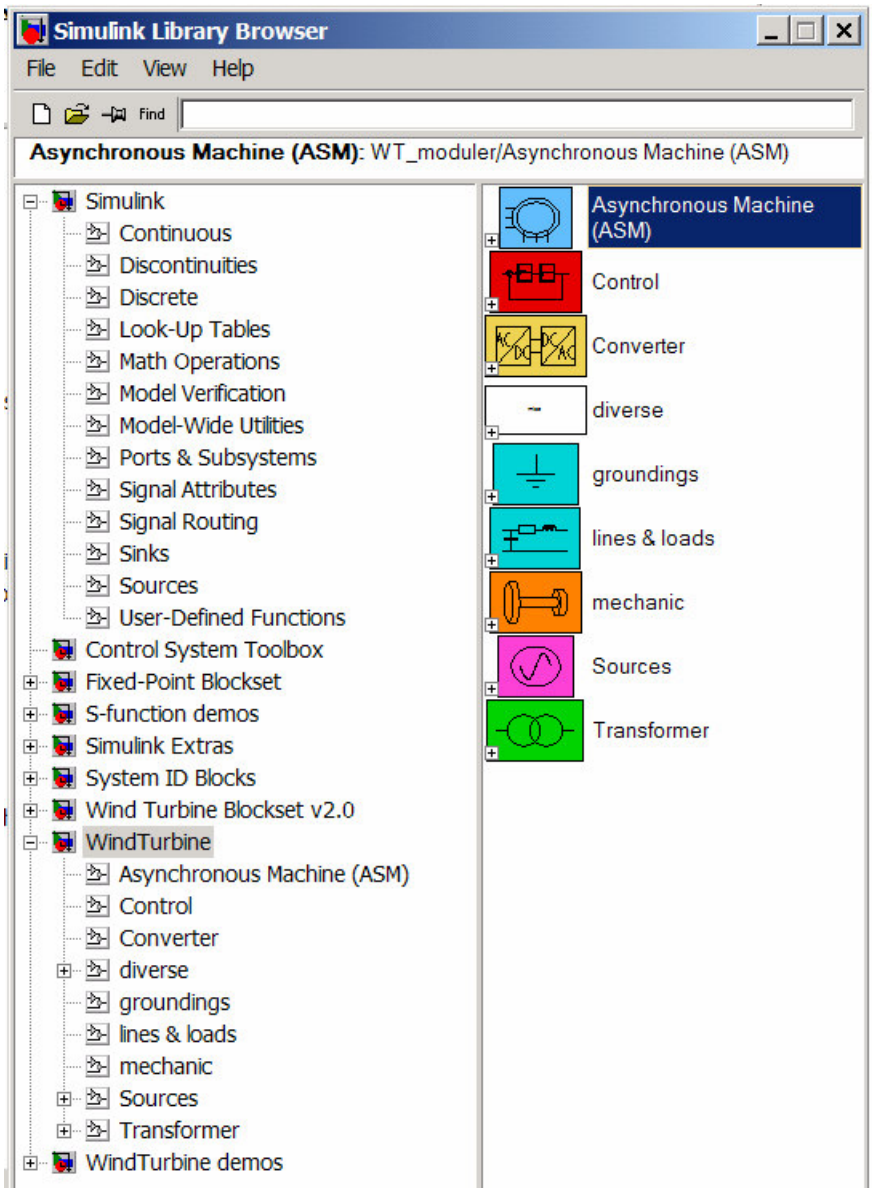

Figure 99 Simulink Library Browser with opened Wind Turbine Toolbox

Through the library the different components models are accessible. In the Asynchronous Machine Library the different advanced machine types can be found (Figure 100). As in this library, various models can be found in the other subgroups. A detailed description of the entire library options extents this work. Therewith this shows only an example about the library.

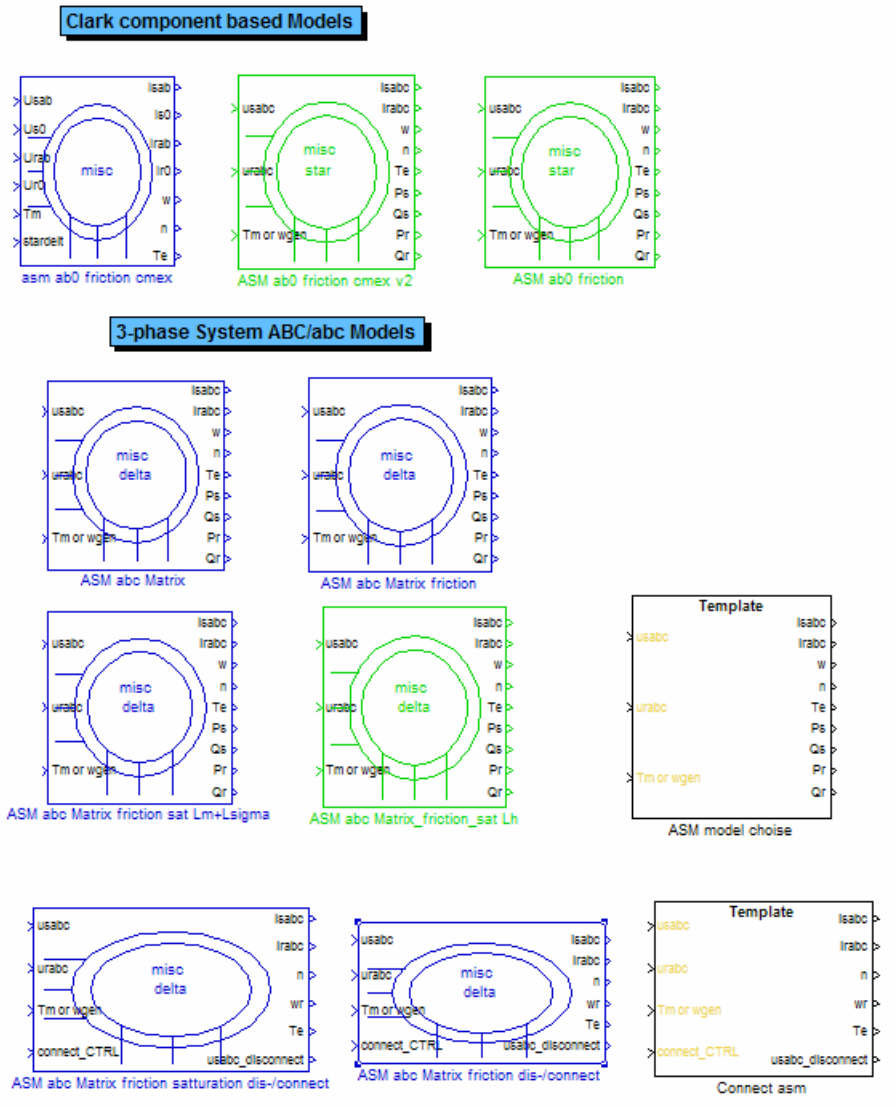

Figure 100 Induction machine/ Asynchronous machine library

To simplify the work with these elements example sheets called “Wind Turbine demos” with some practical assemblies of the elements are included in the library shown in Figure 101.

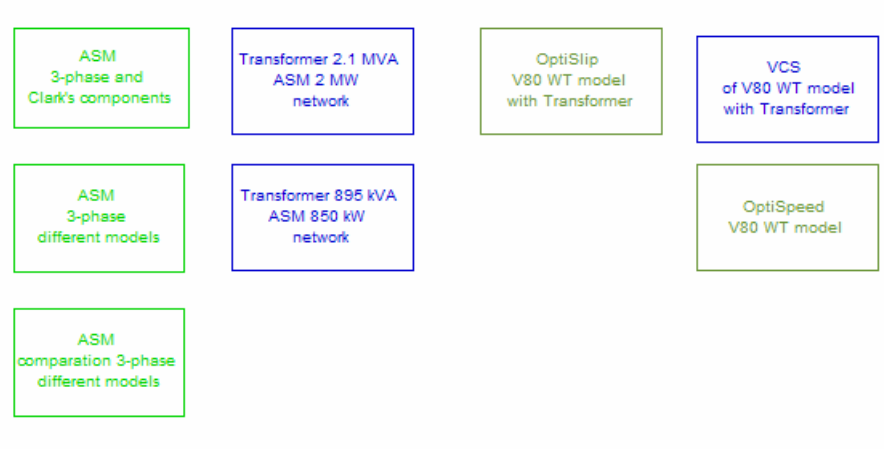

Figure 101 ”Wind Turbine demos” from the Wind Turbine library

As one example the demo model of the Transformer 895 kVA ASM 850 kW network is shown in Figure 102.

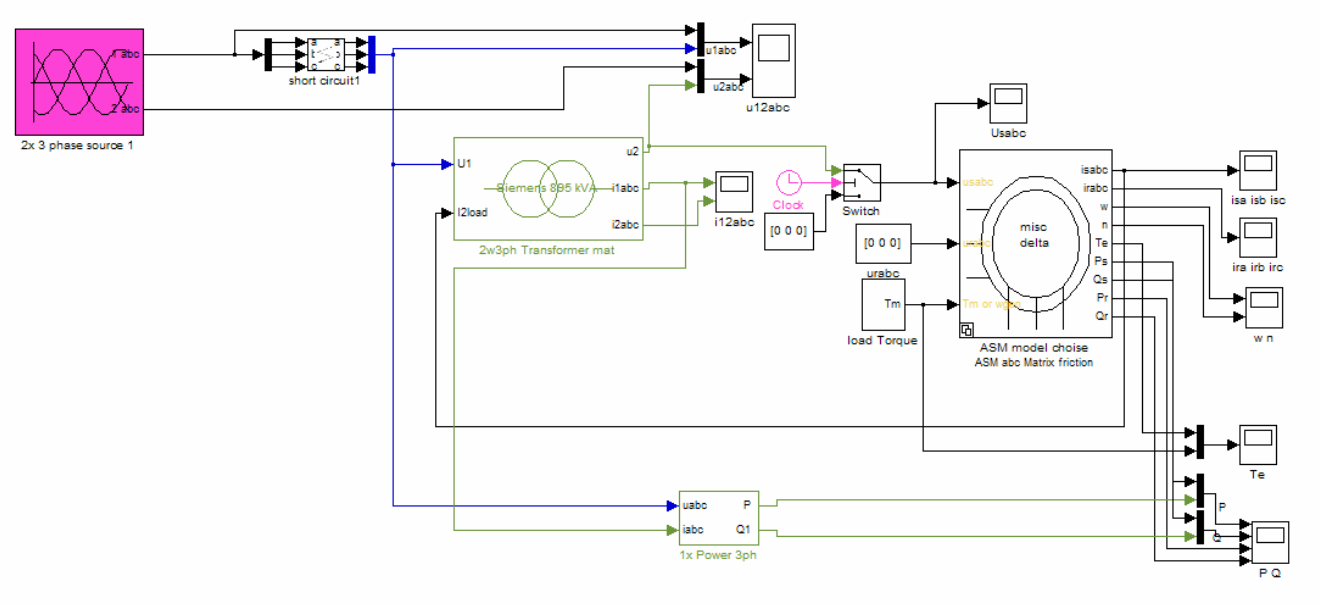

Figure 102 Example model Transformer and ASM network

Furthermore included in the demo model library are the two finished Vestas Wind Turbine models, which will be completed with control system, described in the Chapter 7 and Chapter 8.

Chapter 7

7. Control of a Turbine with controlled rotor resistance

Control of a machine with the help of variation resistor in the rotor circuit of the machine is a well known concept. Vestas uses this concept in a wind turbine called OptiSlip®. The feature allows the wind turbine to stay at the optimal operation point by holding the generator at an optimal power during small speed fluctuations. This leads to a minimisation of torque and power fluctuation during operation, which reduces mechanical stress and flicker level of the turbine. The feature is as beneficial during grid failures as during standard operation e.g. short-circuit power and current is minimized.
The variable resistance is connected to the rotor terminals of a slip-ring induction machine and is controlled by a rotor current controller. In Vestas the system is called Vestas Rotor Current Control (VRCC). The reference for the resistance control is given by the overall wind turbine control, which consists of speed control, pitch control and the power controller. In Figure 103 description of the total control system is shown.

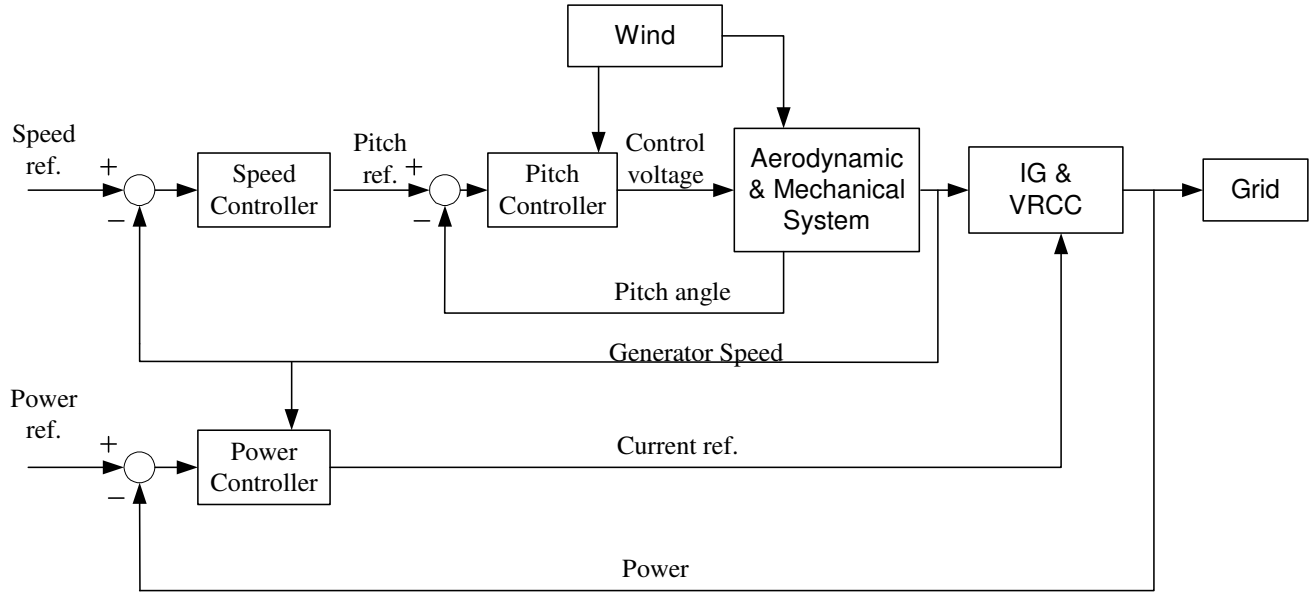

Figure 103 A sketch of the Vestas OptiSlip wind turbine control system

7.1 The rotor current control

The rotor current control for the variation of the resistance represents the inner loop of a power control and/ or speed control as outer loop. In Vestas this unit is called Vestas Rotor Current Control (VRCC) and consists of resistances, a B6 Diode-bridge, an IGBT and the control unit (Figure 104). The IGBT, as controllable switch at the DC side, is used for controlling the rotor current flow though the external rotor resistances. Thereby the effect

of varying rotor resistance on the rotor terminal of the generator is created.

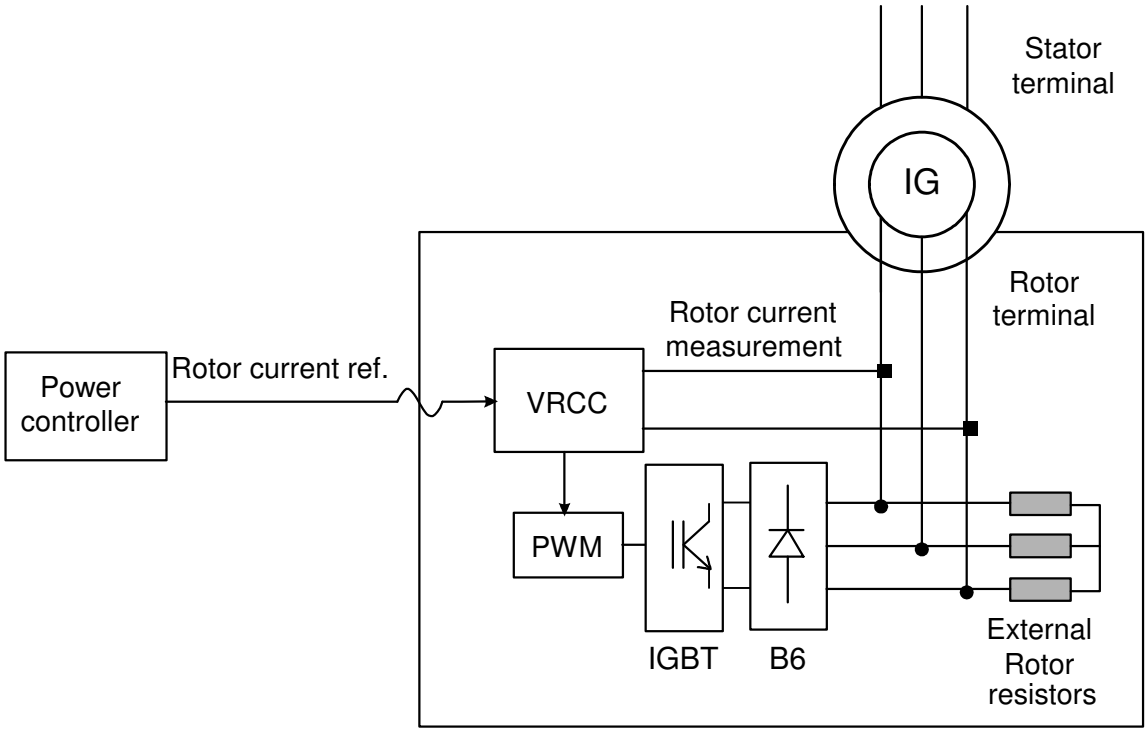

Figure 104 Illustration of the VRCC unit

Variation of the rotor resistance allows the induction machine to operate on different torque – speed characteristics. Figure 105 shows as example three operation points result from resistance change in three different slip points using one torque. This function is well known and it is often used for start-up of motors.

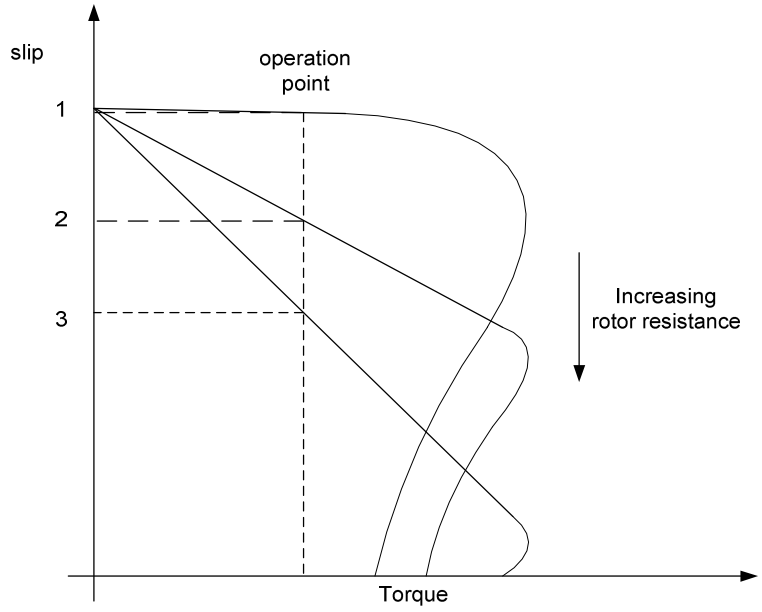

Figure 105 Torque-speed characteristic with increasing rotor resistance

An adaptation of the method for the wind turbine generator either the torque or the power of the generator can remain constant during short term speed changes. Switching the complete external rotor resistance the slip of the generator can be increased up to approx.

12%. For normal control purposes at rated power of the wind turbine only an increase up to slip value of 10% is used. However in fault situations with increased rotor current the IGBT will stop switching and the total resistance will be connected to the rotor terminals. The input for the VRCC is the rotor current reference value, which is received from the power controller and the measured rotor current. The output of the VRCC is the duty cycle for switching the IGBT.

7.1.1 Modelling of the rotor current control

The VRCC unit can be simplified for the researched time frame, since the most interest lies in the damping of the system and minimizing short circuit contribution to the grid. In the model the VRCC is implemented as a continuous controller. The power electronic is simplified by the direct calculation of the active external resistance from the duty-cycle Figure 106. With the resistance the voltage at the rotor terminals can be calculated. The rotor voltage is the input for the generator model.

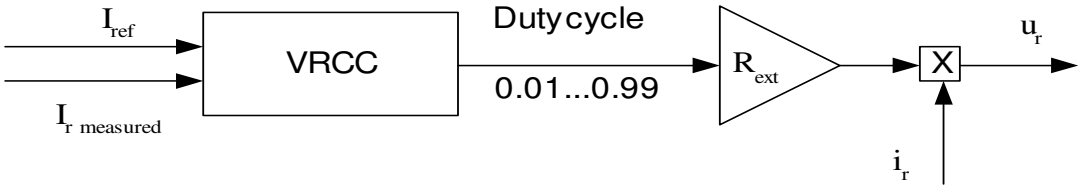

Figure 106 Simplified VRCC model

The VRCC control consists of two cascaded PI-controllers called Master and Slave PI as shown in Figure 107. The Slave-PI controller compensates for the poles of the generator. To increase the dynamic of the control the Master-PI controller is introduced /96/.

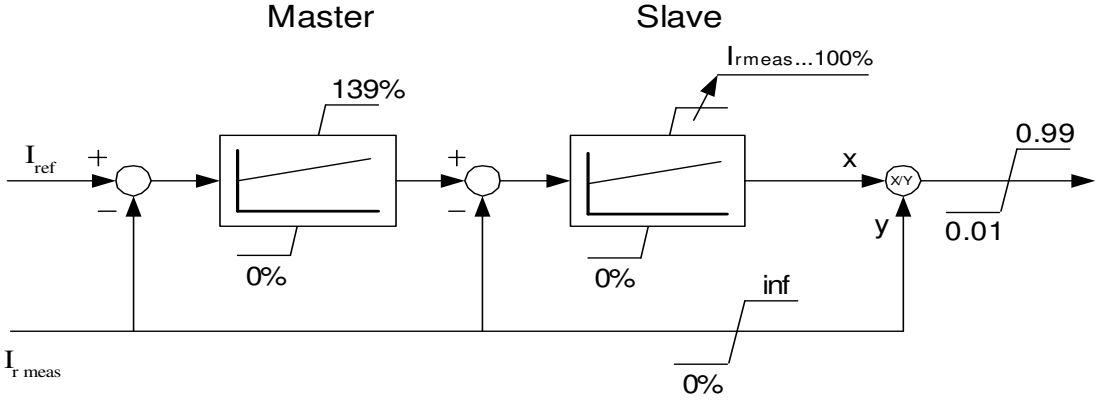

Figure 107 VRCC – controller using two serial PI-controllers

For compensation of the electrical generator poles the integrator time constant of the Slave controller T_{iS} is set to the time constant T_r of the generator.

$$T_r = \frac{L'_{\sigma r} + L_{\sigma s}}{R'_r + R_s} \qquad K_r = \frac{R'_{ext}}{R'_r + R_s} \tag{204}$$

The transfer function of the closed loop slave controller is then:

$$\frac{I_{r\,meas}}{I_{ref}} = \frac{1}{T_{cl\,S} \cdot s + 1} \tag{205}$$

Where:

$$T_{cl\,S} = \frac{T_{iS}}{K_{pS}} \cdot \frac{R_s + R_r^{'}}{R_{ext}} \tag{206}$$

The gain of the slave controller is achieved from equation (206) to:

$$K_{pS} = \frac{T_{iS}}{T_{cl\,S}} \cdot \frac{R_s + R_r^{'}}{R_{ext}} \qquad K_{pS} = \frac{T_{i\,S}}{T_{cl\,S} \cdot K_r} \tag{207}$$

$$T_{i\,S} = T_r \tag{208}$$

The closed loop time constant for the slave controller is deduced from the closed loop time constant of the master controller. The time constant of the master controller is chosen in the way that the closed loop transfer function is representing a first order system.

$$\frac{I_{r\,meas}}{I_{ref}} = \frac{1}{T_{cl\,M} \cdot s + 1} \tag{209}$$

The closed loop master time constant $T_{cl\,M}$ is chosen to be set equal to a desired time constant, which should be much less than the sample time of the overall control. Therewith the closed loop slave time constant can be calculated to:

$$T_{cl\,S} = \frac{T_{cl\,M}}{2} \tag{210}$$

The master time constant $T_{i\,M}$ is simply deduced to:

$$T_{i\,M} = T_{cl\,S} \tag{211}$$

and the gain of the master controller to:

$$K_{pM} = \frac{T_{cl\,S}}{T_{cl\,M}} \tag{212}$$

Simulations made with a variation of the generator speed show the effect of the VRCC. The speed at the generator axis is stepwise changed to express a slip of 2, 4 and 10%, which is rated operation of the wind turbine (see chapter 7.2).
The slip *s* is positive defined for generator operation.

$$s = \frac{n_g}{n_0} - 1 \tag{213}$$

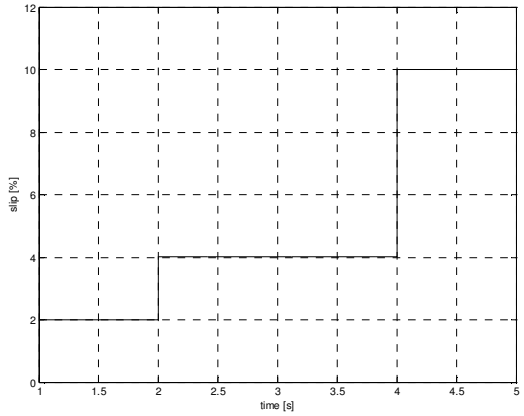

Figure 108 Initiated generator speed changes depicted as slip [%]

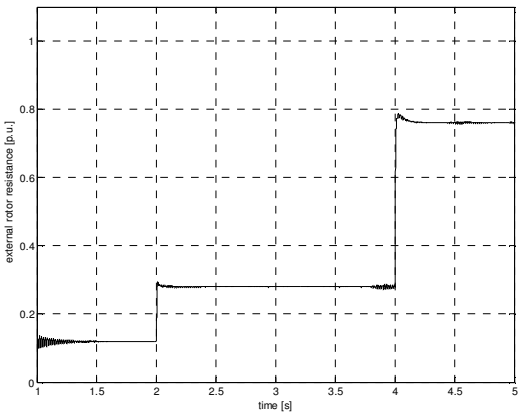

Figure 109 Controlled external rotor resistance as reaction to the speed changes

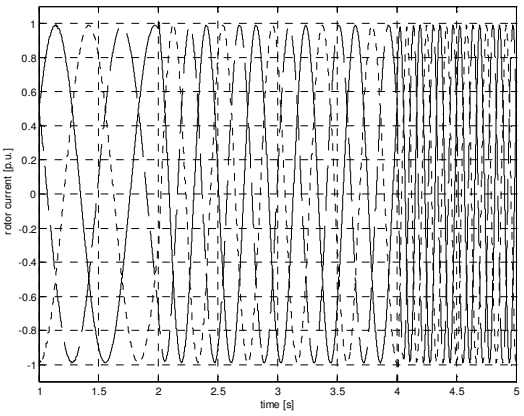

Figure 110 The 3-phase rotor current controlled by the VRCC system

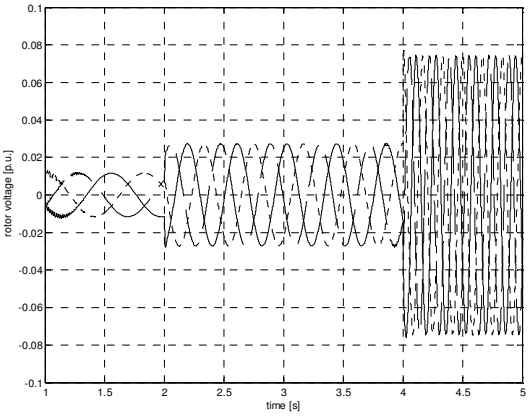

Figure 111 Changes of 3-phase rotor voltage due to the slip changes controlled by the VRCC

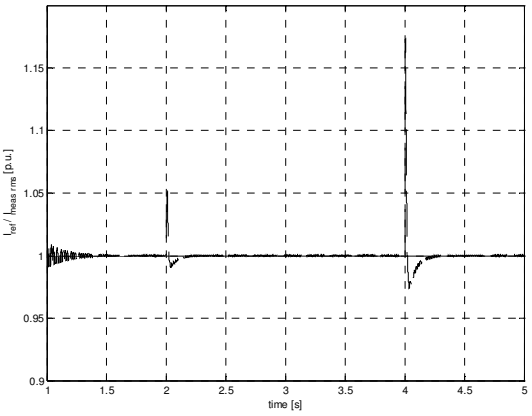

Figure 112 Rotor current reference value (solid line) and feedback rotor current amplitude (dotted line) of the VRCC

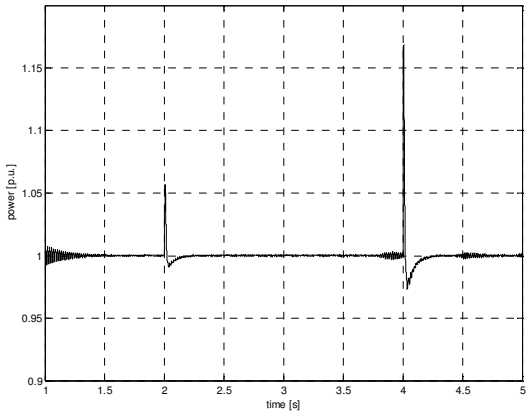

Figure 113 Simulated generator power

7.2 The Power Control

When the wind turbine is connected to the grid the power control is active. The power control represents the outer control loop to the VRCC. The input for the PI power controller is given by a calculation of the power reference on the basis of the generator slip.

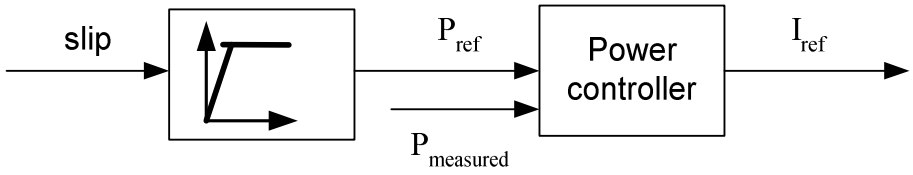

Figure 114 The power control scheme

During start of the wind turbine the wind might not be high enough to produce enough torque on the turbine for running on rated power and the wind turbine is in partial load operation mode. The power is controlled to increase with a generator slip of 2% as shown in Figure 115. If the wind speed rises to a point where rated power can be produced, the wind turbine will switch to rated operation mode. In rated operation mode the power of the wind turbine will be controlled to a constant rated power output, while the rated slip will be controlled by the pitch control to 4%. Short time speed changes at rated power output are controlled by possible slip changes between rated slip of the generator which is approx. 0.5% with no external connected resistance and the max. allowable value of slip=10%.

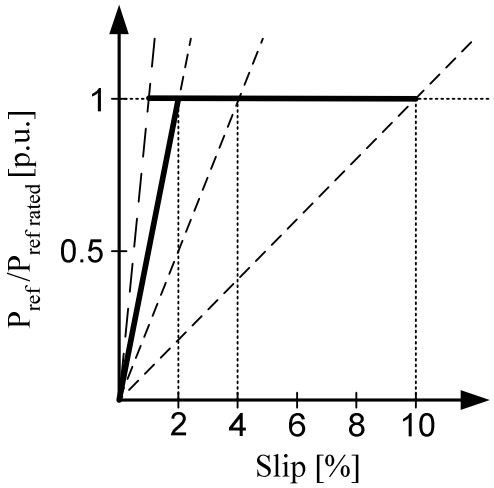

$$P_{ref} = \begin{cases} 0 & for \quad slip < 0\% \\ \dfrac{P_{rated}}{slip = 2\%} \cdot slip & for \quad 0\% \le slip \le 2\% \\ P_{rated} & for \quad slip > 2\% \end{cases}$$

Figure 115 Power – Slip reference curve of the power controller

While the rotor current control is implemented in continuous time domain, the power control is modelled in discrete time steps. In Figure 121 the peak of the sampled feedback power is very small compared to the real power peaks during the speed steps.

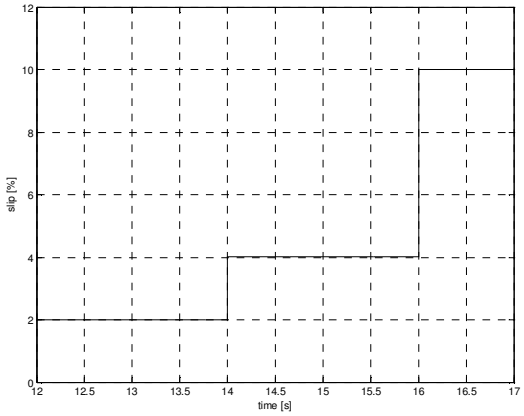

Figure 116 Initiated generator speed changes depicted as slip [%]

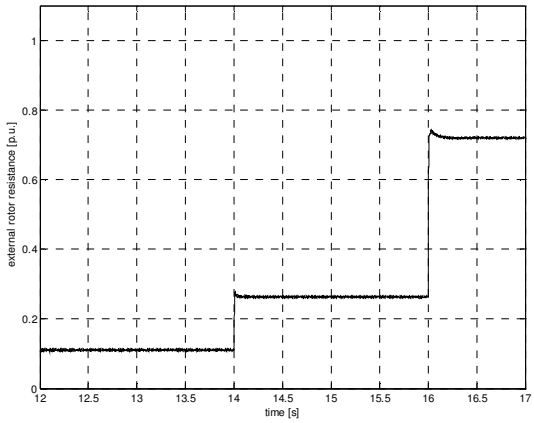

Figure 117 Controlled external rotor resistance as reaction to the speed changes with VRCC and power controller

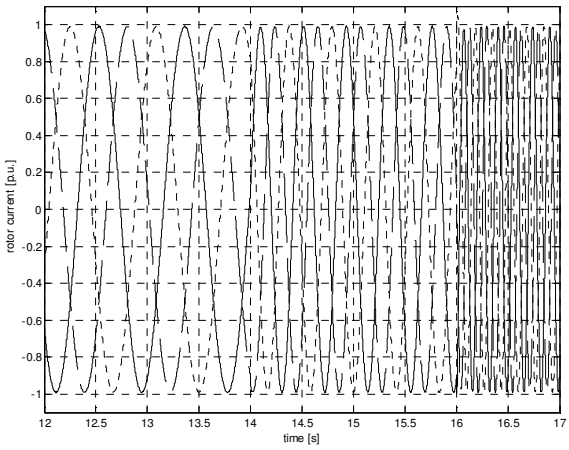

Figure 118 The 3-phase rotor current controlled by the VRCC system and outer power control loop

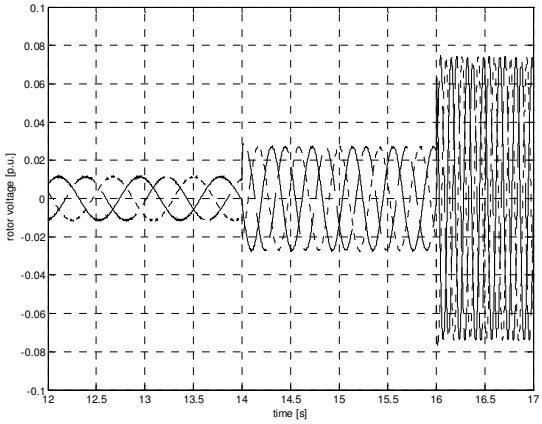

Figure 119 Changes of 3-phase rotor voltage due to the slip changes controlled by the VRCC and outer power control loop

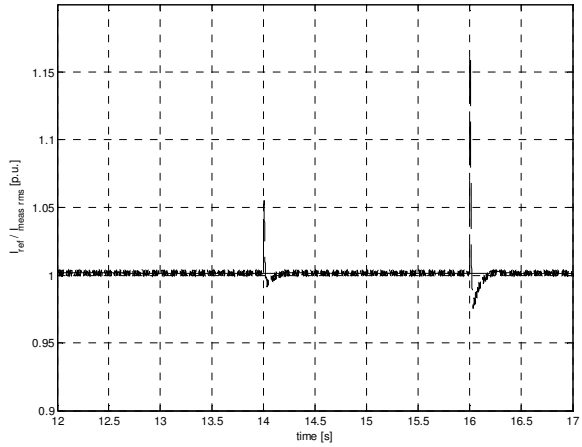

Figure 120 Rotor current reference value (solid line) and feedback rotor current amplitude (dotted line) of the VRCC

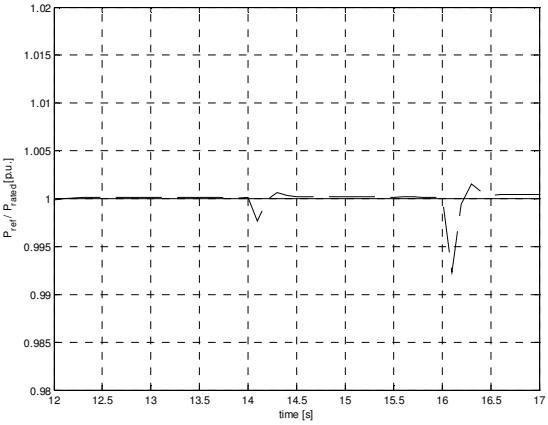

Figure 121 Power reference (solid line) and feedback generator power (dashed line) for the power controller

7.3 The Speed Control

The speed reference and the power reference increase proportionally until the rated values are reached. The rated speed reference is default 4%. If the wind speed and the power output are below the rated values, the slip will be below 2% and the pitch will be controlled from a parameter list based upon the wind speed. This feature is called OptiTip®. If the wind speed is above the rated value, the power output will be almost constant at nominal power and the generator speed is controlled to follow the reference speed by changing the pitch. The speed non-linearity increases the gain if the slip is below or above the rated slip value. The increased gain below or above will speed up the pitch control. The increase above is to avoid over speed errors of the turbine, while the increase below increases the power production by returning fast to rated conditions.

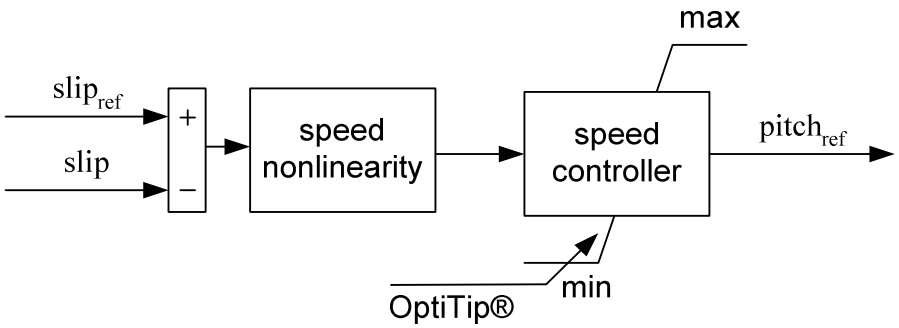

Figure 122 Speed controller of the wind turbine control

7.4 The pitch Control

The turbine has a pitch control system for each blade. Each pitch control system is a servo loop which will make the pitch follow a given reference as quickly as possible and with sufficient damping. The pitch controller is a non-linear controller which compensates for the dead band and the limitations in the proportional valve (see aerodynamic model for actuator description).

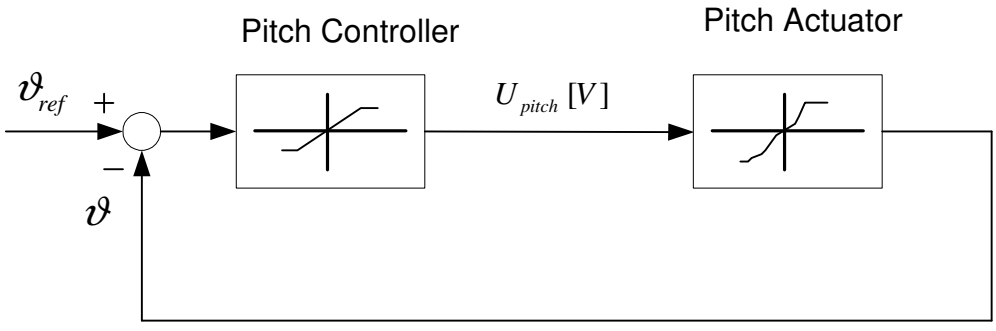

Figure 123 Pitch controller included in the wind turbine controller

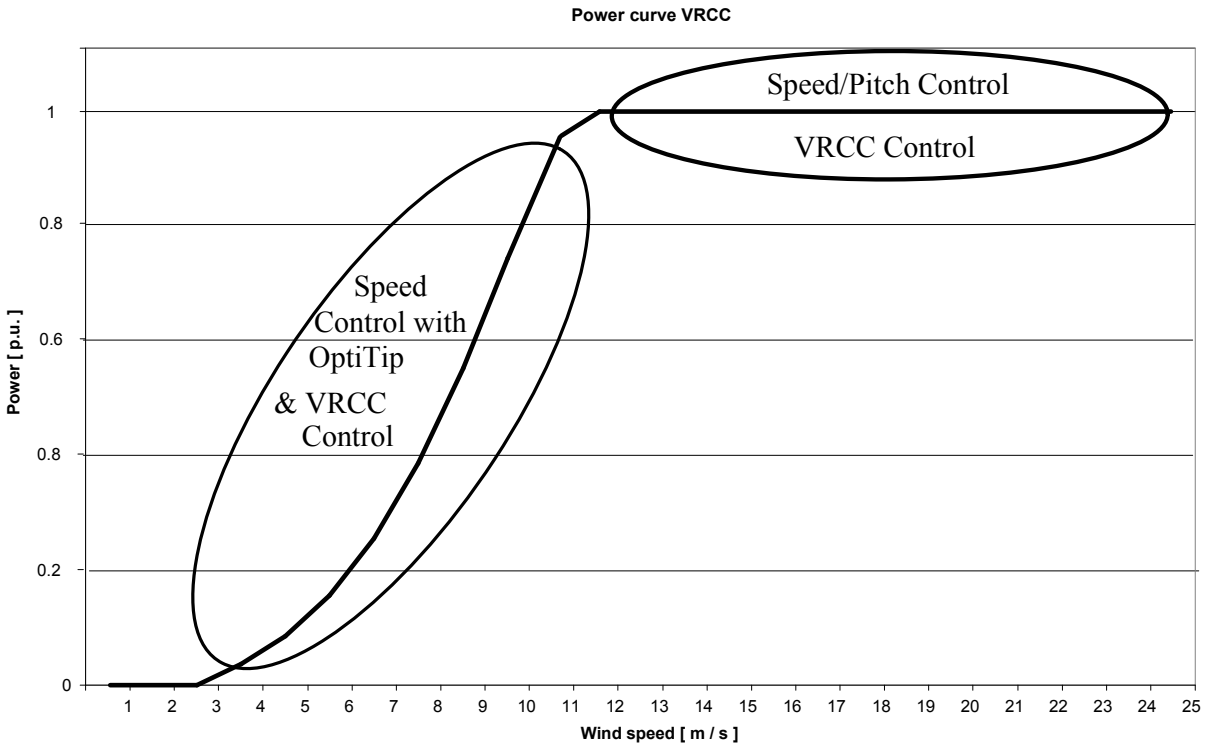

Figure 124 Wind turbine power curve with used control features

7.5 Validation of the OptiSlip® wind turbine model

For validation of the whole turbine model a simplified validated Matlab/ Simulink model /13/ is used. The complete OptiSlip® turbine model is shown in Figure 125.

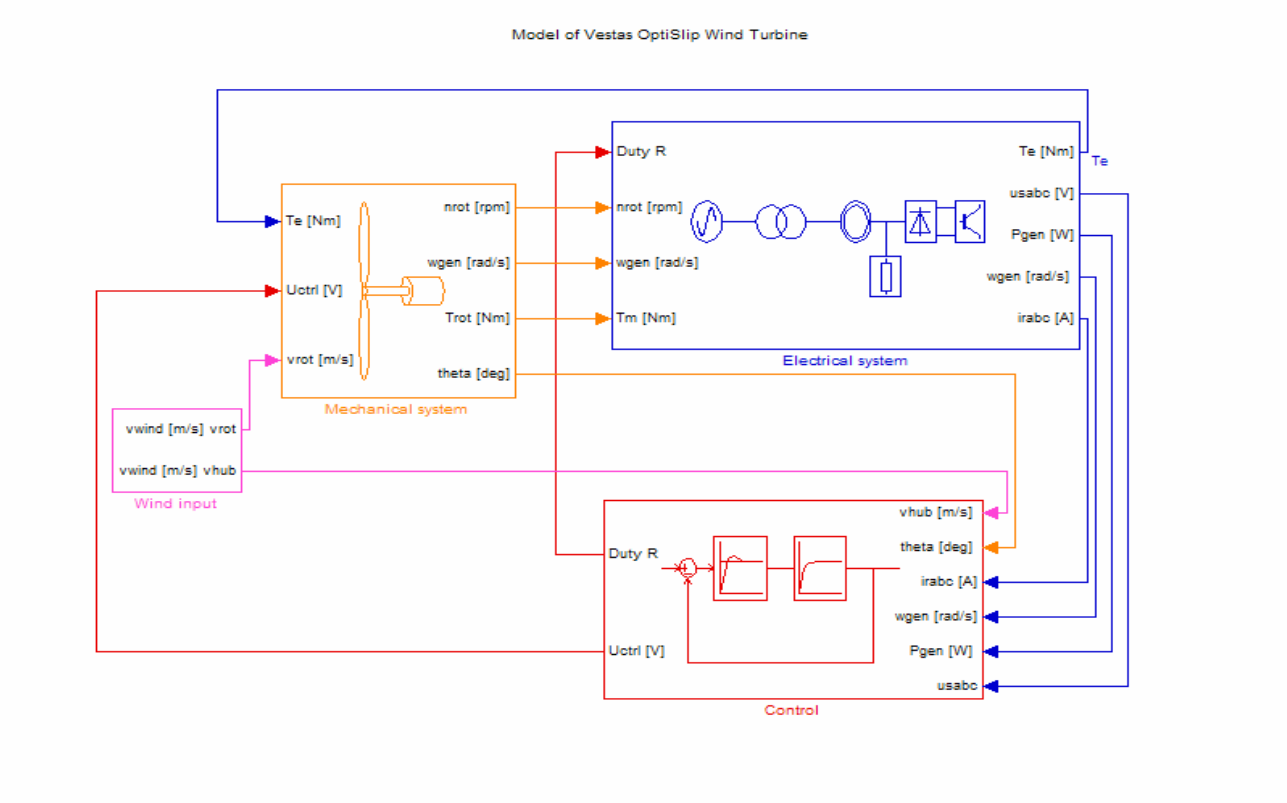

Figure 125 Complete OptiSlip turbine model in Matlab/ Simulink

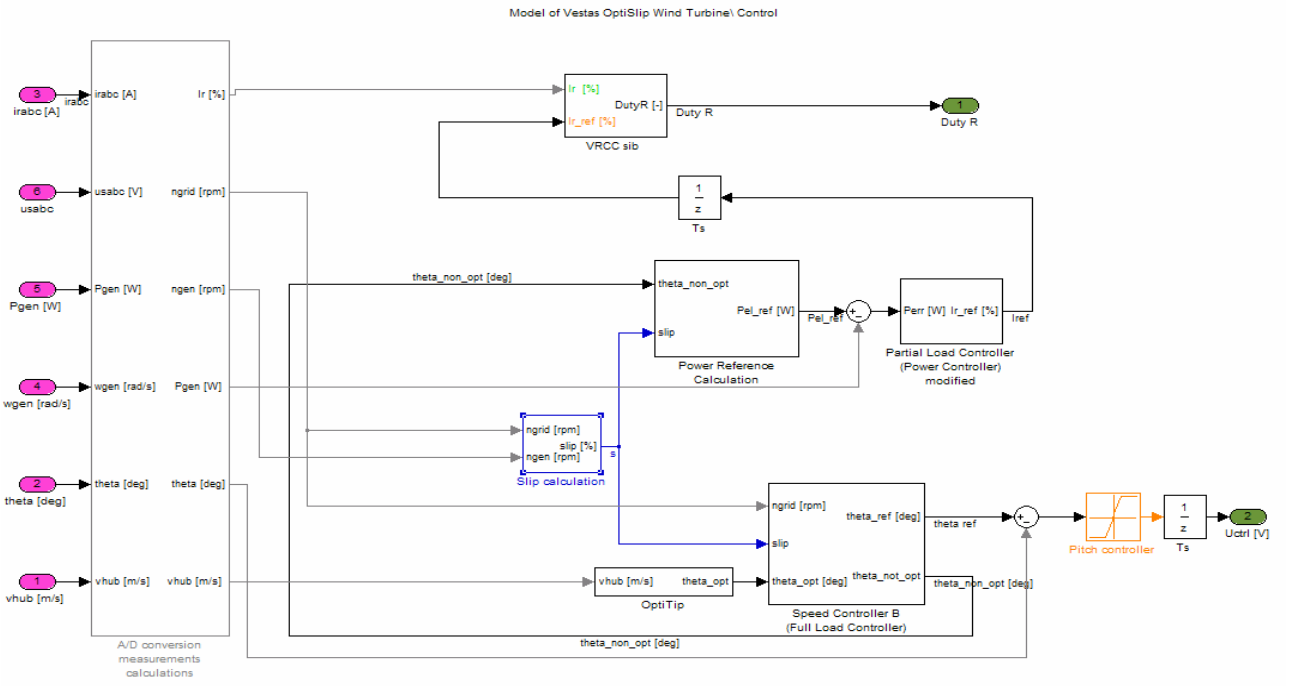

Figure 126 Control of the complete OptiSlip turbine model in Matlab/ Simulink

The inputs of the turbine model are different wind speeds and the electrical grid voltage. The grid voltage is a three-phase voltage with a frequency of 60 Hz. For the simulation a three-phase generator model including the saturation of the main and leakage inductance has been used and compared to a Vestas pre-developed validated OptiSlip model exclusive generator, transformer or grid elements.

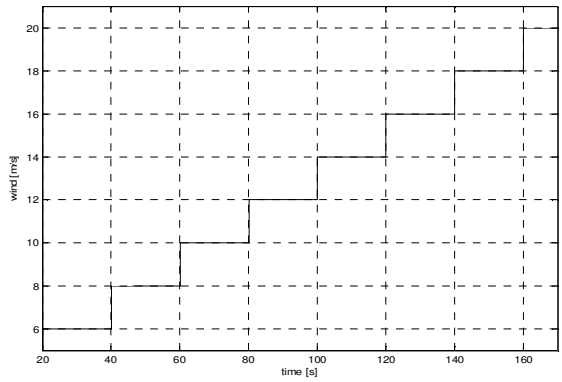

Figure 127 Wind input in m/s

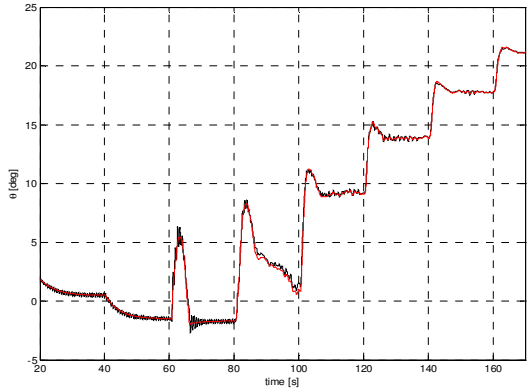

Figure 128 Pitch angle theta [deg] red - validated simple Vestas simulation model; black – new wind turbine model

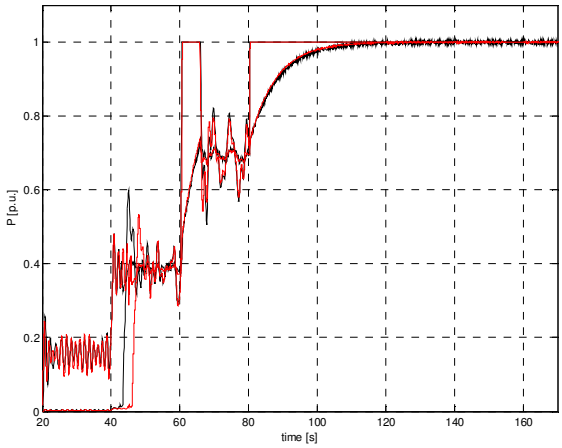

Figure 129 Power controller reference value and feedback for red - validated simple Vestas model; black – new wind turbine model

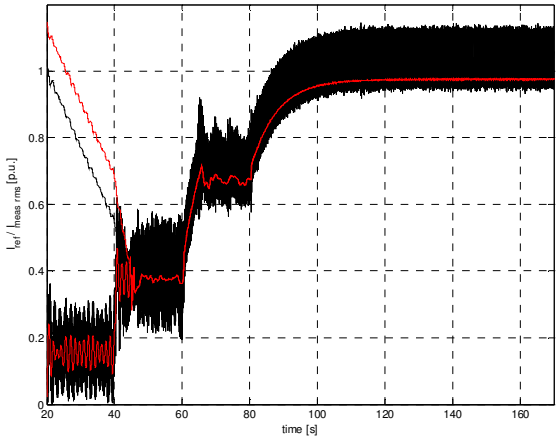

Figure 130 VRCC controller feedback rotor currents – red validated simple Vestas model; black – new wind turbine model

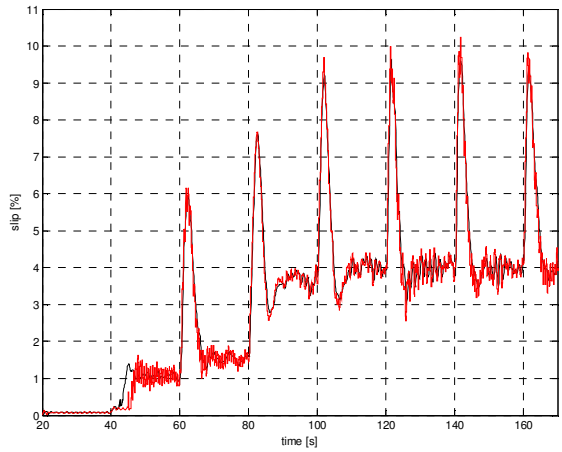

Figure 131 Slip [%] red – validated simple Vestas model; black – new wind turbine model

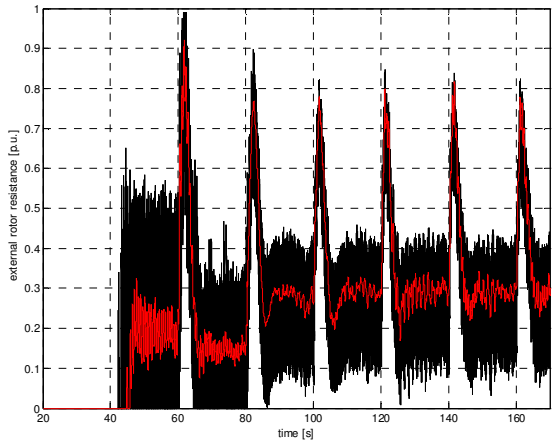

Figure 132 External rotor resistance fro red – validated simple Vestas model; black – new wind turbine model

In the following steady state validation are made. In Table 7-1 values simulated with the V80 VRCC Optislip® wind turbine are shown.

Wind speed [m/s]	P [MW]	speed [rpm]	I rotor [%]	Duty C.	Pitch [deg]
6	0.275	1803	14.5	0.30	0.5
8	0.700	1820	34	0.20	-1.5
10	1.25	1828	62	0.13	-1.7
12	1.78	1866	89	0.27	1.4
14	1.80	1872	89	0.28	9.2
16	1.80	1872	89	0.28	13.8
18	1.80	1872	89	0.28	17.8
20	1.80	1872	89	0.28	21.15

Table 7-1: Simulated steady-state operating points with constant wind speed, deduced from the dynamic simulations shown above

The steady state characteristics of an actual V80 1.8 MW turbine are shown in Table 7-2. These values were gathered from the average values taken from available measurement (.VDF) tracks of a real turbine /44/.

Wind speed [m/s]	P [MW]	speed [rpm]	I rotor [%]	Duty C.	Pitch [deg]
4.01	0.091	1807	5.56	0.446	1.65
4.87	0.220	1812	10.89	0.366	1.26
5.32	0.277	1812	13.67	0.333	0.96
6.45	0.428	1815	20.4	0.246	-0.01
8.07	0.723	1820	34.68	0.185	-1.47
8.65	0.778	1821	37.19	0.185	-1.65
9.74	1.26	1828	59.9	0.144	-1.68
10.08	1.53	1839	72.8	0.167	-1.20
10.85	1.79	1869	86.0	0.286	0.25
11.17	1.71	1858	81.4	0.245	1.80
18.87	1.80	1879	85.7	0.335	17.6

Table 7-2: Measured average steady-state operating points

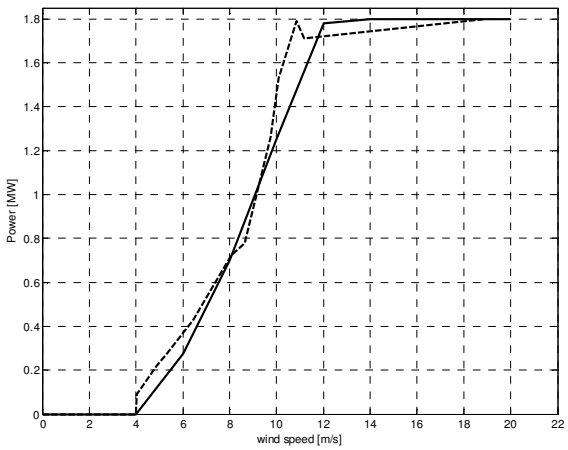

Figure 133 Power curve (simulation – solid line, measured – dotted line)

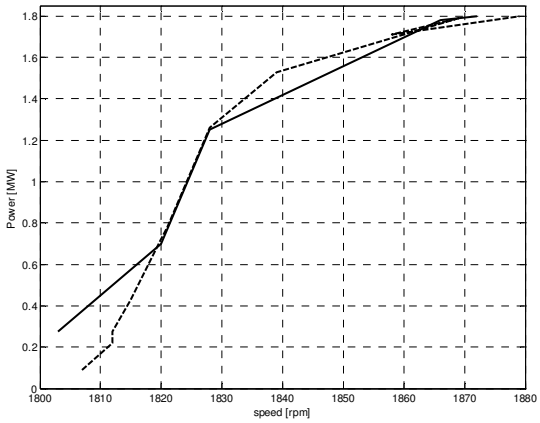

Figure 134 Power speed (simulation – solid line, measured – dotted line)

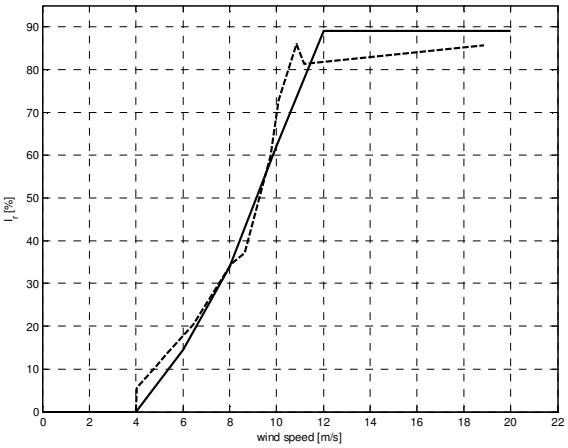

Figure 135 Rotor current –wind speed (simulation – solid line, measured – dotted line)

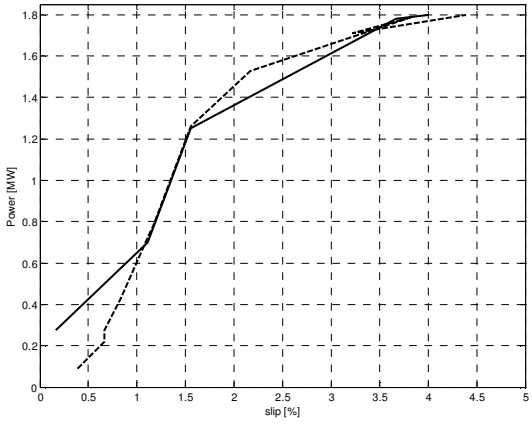

Figure 136 Power slip (simulation – solid line, measured – dotted line)

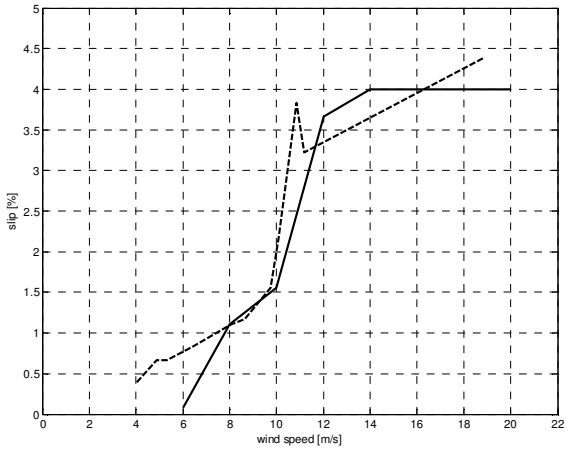

Figure 137 Slip –wind speed (simulation – solid line, measured – dotted line)

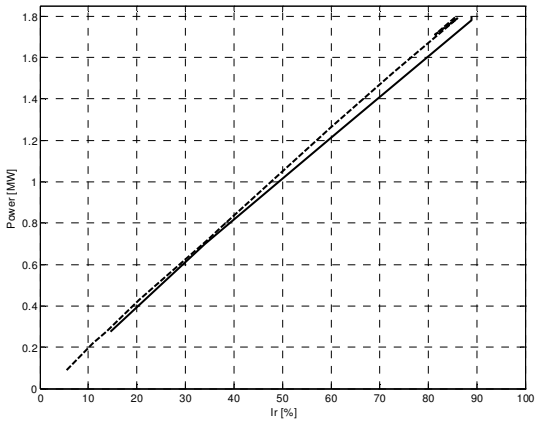

Figure 138 Power – rotor current (simulation – solid line, measured – dotted line)

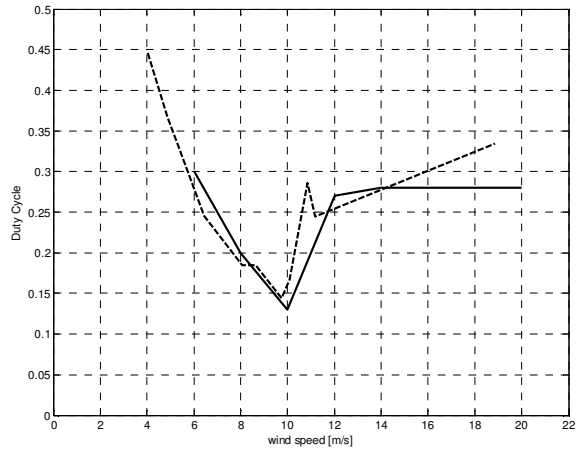

Figure 139 Duty cycle –wind speed (simulation – solid line, measured – dotted line)

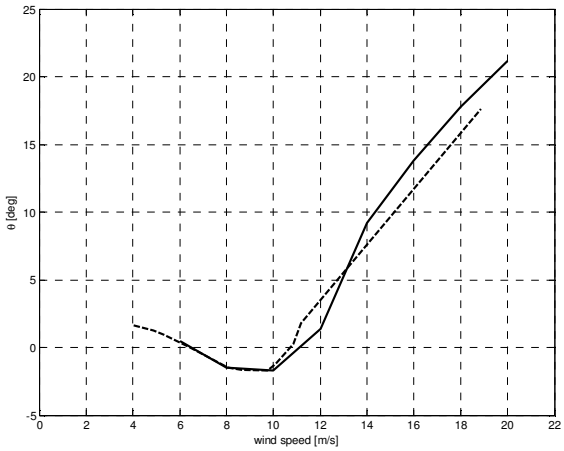

Figure 140 Pitch angle –wind speed (simulation – solid line, measured – dotted line)

7.6 Discussion

The new OptiSlip® turbine model developed in this work shows more oscillations than the validated existing Vestas model /13/ while performing dynamic simulations. There exist a lot of different explanations for this. The existing Vestas model was developed for the different purpose of designing and tuning of the pitch control. The pitch control as outer loop of the whole control is slower than the inner current control loop. The dynamics of the electrical parts have not been of interest for the purpose of pitch control design. Therefore it was sufficient to include a simplified representation of the electrical components. For the present work, with focus especially on electrical dynamics the detailed representation of the electrical components is important, while the control features are identical in the two Optislip® turbine models.

In the Optislip® turbine model developed in this work a clear separation between the modelled parts has been made. The real parts of the turbine, such as generator and drive train are implemented in a continuous time domain with alternating values and the control is represented in the discrete time domain and deals with DC-values. The previous developed Vestas model is based on simplified d, q models, which transforms all alternating values into DC values and is therefore much more stable than the new developed detailed model representation. In order to reduce the oscillations shown in the simulations Figure 127 to Figure 132, some controllers have been improved with an anti windup. The oscillations could be limited to the amount shown in the figures, which is around factor 2 less than before. Furthermore the dynamic limitation of the VRCC Slave PI – controller together with the real generator model leads to mathematical instabilities in Simulink, which causes noise on the signal. Unfortunately a removal or change of this limit has a drastical influence on the behaviour of the whole turbine control. In principle there has been found a good agreement between the two models.

In the second part, steady state simulations from the new OptiSlip® wind turbine model have been compared to the measured average values of a real turbine. The simulated values show good agreement with the real values. Note though, that the model is close to instability, which makes it difficult to get accurate steady state values from the simulation.

Chapter 8

8. Wind turbine with a doubly-fed induction generator control

Nowadays wind turbines equipped with slip-ring induction generators and doubly-fed control are widely used. Vestas introduced their first wind turbine with doubly-fed control, the so called OptiSpeed^{TM} control in 1999 for the wind turbine type V80 2MW. Wind turbines with this control have the advantages of optimizing energy production, minimizing structural loads, limiting noise emission and improvement of the power quality. New challenges gave and give plenty possibilities for improvements in the control and design during this long time usage of this wind turbine concept. Although the control aims have become more complex the basic control from Vestas is built on the principles set forth in the German PhD thesis by D. Arsudis /4/. In Figure 141 a simple sketch of the total Vestas OptiSpeed wind turbine control system is shown. Basically it can be separated into two parts. Firstly the Vestas Converter System (VCS) control, consisting of power controller, rotor current controller and the grid converter controller. The other part is the overall wind turbine control, consisting of speed controller, full-, partial load controller, pitch controller and logic.

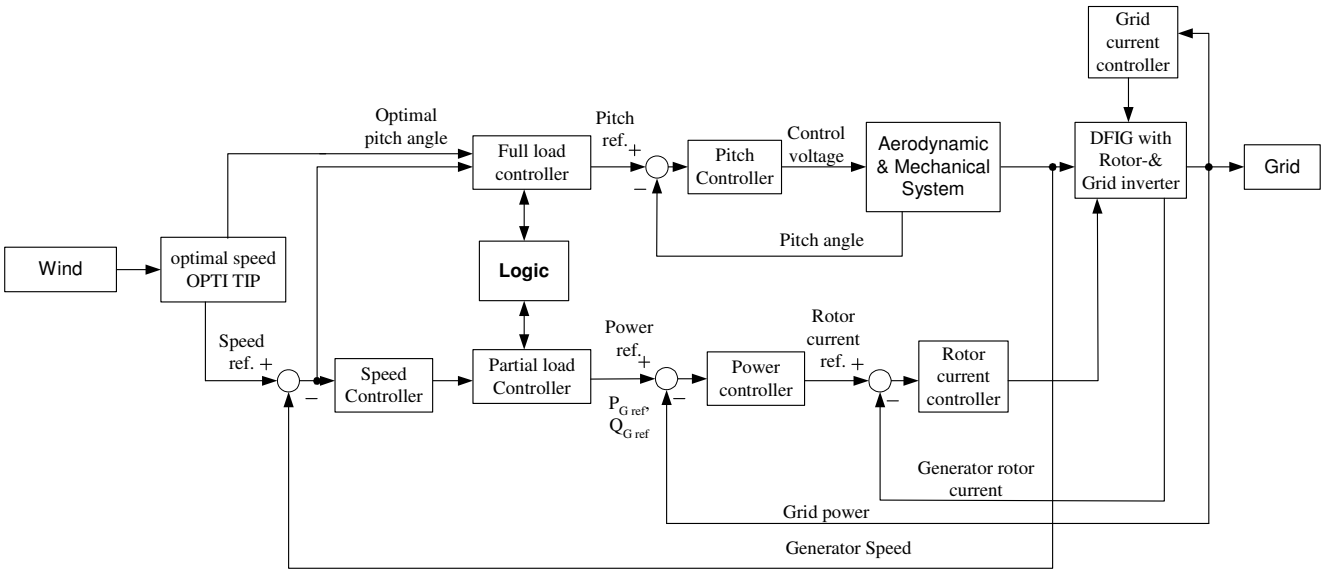

Figure 141 Sketch of the Vestas OptiSpeed control

8.1 The principle of DFIG Control

A usual generator with short-circuit rotor terminals or squirrel-cage is only able to have a minimal rotor speed variation (approx. 1%) dependent on the frequency at the stator terminals of the generator. The Vestas OptiSlip® system already extends this small rotor speed variation range to a variability of 10% as described in the chapters above. Using a doubly-fed generator system allows a variation of the rotor speed from -40% to +30% of the generators synchronous speed, which increases the yearly production approx. 5%

additional to all the other advantages mentioned already in the introduction.
The doubly-fed system, shown in Figure 144 has a converter attached to the rotor terminals of the induction machine. The converter makes it possible to supply or obtain power from the grid through the rotor terminals. This prevents the generator from switching to motor operation while driving at sub synchronous speed. In the so called over synchronous operation the generator's speed is higher than synchronous speed. In this operation power from the stator terminals as well as power from the rotor terminals is supplied to the grid.
The ideal stationary power distribution through the generator is dependent on the slip of the generator as shown in equation (214), (215), (216) and Figure 142, Figure 143.

$$P_M = \omega_r \cdot T_e \tag{214}$$

$$P_S = \frac{P_M}{1+s} = P_M \cdot \frac{\omega_0}{\omega_r} \tag{215}$$

$$P_R = P_M - P_S = P_M \frac{s}{1+s} = s \cdot P_S \tag{216}$$

With: P_M obtained mechanical power through the shaft of the generator
P_S power through the stator of the generator
P_R the power through the rotor of the generator
P_{EL} total to the grid supplied power
ω_0 synchronous speed
ω_r rotor angular speed
s slip ($s > 0, \omega_r > \omega_0$ and $s < 0, \omega_r < \omega_0$)

In sub synchronous operation, when the speed of the generator is below synchronous speed, a part of the stator produced power is fed back into the rotor of the generator through the converter as shown in Figure 142 and Figure 143.

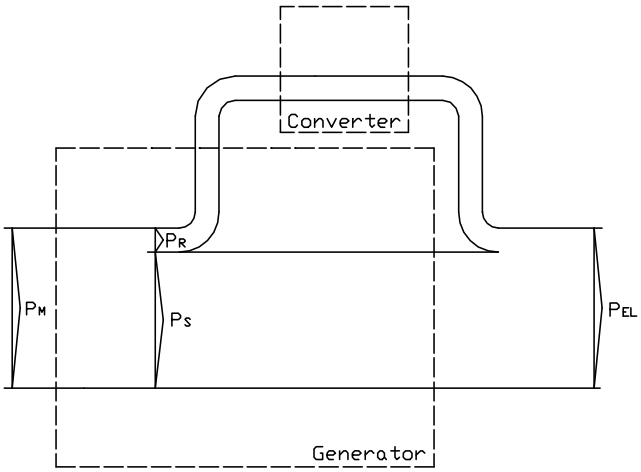

Figure 142: Power flow of an ideal DFIG at over synchronous speed $\omega_r > \omega_0$.

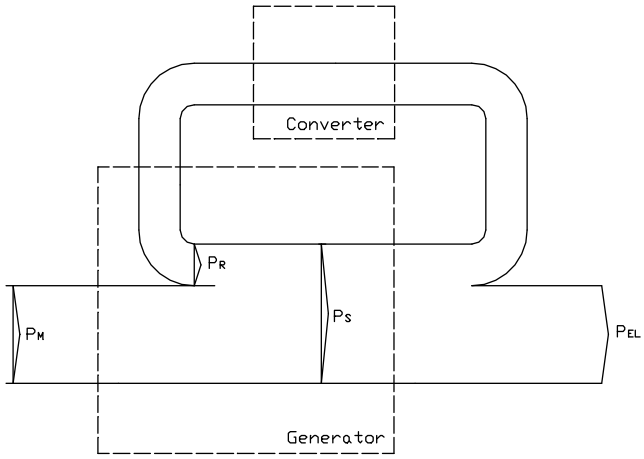

Figure 143 Power flow of an ideal DFIG at sub synchronous speed $\omega_r < \omega_0$

The electrical configuration shown in Figure 144 is the basis for the model of a Vestas wind turbine developed in this chapter. It consists of a 2w3ph autotransformer, a converter, which only will be simplified modelled and the DFIG. The delta-star switch is left out of the

described model, but is easy to include at a later stage.

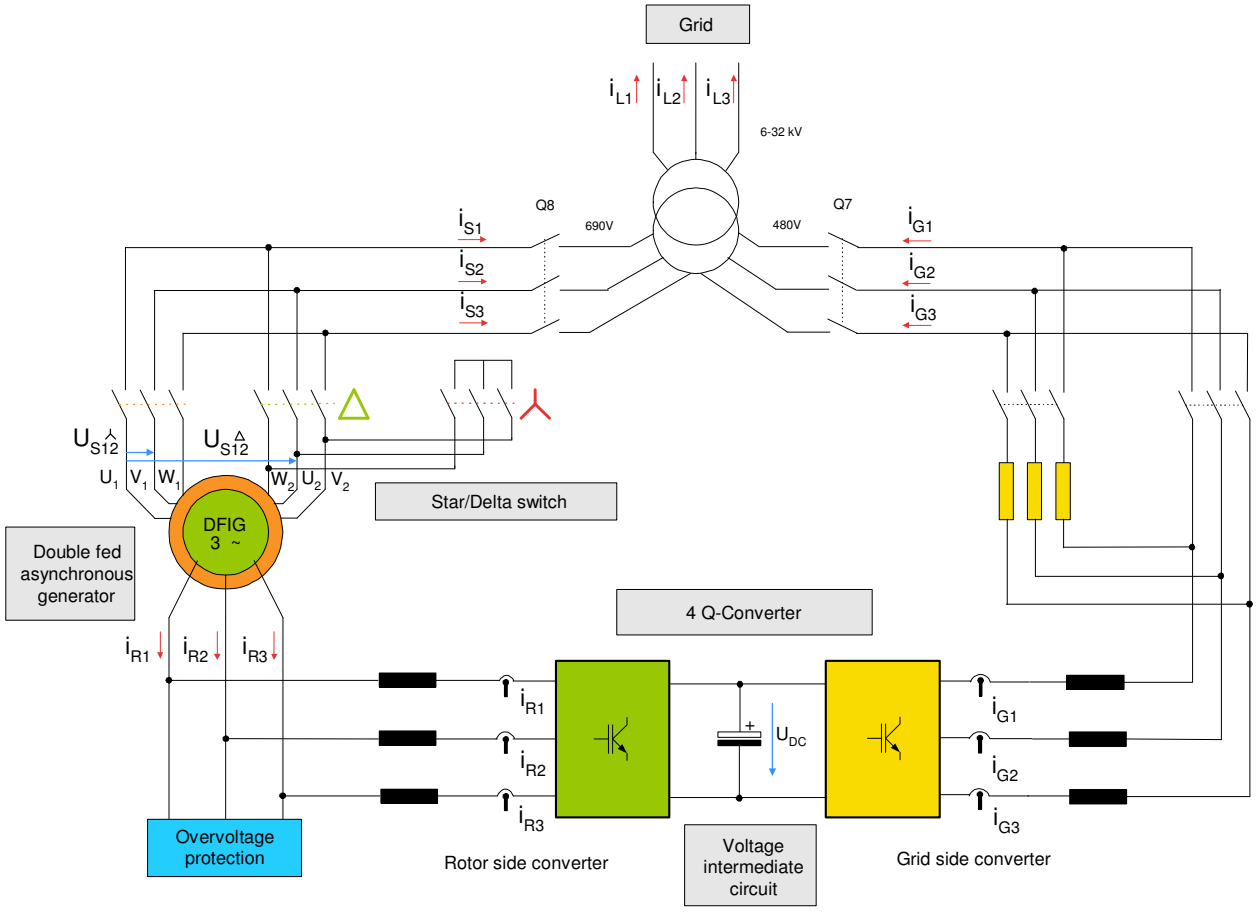

Figure 144 Electrical configuration of the Vestas 2MW OptiSpeed^{TM} turbine

8.2 The DFIG Rotor Converter Control

The active - and reactive power flow of the machine can be controlled through the rotor converter, with the control of the rotor currents. Using the Parks Transformation and orientating all machine equations to the stator field for the control brings mainly two advantages. First of all the alternating time values of current, voltage and flux become DC – values, which are easily to control and secondly it is possible for a decoupled control of active and reactive power, through the two d, q - components.

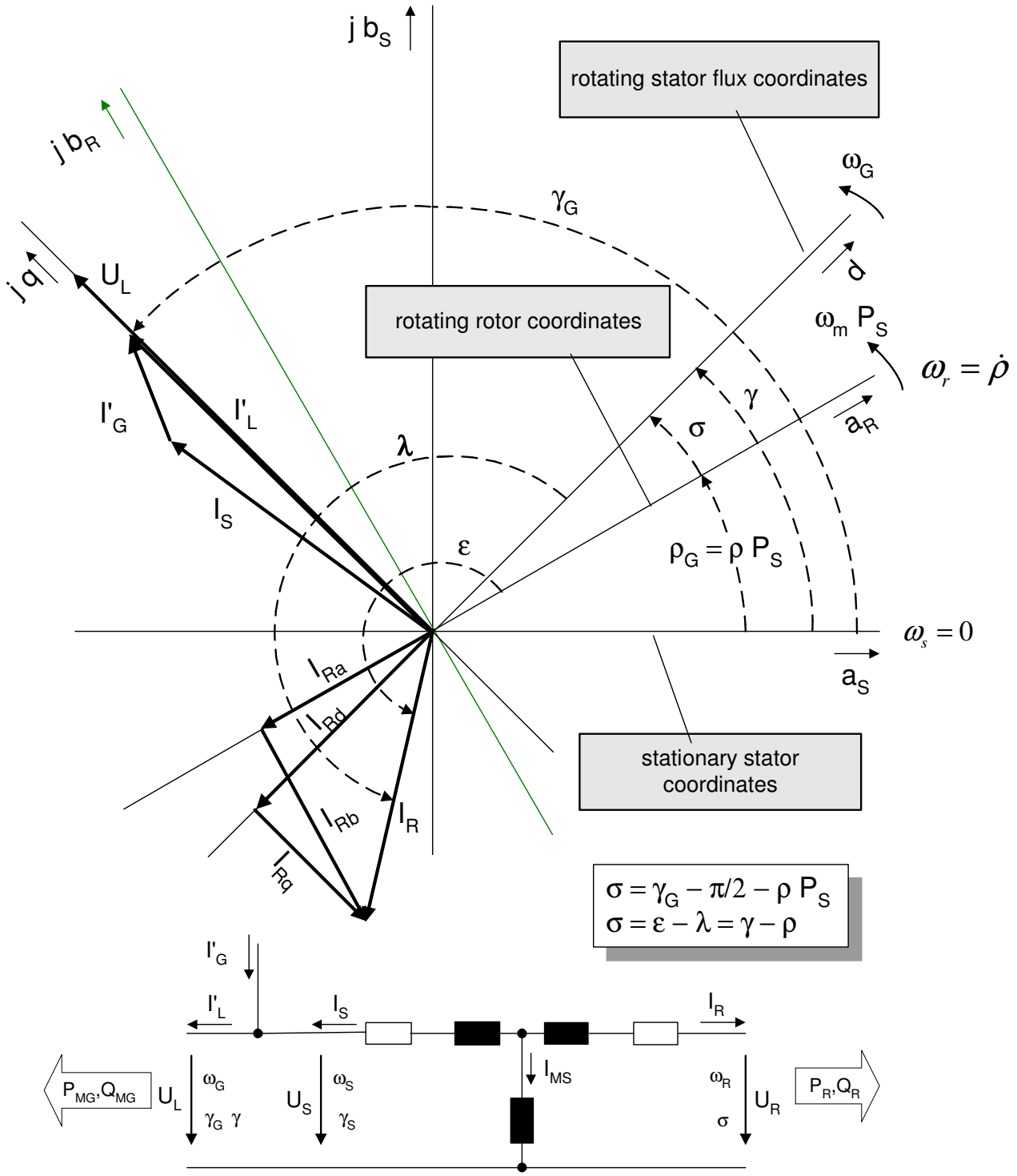

Figure 145 Vector scheme of the doubly fed generator

For the transformation of the machine stator voltage equation, neglecting the zero component, from the stationary stator reference frame into the rotating stator flux coordinate system the equation has to be rotated with the stator flux angle γ

$$\begin{aligned} \underline{u}_s^s &= R_s \cdot \underline{i}_s^s + \frac{d\,\underline{\Psi}_s^s}{dt} \qquad /\cdot e^{-j\gamma} \\ \underline{u}_{sd,q} &= R_s \cdot \underline{i}_{sd,q} + \frac{d}{dt}\underline{\Psi}_{sd,q} + j\dot{\gamma}\underline{\Psi}_{sd,q} \end{aligned} \tag{217}$$

The transformation of the rotor voltage equation, from the rotating rotor reference frame into the rotating stator flux coordinate system the equation have to be turned with the slip angle σ (218). For more detailed explanation about the transformation please go to Appendix 11.3.

$$\begin{aligned} \underline{u}_r^{r'} &= R_r' \cdot \underline{i}_r^{r'} + \frac{d \ \underline{\Psi}_r^{r'}}{dt} \qquad /\cdot e^{-j\sigma} \\ \underline{u}_{rd,q}' &= R_r' \cdot \underline{i}_{rd,q}' + \frac{d}{dt}\underline{\Psi}_{rd,q}' + j \cdot \dot{\sigma} \cdot \underline{\Psi}_{rd,q}' \end{aligned} \tag{218}$$

For the stator flux orientation the necessary angle γ can be derived from the phase angle of the main voltage U_L, whose coordinate system has an negligible small angle difference from the stator flux coordinate system. The main voltage is in synchronism with the stator flux and is shown aligned on the imaginary q axis of the stator flux coordinate system. The measured rotor currents have slip-frequency and are related to the rotating rotor coordinates with the angle ε. Orientation to the rotating stator flux coordinate system has to be done with the slip angle σ, which can be derived from the main grid angle λ and the rotor current angle ε as shown in Figure 145 and (219).

$$\begin{aligned} \gamma &= \gamma_G - \frac{\pi}{2} \\ \sigma &= \varepsilon - \lambda = \gamma - \rho_G \end{aligned} \tag{219}$$

From the Stator flux equation (220) in d, q stator flux coordinates the relation between the stator and rotor current can be derived /4/, where σ_s is the stator leakage factor.

$$\underline{\Psi}_{sd} = (L_{\sigma s} + L_m) \cdot \underline{i}_{sd,q} + \ L_m \cdot \ \underline{i}_{rd,q}' = (1 + \sigma_s) \cdot L_m \cdot \underline{i}_{sd,q} + \ L_m \cdot \ \underline{i}_{rd,q}' \tag{220}$$

Separation of equation (220) into their components and using the magnetizing current $i_{ms} = \Psi_s / L_m$ the following equation can be derived.

$$\begin{aligned} d: \qquad i_{sd} &= \frac{i_{ms} - i_{rd}'}{(1 + \sigma_s)} \\ q: \qquad i_{sq} &= \frac{-i_{rq}'}{(1 + \sigma_s)} \end{aligned} \tag{221}$$

The active and reactive power calculated with the d, q components are shown in equation (222) and (223). The stator voltage d-component is very small and can be neglected. The q – component of the stator voltage can be approximated to be constant under rated condition. Therewith the active power can be controlled by the q-component of the stator current and the reactive power can be controlled by the d-component of the stator current.

$$P_s = \frac{3}{2} \cdot \mathrm{Re}\left\{ \underline{u}_s^{\ *} \cdot \underline{i}_s \right\} = \frac{3}{2}\left(\underbrace{u_{sd} i_{sd}}_{\approx 0} + u_{sq} i_{sq} \right) \tag{222}$$

$$Q_s = \frac{3}{2} \cdot \mathrm{Im}\left\{ \underline{u}_s^{\,*} \cdot \underline{i}_s \right\} = \frac{3}{2} \left(\underbrace{u_{sd} i_{sq}}_{\approx 0} - u_{sq} i_{sd} \right) \tag{223}$$

Like the power, the torque equation can be expressed in stator flux coordinates. Since the d-axis of this coordinate system is aligned with the stator flux, the q-component of the stator flux is zero and therewith the torque can be controlled as the active power through the q-component of the stator current.

$$T_e = \frac{3}{2} \cdot p_p \cdot \mathrm{Im}\left\{ \underline{\Psi}_s^{s^*} \cdot \underline{i}_s^{s} \right\} = \frac{3}{2} \cdot p_p \left(i_{sq} \cdot \Psi_{sd} - \underbrace{\Psi_{sq} \cdot i_{sd}}_{=0} \right) \tag{224}$$

Using equation (221) in equation (222) and (223) the power is expressible with the rotor currents.

$$P_s = -\frac{3}{2} \cdot \frac{u_{sq}}{(1+\sigma_s)} \cdot i_{rq}^{'} \sim -i_{rq} \tag{225}$$

$$Q_s = \frac{3}{2} u_{sq} \frac{-i_{ms} + i_{rd}^{'}}{(1+\sigma_s)} \sim i_{rd} \tag{226}$$

The power controller is a PI-controller, with input the calculated grid power error and as output the reference rotor current for the rotor current control. Thereby the power controller constitutes the outer loop as a cascaded control strategy shown Figure 146.

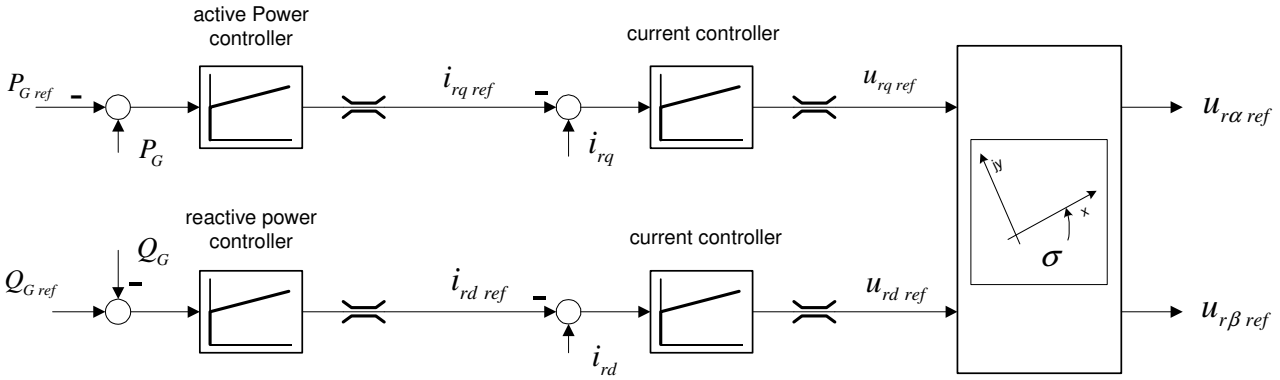

Figure 146 Power and rotor current control for DFIG

The rotor controller is as well a PI-controller with input the rotor currents error and output is the rotor voltage which is used as input to the generator model.

$$\underline{\Psi}_{rd,q}^{'} = (L_m + L_{\sigma r}^{'}) \cdot \underline{i}_{rd,q}^{'} + L_m \cdot \underline{i}_{rd,q} = (1+\sigma_r) \cdot L_m \cdot \underline{i}_{rd,q}^{'} + L_m \cdot \underline{i}_{sd,q} \tag{227}$$

Separation of equation (218) into their components and using the magnetizing current $i_{ms} = \Psi_s / L_m$, the rotor time constant $T_r = L_r / R_r$ and the total leakage factor $\sigma_t = 1 - 1/\left[(1+\sigma_s) \cdot (1+\sigma_r)\right]$ the following equation for the rotor current can be derived /4/.

$$\sigma_t T_r \frac{d}{dt} i_{rd} + i_{rd} = \frac{u_{rd}}{R_r} + (\dot{\gamma} - \dot{\rho}) \sigma_t T_r \cdot i_{rq} - (1 - \sigma_t) T_r \frac{d}{dt} i_{ms} \tag{228}$$

$$\sigma_t T_r \frac{d}{dt} i_{rq} + i_{rq} = \frac{u_{rq}}{R_r} + (\dot{\gamma} - \dot{\rho}) \sigma_t T_r \cdot i_{rd} - (1 - \sigma_t) T_r \frac{d}{dt} i_{ms} \tag{229}$$

Thereby the PI-controller for the current control can be designed. The input of the current controller is the rotor current error and output the rotor voltage.

8.3 The DFIG Grid Converter Control

The main task of grid converter control is to control the DC voltage of the DC link, while exchanging power with grid. Changes of the DC link voltage will occur e.g. when changing the generator torque. The rotor converter control supplies power into the rotor of the generator or the opposite. The power exchange with grid can be controlled by control of the grid current I_L or the grid converter current I_G (230), (231).

$$P_G = \frac{3}{2} \cdot \mathrm{Re}\left\{ \underline{u}_L^* \cdot \underline{i}_L \right\} = \frac{3}{2} |\underline{u}_L| i_{Lq} \tag{230}$$

$$Q_G = \frac{3}{2} \cdot \mathrm{Im}\left\{ \underline{u}_L^* \cdot \underline{i}_L \right\} = -\frac{3}{2} |\underline{u}_L| i_{Ld} \tag{231}$$

If the grid current and the power exchange with the grid is not corrected fast enough the DC – link voltage will decrease or increase. A consequence of a decreased DC voltage can lead to a failure of the generator control or an increased current, which could lead to a damage of the power electronic modules. The increase of the DC voltage can lead to overloading of the DC link capacitor, which can give hard ware damages and a loss of control capabilities of the grid control.
In Figure 147 a schematic of the grid converter with the DC link filter and the grid voltage are shown.

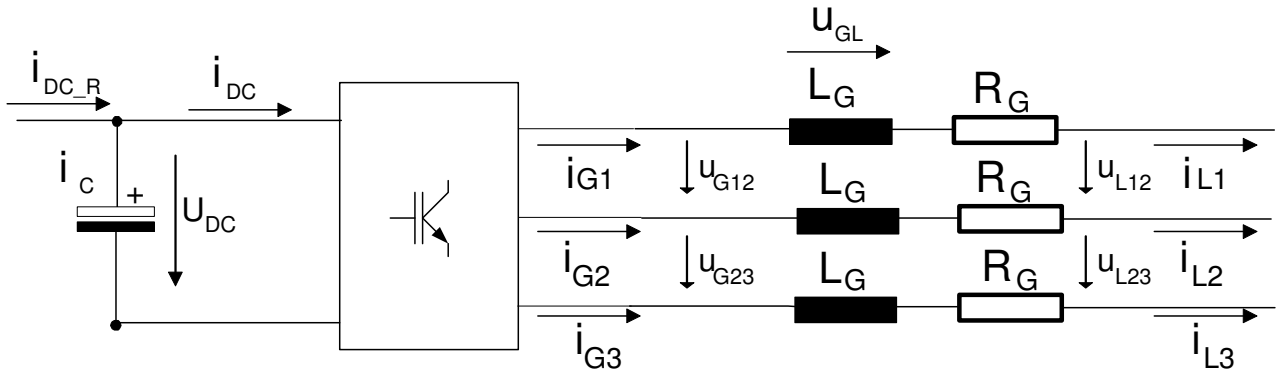

Figure 147 Grid inverter; variables in operation during power supply to the grid

The current through the DC-link capacitor and thereby the DC-link voltage can be calculated from the rotor power of the generator and the grid power (232), (233).

$$i_C = i_{DC\_R} - i_{DC} = \frac{P_R}{u_{DC}} - \frac{P_G}{u_{DC}} \tag{232}$$

$$\frac{d}{dt}u_{DC} = \frac{i_c}{C} = \frac{1}{C}\cdot\left(i_{DC\_R} - i_{DC}\right) = \frac{1}{C}\cdot\left(\frac{P_R}{u_{DC}} - \frac{P_G}{u_{DC}}\right) \tag{233}$$

The grid converter voltage u_G for the grid power calculation can be achieved from the main grid voltage u_L as described with equation (234).

$$\underline{u}_G = R_G \cdot \underline{i}_G + L_G \cdot \frac{d}{dt}\underline{i}_G + \underline{u}_L \tag{234}$$

Transforming the voltage equation with the grid angle gamma into the grid coordinates rotating reference frame as shown in Figure 148 and after separation into their real and imaginary part the equations for the control path are achieved /4/.

$$T_L \frac{d}{dt} i_{Gd} + i_{Gd} = \frac{u_{Gd}}{R_G} + \dot{\gamma} T_G \cdot i_{Gq} \tag{235}$$

$$T_L \frac{d}{dt} i_{Gq} + i_{Gq} = \frac{u_{Gq}}{R_G} - \dot{\gamma} T_G \cdot i_{Gd} - \frac{|\underline{u}_L|}{R_G} \tag{236}$$

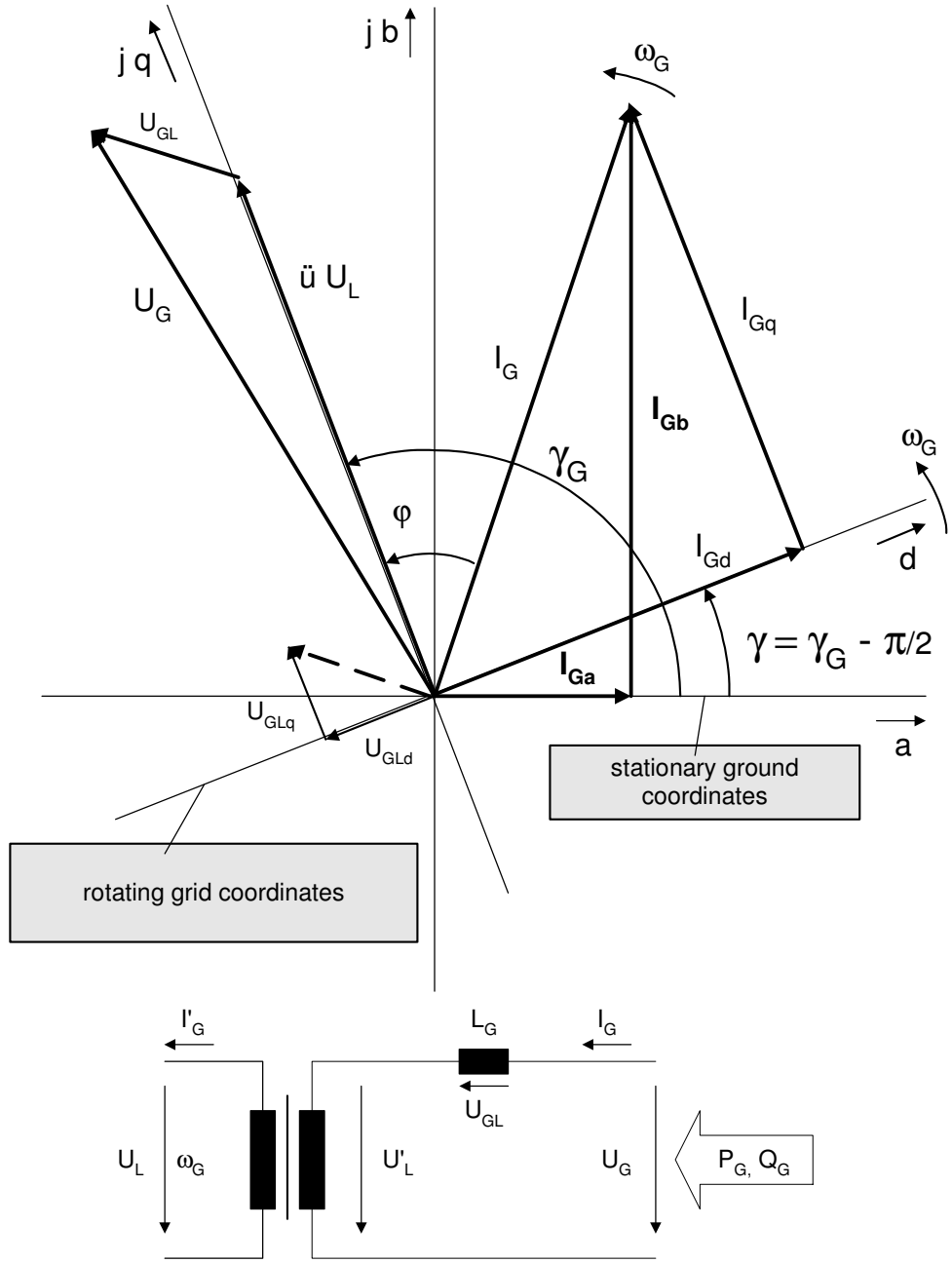

Figure 148 Vector scheme of the grid side inverter

The DC link voltage control is the outer loop of the cascaded control structure shown in Figure 149. The output of the DC-link voltage control gives the input to the grid current controller.

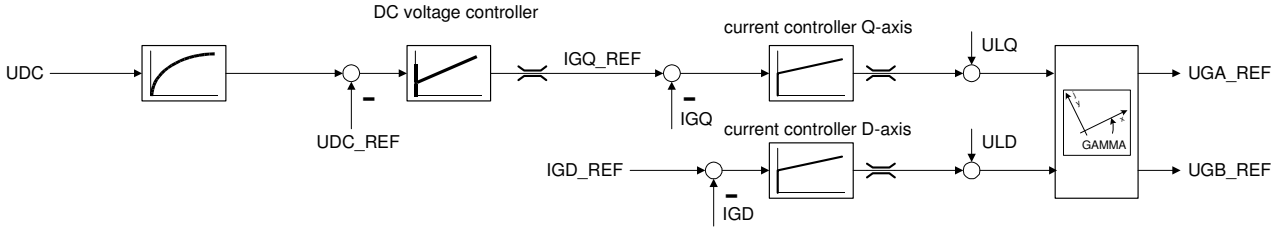

Figure 149 DC-link voltage control structure

8.4 Simulations with the rotor- and grid controller

The following simulations are made with a machine model including all saturation effects, and controlled by the previously discussed rotor inverter control, while the grid converter control secures the stability of the DC-link voltage. In the simulation dynamics caused by short term differences in the DC-link are included. Mechanical dynamics are implemented with a one mass system representing the generator shaft. Two different simulations will be discussed to show functionality of the two control structures. In the simulation a power step at constant speed and a speed step on the generator axes at constant power are initiated. The controller parameters are taken of a real Vestas V80 2 MW wind turbine.

8.4.1 Simulation of power step from partial load to full load

The input grid voltage during these simulations is a constant stiff input Figure 150. At first a step from 0.75 of rated power up to rated power of the 2MW machine is made Figure 151, while the speed is controlled to its rated value Figure 152.

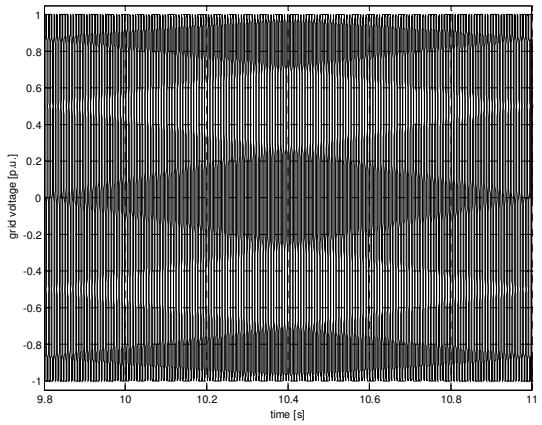

Figure 150 Constant grid voltage during power step

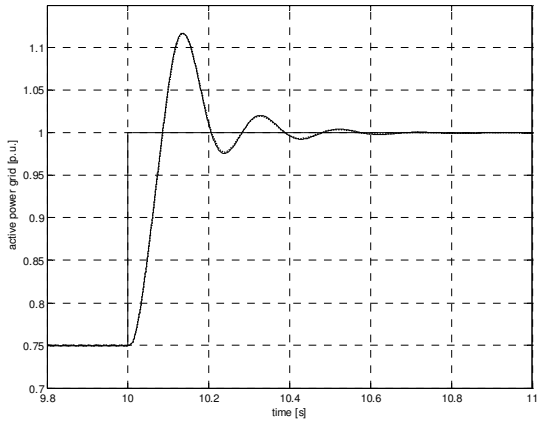

Figure 151 Grid power reference and feedback of the power step

The power step results in a short speed oscillation resulted from the generator reaction torque to the power step seen in Figure 152. The reaction torque is limited as the generator power is limited through the current limit seen in Figure 157 and Figure 158.

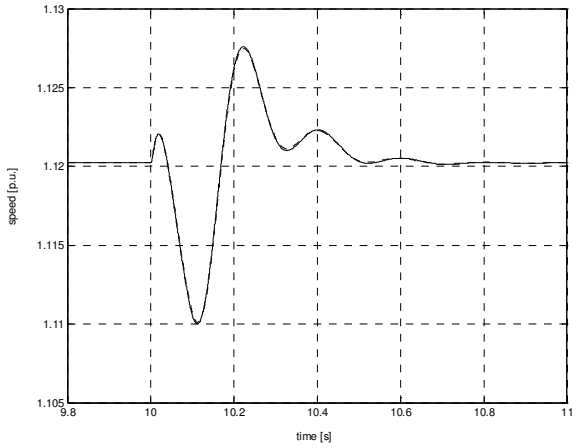

Figure 152 Generator speed during the power step

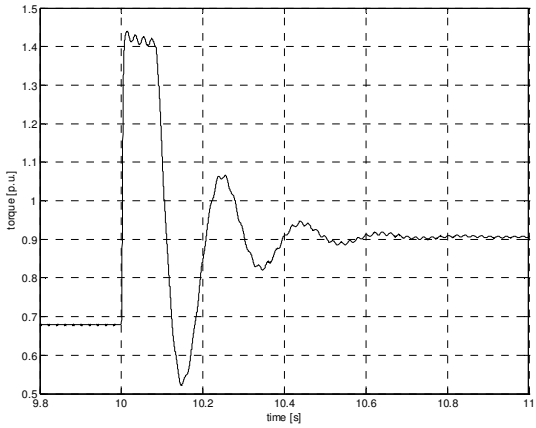

Figure 153 Generator reaction torque to the power step

The reactive power reference is set to zero, though a short reactive power exchange with the grid occurs during the power step. It is to notice that the exchange of reactive power with the grid for the simulation with the machine model including all saturation effects (dotted line in Figure 154) is smaller than with the machine model without saturation effects.

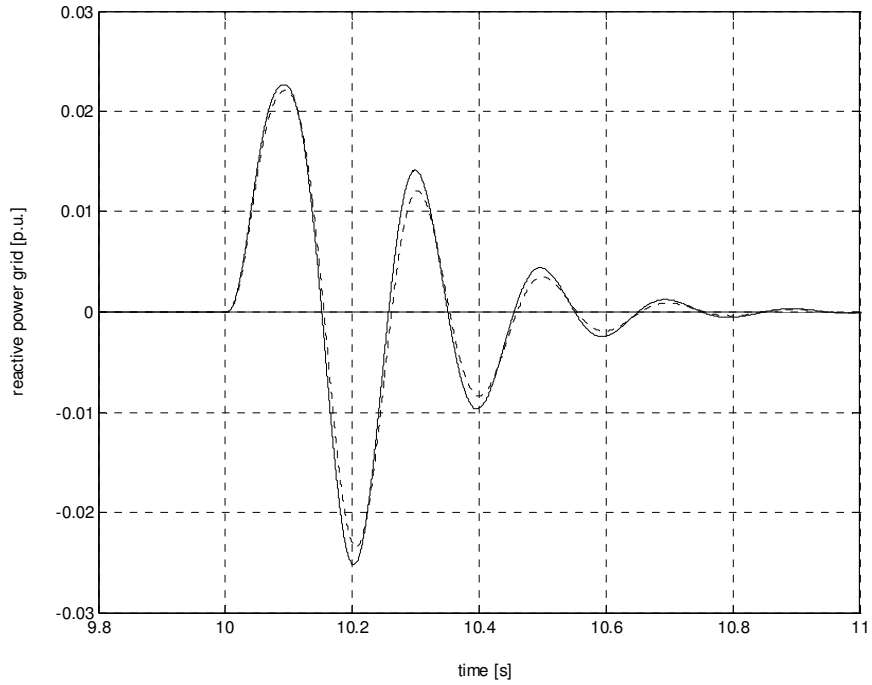

Figure 154 Reactive grid power reference and feedback during VCS-test simulation

The generator active power and the active power of the grid converter sum up to the controlled active grid power. The exchanged power through the grid converter with the grid is a smaller than with the generator rotor exchanged power the through the rotor converter. This is related to the losses in the converter, which are due to the simplified model very small.

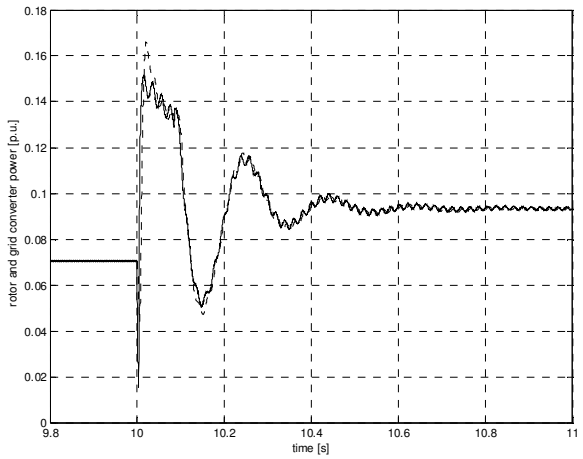

Figure 155 Generator rotor power (dotted line) and grid converter power (solid line)

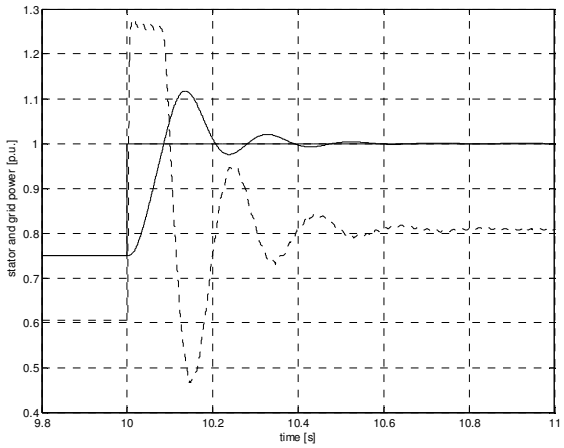

Figure 156 Grid power reference, feedback (solid line) and generator stator power (dotted line)

The supplied power from the stator is limited due to the limit in the rotor current during the dynamic oscillation initiated by the power step.

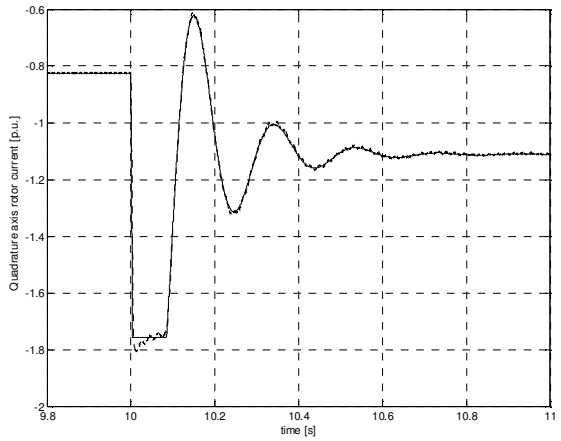

Figure 157 Quadrature axis rotor current reference (solid line) and feedback (dotted line)

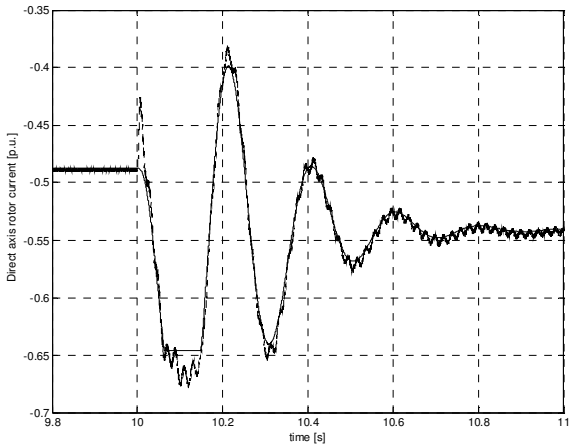

Figure 158 Direct axis rotor current reference (solid line) and feedback (dotted line)

During the power exchange through the converter, the DC-link voltage is controlled to its rated value as shown in Figure 159.

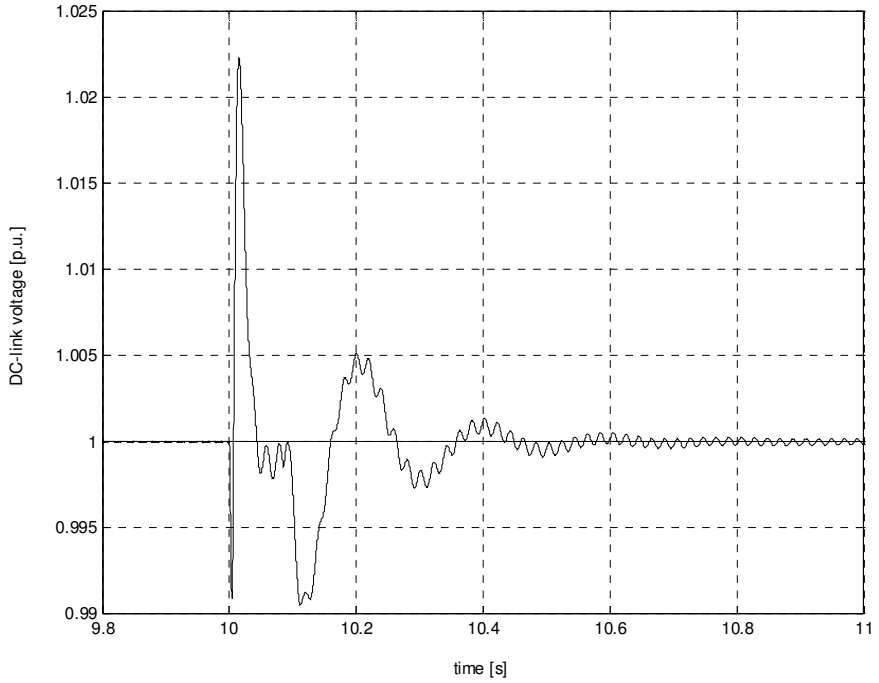

Figure 159 DC-link voltage reference and feedback value

8.4.2 Simulation of a speed step

A speed step from sub-synchronous to over-synchronous speed during the rated power production is simulated. The input grid voltage is kept constant as in the first simulation.

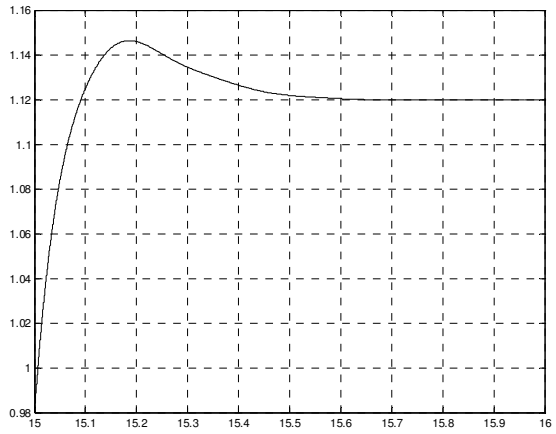

Figure 160 Generator speed step response

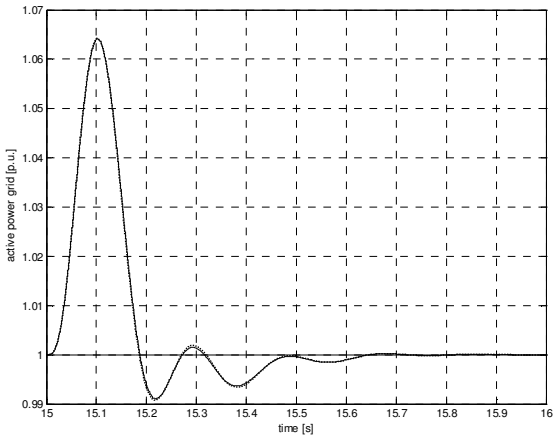

Figure 161 Grid active power reference and feedback during the speed step

The generator reaction torque is shown in Figure 162. During the speed step the current limits are not reached and the power and the generator reaction torque are not limited, as during the power step simulation. The reactive power exchanged with the grid is greater during the speed step as during the power step. Thereby the reactive power oscillation simulated with the machine model including all saturation effects (dotted line) is bigger than the oscillation of the machine model without saturation effects seen in Figure 163.

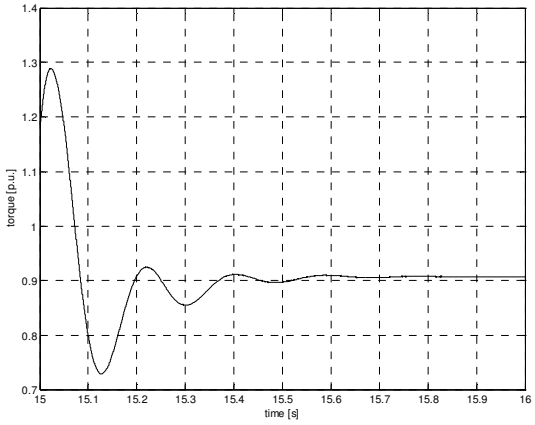

Figure 162 Generator reaction torque

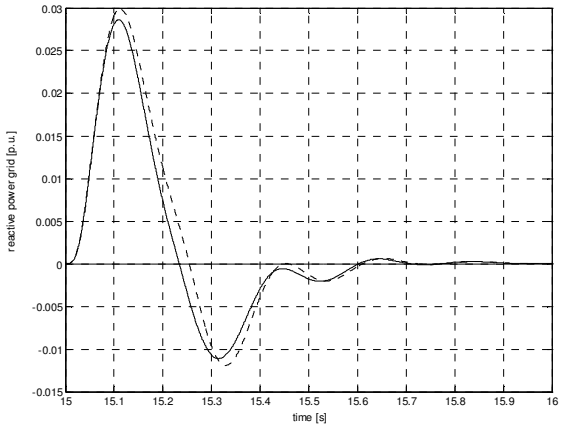

Figure 163 Grid reactive power reference and feedback during the speed step

The differences between the grid converter power and the generator rotor power are again shown in Figure 165. The rotor power compensates for the oscillations in the stator power so that the grid power is controlled to the rated power as seen in Figure 164.

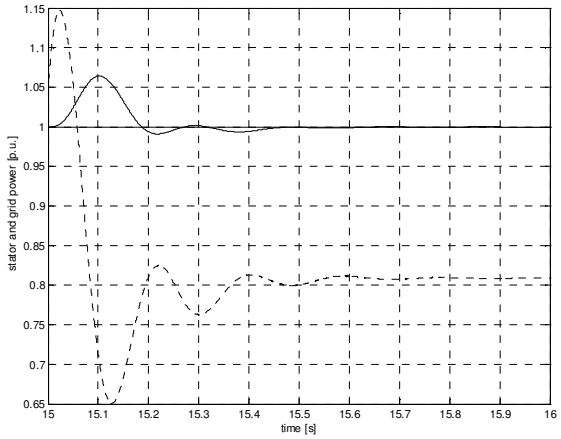

Figure 164 Generator stator power (dotted line) and grid power during (solid line) speed step

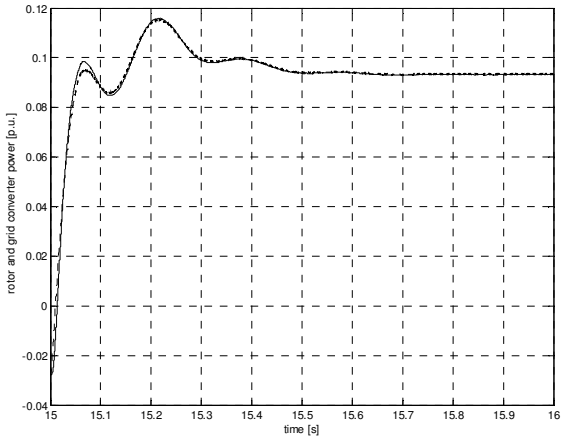

Figure 165 Grid converter power (dotted line) and generator rotor power (solid line) during speed step

In the same way as during the power step simulation, the speed step leads to a dynamic exchange of power through the converter. Therefore the DC-link voltage reacts to the short time changes as well seen in Figure 166.

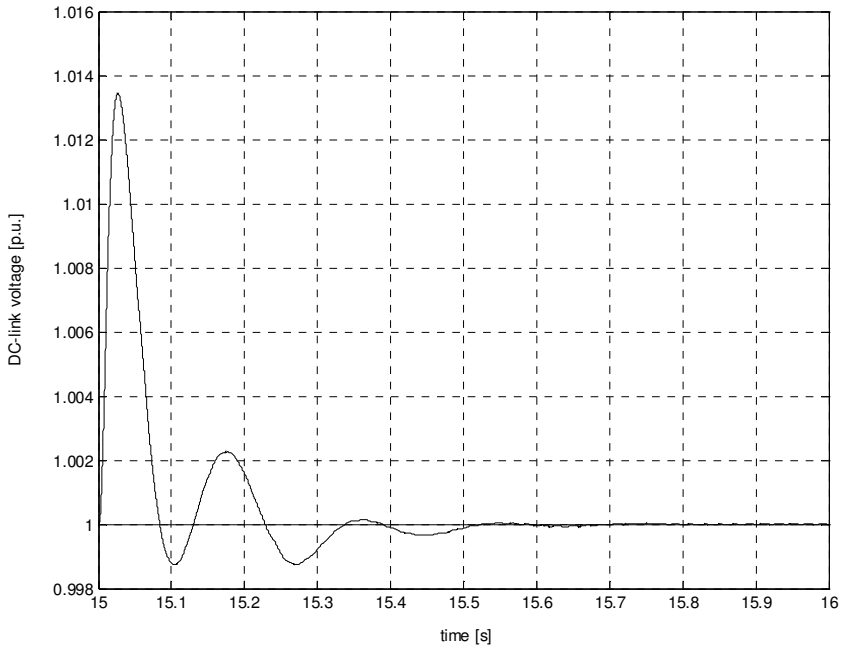

Figure 166 DC-link voltage reference and feedback signal

8.4.3 Validation of the DFIG control system

The following graphs show the measured grid current, grid voltage and DC voltage during a voltage dip test of a 2MW machine in a test bench. The measured line stator voltage depicted in Figure 167 is used as input for the model to simulate the case with the developed DFIG control system model.

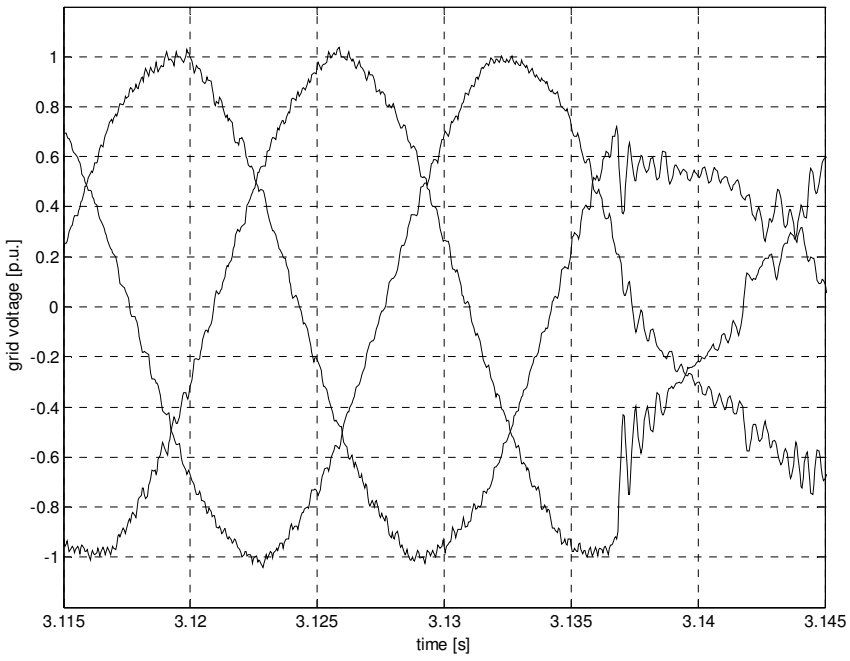

Figure 167 Measured stator voltage from a 2MW test bench

The active power reference is set to the rated power output and the reactive power reference is given to zero. The simulated active power signal is difficult to identify in Figure 168, because it is hidden behind the measured signal. The reactive power in Figure 169 shows the same behaviour.

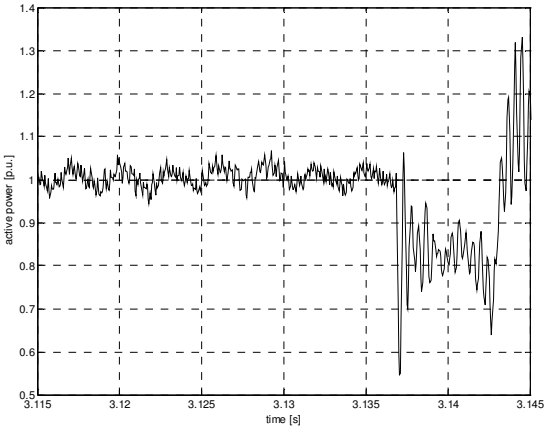

Figure 168 Measured active power p.u. (solid line) and simulated (dashed line) in the test bench

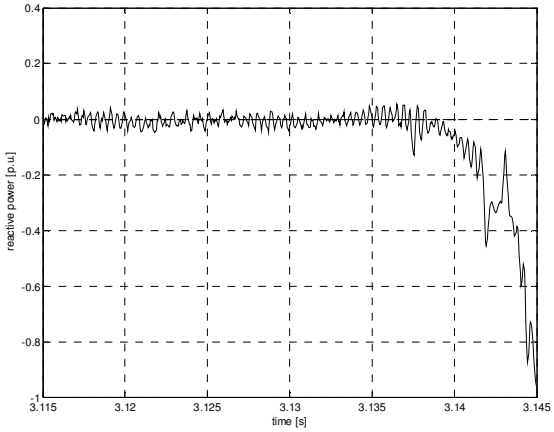

Figure 169 Measured (solid line) and simulated (dashed line) reactive power p.u.

In Figure 170 the DC-link voltage before and after the voltage dip is shown. The DC link voltage starts rising immediately after the decrease of the grid voltage. The internal protection system starts a disconnecting procedure after reaching 1.125 of the rated DC-voltage. This limit is reached at 3.142s and the over voltage protection circuit (OVP) will start operation immediately because the disconnection of the whole system is delayed due to delays caused by physical contactor operation time during initiation and opening. A non interruptible current, driven by the inductances in the circuit, causes a further rise of the converters DC-link voltage.

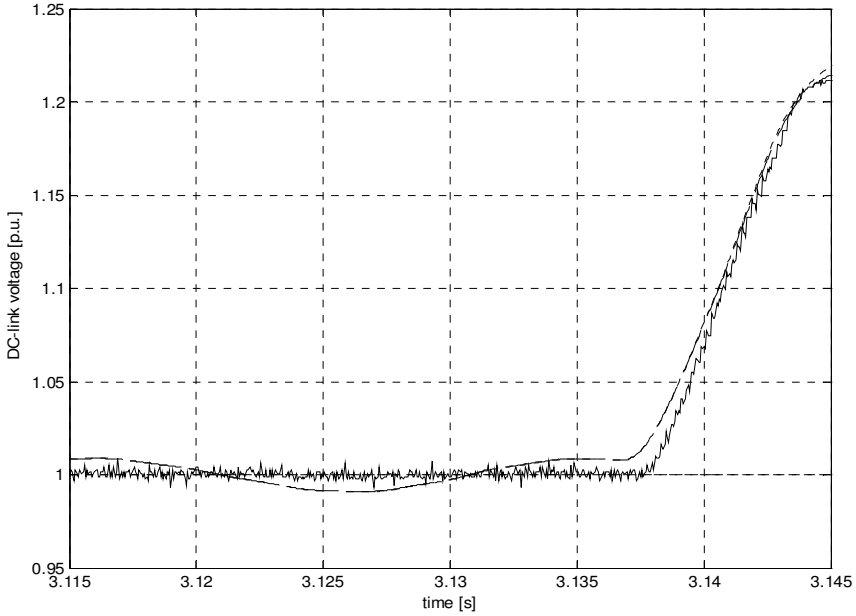

Figure 170 DC-link voltage measured (solid line), simulated with machine model including saturation effects (dashed line) and simulation with machine model without saturation effects (dotted line)

In Figure 171 the stator currents of the generator are shown. The simulated values follow the measured current in the steady state with an error less than 1%. With the voltage dip the protection devices are activated. This changes the current circuit and the current probes are not detecting the full current anymore, which causes the discrepancy between the measured stator current and the simulated current values. The considered over voltage protection can be seen in the end of the shown grid current plot shown in Figure 171.

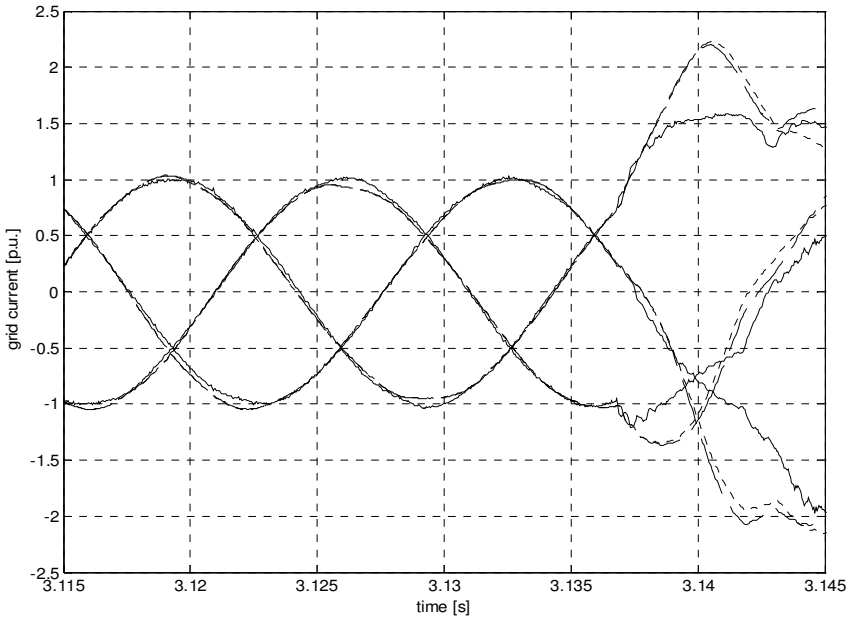

Figure 171 Grid current measured (solid line), simulated with machine model without saturation effects (dotted line) and simulation using machine model with saturation effects (dashed line)

8.4.4 Discussion of the simulation results

The simulated power step and speed step show the functionality of the doubly-fed induction generator control system, which consists of the grid – and rotor converter control. The different controllers have been able to control the signals to their reference values in both cases, which are extreme situations and are not likely to occur in reality. It has been shown; that the control operates satisfactorily in partial and full load operation. A fine tuning of the control parameters would be advisable to improve the speed of the control during the fast oscillation. Using a simplified converter model instead of a fixed DC-link voltage gives the possibility for a more realistic behaviour, since power from the rotor of the generator through the converter is supplied back into the stator of the generator. A good example for the importance of this possibility is in the simulated case of the power step. While the rotor currents are limited and therewith the power of the generator is limited as well, the power supplied through the converter equalizes this nonlinearity. It is not possible to see the limit and strong oscillation in the total grid power and therewith in the grid. Using the stator power as power supplied to the grid instead of the sum of stator and rotor power, would give a wrong impression about the wind turbines behaviour and power quality on the grid.

The simulated values done with the measured input approve the usability of the developed model. Simulated model values show less than 1% difference to the measured values and lies thereby inside the measurement tolerance band. It is to notice there is only a minimal influence of the saturation effects during the doubly fed operation. In the doubly fed operation the influence of machine effect seems negligible and the control is able to compensate for the nonlinearities in the machine. The characteristics of the generator come forward again in failure situation, especially when the control is disabled and the generator is operating with short circuit rotor terminals, as it is already indicated in Figure 171. The influence of machine saturation effects will be studied further during the simulations with the complete OptiSpeed Turbine model in failure situations.

8.5 The OptiSpeed^{TM} wind turbines overall control strategy

Although the optimal way to gain energy from the wind is a major control target it plays especially a role in partial load operation, under the absence of noise restrictions, while in the full load the power is limited and the optimal operation is irrelevant.
Maximum energy from the wind is obtained when the rotor is operating at its aerodynamic optimum. The aerodynamic optimum is reached, if the tip-speed ratio λ_{opt} and the pitch angle ϑ_{opt} are at their optimum. To keep the tip-speed ratio at its optimum the rotor with the radius R has to be operated with a rotor speed ω_{rot} proportional to the wind velocity v_w (237).

$$\omega_{rot} = \frac{\lambda_{opt} v_w}{R} \tag{237}$$

The stationary power obtained by the blades on this optimum condition is:

$$P_{w,el} = \frac{1}{2}\eta\rho_{air}\pi R^2 c_{P,opt} v_w^3 \tag{238}$$

However, it is not always beneficial or possible to operate the turbine at a point for maximal energy gain. The operational wind speed area is limited, due to the turbines operation area. The operation area can be defined by introducing rotor speed limits. Between the minimum and rated rotor speed $[\omega_{\min}, \omega_{rtd}]$ 4 different control strategies apply /56/.
The first is an operation at wind speeds less than the wind speed correlated to the minimum rotor speed v_1 (239). The rotor can not operate on its optimal tip-speed and therefore the controls main task is to keep the minimum rotor speed.

$$v_1 = \frac{R\omega_{\min}}{\lambda_{opt}} \tag{239}$$

In the partial operation range between minimum rotor speed and maximal rotor speed, the turbine is controlled to operate with the optimal tip-speed ratio.

$$v_2 = \frac{R\omega_{rtd}}{\lambda_{opt}} \tag{240}$$

If the wind speed is above defined v_2 the turbine can not operate further with the optimal tip-speed ratio, since the speed is restricted to the rated generator speed.
With further rising of the wind speed, the turbine switches from the partial load operation into full load operation (fourth control strategy). Consideration about the optimal rotor efficiency are in the last control areas not necessary, hence the power is limited to the rated power.

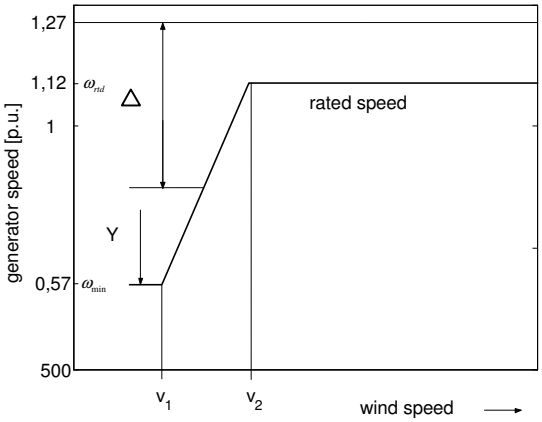

Figure 172 Stationary generator speed vs. wind speed for an OptiSpeed^{TM} wind turbine

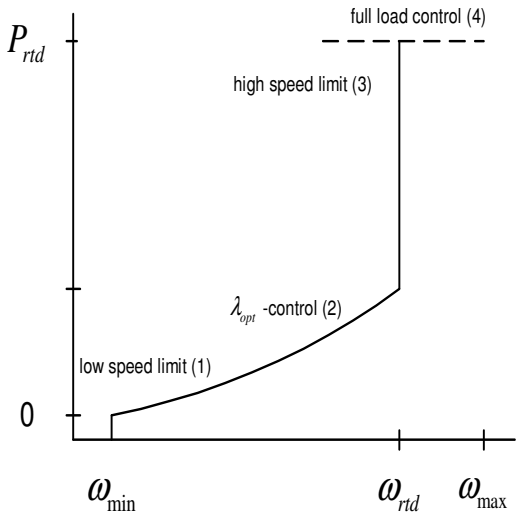

Figure 173 Steady state operation curve power vs. generator speed for an OptiSpeed^{TM} wind turbine

The shift between the different control areas is done with a logic block (Figure 174). This logic decides between the partial load controller, which is designed to keep the turbine operating on an optimal power set point, and the full load controller, which is controlling the speed, while the power is limited to the rated power. Both controllers are very similar to the described controllers used in the OptiSlip wind turbine model. The OptiTip feature introduced for the OptiSlip wind turbines pitch control is used in the OptiSpeed wind turbine is as well /56/.

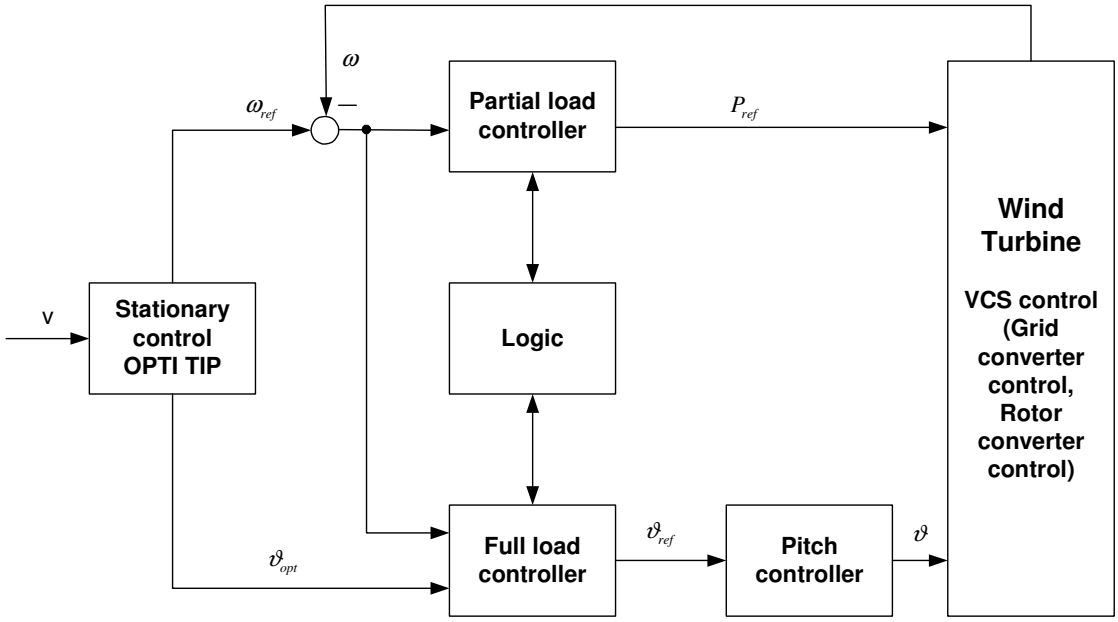

Figure 174 Overall control scheme for the OptiSpeed turbine

The OptiTip control strategy is useful to optimize the energy capture at partial load operation, while the turbine is operating at the low or high speed limit. In these areas it is not possible to operate at the aerodynamical optimum controlled by the speed. With adjusting the pitch angle according to a function found from the maximum of the c_p – curves described for every tip speed ratio this is improved:

$$\vartheta_{opt}(\lambda): \quad c_p(\lambda, \vartheta_{opt}) = \max\{c_p(\lambda, \vartheta)\} \tag{241}$$

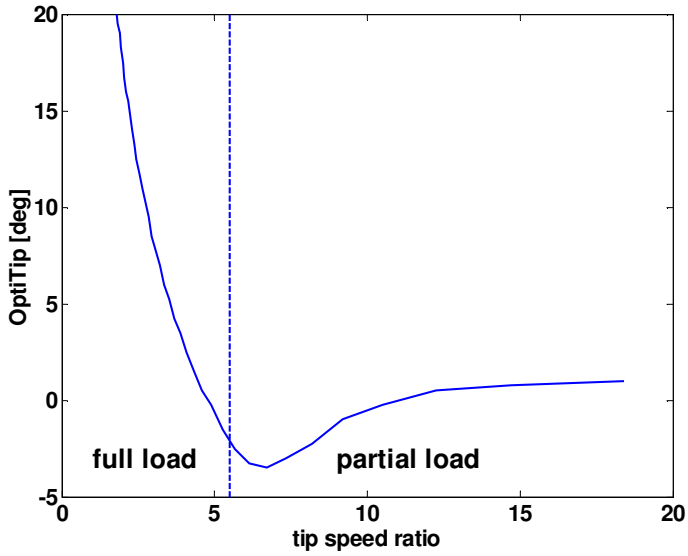

Figure 175 optimum pitch angle vs. tip speed ratio e.g. V80 rotor

The model of the wind turbine with doubly-fed control is structured in the same way as the wind model with the variable rotor resistance in Matlab/ Simulink. There are three basic blocks. In the block “Electrical System” all electrical components as the DFIG, the transformer and the grid are implemented. In the block “Mechanical system”, the model of the pitch system, blades and drive train is in the same way implemented as described in

Chapter 6. The complete control system, wind turbine controller and doubly-fed control as described above are included in the block “Control”.

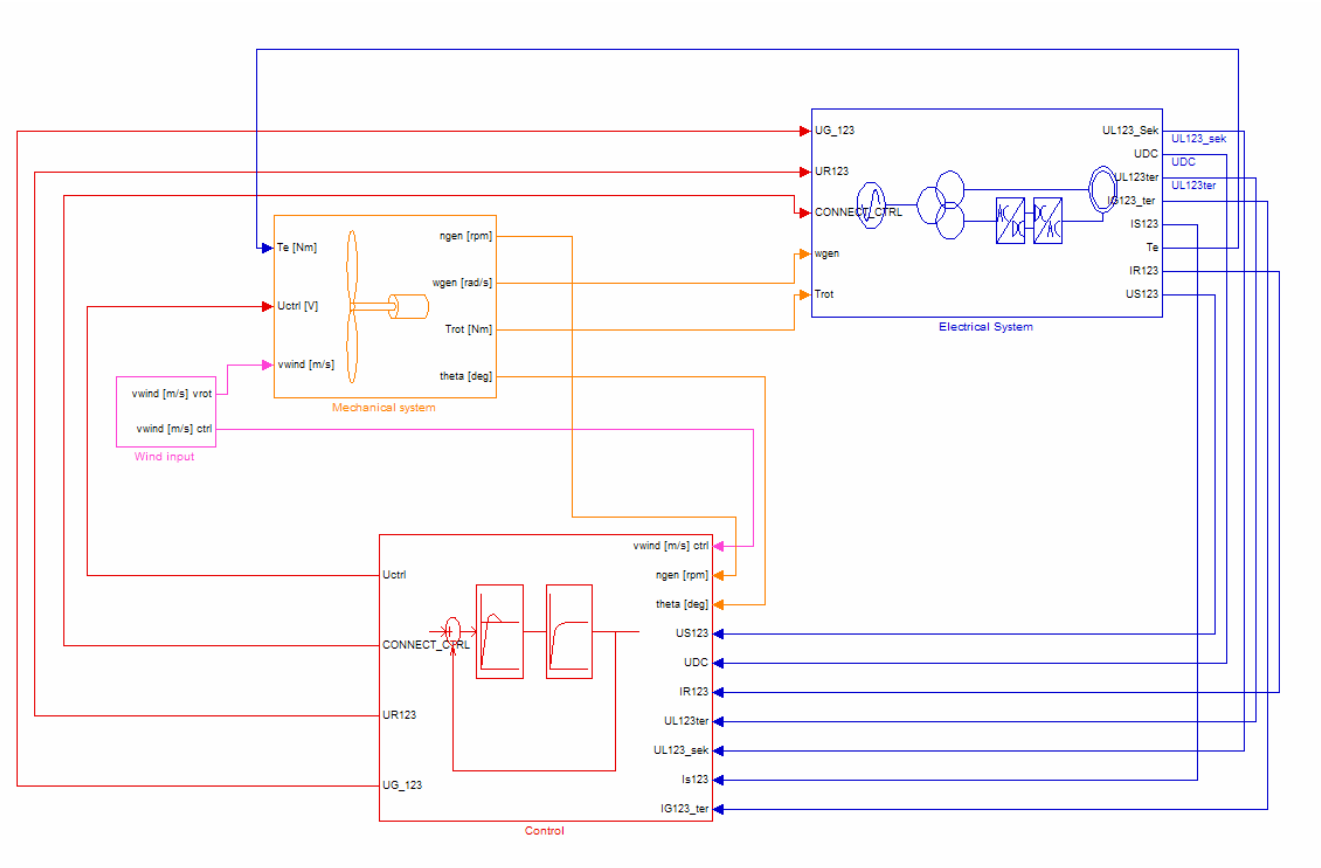

Figure 176 Overall structure of the OptiSpeed wind turbine model in Matlab/ Simulink

Chapter 9

9. Fault simulations with total turbine models

With the two developed wind turbine models it is possible to investigate various operations from normal operation to fault situations. The main focus for the fault simulations is the clarification of the peak current after the incident to determine the necessary values for protection equipment design, the load torque on the shaft as design criteria for the gear box and coupling and the short circuit power contribution. These all are important design criteria for the wind turbine and for the grid connection of wind turbines. The simulated values are prospective, which means the wind turbine models continue operating during the fault, whereas in reality the protection mechanism would interrupt the wind turbines operation in order to protect the wind turbine. This is a well known method for researching the impacts during fault situations.

9.1 Wind turbine model with variable rotor resistance

In this chapter simulations with the V80 1.8 MW Vestas OptiSlip turbine have been made (Figure 177).

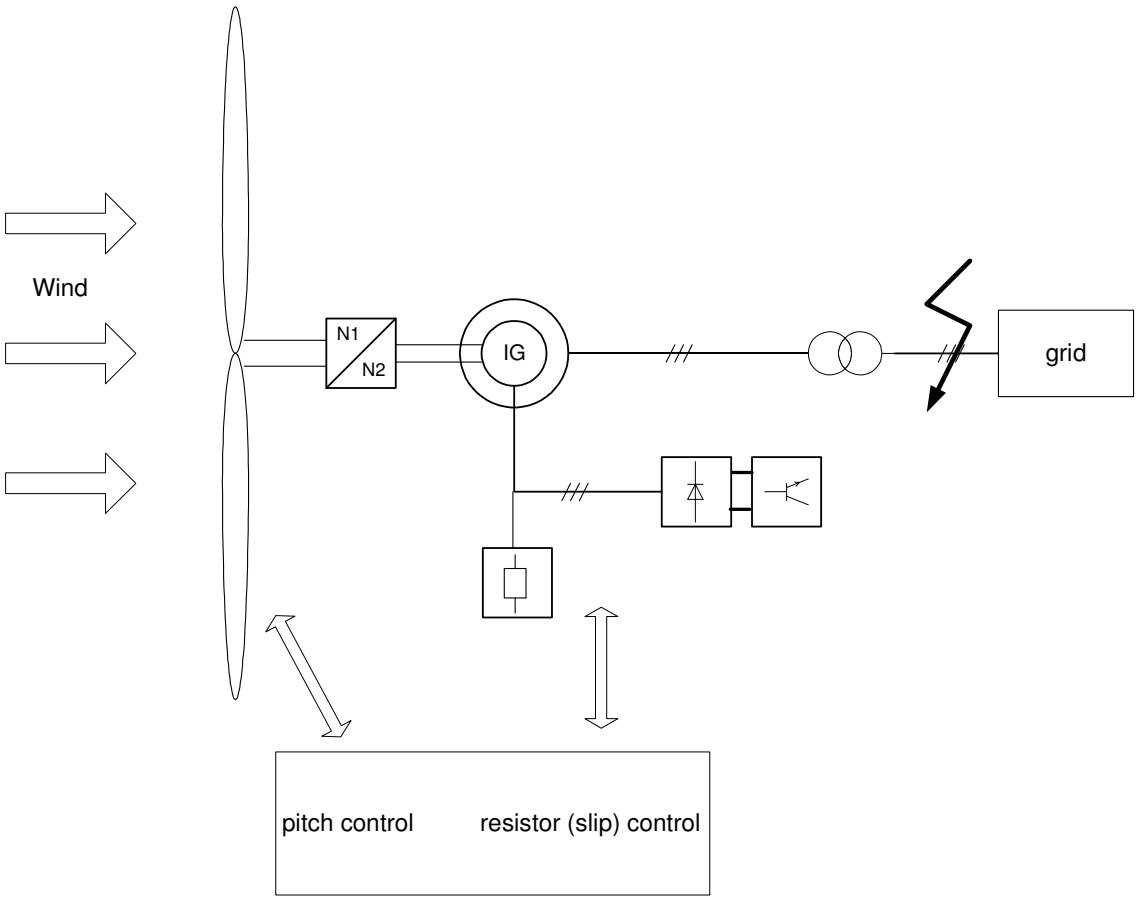

Figure 177 Outline of the wind turbine simulation model for fault simulation

Besides extreme fault conditions, e.g. three phase short circuit wind turbine operation at the border of the permitted operation limits are studied. Thereby the stability of the control system as well as the operation of the wind turbine can be proven. One of these limits is an occurrence of voltage drop as discussed in chapter 2.3.
The standard wind turbine is specified to disconnect with occurrence of the voltage changes, excluding additional modifications, as shown in Table 9-1 and Figure 178. The different levels are implemented to distinguish the occurrences importance.

Table 9-1 Voltage parameter limit values for V80 with variable resistance

	voltage value [%]	Time [s]
High voltage	+10	60
Extreme high voltage	+13,5	0.20
Extreme extreme High voltage	+20	0.08
Low voltage	-6	60
Extreme low voltage	-15	0.4
Extreme extreme low voltage	-25	0.08

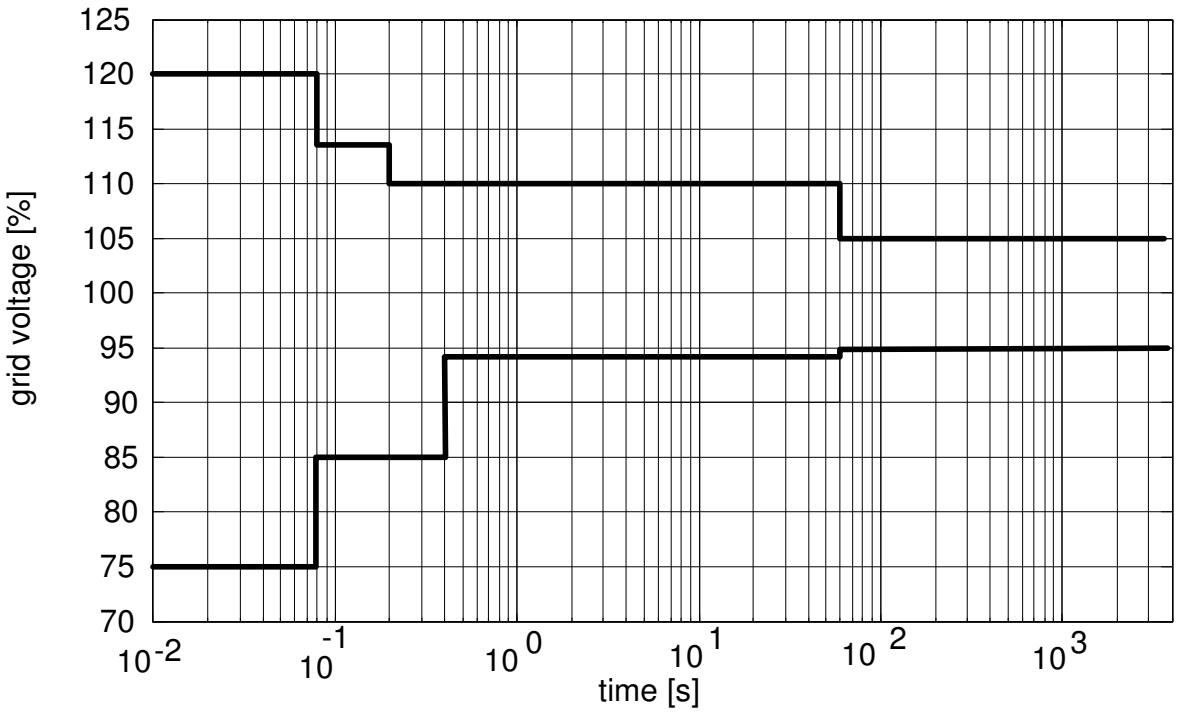

Figure 178 Operational voltage limits for the OptiSlip V80 1.8 MW wind turbine

9.1.1 Simulation of a 15% voltage dip

The turbine experiences a wind speed of 18 m/s and the turbine is controlled to produce the rated power of 1.8 MW. A short term voltage dip to 85% of the rated voltage, which is cleared within 400 ms should not lead to a disconnection of the turbine. In the simulation the grid voltage (primary transformer side) is tripping for 400 ms to 85% as shown in Figure 179. The voltage on secondary side of the transformer, the generator stator voltage, follows smoothly this dip Figure 180.

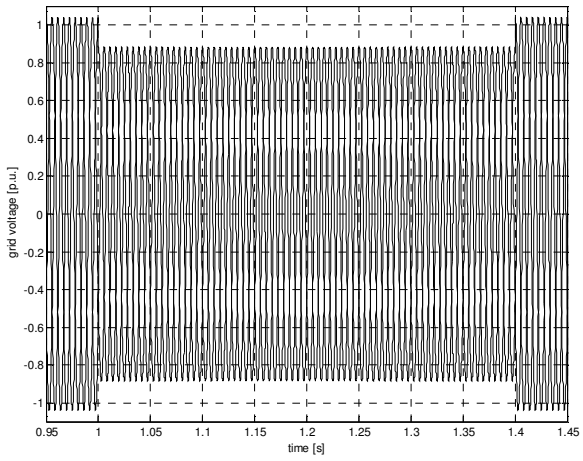

Figure 179 Grid voltage dip in p.u. (simulation input)

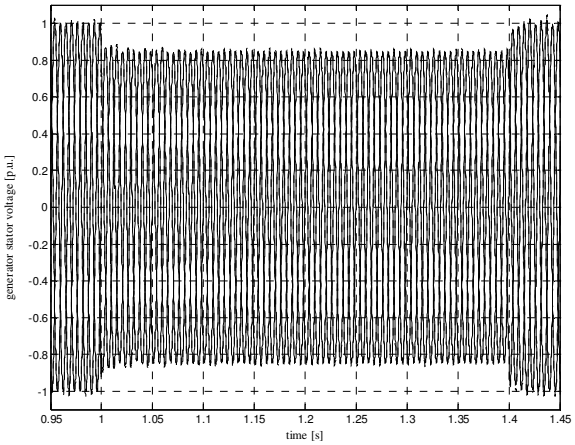

Figure 180 Voltage at generator stator in p.u.

The occurrence can be separated into two incidents. The first is the drop of the voltage to 85% rated voltage and the second, which usually is more stressing, the rising of the voltage back from 85% to rated voltage. To reinforce the research on the influence of different generator models the same simulations have been made including a generator model without saturation effects and one with saturation effects. Both simulations are shown together in the simulations in Figure 181.

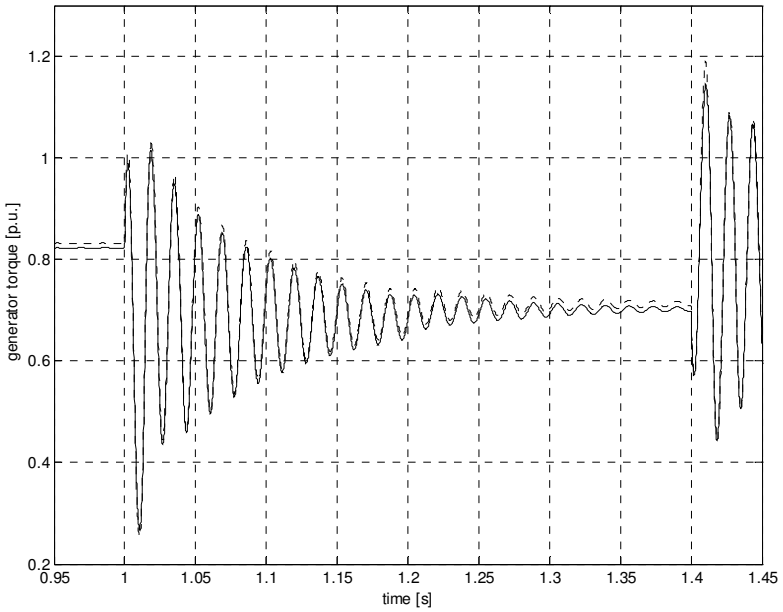

Figure 181 Developed torque by the generator with different generator models with saturation effect (dotted line) and without saturation effects (solid line)

At a wind speed of 18 m/s the torque on the shaft is high enough to produce maximal power of the turbine as shown in Figure 182.

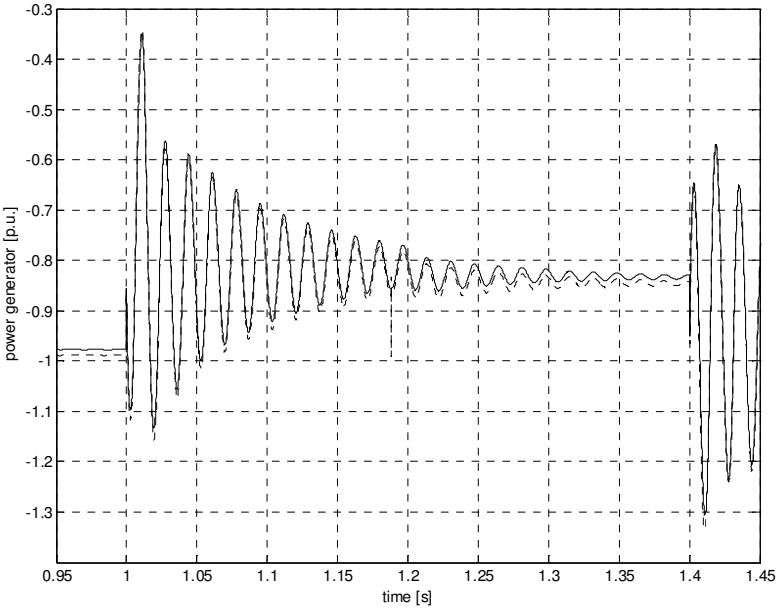

Figure 182 Generator power during the 15% voltage dip while using a machine model including saturation (dashed line) and a model without saturation (solid line).

The sign of the power is negative, which shows the flow of the power to the grid. During the voltage dip the current would increase however the rotor control system (VRCC) prevents this by increasing the external rotor resistance as shown in Figure 183.

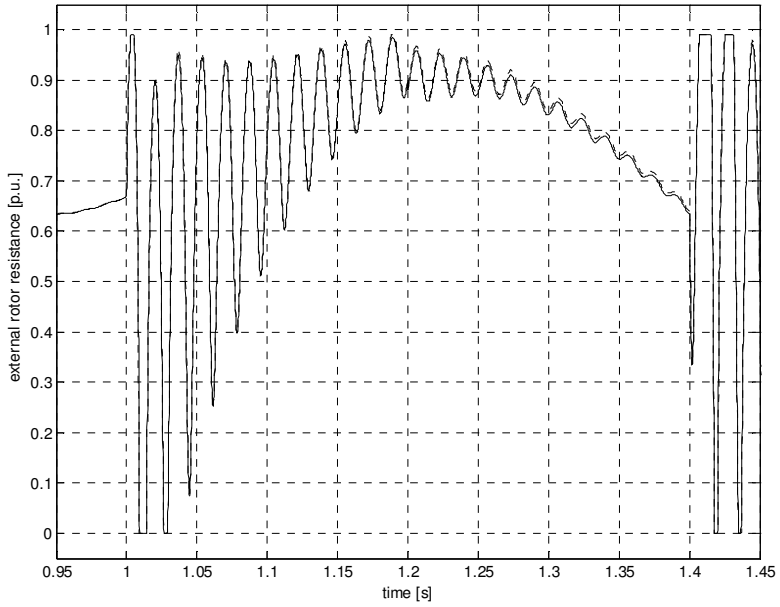

Figure 183 External rotor resistance during the 15% voltage dip, model with saturation (dashed line) and without saturation (solid line)

The increased rotor resistance results in an increased speed as shown in Figure 184.

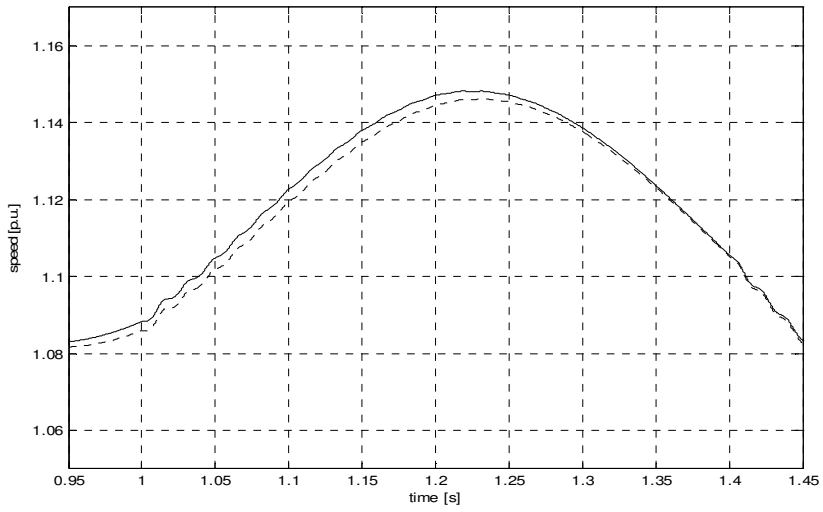

Figure 184 Generator speed during 15% voltage dip using a machine model with saturation effects (dotted line) and without saturation (solid line).

With the rotor current control the rotor current Figure 185 as well as the stator current Figure 186 are controlled to their rated values shortly after the start of the voltage drop as well as after the recovery of the voltage.

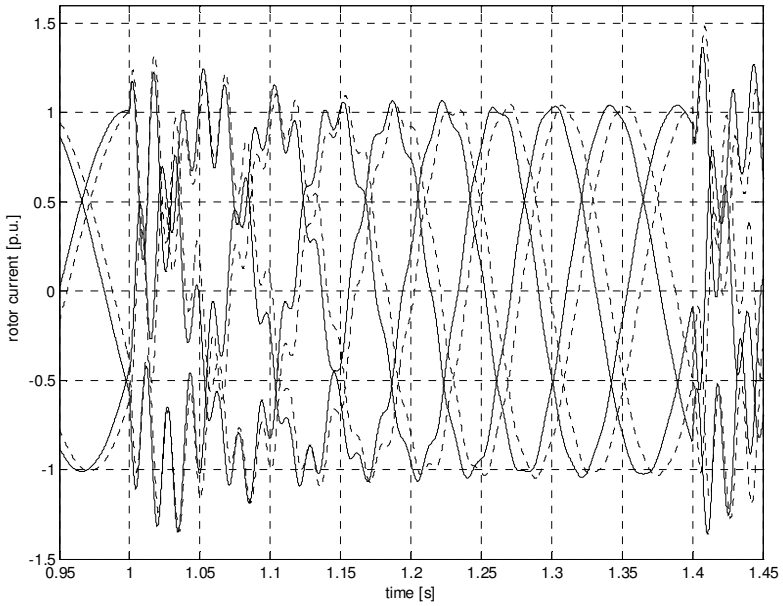

Figure 185 Rotor current during 15% voltage dip, machine model with saturation (dotted line) and without saturation effects (solid line)

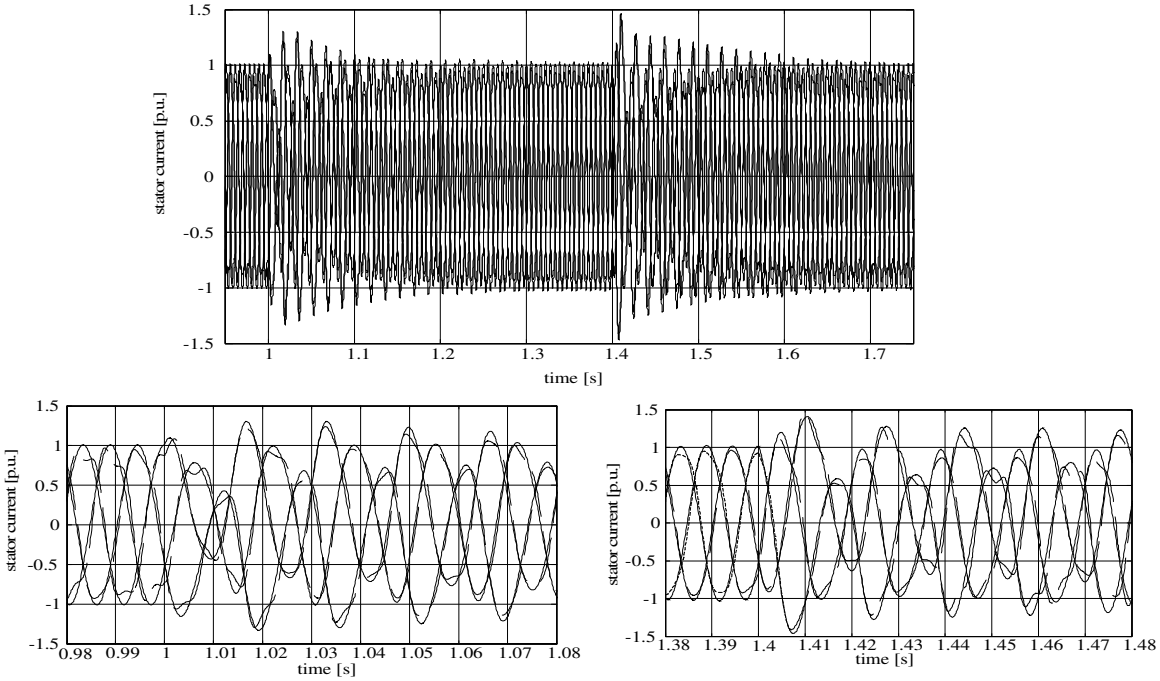

Figure 186 Generator stator current during 15% voltage dip using machine model with saturation effects (dashed line) and machine model without saturation effect (solid line)

Because the power control is very slow, the rotor current reference is constant during the voltage drop. The rotor current control keeps the rotor current continuously to the rated current. The reduced voltage and the constant current results in a decrease of the power supplied to the grid and therewith a decreased reaction torque of the machine, while the torque of the turbine shaft decreases much more slowly Figure 188. To keep the energy balance during the voltage dip the generator speed increases and the rotor power increases as shown in Figure 187. After the decrease of the shaft torque, the rotor power

and the speed decrease as well.

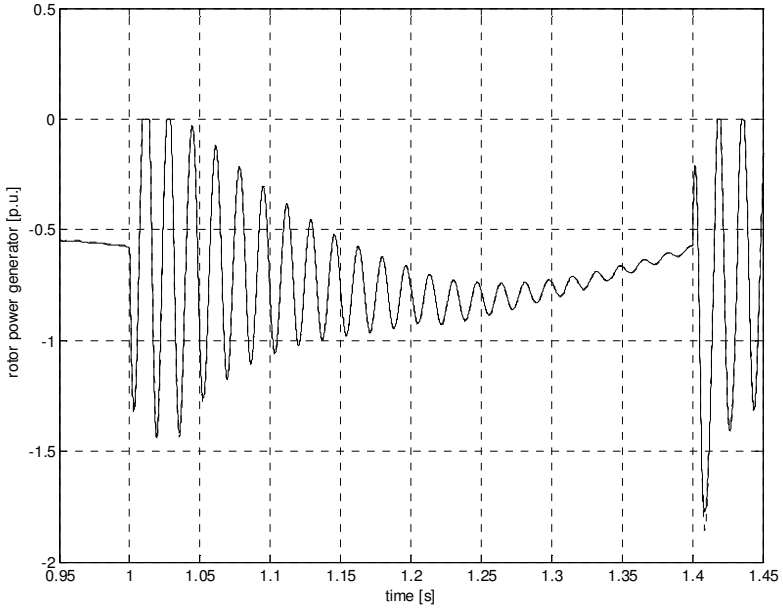

Figure 187 Rotor power using a machine model with saturation effects (dotted line) and without saturation (solid line)

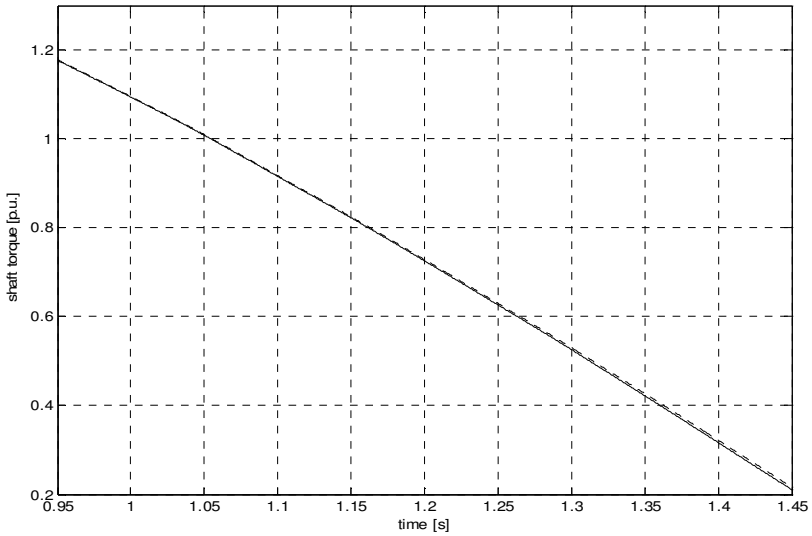

Figure 188 Shaft torque during 15% voltage dip

The OptiSlip turbine model shows a reliable operation during the voltage dip. Although the controller has to use the maximal available external rotor resistance the rotor current limits do not exceed the limits. The wind turbine is continuing in normal operation without any stability problems, which could cause a disconnection of the turbine.

9.1.2 Simulation of a 2 phase short circuit

Preventing the wind turbine from permanent damage, it is important to be able to know the loads during extreme incidents such as 1-, 2- or 3-phase short circuits. The 3-phase short circuit is considered as the worst case, though it is symmetrical and not as frequent as the other two faults. Researching a 1-phase short circuit is not an easy task, since it requires access to the data for the grounding of the power system the wind turbine is connected to. Stressing the simulation model capabilities for researching asymmetrical conditions the 2-phase short circuit without ground connection is researched.
The 2-phase short circuit occurs at the primary side of the transformer terminals as shown in Figure 189. Due to the coupling in the transformer the secondary transformer voltage (the generator stator voltage) changes to an extreme voltage dip in phases one and two to a voltage level of approx. 50% and in phase three to a voltage level of approx. 9%.

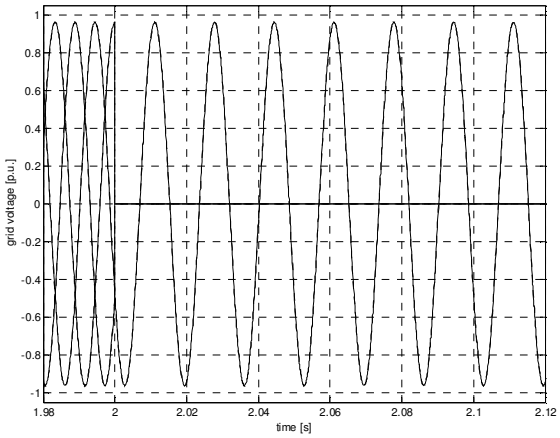

Figure 189 Grid voltage of a 2-phase short-circuit at transformer terminals (simulation input)

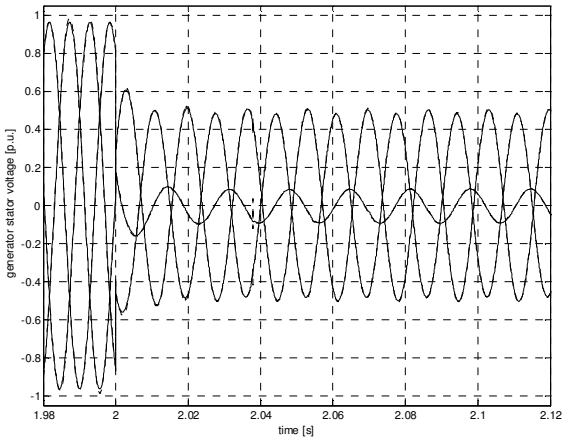

Figure 190 Voltage at the generator stator during 2-phase short circuit at the transformer terminals

After the fast dropping of the voltage, the generator currents of all three phases rise as seen in Figure 191. Though the stator current is increased the field in the machine is decreased with accordingly a lower voltage, and it is not able to produce the amount of power as before, see Figure 192.

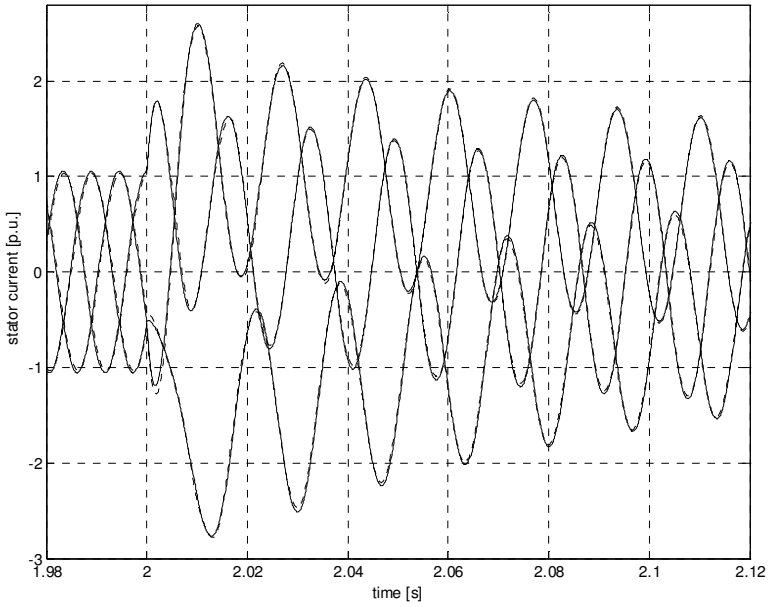

Figure 191 Stator current during a 2-phase-short circuit at transformer terminals, model with saturation (dotted line), without saturation (solid line)

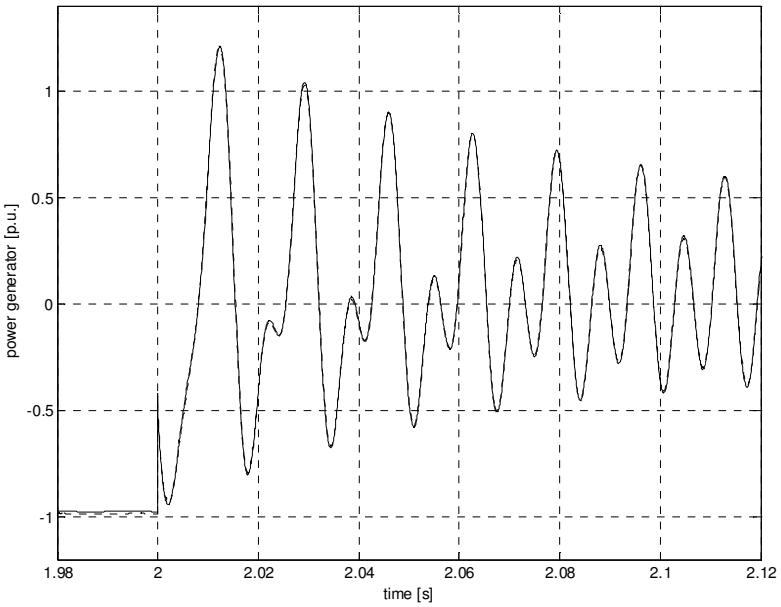

Figure 192 Generator power during a 2-phase-short circuit at transformer terminals, model with saturation (dotted line), without saturation (solid line)

The torque of the generator stresses the coupling on the shaft of the machine with short time torque oscillations see Figure 193.

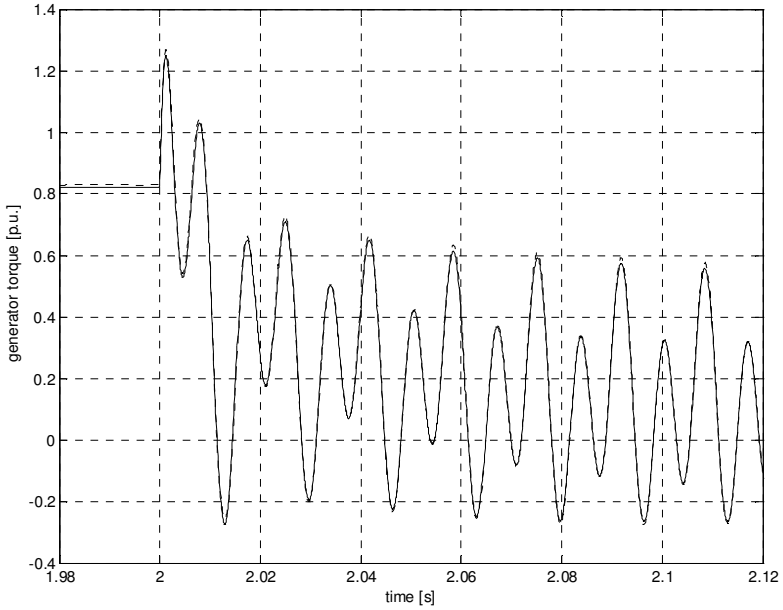

Figure 193 Generator reaction torque (air gap torque) during a 2-phase-short circuit at transformer terminals, model with saturation (dotted line), without saturation (solid line)

The rotor current control of the machine tries to reduce the current by increasing the external rotor resistance (Figure 194). This leads to a higher slip and therewith an increase of the generator speed (Figure 195).

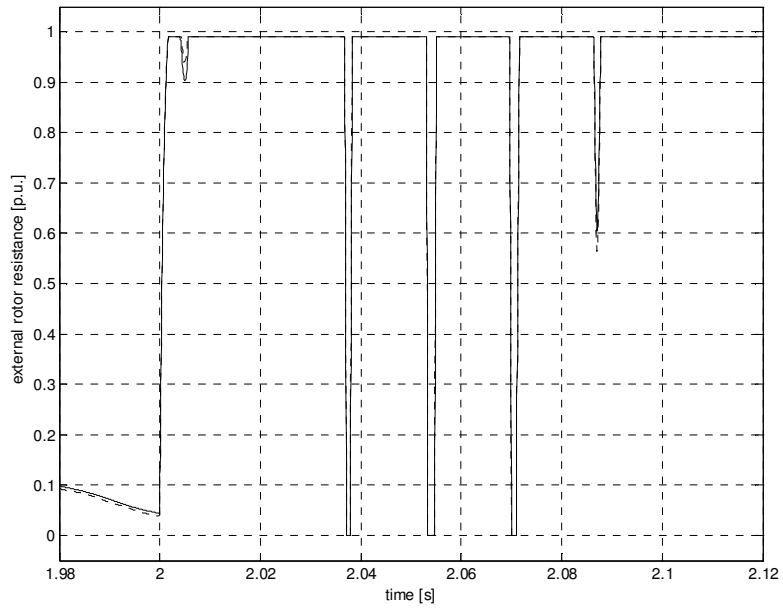

Figure 194 External rotor resistance during a 2-phase-short circuit at transformer terminals, model with saturation (dotted line), without saturation (solid line)

The external resistance shown in Figure 194 breaks to zero during the short circuit, because of the oscillations. In reality the external rotor resistance would keep its maximum value until the protection system short circuits the rotor terminals. Hence no protection system is implemented in this simulation you see the behaviour in case of continuing

control under a 2-phase short circuit.

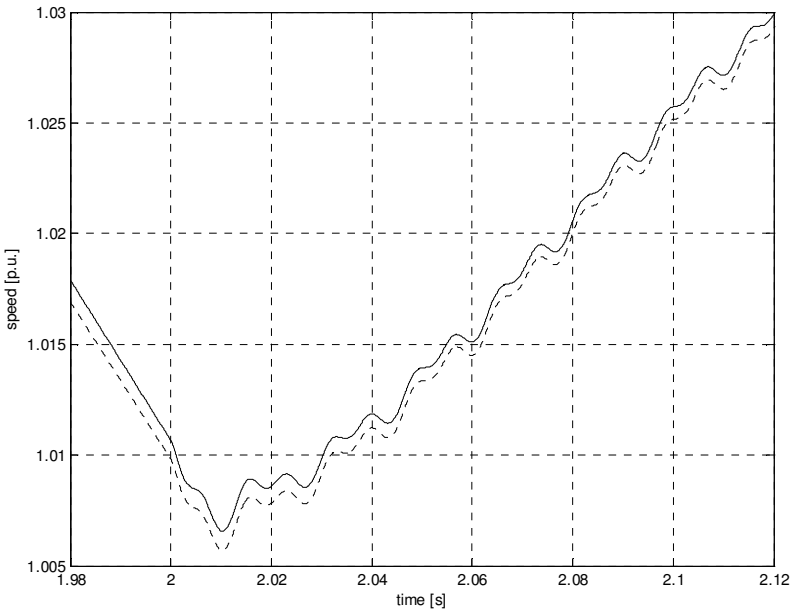

Figure 195 Speed during a 2-phase-short circuit at transformer terminals, model with saturation (dotted line), without saturation (solid line)

The existing energy is in this case supplied to the rotor of the machine and dissipated in the rotor resistance as it can be seen in Figure 196. This would damage the IGBT placed in the rotor circuit for the rotor control. In reality the IGBT protection system will stop the switching of the IGBT's, which means the current will be going directly through the total connected resistances and not only through the controlled fraction of the resistance. In the presented case this will not help to reduce the current in the given time and will initialize as disconnection of the generator ca. 40 ms after the current is higher than 1.5 of rated rotor current (Figure 197). The limit is reached shortly after the 2-phase short-circuit start and therewith expected disconnection and stop of the wind turbine is ca. at time 2.04 s (40 ms after).

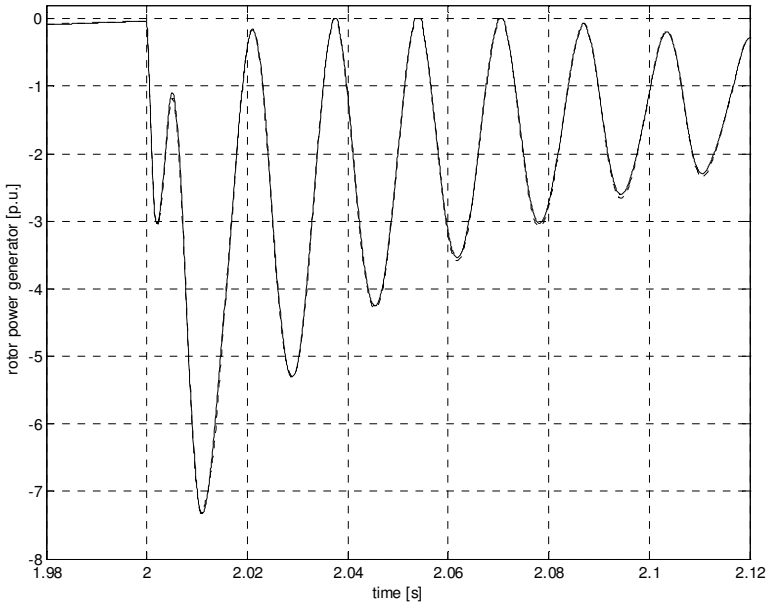

Figure 196 Rotor power during a 2-phase-short circuit at transformer terminals, model with saturation (dotted line), without saturation (solid line)

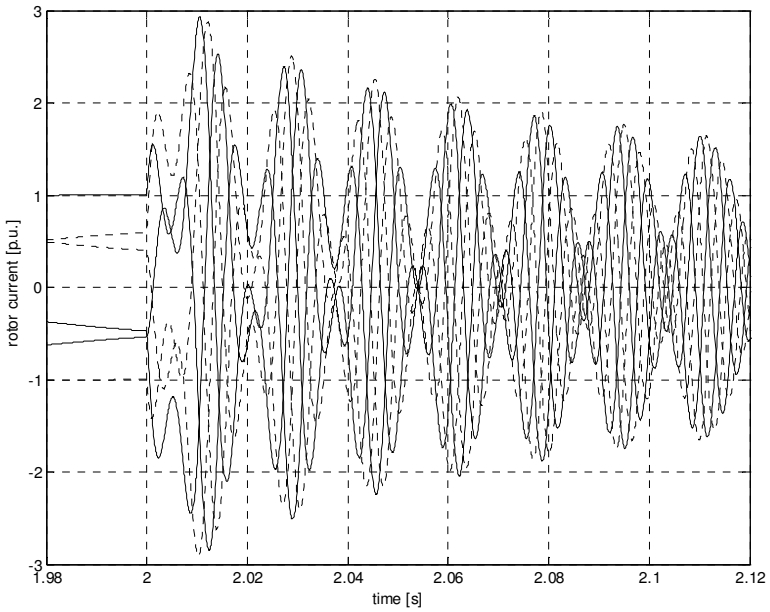

Figure 197 Rotor current during a 2-phase-short circuit at transformer terminals, model with saturation (dotted line), without saturation (solid line)

9.2 Discussion

Two cases with the OptiSlip wind turbine model have been simulated. Thereby each simulation has been carried out with two different precise generator models. The results of the simulation with the generator model including saturation effects and the simulation made with the generator model without saturation effects are depicted in the same graphs.

Due to the high changes during the fault occurrence the percentage differences between the simulated values are very small. In the shown cases the control of the wind turbine is reacting similarly with both generator models and the saturation effects do not lead to a general malfunction of the wind turbine. Therefore saturation effects can be neglected in the control itself.
The simulated absolute values are somewhat different in both simulations, but it is difficult to compare. Even the primary transformer voltage is equally in both cases the secondary voltage of the transformer is dependent the current flowing through the transformer. The simulation with the generator model including saturation effects finds a stationary operating point with a 2% higher generator stator voltage as the generator voltage in the simulation with the generator excluded saturation effects (Figure 198).

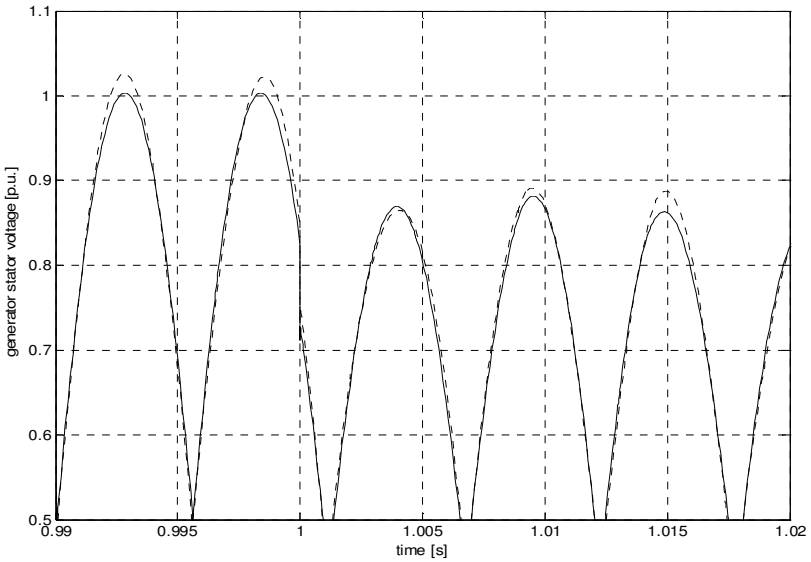

Figure 198 Zoom into the generator stator voltage during 15% voltage dip, model with saturation (dotted line), without saturation (solid line)

The generator current is therefore smaller compared to the current in the model without saturation effects, while the average power is equal in both simulations due to the power control of the system. The absolute difference of the stator current peak during the occurrence start of 15% voltage dip is 4% and at the end of the dip during the voltage rise it is 6%.
The differences during the 2-phase short circuit are similar. Due to the shown small differences in the simulation model including and excluding saturation effect the neglecting of these influences could be easily drawn.
However, these shown cases are made with only one machine type from supplier A having an R/X close to 0.05. Using a different machine supplier B with an R/X of 0.09 draws a total different picture of the influence of the saturation. Rushing into the conclusion to neglected saturation effects would exclude results using another machine type. The second machine B with the higher R/X value shows an increase of the currents to a 6% higher value during the 2-phase occurrence, while it is lower during rated conditions.

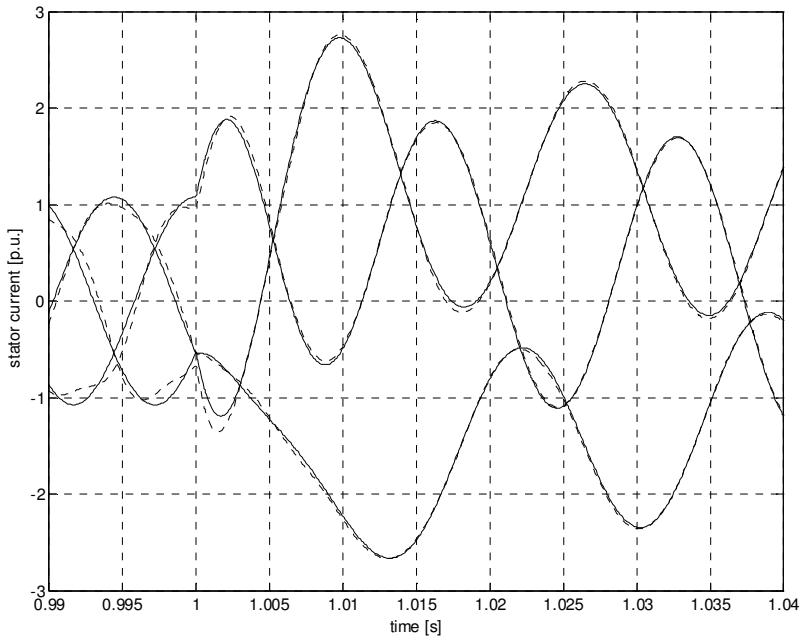

Figure 199 Zoom into the generator stator current during 15% voltage dip with machine B, model with saturation (dotted line), without saturation (solid line)

As shown in the case it can have consequences, while rushing into conclusions from one example. The saturation effects could be easily excluded while using the machine type A while using the machine type B it would not be advisable. However, neglecting these effects in the start would have never shown these differences.
To draw any general conclusions on the influence of saturation effects on the wind turbine behaviour more studies with different cases and different machines have to be investigated. Since this has not been done yet it is advisable to include saturation effects in the simulation of faults, hence it shows difference from 4 % and more and in the machine range (>600 kW) it might just give the difference of an enforced gear box or larger contactor in order to handle the stress during the fault.

9.3 Wind turbine model with DFIG

Similar to the study with the OptiSlip wind turbine model, simulation with the OptiSpeed wind turbine model have been made.

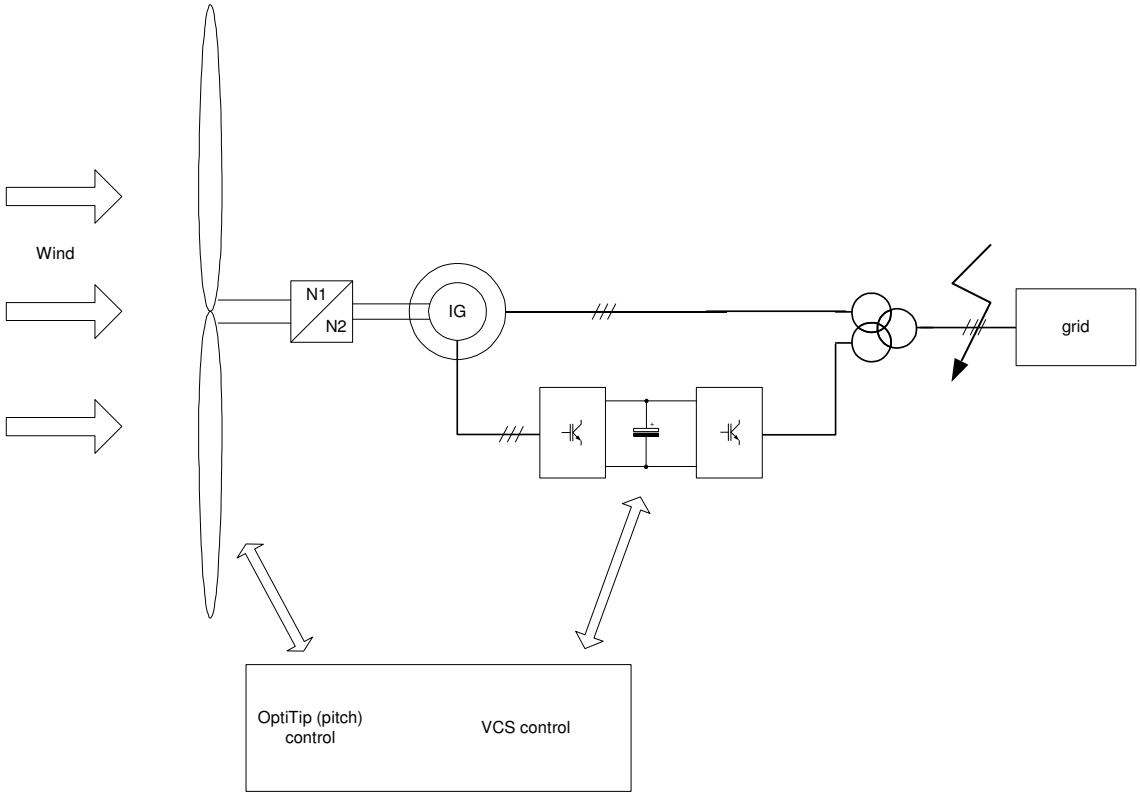

Figure 200 Outline of the OptiSpeed wind turbine model for fault simulations

The voltage availability of the standard V80 2MW wind turbine with DFIG is shown in Table 9-1 and Figure 201. As in the case with the OptiSlip wind turbine a simulation with a voltage dip is performed.

Table 9-2 Voltage values for the V80 2MW with DFIG

	voltage value [%]	Time [s]
High voltage	+10 – +6	60
Extreme high voltage	+13,5	0.20
Extreme extreme High voltage	+20	0.08
Voltage operation band	+/- 5	
Low voltage	-10	60
Extreme low voltage	-15 - -13	0.4
Extreme extreme low voltage	-25 - -20	0.08

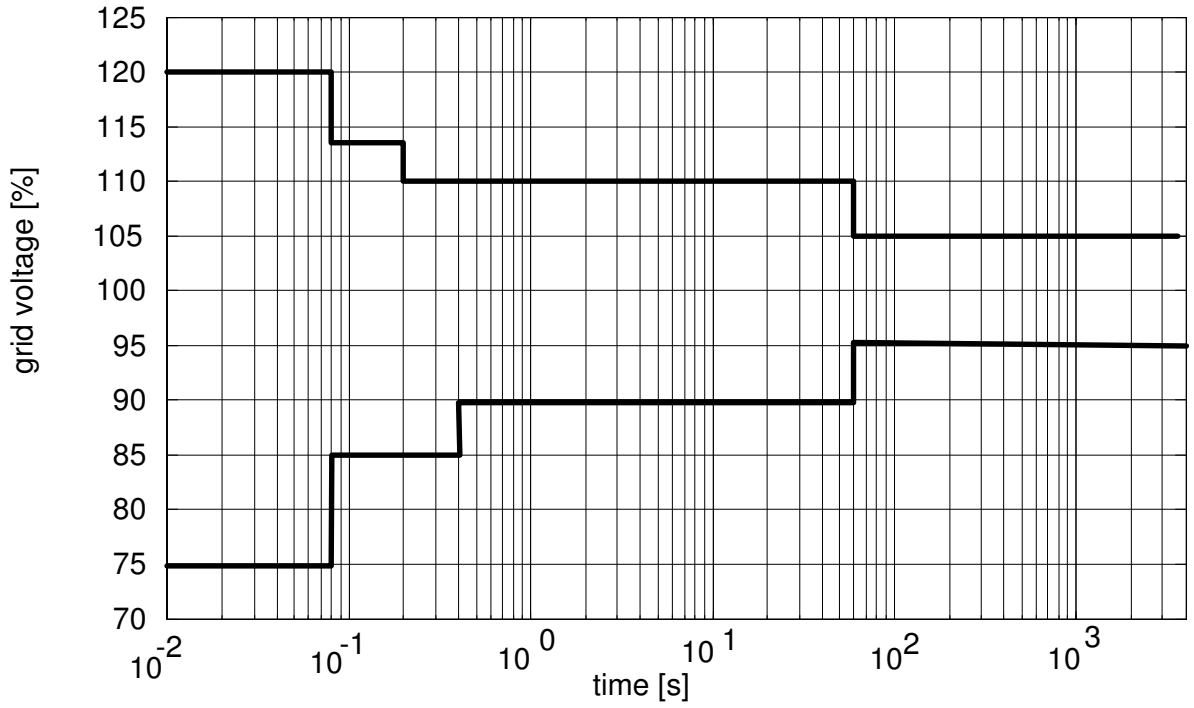

Figure 201 Trip voltage limits for the OptiSpeed wind turbine

9.3.1 Simulation of a 25% voltage dip

The standard V80 2MW wind turbine will disconnect if a short term voltages dip to 75% for 80 ms occurs. In other words the turbine should withstand a short term voltage dip to 75% as long it is shorter than 80 ms. To show the effects of such a short term voltage dip it is initiated at the high voltage side of the transformer (Figure 203). The average input wind speed during the voltage dip is 10 m/s (Figure 202).

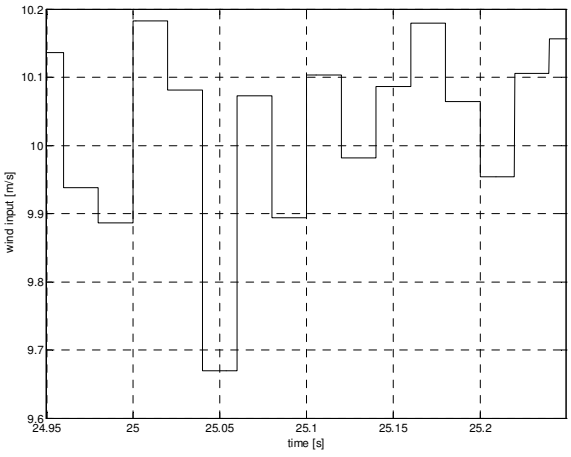

Figure 202 Input Wind Speed into the wind turbine model

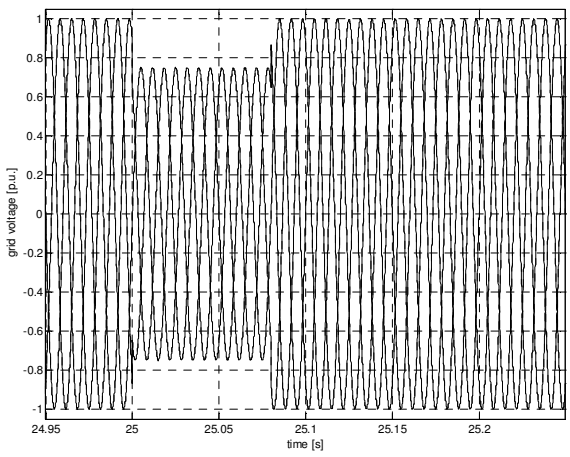

Figure 203 25% voltage dip of the grid voltage as input into the wind turbine model

The rotor load torque at the generator shaft is calculated from the wind speed and the cp-

tables and includes oscillations according to tower shadow effects. At 25 s the voltage dip is initiated and after 80 ms cleared. The two incidences of voltage drop and voltage rise are close together and cannot clearly be separated though a difference in the simulation between the machine model including all saturation effects and the machine model without saturation effects is negligible during steady state operation. In dynamic situations the effects of saturation can clearly be seen. The simulation including the saturation effects shows a 3% higher generator reaction torque during the dynamic period.

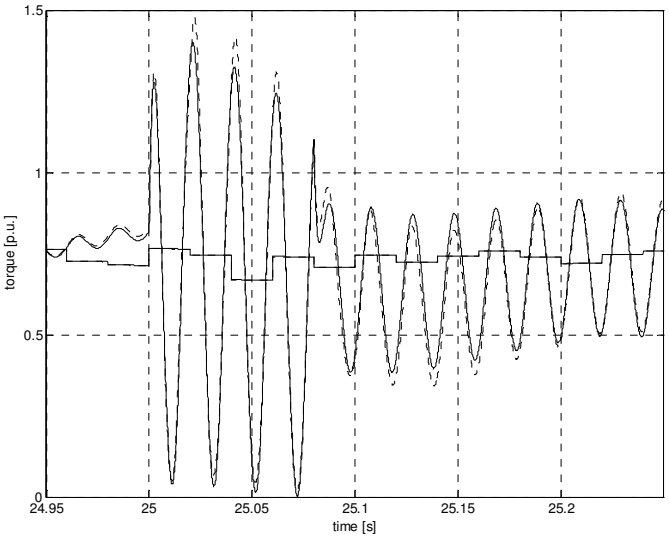

Figure 204 Rotor torque (sampled value) and generator reaction torque – machine model with saturation (dotted line) and machine model without saturation effects (solid line) during 15% voltage dip

The generator speed is not steady before initiating the voltage dip. Figure 205 show a poorly damped drive train oscillation in the generator speed, which is not related to the 25% voltage dip. The fall and rise of the generator speed seen in Figure 206 is part of this oscillation. In the zoom some smaller superpose near 50Hz oscillation can be seen, which are related to the voltage dip.

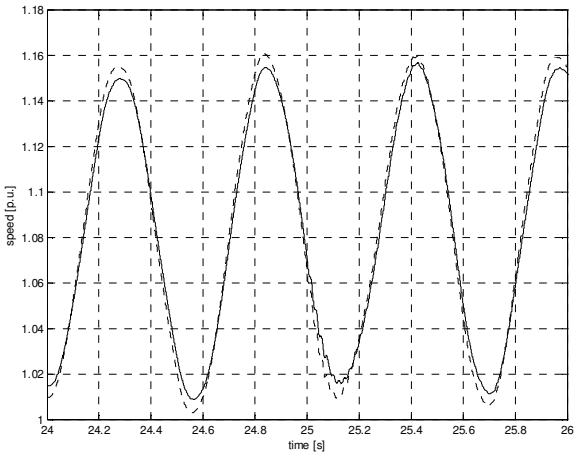

Figure 205 Generator speed during operations of wind turbine model using a machine model with saturation (dashed line) and without saturation (solid line)

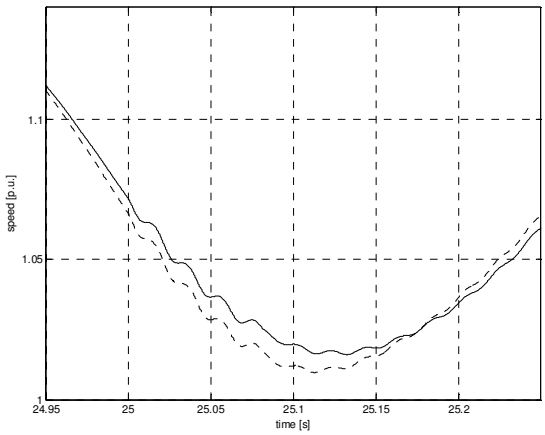

Figure 206 Zoom into the generator speed during 25% voltage dip of the wind turbine model using a machine model with saturation (dashed line) and without saturation (solid line)

The turbine is operating in partial load and follows the optimal power output (strategy 2 in chapter 8.5). While the active grid power is controlled to a smooth output Figure 207, the generator stator power and the generator rotor power react to the voltage dip. The power flow through the converter from the rotor terminals to the grid is shown in Figure 208.

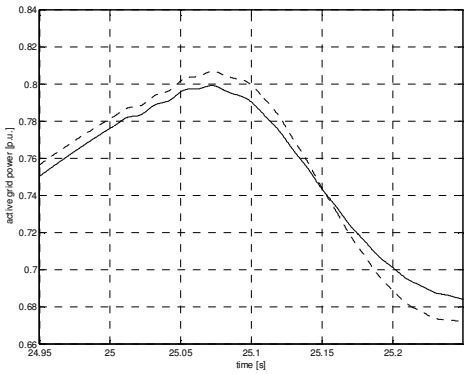

Figure 207 Generator active power reference (solid line) and feedback (dotted line) during a 25% voltage dip

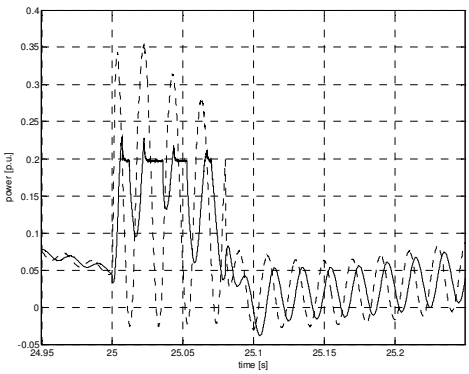

Figure 208 Generator rotor power (dotted line) and grid converter power (solid line) during 25% voltage dip

Due to the dynamics in the power transported through the DC-link, the DC-link voltage is oscillating as shown in Figure 209. The oscillations in all signals excited with the voltage dip are disappeared at ca. 27 s after the grid voltage is restored.

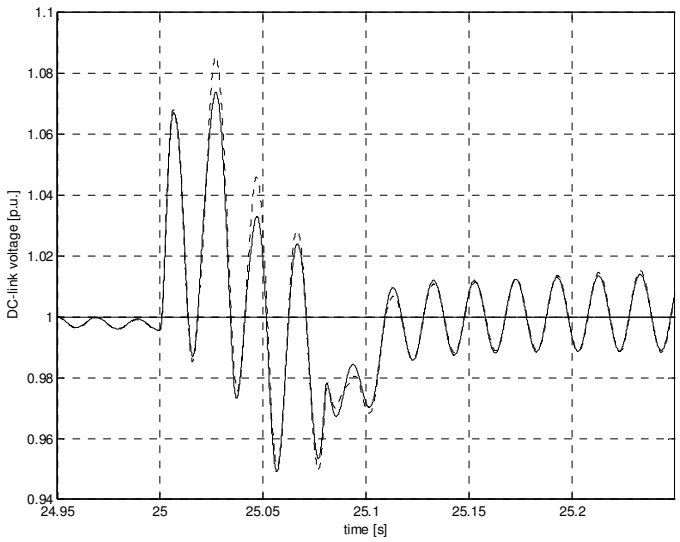

Figure 209 DC-link voltage during 25% voltage dip on the wind turbine model using a machine model with saturation (dotted line) and a model without saturation (solid line)

The grid current and the generator stator current increase during the voltage dip to 1.5 – 2 times of the rated current output and have asymmetric behaviour as well. Approx. 2 s after the occurrence the rated steady state conditions are restored again.

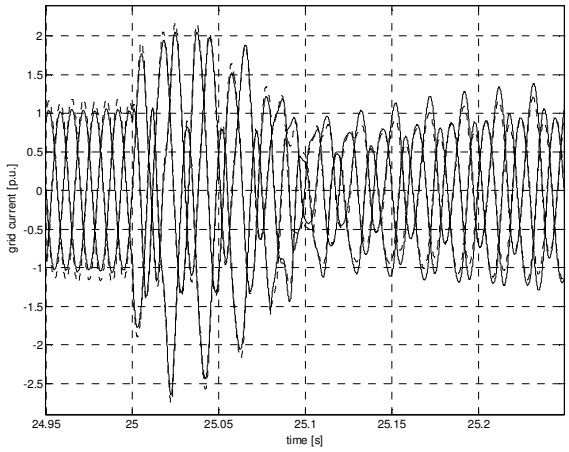

Figure 210 Grid current of the wind turbine model using a machine model without saturation (solid line) and with saturation effects (dotted line)

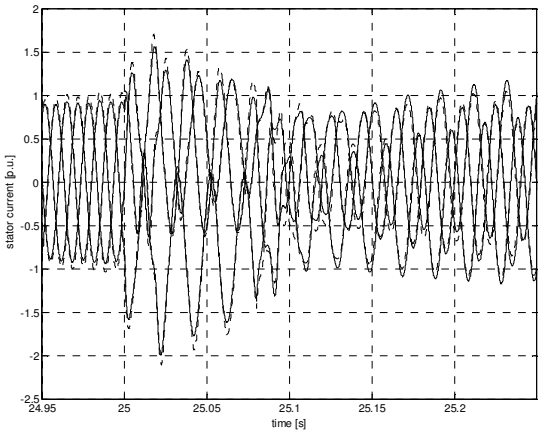

Figure 211 Generator stator current during 25% voltage dip using a machine model without saturation (solid line) and with saturation effects (dotted line)

9.3.2 Simulation of 2 phase short circuit

As mentioned in the study of the OptiSlip turbine, short circuits are an important issue to investigate in respect to loads at the wind turbine and the grid connection. The two phase short circuit is especially interesting, since it occurs frequently and it is due to the asymmetrical nature difficult to calculate with simple calculation methods.
In the simulation a two phase short circuit on the transformer primary terminals is initiated

(Figure 212)

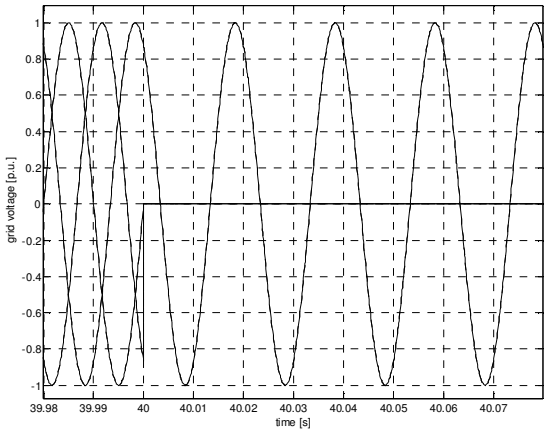

Figure 212 Grid voltage for a 2-phase short circuit on the V80 2 MW wind turbine model

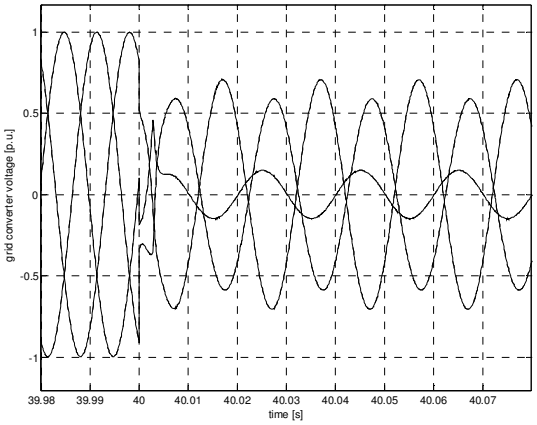

Figure 213 Grid converter voltage on the tertiary transformer side of the wind turbine model

The average wind input to the turbine during the 2-phase short circuit is 12 m/s. Having the same wind speed as input into the wind turbine simulation model using a machine model with saturation effects and without, the consideration of saturation effects lead to 2 different operation points, which can be especially seen in the pitch angle.

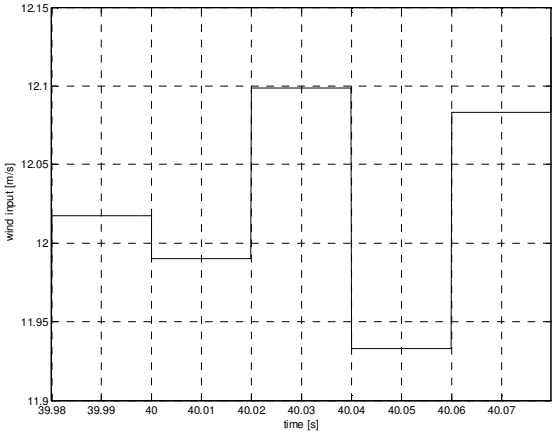

Figure 214 Sampled wind input signal during the two phase short circuit of the V80 2 MW wind turbine model

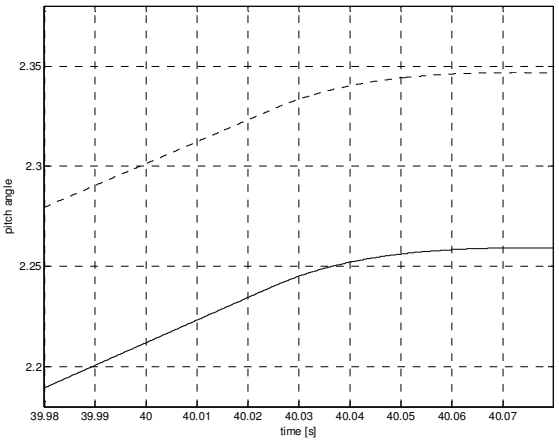

Figure 215 Pitch angle, simulated using a machine model with saturation effects (dotted line) and without saturation effects (solid line) during

The differences related to the saturation effects are minimal in the generator speed or torque. The wind turbine model including saturation effects has a steady state generator speed (Figure 216), which is 0.04% (ca 0.6 rpm) lower compared to the model without included saturation effects. While the rotor torque is nearly constant during the voltage dip, the generator reaction torque is reacting to the 2-phase short circuit (Figure 217).

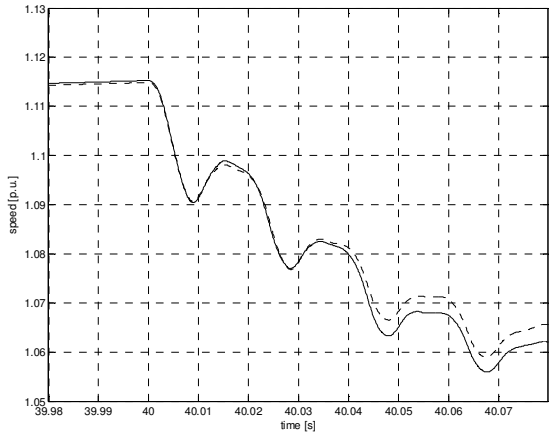

Figure 216 Generator speed during 2-phase short circuit using a model with saturation effects (dotted line) and a model without saturation (solid line)

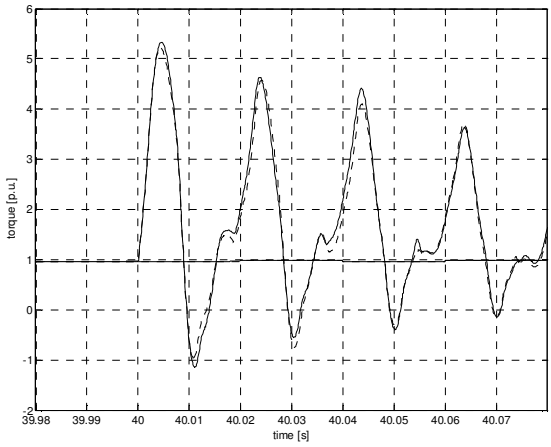

Figure 217 Rotor torque and generator reaction torque using a model with saturation effects (dotted line) and without saturation effects (solid line)

The active and reactive grid power, which is the addition of generator stator power and generator rotor power or grid converter power are decreasing due to the grid voltage drop.

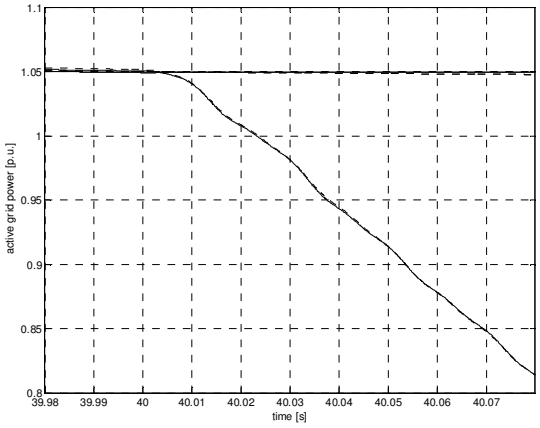

Figure 218 Active grid power reference and feedback during 2-phase short circuit of the OptiSpeed V80 2 MW wind turbine model

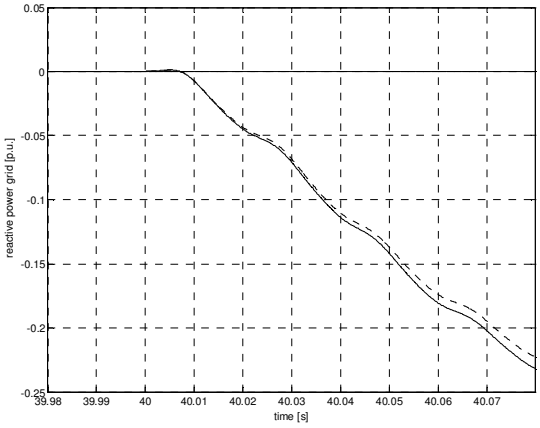

Figure 219 Reactive grid power reference and feedback signal during the 2-phase short circuit of the wind turbine

Though the power exchange with the grid is very smooth during the short circuit occurrence there is a huge dynamical exchange between stator and rotor of the generator.

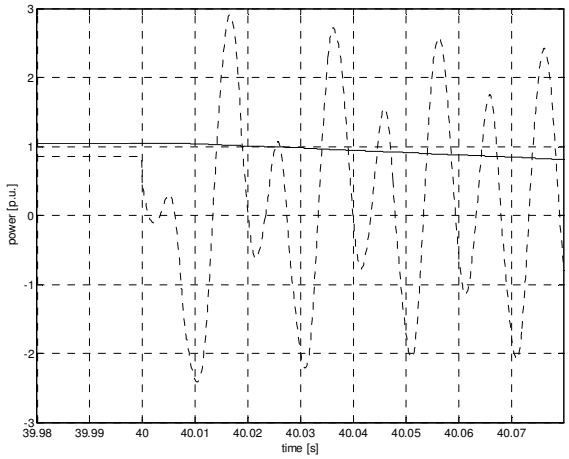

Figure 220 Grid power (solid line) and generator stator power (dotted line) during the 2-phase short circuit of a OptiSpeed V80 2 MW wind turbine model

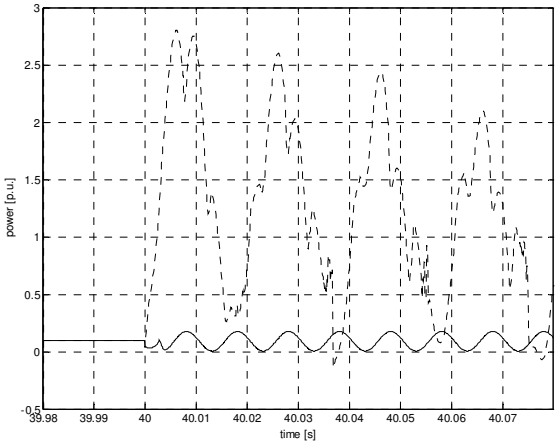

Figure 221 Grid converter power (solid line) and generator rotor power (dotted line) during the 2-phase short circuit on the wind turbine

The current exchanged with the grid is shown in Figure 222. The current peak caused by the sudden voltage drop is approx. 13.1 p.u. for the machine model without saturation effects and 12.2 p.u. for the simulations using the machine model including saturation effects.

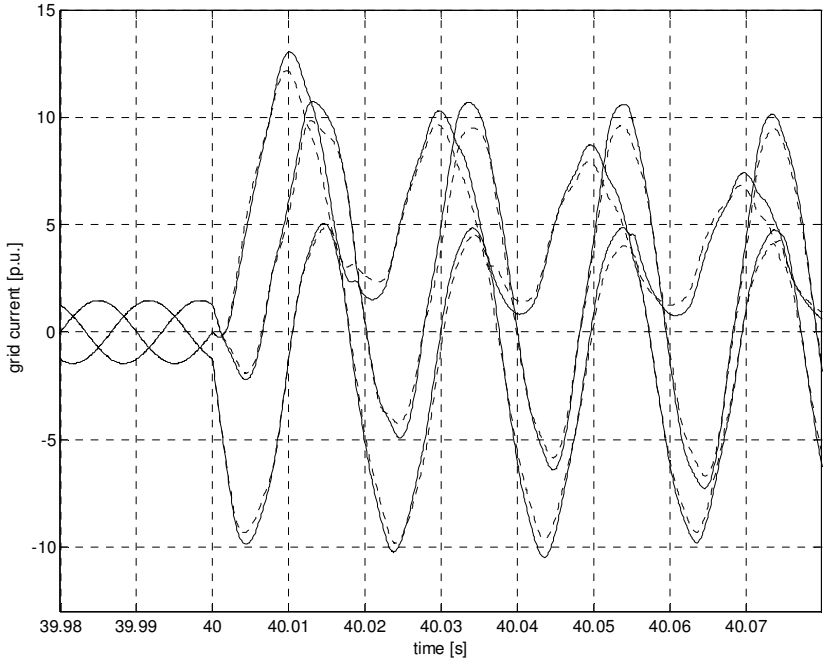

Figure 222 Grid current during the 2-phase short circuit on a V80 2MW wind turbine model using a machine model with saturation effects (dotted line) and without saturation effects (solid line)

However in reality the short circuit current contribution is much less than shown in Figure 222, since the over voltage protection system will trigger as soon the DC-link voltage (Figure 223) is 1.18 p.u. The grid current at this time is approx. 5 p.u.

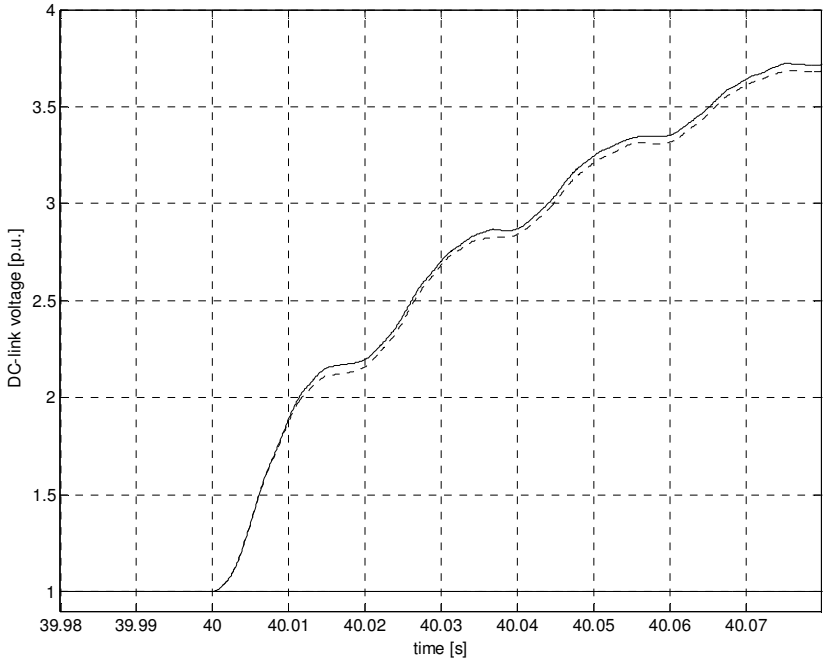

Figure 223 DC-link voltage of the converter during the 2 phase short circuit

9.4 Discussion of the simulation results

The above chapters show a study with the Vestas OptiSpeed wind turbine model. An example for a simulation on the operation limit and a fault simulation has been made. Furthermore for the simulations two different machine models, one model including all saturation effects and one without any saturation effects have been used. The influence of machine saturation during general operation of the OptiSpeed wind turbine is negligible. The turbine finds its steady state in a minimal different operation point, which is due to the control characteristics of the speed control. In the simulations made only with the electrical system, neglecting the mechanical and aerodynamically elements of the turbine show no difference at all during simulation using the machine model with included saturation effects or without. Oscillations caused by the saturation effects are not clearly identified. Existing oscillations are due to drive train oscillation, which get energized partly from the control in the rotor terminals of the generator. This energizing of the oscillation on the other hand can be a sign of angle error supplied rotor currents at the rotor terminals. It is recommended to investigate this in future work. Another method to reduce oscillations is an active damping, which is used in the wind turbines. The effect of this active damping function can be seen in the two different simulation results of chapter 9.3.1 and 9.3.2. In the simulation of the two phase short circuit a changed damping parameters value has been used, which reduced the oscillations by about 9% compared to the simulation of the voltage dip, where the default value for the active damping has been used. (Figure 224, Figure 225).

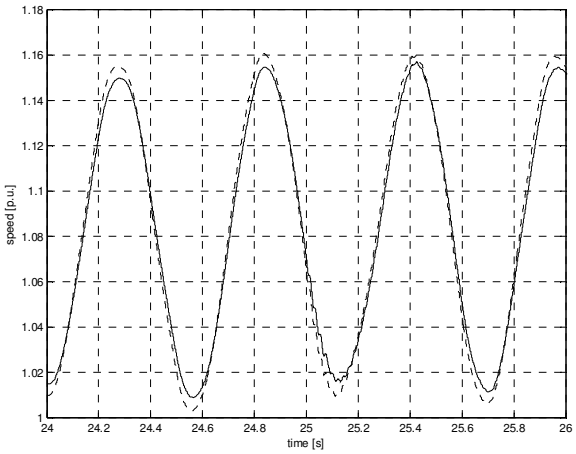

Figure 224 Generator speed during operations of the OptiSpeed^{TM} wind turbine model with default drive train damping parameter

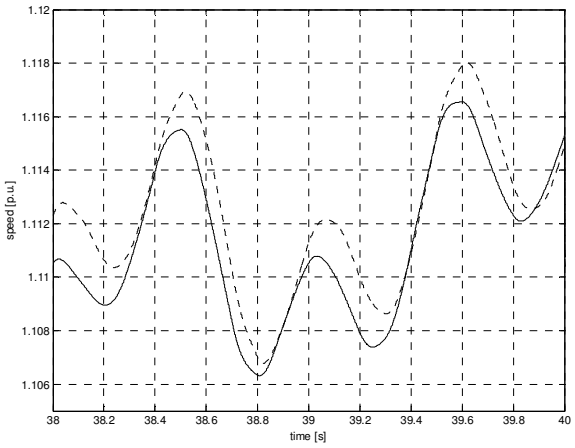

Figure 225 Generator speed during operations of the OptiSpeed^{TM} wind turbine model with different drive train damping parameter value

However, the OptiSpeed wind turbine is operating through the voltage dip and stays inside the electrical operation limits. The gearbox of the turbine has to withstand load oscillations during the incident. These stresses are important to consider during dimensioning in order to keep the expected life time of the turbine. It is to notice though, that the model is not optimally tuned and the used parameters for these simulations are general predefined parameters. The possible exchanged power over the grid converter is limited due to the DC-link voltage and the maximal current through the inverter elements. This limit is reached as seen in Figure 208.

Despite the oscillations in the drive train the grid power is smoothly controlled. The oscillation of the generator stator power is compensated with the addition of the generator rotor power. Generally it can be concluded, that the wind turbine with DFIG control is better grid compliant as the wind turbine with controlled rotor resistance. However the stress for the wind turbine components itself due to grid faults (torque oscillation and dynamic power exchange between stator and rotor of the generator) is considered harder on the wind turbine with the presented DFIG control. On the other hand the wind turbine's stress is less under rated conditions compared to the wind turbine with controlled resistance.

The influences of generator saturation effects are negligible in normal operation. In fault situation, the OVP will short circuit the rotor terminals of the generator, which enforces the natural behaviour of the induction machine and therewith increase the influence of saturation.

Chapter 10

10. Conclusion

In order to research and gain knowledge about wind turbine behaviour during grid faults or abnormal operations new wind turbine models have to be developed. Approximated behaviours are not sufficient for today's tasks and therefore detailed multifunctional models have to be developed. In this thesis a detailed model of two wind turbine types has been developed to gain better understanding about dynamic behaviour during faults e.g. two phase short circuits or voltage dips. As a key issue, the induction generator's behaviour has been investigated with a detailed three phase model.

10.1 Summary of the work

This thesis is focused on the development of a variable speed wind turbine model with an induction generator to be used in normal operation as well as in fault situations. To achieve this in detail, two specific wind turbine types from Vestas have been implemented in Matlab/ Simulink. The models shall provide opportunities for the investigation of a wide range of wind turbine sizes and different conditions while retaining easily accessible parameters which are used as input for the model.
It is important to have adequate wind turbine models for the study of grid connection conditions. In Chapter 2 a few existing grid connection requirements are discussed and compared.
The basis for a realistic representation of the wind turbine and their properties is an accurate model of the generator. The third chapter introduces therefore an analytical three phase machine model and discusses the improvement achieved by considering the effects of saturation. The behaviour of the model under normal operating conditions is validated by comparison with steady state measurements, and the applicability of the machine model during dynamic fault situations is validated with a direct on line start of a machine in a test bench. It is shown, that the consideration of leakage inductance saturation of the machine is especially important during fault situations. A simulated stator current with a machine model including main and leakage inductance saturation effects shows an error of less than 2% compared to the test bench test measurements, while during high currents an error of 20 % in peak values is observed. Though a 20 % error is large it none the less represents a 10% reduction in error compared to simulations with the simple machine models neglecting any additional effects. A further reduction of the error could be achieved while including further additional affects such as skin, proximity effect and iron losses, which are not included in this work.
In addition to the three phase generator model, the whole electrical network is depicted in a three phase system. Development of three phase models and the implementation into Matlab/ Simulink turned out to be a rather challenging task. The transformations that are commonly used to simplify the mathematical representation of the system e.g. Park Transformation are appropriate for other purposes e.g. for control strategy development, but inadequate for the demands on these models. Though it is certainly possible to investigate symmetrical fault situations of wind turbines with a model system based on dq-components (i.e. the Park - transformation), it presumes very detailed knowledge about

the total system configurations and has limited scope for adaptation to expansion and variations to other uses e.g. for asymmetrical simulations. Using a three phase system avoids any invalid assumptions introduced by the transformation theory and therefore introduces less error and represents more closely the physical system, which is a priority for the model.
In chapter 4 the models of a three-phase two-winding, a three-phase three-winding and a three-phase autotransformer are developed, using the experiences gained from the machine modelling. The following Chapter 5 presents the modelling method “Dynamic Node technique”, which is needed in order to connect the electrical elements generator, transformer, grid elements and source to be able to simulate the complete wind turbine.
The development of the wind turbine model is concluded by the implementation of a model for the aerodynamics (modelling the wind obtained power, pitch of the blades and 3p-effect), the mechanical model (using two masses: representing the mass of the blades and the drive train, and including the generator axis) and the control systems. The models for the aerodynamical, the mechanical components and the control systems have been developed in different projects previously and have undergone several verification processes. The main challenge encountered during this work was related to combine the existing models with the own developed advanced electrical models into an efficient complete model.
Because the control systems of the two investigated wind turbines types are different, a complete wind turbine model for the Vestas OptiSlip wind turbine and a complete model of the Vestas OptiSpeed turbines have been made. The control systems of the wind turbine with controlled resistance is shown and discussed in chapter 7 and the wind turbine control with DFIG is seen in chapter 8.
With the two developed models, simulations of faults according to current grid connection requirements for wind turbines have been carried out. From the many presented requirements discussed, a two phase short circuit and a voltage dip were chosen for investigation. The two phase short circuit is an interesting case, because it occurs relatively often and presents an asymmetrical case. Further a voltage dip inside the operation limits of the two turbines has been investigated. Both faults were simulated with a generator model both including and excluding saturation effects. While in the simulation of an uncontrolled machine, these effects play an important role, they are minimal in a controlled wind turbine. In normal conditions the influence of machines saturation is minimal and can be neglected using the studied machine type. However, in fault situations the saturation effects do have a greater influence for some machine types. The two specific examples which have been investigated do not provide suitable basis to draw a general conclusion. Because of this it is an advantage to consider saturation effects during grid fault studies until a general conclusion can be drawn.

10.2 Results obtained in the thesis

The present thesis contributes to the body of research in the field of wind turbine behaviour in fault situations and their mathematical representation.

The main contributions have been:

- **Overview of existing grid codes**
  - Methods for comparing different grid connection requirements have been presented.

- Presentation of the perspective of network operators as well as the wind turbine manufacturer has been made.
- Emphasis of important points for the development of wind turbine grid codes is made.

- **Modelling and analysis of the induction machine model**

  - Analysis of different analytical induction machine representations has been made.
  - An advanced three phase ABC/abc induction machine model is developed in Matlab/ Simulink. The model includes a representation of leakage and main inductance saturation, as well as friction and windage losses. A discussion of the saturation influences due to faults is presented.
  - Measurements on a test bench at full-scale verifies the achieved model.

- **Modelling of electrical three-phase components**

  - A three phase transformer model has been developed in Matlab/ Simulink. A two-winding three-phase autotransformer is presented.
  - A three phase 6^{th} order transmission line has been implemented as well as a simplified three phase line model for the simulation of a grid.
  - Different three phase sources for the simulation of voltage dips, phase changes, frequency changes, voltage ramp and frequency ramps and harmonics are developed.

- **Modelling of two complete wind turbine systems (OptiSlip, OptiSpeed)**

  - The models are reliable for research in symmetrical as well as asymmetrical fault situations and short circuits due to the three phase representation of the electrical system.
  - The models represent the two standard used control strategies and include previously validated aerodynamical and mechanical models. Completed with the electrical models it is believed to have a real representation of the behaviour of the wind turbines.
  - The model has particular importance for wind turbine component design and it is useful for studies of e.g. load and controller design.
  - Because it models the grid, it can be used for simple grid fault simulations and therefore it is useful as documentation for customers and useful as a supportive component for larger grid connection studies.
  - The model is easy to handle, since all input parameters used for the simulations are available by documentation inside the company.
  - The usage of Matlab/ Simulink keeps the specific model open for adaptation to a variety of uses, for example for the purpose of harmonic studies.

- **Results obtained from the models**

  - The generator effects like saturation are alleviated by doubly-fed operation and are more likely to be experienced with an induction machine with a short-circuited rotor.
  - While the OptiSlip wind turbine model shows especially stresses of the electrical system during fault situations the OptiSpeed wind turbine model shows more stresses of the mechanical system compared to the electrical system, which is based on the control strategy.
  - The investigation with the OptiSpeed wind turbine model show high stresses internally in the turbine in order to retain good power quality.
  - The simulated examples show a satisfactory wind turbine operation within the accepted operation limits.
  - During modelling of the turbines a review of the control systems has been conducted.

10.3 Future work

The research captured in this work represents the state of the art of today, though it is only a step in the effort to clarify the influences of faults in wind turbines and their impact on the grid. The following are opportunities for future work:

- An important part the wind turbine model yet to be implemented, is the total protection system of the turbine. A model encompassing this would to enable further fault studies.
- Extending the model with recently developed control strategies for fault ride through capability.
- Further validation of the transformer and the complete turbine models with measurements should be performed.
- Implementation of other machine phenomena such as slots effects, skin effects and the implementation of a realistic converter model (switching model) to capture harmonic contributions to the turbine (flicker) and investigate overload conditions of the converter.
- Expanding the study in order to clarify the influence of several different generator types and finding a rule for the machine phenomena.
- Measurement of an asymmetrical fault to further validate the machine and wind turbine model.

Another major challenge to modelling such a complex system with many nonlinear elements in Matlab/ Simulink is the stability of the simulation itself. Therefore one of the major issues beside the scientific work mentioned above is an optimisation of the models for the use in Matlab/ Simulink. Another possibility is to translate the achieved models from their representation in Simulink to Matlab (without Simulink) and use the graphical user interface programming which was recently introduced by Matlab or the use of another simulation platform altogether.

Chapter 11

11. Appendix

11.1 REFERENCES

/1/ ABB Calor Emag, *Switchgear Manual*, Cornelsen Verlag Berlin, 10th revised edition, 1999 ISBN 3-46448236-7

/2/ V.Akhmatov, H. Knudsen, A.H. Nielsen, *Advanced simulation of windmills in the electric power supply*, International Journal of Electrical Power and Energy Systems, 22 (6) , p. 421-434, Elsevier 2000

/3/ Vladislav Akhmatov, *Analysis of Dynamic Behavior of Electric Power Systems with Large Amount of Wind Power*, PhD Thesis April 2003, Ørsted DTU, Denmark

/4/ Dimitios Arsudis, *Doppeltgespeister Drehstromgenerator mit Spannungzwischenkreis-Umrichter im Rotorkreis für Windkraftanlagen*, Dissertation TU Braunschweig, 1989 Germany

/**5**/ S.B. Bayne, M.G. Giesselmann, *Effect of blade passing on a wind turbine output*, Conversion Engineering Conference and Exhibit, 2000. (IECEC) 35th Intersociety

/6/ Gotthard Berger, *Beitrag zur Realisierung der feldorientierten Drehzahlregelung einer von einem Pulsspannungswechselrichter gespeisten Drehstromasynchronmaschine,* Dissertation, 1982, TU Ilmenau, Germany

/7/ F. Blaschke, *Das Verfahren der Feldorientierung zur Regelung der Asynchronmaschine*, Dissertation 1974, TH Ilmenau

/8/ E. Bogalecka, *Power control of a double fed induction generator without speed or position sensor*, EPE 1993

/9/ E. Bogalecka, *Stability Analysis of a Double Fed Induction generator with the PLL Controller*, IECON Proceedings (Industrial Electronics Conference), 1 , p. 67-72. IEEE 1994

/10/ Ion Boldea, S. A. Nasar, *Electric Drives,* CRC Press LLC, 1999, ISBN 0-8493-2521-8

/11/ Sigrid M. Bolik, Jens Birk, Björn Andresen, John G. Nielsen, *Vestas Handles Grid Requirements: Advanced Control Stradegy for Wind Turbines,* EWEC'03, Juni 2003, Madrid, Spain

/12/ Sigrid M. Bolik, *Grid requirements challenges for Wind Turbines,* Proceedings Fourth International Workshop on Large-Scale Integration of Wind Power and Transmission Networks for Offshore Wind Farms, October 2003, Billund, Denmark

/13/ P. B. Christensen, M. Pronk, *Combined Speed and Pitch Control of a Vestas V44-600 kW Wind Turbine,* Aalborg University, Departement of Control Engineering,1997, Denmark

/14/ Peter Christiansen, Jesper R. Kristoffersen, *The Wind Farm Main Controller and the Remote Control System of the Horns Rev Offshore Wind Farm,* Proceedings Fourth International Workshop on Large-Scale Integration of Wind Power and Transmission Networks for Offshore Wind Farms, October 2003, Billund, Denmark

/15/ M. Davidson**,** *Interaction of a Wind Farm with the Distribution Network and its effect on Voltage Quality*, Embedded Generation on Distribution Networks (Digest No. 1996/194), IEE Colloquium on the Impact of , 1996

/16/ Li Dongxia, Wang Zanji, Liu Xiucheng (1999), A *new ATP add-on for modeling internal Faults in Power Transformers*, ICEMS 2001

/17/ Jürgen Ehrenberg , Björn Andrese, Anders Rebsdorf, Windkraftanlagen für den Megawattbereich, Digitale Steuerung eines doppelt gespeisten Asynchrongenerators ohne Lagegeber, Teil 1 , Zeitschrift Elektronik 2001, issue 18, page 60 ... 67, Germany

/18/ Jürgen Ehrenberg , Björn Andrese, Anders Rebsdorf, Windkraftanlagen für den Megawattbereich, Digitale Steuerung eines doppelt gespeisten Asynchrongenerators ohne Lagegeber, Teil 2 , Zeitschrift Elektronik 2001, issue 19, page 78 ... 87, Germany

/19/ Jürgen Ehrenberg, Karl Stapelfeldt (1998), Software Documentation, Sican GmbH, Braunschweig, Gemany

/20/ J.B. Ekanayake, L. Holdsworth, N.Jenkins, "Comparation of 5th order and 3th order machine models for doubly fed induction generator (DFIG) wind turbines", Elsvier Power System Research 67, 2003, pp. 207-215

/21/ Eltra, Elkraft System, *Vindmøller tilsluttet net med spændinger under 100 kV*, Draft, May 2004, Denmark

/22/ E.ON Netz, *Ergänzende Netzanschlussregeln für Windenergieanlagen*, December 2001, Germany

/23/ E.ON Netz, *Netzanschlussregeln Hoch- und Höchstspannung*, August 2003, Germany

/24/ ESB National Grid, *Wind Farm Connection Requirements,* Draft Version 1.0, February 2002, Ireland

/25/ A. E. Fitzgerald, Charles Kingsley,Jr. , Stephen D. Umans, *Electric Machinery,* McGraw-Hill Book Company, 1992, ISBN 0-07-112946-4

/26/ Frank Flinders, Wardina Oghanna, Steven Semini, *Mixed electrical and mechanical simulations using dynamic system analysis packages*, Proceedings of IEEE/ ASME Joint Railroad Conference, Pittsburgh, April 6-8, 1993 , p. 87-93

/27/ Frank Flinders, Wardina Oghanna, Steven Semini, *Power electronics simulation laboratory using "Simulink" dynamic systems analysis packages*, IMACS - TC1 '93. 4th International Conference Proceedings, 1993, p. 643-50

/28/ J. Fortmann, *Validation of DFIG model using 1.5 MW turbines for the analysis of its behaviour during voltage drops in the 110 kV grid*, Fourth International Workshop on Large-Scale Integration of Wind Power and Transmission Networks for Offshore Wind Farms, Oct. 2003, Billund, Denmark

/29/ A.H. Ghorashi, S.S. Murthy, B.P Singh, *Field Studies and Transient Analysis Related to Wind Electric Systems*, Proceedings of Power Electronics, Drives and Energy Systems for Industrial Growth, 1996, Volume: 1 , 1995, p. 271 -279 vol.1

/30/ C. Goldemberg, A. de Arruda Penteado, F. A. M. Salotti, *Induction motor analysis in the ABC/abc refernce frame including saturation effects*, *Proceed. of the ICEM 2000,pp.397-401*

/31/ Clovis Goldemberg, Aderbal de Arruda Penteado Jr., *Improvements on the inductance matrix inversion simplifying the use of the ABC/abc induction machine model,* 1999, IEEE 0-7803-5293-9/99

/32/ L. H. Hansen, *Generator Concepts and their Progress" presented at Seminar on Control concepts of Wind Turbines*, Oct. 2000, Aalborg University, Denmark

/33/ J. H. S. Hansen, M. Lau, P. F. Sørensen**,** *Sensorless Control of a double fed Induction generator for wind turbine Applications*, Aalborg University 1998, Denmark

/34/ E. Hau, *Windkraftanlagen - Grundlagen, Technik, Einsatz, Wirtschaftlichkeit*, Springer Verlag Berlin, 2. Auflage, 1996, ISBN: 3540574301
/35/ S. Heier, *Grid Integraton of Wind Energy Conversion Systems*, John Wiley & Sons Ltd, 1998, ISBN 0-471-97143-X
/36/ W. Hofmann, A. Thieme, *Control of a Double-fed Induction generator for Wind-Power Plants*, PCIM'98 May 1998 Nürnberg, Germany
/37/ W. Hofmann, *Optimal reactive power splitting in wind power plants controlled by double-fed induction generator*, IEEE AFRICON Conference, 1999, p. 943 -948 vol.2
/38/ W. Hofmann, B. Rabelo, *Optimal Active and Reactive Power Control with the Double-Fed Induction Generator in the MW-Class Wind-turbines*, PEDS´01
/39/ Prashanth S.S. Holenarsipur, Ned Mohan, Vermon D. Albertson, Jack Christofersen, *Avoiding the use of negative inductances and resistances in modeling three-winding transformers for computer simulations*, IEEE 1998, 0-7803-4403-0/98
/40/ B. Hopfensperger, D.J. Atkinson, R.A. Lakin, *Kaskadierte doppeltgespeiste Maschinen als drehzahlvariable Generatorsysteme: ein Ueberblick*, DEWEK '96. 3. Deutsche Windenergie-Konferenz. Tagungsband, Wilhelmshaven, Germany
/41/ http://www.control-design.de/home_deu/Applikationen/Windenergie/hauptteil_windenergie.html
/42/ F. Iov, F. Blaabjerg, A.D. Hansen, P. Sørensen, *Analysis of reduced order models for large squirrel-cage induction generators in wind turbine applications*, Proceed. of EPE'03,2003
/43/ F. Iov, A.D. Hansen, F. Blaabjerg, *A New Matlab/ Simulink Toolbox for Wind Turbine Applications*, Proceed. Nordic MATLAB Conference 2003 in Copenhagen
/44/ L. Jánosi, A. D. Hansen, P. Sørensen, F. Blaabjerg, J. Bech, B. Bak-Jensen, *Simulation of 12 MW Wind Farm*, EPE´2001
/45/ N. Jenkins, G. Strbac**,** *Impact of embedded generation on distribution system voltage stability*, IEE Colloquium on Voltage Collapse (Digest No: 1997/101), p. 9/1-4, 1997
/46/ Martin Høgdahl Jensen, *Broadband model of the distribution network*, Dissertation Aalborg University, Institute of Energy Technology, 2003, ISBN 87-89179-43-9
/47/ Martin Høgdahl Jensen, *Evaluation of the V80 VRCC Optislip*, Internal Vestas Documentation
/48/ H. Jordan, V. Klima, K. P. Kovacs, *Asynchronmaschinen,* Vieweg & Sohn Verlagsgesellschaft, 1975, ISBN 3-528-04600-7
/49/ Mladeb Kezunovic, Bogdan Kasztenny, Zijad Galijasevic, Donna Williams (1999), *New ATP add-on for modeling internal Faults in Power Transformers*, Proceedings of the American Power Conference. Kezunovic, Mladen 2000, 62 , p. 132-137
/50/ K. P. Kovacs, *Symmetrische Komponenten in Wechselstrommaschinen*, Birkhäuser Verlag, 1962
/51/ K. P. Kovacs**,** *Transient Phenomina in Electrical Machines*, ELSEVIER, 1984, ISBN 0-444-41713-3
/52/ P. C. Krause, O. Wasynczuk, S. D. Sudhoff, *Analysis of electrical Machinery, IEEE PRESS, 1994 ISBN 0-7803-1101-9*
/53/ Thomas Krüger, Björn Andresen, *Vestas OptiSpeed^{TM} – Advanced Control Strategy for Variable Speed Wind Turbines*, EWEC 2001, Copenhagen, Denmark
/54/ Thomas Krüger, Jens Birk, *Metode til kontrol af vindturbine under perioder med afbrydelse af elnettet,* Patent DK 174411 B1, February 2003
/55/ Prabha Kundur, *Power System Stability and Control*, McGraw-Hill Inc. 1993, ISBN 0-07-035958-X
/56/ W. Langreder, *Models for Variable Speed Wind Turbines*, Risø 1996

/57/ W.E.Leithead, S. de la Salle, D. Reardon, *Role and objectives of control for wind turbines*, IEE Proceedings-C, Vol.138, No. 2, March 1991
/58/ J. A. Peças Lopes, N. Hatziargyriou, H. Vasconcelos, C. Monteiro, *Control Requirements for Optimal Operation of Large Isolated Systems with Increased Wind Power Penetration*, EWEC, April, 1999
/59/ W. Leonard, *"Control of Electrical Drives",* Springer Verlag, 1996, ISBN 3-540-59380-2
/60/ Per Lund, *Undersøgelse af transiente forløb på Kraftværker med speciel vægt på Egenforsyningen*, Akademiet for de tekniske Videnskaber, 1985
/61/ Julija Matevosyan, Thomas Ackermann, Sigrid Bolik, Lennart Söder, *Comparison of International Regulations for Connection of Wind Turbines to the Network*, NWPC '04, Grid Integration and Electrical Systems of Wind Turbines and Wind Farms, Chalmers University of Technology, 1-2 March 2004, Göteborg, Sweden
/62/ Nicholas W. Miller, *Power System Dynamic Performance Improvements From Advanced Power Control of Wind Turbine-Generators*, Fourth International Workshop on Large-Scale Integration of Wind Power and Transmission Networks for Offshore Wind Farms, Oct. 2003, Billund, Denmark
/63/ Ministerium für Bildung der DDR, *Lehrbriefe Elektroenergiesysteme 1 – 6,* Zentralstelle für Lehr- und Organiationsmittel des Ministeriums für Bildung, 1982/1983, Bestell-Nr. 021435012
/64/ L. Morel, H. Godfroid, A. Mirzaian, J.M. Kauffmann, *Double-fed induction machine: converter optimisation and field oriented control without position sensor*, IEE Proceedings Electric Power Applications 1998, 145 (4) , p. 360-368.
/65/ J. Morren, S.W.H. de Haan, P. Bauer, J.T.G. Pierik, J. Bozelie, "Comparison of complete and reduced models of a wind turbine with Doubly-Fed Induction Generator", Proceed. of EPE'03, 2003
/66/ Germar Müller, Grundlagen e*lektrischer Maschinen*, VCH Verlagsgesellschaft mbH, 1994, ISBN 3-527-28390-0
/67/ NECA, *National Electricity Code*, Version 1.0 Amendment 8.0, 1999 – 2003, Australia
/68/ Peter Novak, Inge Jovik, Bengt Schmidtbauer (1994), *Modeling and Identification of Drive-System Dynamics in a Variable-Speed Wind Turbine*, IEEE 0-7803-1872-2/94
/69/ P. Novak, T. Ekelund, I. Jovik, B. Schmidtbauer (1995), *Modeling and Control of Variable-Speed Wind-Turbine Drive-System Dynamics*, IEEE 0272-1708/95
/70/ D. W. Novotny, T. A. Lipo, *Vector Control and Dynamics of AC Drives,*Clarendon Press, 1996, Oxford, ISBN 0-19-856439-2
/71/ W. Nürnberg, *Die Asynchronmasch*hine, Springer Verlag, 1963
/72/ W. Nürnberg, *Die Prüfung elektrischer Maschinen,* Springer – Verlag, 1965
/73/ J. Olav, G. Tande, *Impact of Wind Turbines on Voltage Quality*, ICHQP'98 (Athen, Greece), IEEE 1998
/74/ Chee-Mun Ong, *Dynamic Simulation of Electric Machinery using Matlab/Simulink,* PRENTICE HALL, 1994, ISBN 0-13-723785-5
/75/ Jørgen Kaas Pedersen, Skjold Saxe (1974), *Magnetiske Kredse og Transformere*, Den private ingenørfond ved DtH, Laboratoriet for Almen Elektroteknik, Danmarks tekniske Højskole, 2800 Lyngby
/76/ J.K. Pedersen, M. Akke, N.K. Poulsen, K.O.H Pedersen, *Analysis of wind farm islanding experiment*, Energy Conversion, IEEE Transaction on , Volume: 15 Issue: 1 , March 2000
/77/ T. Petru, *Modeling of Wind Turbines for Power System Studies*, Thesis, Chalmers University of Technology, 2003
/78/ T.Petru, T. Thiringer, *Modelling of Wind Turbines for Power System Studies*, 2002, IEEE 0885-8950/02

/79/ P. Pillay, V. Levin, *Mathematical models for induction machines*, *Proceed. of IAS-95, Vol.X.pp.606-616*
/80/ U. Rädel, D. Navarro, G.Berger, S. Berg, *Sensorless Field-Oriented Control of a Slipring Induction Generator for a 2.5 MW Wind Power Plant from Nordex Energy GmbH*, EPE 2001
/81/ Rudolf Richter , *Elektrische Maschinen/ Die Transformatoren,3*. Band, Birkhäuser Verlag, 1963
/82/ Rudolf Richter, *Elektrische Maschinen/ Die Induktionsmaschinen,* 4. Band, Birkhäuser Verlag, 1954
/83/ Pedro Rosas, *Dynamic Influences of Wind Power on the Power System*, PhD Thesis March 2003, Ørsted DTU, Denmark
/84/ J.R. Saenz, G. Tapia, X. Ostolaza, A. Tapia, R. Criado, J.L. Berastegui, *Simulation of a wind farm performance under wind speed changes*, Electricity Distribution, 2001. Part 1: Contributions. CIRED. 16th International; Conference and Exhibition on (IEE Conf. Publ No. 482) , Volume: Summaries , 2001
/85/ Z. Saad-Saoud, N. Jenkins, *Simple wind farm dynamic mode*l, Generation, Transmission and Distribution, IEE Proceedings- , Volume: 142 Issue: 5 , Sept. 1995
/86/ Slavomir Seman, Antero Arkkio*, An Induction Motor Transient Model in Simulink Including Saturation and Skin Effect in Rotor Bars*, NorMUD Summer Seminar 2002, Tiapalsaari, Finland
/87/ I. Serban, F. Blaabjerg, I. Boldea, Z. Chen, *A study of the Doubly-Fed Wind Power Generator Under Power System Faults*, proceed. of EPE'03,2003
/88/ J.G. Slootweg, H. Polinder, W. L. Kling, *Dynamic Modelling of a Wind Turbine with Douply Fed Induction Generator*, 2001, IEEE 0-7803-7173-9/01
/89/ Poul Sørensen, Anca Hansen, Lorand Janosi, John Bech, Birgitte Bak-Jensen, *Simulation of Interaction between Wind Farm and Power System*, Risø National Laboraty, Roskilde, Dec. 2001, Risø-R-1281(EN)
/90/ SP Transmission & Distribution, Scottish Hydro Electric, *Guidance Note for the connection of Wind Farms*, Issue No. 2.1.4, December 2002, Scotland
/91/ Tao Sun, *Power Quality of Grid-Connected Wind Turbines with DFIG and Their Interaction with the Grid*, PhD Thesis May 2004, Aalborg University, Denmark, ISBN 87-89179-49-8
/92/ A. Tapia, G. Tapia, J.X. Ostolaza, J.R. Saenz, R. Criado, J. L. Berasategui, *Reactive Power Control of a Wind Farm made up with Doubly Fed Induction Generators*, Porto Power Tech Proceedings (Cat. No.01EX502), 2001, p. 6 pp. vol.4.
/93/ A. Tapia, G. Tapia, X. Ostolaza, E. Fernandez, J.R. Saenz, *Modeling and dynamic regulation of a wind farm*, Power Electronics Congress, 2000. CIEP 2000. VII IEEE International , 2000
/94/ Peter Vas, *Sensorless Vector and Direct Torque Control,* Oxford University Press, 1998, ISBN 0-19-856465-1
/95/ Peter VAS, *Electrical Machines and Drives, A Space-Vector Theory Approach,* Oxford University Press, 1992, ISBN 0-19-859378-3
/96/ Internal Vestas Documentations no. 8729
/97/ John G. Vlachogiannis, *An accurate autotransformermodel for load flow studies effect on steady-state analysis of Hellenic transmission system*, Electric Power Systems Research. 1999, 50 (2) , p. 147.
/98/ K. Vogt, *Berechnung elektrischer Maschinen*, VCH Verlag, 1996, ISBN 3-527-28391-9
/99/ S. Vørts, *Elektriske Fordelingsanlæg*, Polyteknisk Forlag, 1990, ISBN 87-502-0707-5

/100/ H. Weh, *Elektrische Netzwerke und Maschinen in Matritzendarstellung*, Hochschultaschenbücherverlag, 1968
/101/ Wu Xueguang; Wang Weisheng; Dai Huizhu; Chen Yunping, *Application of models of the wind energy conversion system to wind power dynamic analysis*, Power System Technology, 1998. Proceedings. POWERCON '98. 1998 International; Conference on , Volume: 2
/102/ I. V. Yakimets, V. G. Narovlyanskii, *Autotransformer with a voltage stabilized tertiary winding*, Electrical Technology No. 1. pp. 21-30, Elsevier 1995
/103/ X. Zhao, *Neue Umrichtertechnologien sind in Entwickliung*, Erneuerbare Energien 9/2001
/104/ Zhongming Ye, Bin Wu, *Simulation of Electrical Faults of Three Phase Induction Motor Drive System*, *Power System Technology, Proceed. of. PowerCon 2000 , Vol. 2 pp. 789 -794*

11.2 Glossary of Symbols

Symbols

a , j	complex Versors[1]
a , D	distance between the conductors
a_{12} , a_{23} , a_{13}	Transformer ratio between side 1-2, 2-3 and 1-3
c_p	Power coefficient
e	induced voltage
f_1	Grid frequency
f_1 , f_2 , f_3 , f_4 , f_5 , f_6 , f_7	Functions of angle difference between phases used in machine and transformer induction matrix
i	current
m	number of phase
n	Number; gear ratio
n_g	Generator speed
n_0	Synchronous speed
p_p	pairs of poles
r	radius
r_T	equivalent circle radius
r_P	distance to a point
r_B	equivalent radius of the n-bundle conductor
s	slip
u	voltage
ue	ratio between stator and rotor winding
v_w	Wind speed
w_1 , w_2	Primary, secondary winding turns
A	Area
B	magnetic field strength
C	Capacitance
D	damping factor
$D\omega_r$	damping torque
E_s	from stator induced voltage
H	electric field strength
I	Rms current
$I_{r\,meas}$	Measured rotor current amplitude
I_{ref}	Desired rotor current
J	Inertia
J_{ges}	Total inertia
K_{jj} , K_{kk} , , K_{jk} K_{kj}	Capacitance coefficients
K_r	Generator constant
K_{pS}	Gain of the slave PI-controller
K_{pM}	Gain of the master PI-controller
L	inductance
L_m , L_h	main flux inductance

$L_{ms,}\ L_{mr}$	mutual inductance stator, rotor
L_{msr}	stator – rotor couple inductance
L_{σ}	leakage flux inductance
N	number of turns
$N\,\xi$	effective number of turns
$N_1,\ N_2$	number of slots (stator, rotor)
P	active power
P	Potential used in line theory
P_M	Mechanical power
P_w	Power obtained from the wind
Q	reactive power
Q	Charge used in line theory
R	Resistance
R'_{ext}	External rotor resistance
S	Apparent power
T_A	Aerodynamic torque
$T_{cl\,S}$	Closed loop slave controller time constant
$T_{cl\,M}$	Closed loop master controller time constant
$T_{i\,S}$	Integrator time constant for the slave PI-controller
$T_{i\,M}$	Integrator time constant for the master PI-controller
T_e	electromagnetic torque
T_m	mechanical load torque
T_r	Generator time constant
T_S	Shaft torque
U	Rms voltage
X	Reactance
Z	Impedance
ε	Permittivity
$\theta,\ \varphi$	General angle
γ	Angle to arbitrary rotating reference frame
$\kappa_{fe},\ \kappa_w$	electrical conductivity of the core, winding material
λ	Tip speed ratio
μ	order of rotor harmonics
$\mu_{fe},\ \mu_{air}$	Permeability of the core, air
υ	order of stator harmonics
π	Constant pi
ω	Angular speed
ω_r	angular rotor speed
ω_e	electrical angular rotor speed
ϑ	Pitch angle
ρ	rotor angle
$\dot{\rho}$	rotor angle velocity = ω_r
$\ddot{\rho}$	rotor angle acceleration
σ	Angle between rotor and flux reference frame
Φ	flux
Θ	mmf or magnetomotive force

Ψ	Flux

Upper index

s	stator reference frame
r	rotor reference frame
μ	flux reference frame

Lower index

abc	3-phase rotor system of a machine
a, b, c	Phase a, b, c
d , q	components of Park's transformation
fw	Friction and windage
g	generator
k	Short circuit
rtd, n	Rated/ nominal
o	No load/ open circuit
ref	reference
s, r	Stator, rotor
ABC	3-phase stator system of a machine
G	Grid converter
L	grid
R	rotor
0	Zero component
123	3-phase systems of transformers
1, 2, 3	Primary, secondary, tertiary
α , β	components of Clark's transformation
μ, *m*	Magnetizing parameter

Special Symbols

→	vector
_	complex vector
´	transposed systems with using ratio ue
*	conjugate complex

Abbreviation

DC	Direct Current
DFIG	Doubly Fed Induction Generator
DOL	Direct On Line
EMK	electromotive force
IG	Induction Generator
2w3ph	2 winding 3 phase
3w3ph	3 winding 3 phase
OVP	Over Voltage Protection
VRCC	Vestas Rotor Current Control
VCS	Vestas Converter System

[1]**Versor** [NL., fr. L. vertere, versus, to turn.] (Geom.) The turning factor of a quaternion. Note: The change of

one vector into another is considered in quaternions as made up of two operations; 1st, the rotation of the first vector so that it shall be parallel to the second; 2d, the change of length so that the first vector shall be equal to the second. That which expresses in amount and kind the first operation is a versor, and is denoted geometrically by a line at right angles to the plane in which the rotation takes place, the length of this line being proportioned to the amount of rotation. That which expresses the second operation is a tensor. The product of the versor and tensor expresses the total operation, and is called a quaternion. See Quaternion.

11.3 Coordinate transformation

Vektor in Stator coordinates (a_s, b_s)

$$\underline{V}^s = \left|\underline{V}\right| \cdot e^{j \cdot \varphi_s} = V \cdot e^{j \cdot \varphi_s}$$

Vektor in Rotor coordinates (a_r, b_r)

$$\underline{V}^r = \left|\underline{V}\right| \cdot e^{j \cdot \varphi_r} = V \cdot e^{j \cdot \varphi_r}$$

Vektor in Flux coordinates (d, q)

$$\underline{V}^\mu = \left|\underline{V}\right| \cdot e^{j \cdot \varphi_\mu} = V \cdot e^{j \cdot \varphi_\mu}$$

angle correlation

$$\varphi_s = \varphi_r + \rho$$
$$\varphi_r = \varphi_s - \rho$$
$$\varphi_\mu = \varphi_s - \gamma = \varphi_r + \rho - \gamma$$
$$\gamma = \gamma_r + \rho$$
$$\varphi_\mu = \varphi_s - \gamma = \varphi_r - \gamma_r$$

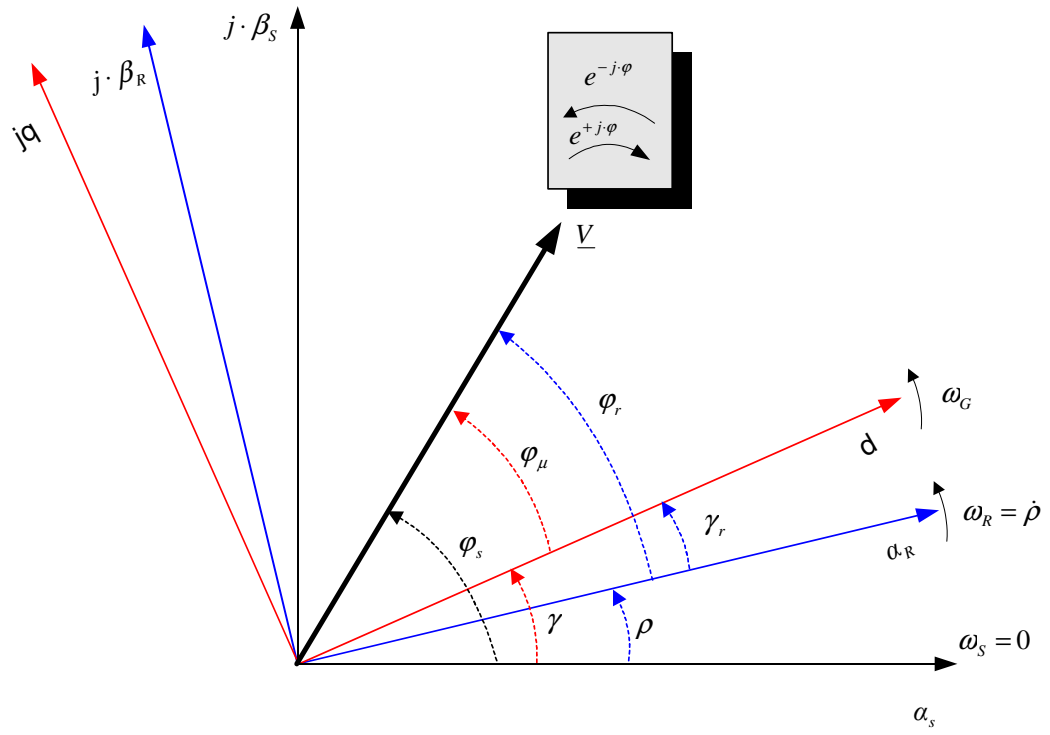

Figure 226 coordinate correlation

Overview over transformation of an vector in different reference frames

$\cdot e^{-j\varphi}$	$\cdot e^{j\varphi}$
Stator – Rotor $\underline{V}^s \cdot e^{-j\rho} = V \cdot e^{j\varphi_s} \cdot e^{-j\rho} = V \cdot e^{j(\varphi_r+\rho)} \cdot e^{-j\rho}$ $= V \cdot e^{j\varphi_r} = \underline{V}^r$	Rotor – Stator $\underline{V}^r \cdot e^{j\rho} = \underline{V}^s$
Stator – Flux $\underline{V}^s \cdot e^{-j\gamma} = V \cdot e^{j\varphi_s} \cdot e^{-j\gamma} = V \cdot e^{j(\varphi_\mu+\gamma)} \cdot e^{-j\gamma}$ $= V \cdot e^{j\varphi_\mu} = \underline{V}^\mu$	Flux - Stator $\underline{V}^\mu \cdot e^{j\gamma} = \underline{V}^s$
Rotor – Flux $\underline{V}^r \cdot e^{-j\gamma_r} = \underline{V}^r \cdot e^{-j(\gamma-\rho)} = V \cdot e^{j\varphi_r} \cdot e^{-j(\gamma-\rho)}$ $= V \cdot e^{j(\varphi_\mu+(-\gamma+\rho)} \cdot e^{-j(\gamma-\rho)}$ $= V \cdot e^{j\varphi_\mu} = \underline{V}^\mu$	Flux – Rotor $\underline{V}^\mu \cdot e^{+j(\gamma-\rho)} = \underline{V}^r$
Stator – Rotor	Rotor – Stator

$\frac{d\,\underline{V}^s}{dt}\cdot e^{-j\rho} = \frac{d\left(V\cdot e^{j(\varphi_r+\rho)}\right)}{dt}\cdot e^{-j\rho}$ $= \frac{d\left(\underline{V}^r\cdot e^{j\rho}\right)}{dt}\cdot e^{-j\rho}$ $= \frac{d\,\underline{V}^r}{dt}\cdot e^{j\rho}\cdot e^{-j\rho} + j\cdot\dot{\rho}\cdot\underline{V}^r\cdot e^{j\rho}\cdot e^{-j\rho}$ $= \frac{d\,\underline{V}^r}{dt} + j\cdot\dot{\rho}\cdot\underline{V}^r$	$\frac{d\,\underline{V}^r}{dt}\cdot e^{j\rho} = \frac{d\left(V\cdot e^{j(\varphi_s-\rho)}\right)}{dt}\cdot e^{j\rho}$ $= \frac{d\left(\underline{V}^s\cdot e^{-j\rho}\right)}{dt}\cdot e^{j\rho}$ $= \frac{d\,\underline{V}^s}{dt}\cdot e^{-j\rho}\cdot e^{j\rho} - j\cdot\dot{\rho}\cdot\underline{V}^s\cdot e^{-j\rho}\cdot e^{j\rho}$ $= \frac{d\,\underline{V}^s}{dt} - j\cdot\dot{\rho}\cdot\underline{V}^s$
Stator – Flux $\frac{d\,\underline{V}^s}{dt}\cdot e^{-j\gamma} = \frac{d\,\underline{V}^\mu}{dt} + j\cdot\dot{\gamma}\cdot\underline{V}^\mu$	Flux - Stator $\frac{d\,\underline{V}^\mu}{dt}\cdot e^{j\gamma} = \frac{d\,\underline{V}^s}{dt} - j\cdot\dot{\gamma}\cdot\underline{V}^s$
Rotor – Flux $i_d + j\cdot i_q = \left(i_\alpha + j\cdot i_\beta\right)\cdot e^{-j\cdot\varphi}$ $\frac{d\,\underline{V}^r}{dt}\cdot e^{-j(\gamma-\rho)} = \frac{d\,\underline{V}^\mu}{dt} + j\cdot(\dot{\gamma}-\dot{\rho})\cdot\underline{V}^\mu$	Flux – Rotor $\frac{d\,\underline{V}^\mu}{dt}\cdot e^{j(\gamma-\rho)} = \frac{d\,\underline{V}^r}{dt} - j\cdot(\dot{\gamma}-\dot{\rho})\cdot\underline{V}^r$

Correlation between Clark and Park transformation in with Space Vectors

The Clark and Park transformation or the α,β-coordinates and d, q coordinates are very similar. They are both in a space vector expressed 3-phase system. The only difference is the orientation α,β-coordinates are refereed to the non-rotating stator reference frame, the d, q components are oriented to an rotating reference frame.

The d, q – components in an arbitrary rotating frame can be achieved from the α,β - components with the transformation shown in equation (242), (244) and back transformation with equation (243), (245).

$$i_d + j\cdot i_q = \left(i_\alpha + j\cdot i_\beta\right)\cdot e^{-j\cdot\varphi} \tag{242}$$

$$i_\alpha + j\cdot i_\beta = \left(i_d + j\cdot i_q\right)\cdot e^{j\cdot\varphi} \tag{243}$$

$$\begin{pmatrix} i_d \\ i_q \end{pmatrix} = \begin{pmatrix} \cos(\varphi) & \sin(\varphi) \\ -\sin(\varphi) & \cos(\varphi) \end{pmatrix}\cdot\begin{pmatrix} i_\alpha \\ i_\beta \end{pmatrix} \tag{244}$$

$$\begin{pmatrix} i_\alpha \\ i_\beta \end{pmatrix} = \begin{pmatrix} \cos(\varphi) & -\sin(\varphi) \\ \sin(\varphi) & \cos(\varphi) \end{pmatrix}\cdot\begin{pmatrix} i_d \\ i_q \end{pmatrix} \tag{245}$$

GRID REQUIREMENTS CHALLENGES FOR WIND TURBINES

Sigrid M. Bolik

Research and Development Departement
Vestas Wind Systems A/S, E. F. Jacobsensvej 7, DK - 6950 Ringkøbing
phone: +45 97301446, fax: +45 97301308, e-mail: sib@vestas.dk

ABSTRACT: The produced electrical power from wind has dramatically increased in the last years. Therefore today's wind turbines, which typically are centralised in wind parks, have a significant influence on the power production. Network operators have to ensure well function power transmission and supply to their customers. For this reason, there exist different requirements in the distribution and transmission net, which deal with controlled power production, connect/ disconnect requirements and behaviour during faults in the grid. Several Network operators have also introduced special grid connection requirements for wind turbines, which are mainly based on existing requirements for power plants. These requirements are a challenge for wind turbine producers. New hardware and control strategies have to be developed and existing control strategies have to be changed. The important changes are due to pitch control, power control, grid connection and error handling. The changes should not affect the already existing advantages of the wind turbines control strategies.
The paper contributes a discussion of the existing grid codes and furthermore a control strategy developed by Vestas is presented.

Keywords: wind power generation, grid code, wind turbine control

1. INTRODUCTION

It takes typically three to five years for the development of a new wind turbine from design to sale. As example the Vestas products over the past years are shown in Figure 6.
A wind turbine is a state of the art product, which must meet the market demands. In addition, the cost per kilowatt should be low. The market for wind turbines and the demands imposed on the wind turbines are changing rapidly and are usually only satisfied by new technical solutions. The demands due to grid connection are especially challenging. Historically there were no demands, because the contribution into the electrical grid was insignificant.

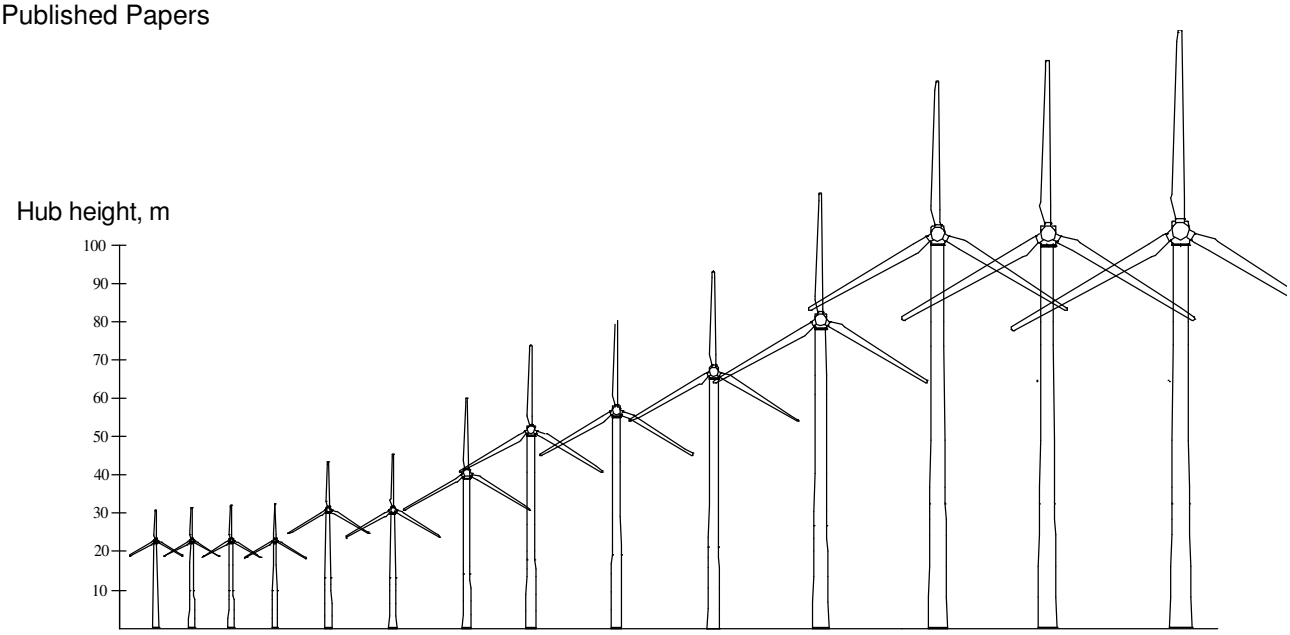

Capacity	55 kW	75 kW	90 kW	100 kW	200 kW	225 kW	500 kW	600 kW	660 kW	850 kW	1750 kW	2000 kW	3000 kW
First install.	1981	1984	1986	1987	1988	1989	1991	1995	1997	2000	1999	2000	2002
Rotor	15/16 m	17 m	19 m	20 m	25 m	27/29 m	39 m	44 m	47 m	52 m	66 m	80 m	90 m
Control	Stall	Stall	Stall	Stall	Stall	Pitch	Pitch/OptiSlip	Pitch/OptiSlip	Pitch/OptiSlip	Pitch/OptiSpeed	Pitch/OptiSpeed	Pitch/OptiSpeed	Pitch/OptiSpeed
Tower	22 m	22 m	22 m	31 m	31 m	39 m	50 m	50 m	55 m	49- 65 m	60-78 m	60-100 m	80 m
MWh/year	217	265	301	346	662	860	1671	1904	2372	2998	5303	7041	

Figure 227 *Vestas Type Development*

Today wind turbines are typically connected in wind farms or parks. Their power contribution to the grid is similar to a power plant, which is connected to the distribution or to the transmission net. For every grid exist connection requirements (grid codes, connection codes or distribution codes) to ensure a save operation and fulfilment of quality demands. These requirements are besides juristic terms concerning frequency, voltage, power production and many others characteristics of the system.
Unfortunately are wind farms only similar to conventional power plants. Unlike power production from nuclear power plants or coal power plants, where the possible power production is dependent on the mass of raw material and the consumed power, wind turbines are dependent on wind forecasting to guarantee a predicted power production. This forecasting of power production from wind turbines is not a simple task. A wind turbine has though some advantages compared to a conventional power plant.
However typical demands for the generating units do not meet wind turbine characteristics. Special connection conditions have to be discussed. A few countries are already working on grid codes especially for wind turbines or wind parks or a modification of the existing code, which also meets wind turbine characteristics /23/. Figure 7 is visualising the grid code development compared to the turbines development and approximate turbine development time.

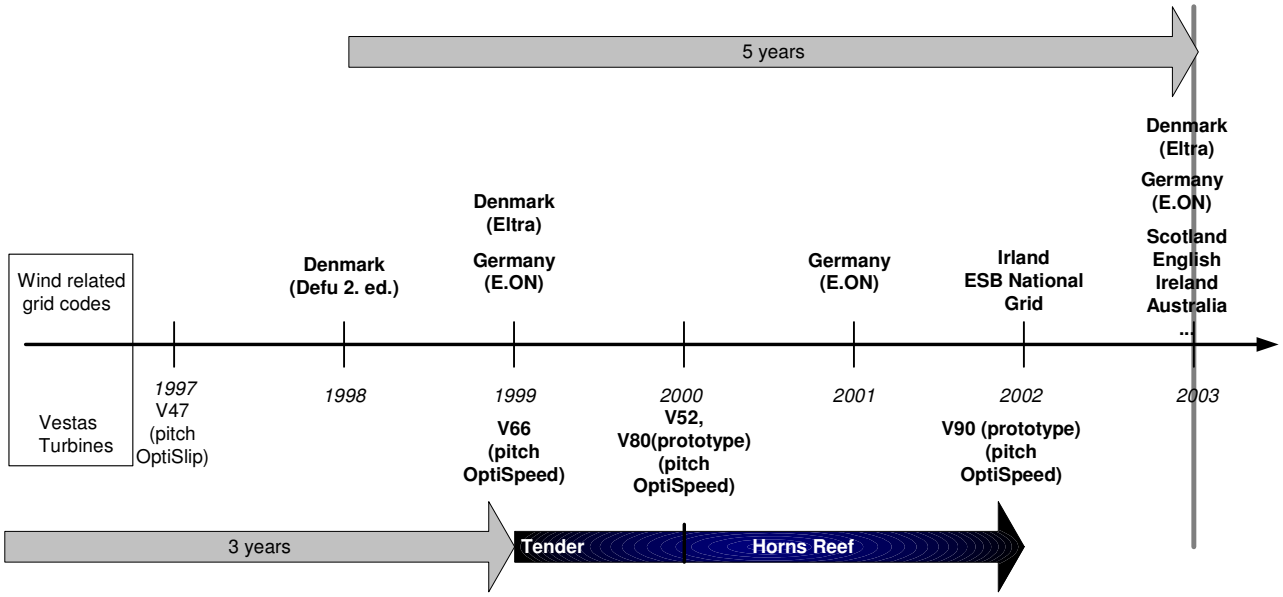

Figure 228 *Wind Turbine development time and grid code demands*

Regrettably not all countries, where wind turbines are installed, have specific or modified grid codes. This makes development of future wind turbines very difficult. There is a big risk involved in developing new techniques to fulfill unspecified demands.
An example how to tackle the grid requirements is the Vestas wind turbine V80. The V80 turbine is capable to expand their functionality to fulfill the most common grid requirements. One possible solution, which will be discussed later in this paper, is the system which was developed and introduced in the offshore park at “Horns Reef” in Denmark with a total capacity of 160 MW.

2. TO BE OR NOT TO BE - GRID CONNECTION DEMANDS

The most wind turbine producers today deliver wind turbines to an international marked and are faced with a various number of grid requirements. Looking at a few of the existing grid codes it appears that there are very different in the most important characteristics. An example is the demand on the voltage tolerance of a system. Where in Australia the grid connected unit has to sustain 0% voltage for 175ms in Denmark it is only 25% voltage for 100ms without disconnecting from the grid (see **Figure 231**). There is a huge difference for the turbine, if there is still some voltage available or not. However a voltage drop is always a very critical condition, because of e.g. the rising current, which can cause serious damage on the system. Usually the turbine gets disconnected to protect itself. A similar difference is seen in the active - reactive power capability and frequency fluctuation of the grid. (see **Figure 10** and **Figure 9**)

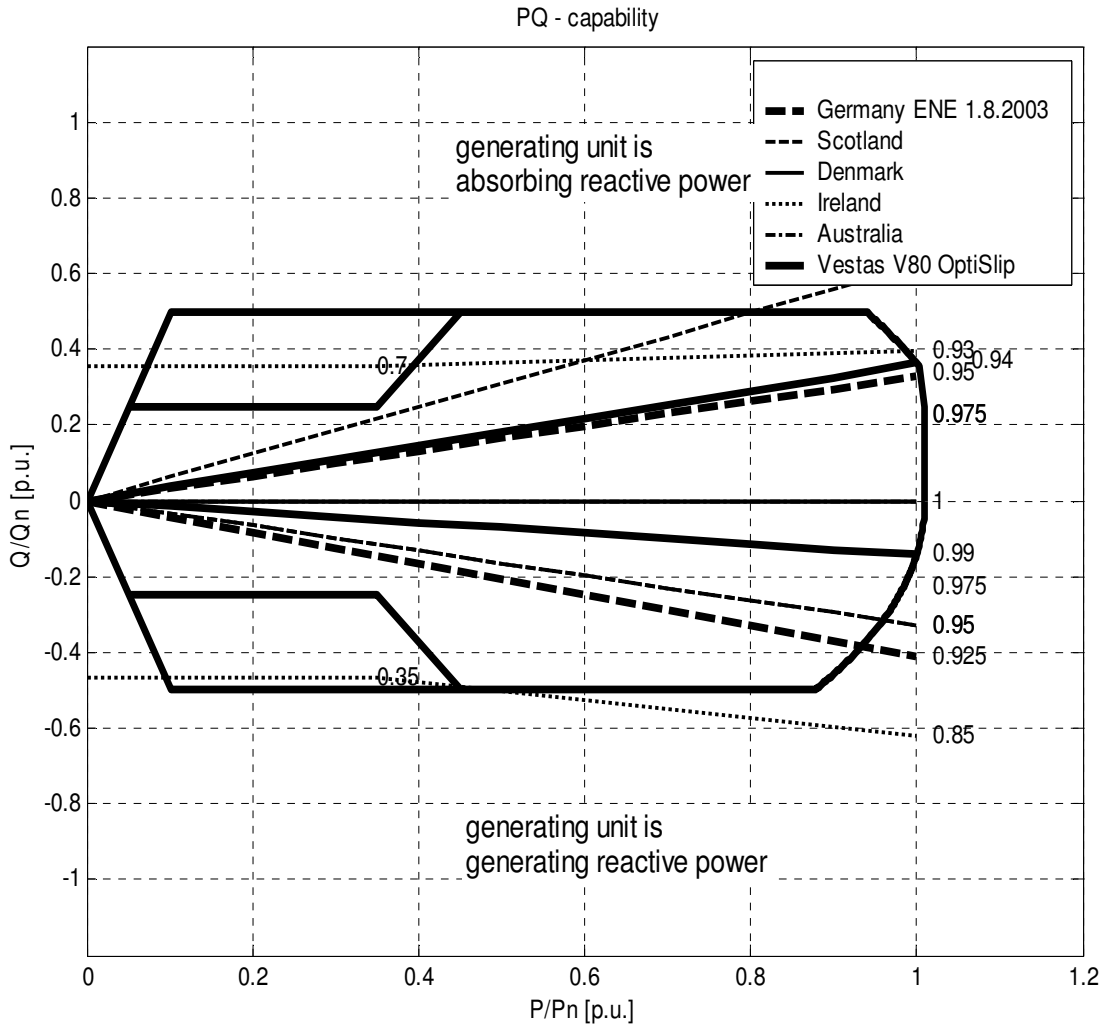

Figure 229 *active power (P) – reactive power (Q) demands*

The active - reactive power capability is typically described in one point, for a static reactive power exchange with the grid during 100% power supply. But why is the demand only for static condition and why only at one point? The answer lies in the history.
The connection demands, which are also base for draft versions of wind turbine connection requirements, are primary made for integration of “generating units” into the grid. These “generating units” usually produces the full power after connecting to the grid and are slow in decreasing or increasing the power. The power production of a wind farm can vary between 0 and 100%, depending on the wind reserve and type. Because of the nature of wind power production from fluctuating wind, wind turbines have a fast power control. Wind farms therefore are capable in a short time to adjust power production.

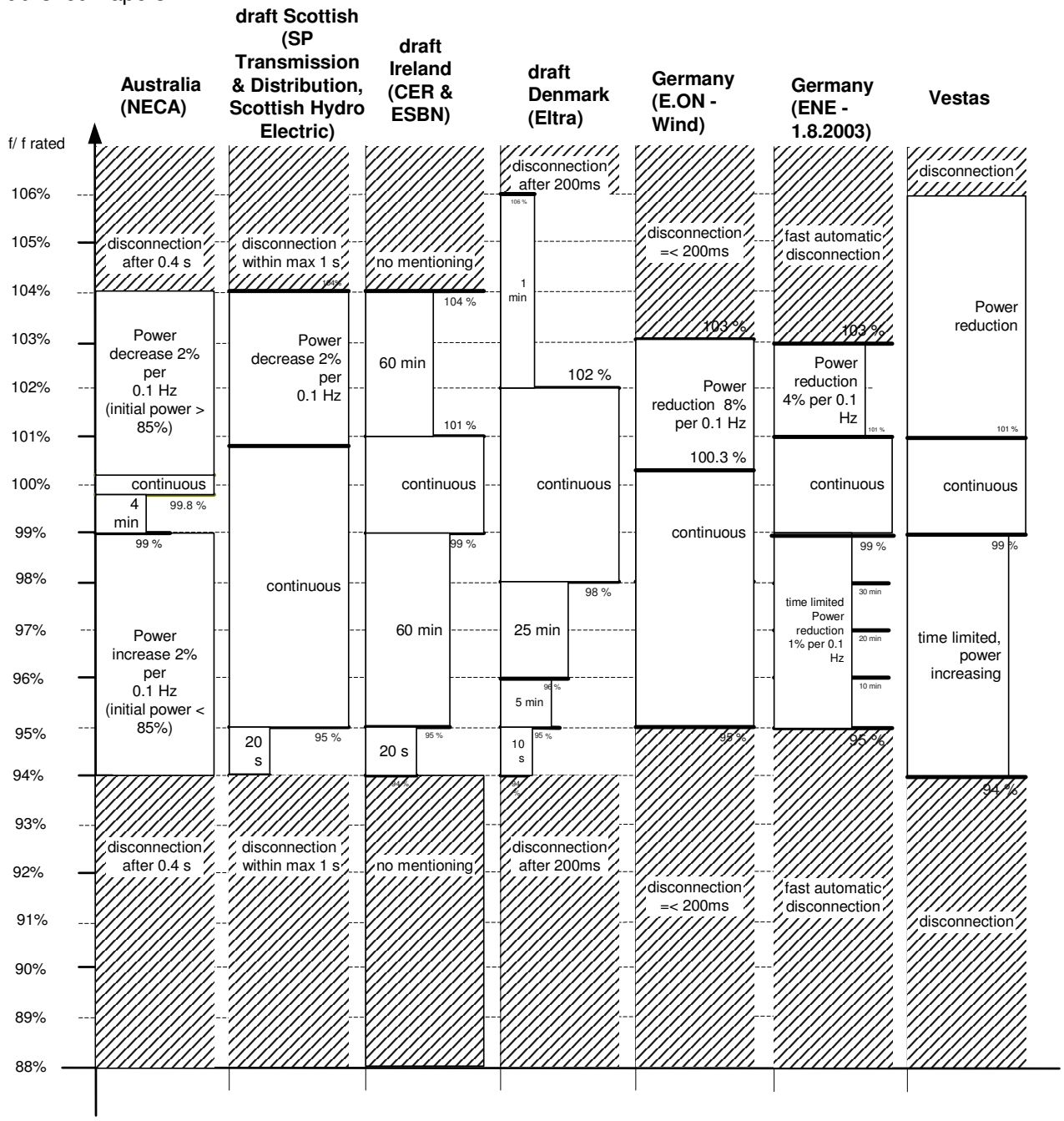

Figure 230 *Frequency fluctuations*

Historical power plants or “generating units” have big synchronous generators. Direct grid connected synchronous machines have stability problems due to load changes and frequency changes. Therefore an important issue is to operate in a wide range of frequencies (see **Figure 9**). A frequency change in a grid can be caused by loss of transmission and sudden demand changes or some problems of bigger power plans (loss of generation), which normally stabilise the grid frequency. Wind turbines with induction generators have no problem with asynchronous operation. Frequency operation range is more an issue of control strategy. A big frequency operation range for wind turbines and frequency control is therefore only interesting, if the net operator uses the wind farm for stabilising the grid frequency. Though wind turbines are able to tolerate big frequency changes they have difficulties to support frequency supporting operation in a wide range, hence the inertia in the system is very small. Anyhow it is a chance to include big wind

farms into superior grid control, because of the fast control possibilities.

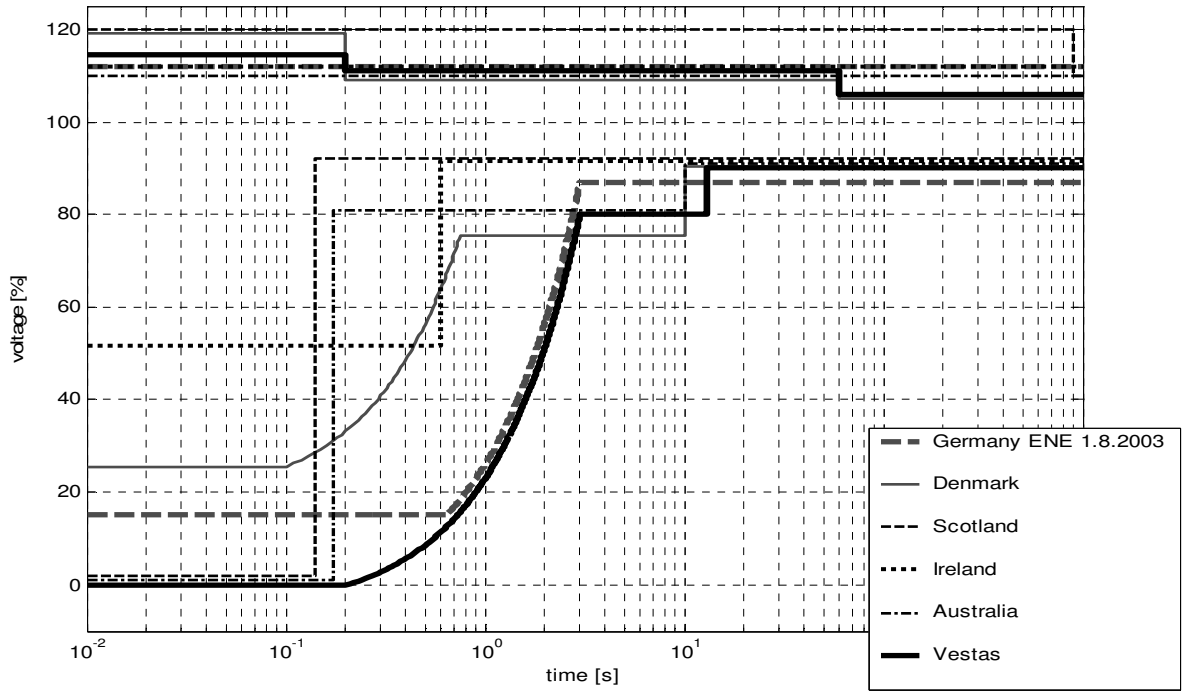

Figure 231 *Voltage tolerance curves*

For example it is possible to use the wind turbines reactive power capability for compensation or support of the grid in situation, where no active power is needed. In **Figure 10** the possibility of the V80 to supply reactive power is shown. Hence Vestas is changing to star connection in small power ranges the reactive power capability is less as well. But it is possible to stay in delta connection with a loss of some efficiency. Even the wind turbine is in smaller power capable of an excellent power factor control it will cost extra money to expand the range, especially at rated power to generate reactive power.
The in **Figure 10**, **Figure 9**, **Figure 231** visualised data can be found in Table 3. This table show some chosen demands from the grid codes with the purpose of comparison the most important demands. The last column shows data for a standard V80 turbine with the modifications towards technical solutions developed for the “Horns Reef” project.

But what is important, missing, or improvable in grid codes for wind turbines?

- Turbine should start automatically with a pre-defined time delay and power ramp
- Turbine should stop automatically with a pre-defined disconnection procedure (high wind or fault) and power ramp
- The continuous frequency range should be defined.
- A distinction between synchronous and asynchronous generator should be made.
- A dynamical description during rated operation and fault situations regarding voltage, active power and reactive power should be made.

The new grid connection demands from Germany /23/ have already included a lot of these points. Even they are not the best suited demands for wind turbines a big effort has been made to describe the expected behaviour.

3. CONTROL STRATEGIES

A good example how to include wind farms control into the superior control can be shown in the “Horns Reef” wind farm. In this farm many of the listed demands are taken into account. Especially challenging were the demands during grid fault. Vestas developed a feature, which is specially designed to tolerate short time voltage reductions (fault-ride–through capability). The grid support option limits the time before the turbine resumes pre-fault power production and limits the risk of voltage collapse due to a very low reactive power draw after the clearance of the grid fault. The method takes advantage of the benefits of having a pitch controlled variable speed wind turbine. The doubly fed induction generator (DFIG) is operated with variable speed and active and reactive power of the generator is controllable via the back to-back Vestas Converter System. The turbine will always be connected to the grid, even at 0 voltage for 200ms (**Figure 231**). To ensure a safe operation point the pitch system is optimised to keep the turbine within normal speed condition and a UPS backup system secures power to the essential units.
In order to use the method, new hardware and control strategies had to be developed and existing control strategies had to be changed. The important changes are due to:

- Pitch control
- Power control
- Grid connection (Synchronisation) /Disconnection
- Error handling
- Backup

In Figure 232 a simulated example for the control algorithm implemented in a V66 turbine is shown. After an occurrence of an error in the grid (such as a sudden voltage drop) the following steps are performed:

1. The stator of the generator is disconnected from the grid
2. The pitch reference is set to a no-load angle θ_0, where the rotor power is 0. θ_0 is continuously calculated based on the wind speed, generator speed and the Cp-curves.
3. When the actual pitch position is close to θ_0 the controller is switched to speed control. The reference speed is set equal to the speed immediately before the error (although limited to the max. static speed).
4. When the grid error is gone the normal procedure for connecting the wind turbine to the grid is started.

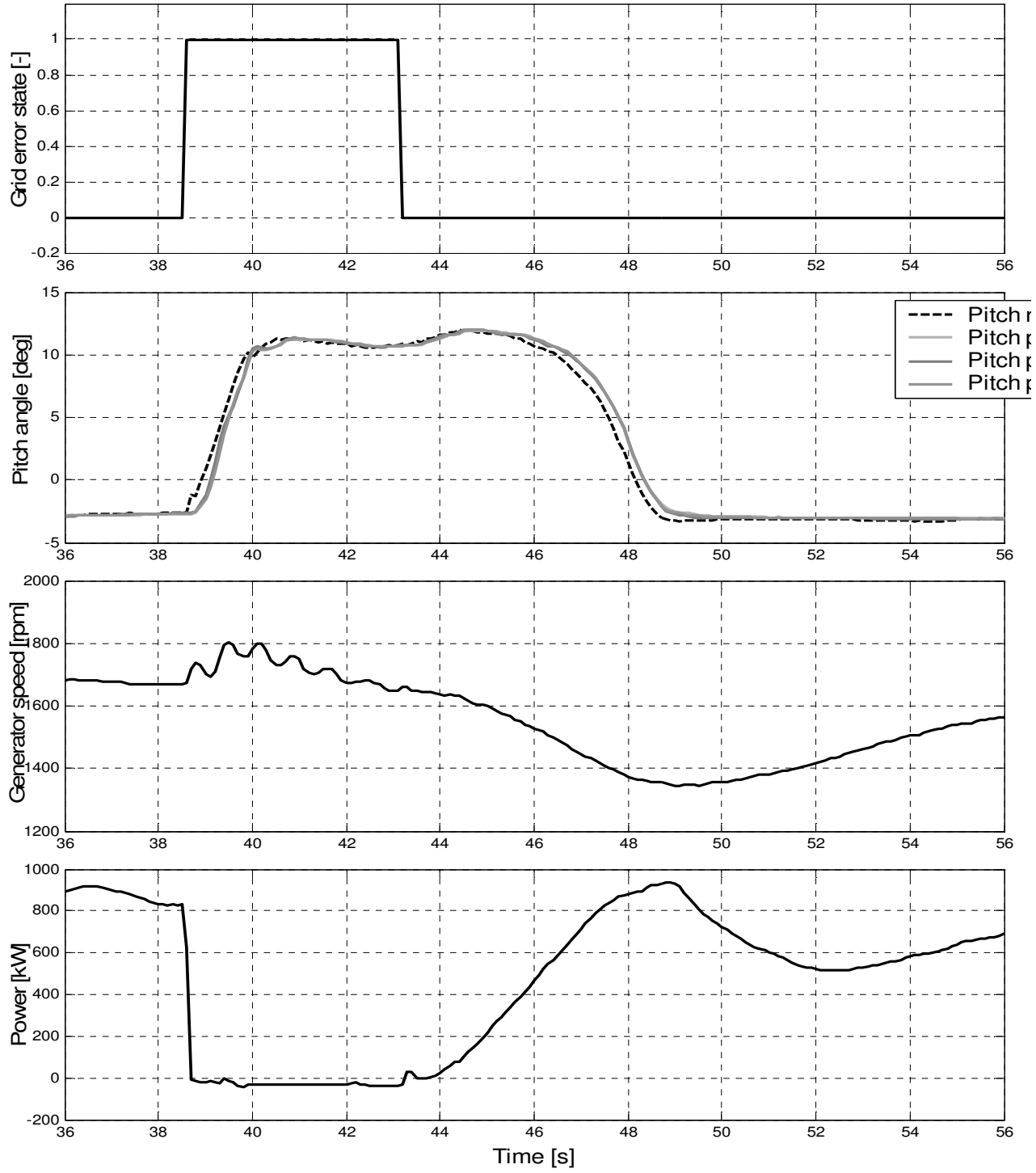

Figure 232 *Control example simulation (V66-1.75 MW, wind speed 10 m/s) 1) grid error state – characterise the voltage drop in the grid, 2) pitch angle [deg], 3) generator speed [rpm], 4) active power [kW]*

Figure 233 shows a measurement during two subsequently occurring grid faults. Thereby the same control steps like in the simulated example are performed.

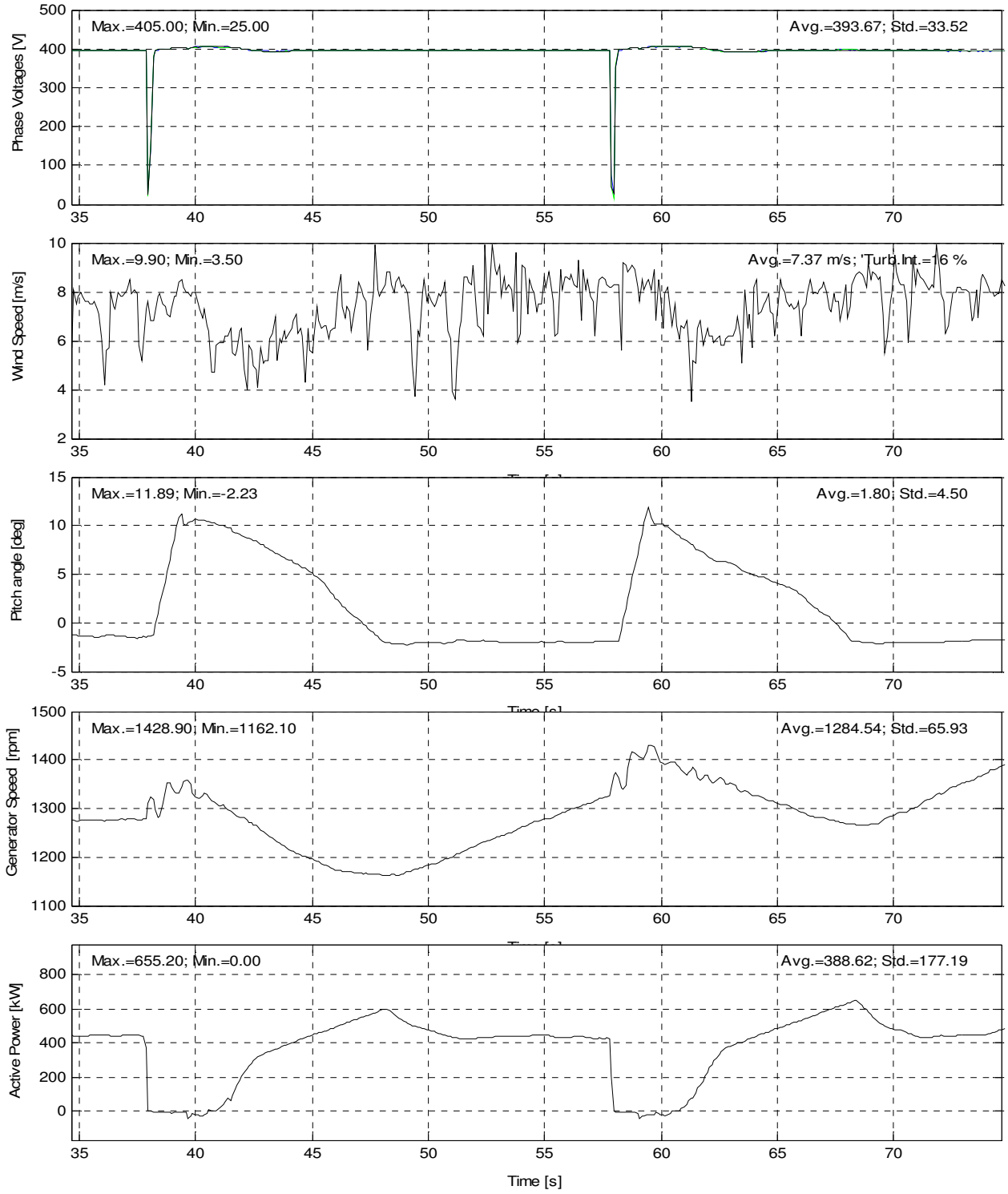

Figure 233 *Measured wind turbine response (V80-2 MW, wind speed 7 m/s) 1) grid rms voltage [V], 2) wind speed, 3) pitch angle [deg], 4) generator speed [rpm], 5) active power [kW]*

4. CONCLUSION

There exist a lot of different grid codes all over the world. All wind turbine producers have a numbered product range, which should be able to fulfil as many grid requirements as possible. With the lack of conformability wind turbines will be designed for the codes for the biggest marked and the outer limits. This is limiting the prize reduction of wind turbine technology. Therefore a close working relationship between all grid operators, costumers and wind turbines producers is required to find acceptable demands in the near future.

5. APPENDIX

Table 3: Grid Codes Overview

Condition	Scotland (SP Transmission & Distribution, Scottish Hydro Electric)	Denmark (Eltra)	Ireland (ESB National Grid)	Germany (E.ON additional WT - rules)	Germany (E.ON)	Australia (NECA)	Vestas (V80, Horns Reef)
High wind speed shut down	neg power ramp within 30 min.	stop wind speed e.g. 25 m/s					25 m/s
start	15 min. warning then power ramp rate limit (>5 MW)	5 - 10 min after fault				1 hour, update every 5 min	10 min after fault clearance
Power Control		Yes	Yes		yes		Yes
Power ramp rate limit	< 15 MW 60 MW per hour, max 10 MW per 10 min, max 3 MW per min 15 - 150 MW 4xrated power per hour, rated power/1.5 per 10 min, rated power/5 per min >150 MW 600 MW per hour, max 100 MW per 10 min, max 30 MW per min	1 min average 0 - 5% of rated power/ min	15 min average 5% of rated power/ min (<= 100 MW) 4% of rated power/ min (<= 200 MW) 2% of rated power/ min (> 200 MW)	after 0Volt - max 10%/ min general - min 10%/min	min. 1% from Prated/min 20%/s or 5%/s after fault		typical: start/ disconnection 50 kW/s delta/ star change 100 kW/s
Power factor / reactive power capability	0.95 lead to 0.85 lag	Unity power control Q = + - 10%P	0.93 lead to 0.85 lag (100% power) 0.7 lead to 0.4 lag (35% power)	P generating 0.975 lead to 0,975 lag P consumtion 1 lead to 0.95 lag Q trin: <= 0.5% , >= 25 kVar	0.95 lead 0.95 lag (<100MW) >=100 MW dependant on voltage range 0.925 unit generating reactive power	0.98 lagging to unity (> 400 kV) 0.96 lagging to unity (250 kV - 400 kV) 0.95 lagging to unity (50 kV - 250 kV) 0.90 lagging to 0.90 leading (> 50 kV)	unity to 0.98 cap.
						0.93 lead to 0.9 lag synchronous generator unity to 0.95 lagging asyncronous generator	0.98 cap 0.96 ind. (100% power) limited constant reaktiv power (0 - 100% aktiv power) 0.2 cap. 0.2 ind. (power -> 0) power factor adjustments due to voltage, power control, power factor control, customer demands
Voltage range (Continuous operation)	+ - 10% (132 kV, 275 kV) + - 5% (400 kV)	95% to 106%	92.5% - 102.5% (400 kV) 95.45% - 109.1% (110 kV & 220 kV)	350 - 420 kV (380 kV) -> 92.1% - 110.5% 193 - 245 kV (220 kV) -> 87.7% - 111.4% 96 - 123 kV (110 kV) -> 87.2% - 111.8% 54 - 70 kV (60 kV) -> 90% - 116.7%	350 - 420 kV (380 kV) -> 92.1% - 110.5% 193 - 245 kV (220 kV) -> 87.7% - 111.4% 96 - 123 kV (110 kV) -> 87.2% - 111.8%	90% - 110%	+ - 5% (medium voltage) + - 10% (low voltage)
Voltage control	Yes		Yes				
Voltage range	+10% (400 kV) +15% (275 kV) +20% (132 kV) (15 min. operation) 90% for 500ms	85% - 110% (60 min)	87.5% - 102.5% (400 kV) 90.9% - 109.1% (220 kV) 90 % - 111.82% (110 kV)	80% 3 s - 5 s 110% <= 100 ms	U>Umax - 30min U<Umin at 110kV -> continous different U<80% disconnection after min 3 s og max 5s generator terminal short circuit 70% - 700ms 70% - Umin for 700 - 1500ms	0% <= 0.175 s 80% -110% 10 s 90% - 110% 3 min	+ - 10% (60 s) + 13.5% (0.2 s) add on 0% (0.2s) 0% - 80% (3s) 80% (13s)
Voltage dip - no trips	jan. 2004 - now 0% - 15% 140ms (132 kV) 0% - 15% 100ms (275 kV)	90% (minim. 10 to 60 s) 106% (minim. 60s) 110% (minim. 200 ms) 120% 0.1 s 25% 0.1 s	step <=10% dip 95% (HV) 0.2 s dip 50% 0.6 s	0% for 150 ms	generator IK > 2*Irated 0% for 150ms IK < = 2*Irated 15% for x<700ms		
Harmonics	G5/4 limits	voltages <= 4% (10-20kV) <=3% (50 - 60 kV)	IEC/TR3 6100-3-6, 61000-3-7			IEEE519 - 1992 Isc/IL THD <50 2.5 50 3.75	all known standarts
nominal frequency	50 Hz + - 0.5 Hz	50 Hz	50 Hz	50 Hz	50 Hz	50 Hz	50 Hz
Frequency range (Continuous operation)	47.5 to 50.4 Hz	49 to 51 Hz	49.5 to 50.5 Hz 49.8 to 51.0 Hz minimum operation stay connected at frequ. Change 0.5 Hz/s	47.5 to 51.5 Hz	49,5 to 50,5 Hz (99% to 101%)	49.9 to 50.1 Hz	49.5 to 50.5 Hz
Frequency range (Limited Operation)	47 to 47.5 Hz - 20s <47 Hz & >52 Hz tripp within 1s	51 to 53 Hz - 1 min 48 to 49 Hz – 25 min 47.5 to 28 Hz – 5 min 47 to 27.5 Hz – 10 s trip efter 200 ms	47.5 to 52.0 Hz - 60 min 47.0 to 47.5 Hz - 20 s (if f<47.5 Hz)	47.5 to 49 Hz P>90%	<47.5 Hz;> 51.5 Hz (95% , 103%) no delayed disconnection 47.5 to 51.5 Hz no disconnection!	49.75 Hz to 50.25 Hz disconnected if outside the range for more than 0.4 49.5 Hz to 49.9 Hz 4 min	47 to 49.5 Hz (Power increase) 50.5 to 53 Hz (Power decrease)
Frequency Control	Yes	Yes	Yes (3% - 5%)	yes	yes	Yes	Yes
	set value, min value, max value power reduction: 10%, 0%, 25% deadband: 0.1Hz,0 Hz, 0.5 Hz droop: 5%, 3%, 20%	UCTE grid second and minute reserve	1.automatical 30 s after f change 2. manually 5 s to 10 min after f change	UCTE grid second and minute reserve	<100 MW volatatry >=100 MW volantary minute reserve (secondary control) >= 100 MW participation in second reserve (primary control) - + 2% Prated start +- 0.2 Hz in 30s to 15 min sensibility +- 0.01 Hz		
Power reduction at high frequency	2% reduction per 0.1 Hz above 50.4 Hz max. 10s			8% reduction per 0.1 Hz above 50.25 Hz	4% reduction per 0.1Hz above 50.5Hz frequency gradient <=0.5% per min voltage gradient <=5% per min	2% power increase + decrease (initial power < 85%) per 0.1 Hz f reduction	2% power per 0.1 Hz
current fault level	calculation of fault infeed from max. 3-phase short circuit	max. 3-phase short circuit of 3 - phase short cicuit		current < = 1.2 Irated at start short circuit duration to 3 s supply max apparent current	Σcurrent = 2 x rated current for >150ms		supply current 1 to 5 p.u. (ca. 60-100 ms)

REFERENCES

/1/ SP Transmission & Distribution, Scottish Hydro Electric, *Guidance Note for the connection of Wind Farms*, Issue No. 2.1.4, December 2002 (Scotland)

/2/ ESB National Grid, *Wind Farm Connection Requirements,* Draft Version 1.0, February 2002 (Ireland)
/3/ E.ON Netz, *Ergänzende Netzanschlussregeln für Windenergieanlagen*, December 2001 (Germany)
/4/ E.ON Netz, *Netzanschlussregeln Hoch- und Höchstspannung*, December 2001 (Germany)
/5/ E.ON Netz, *Netzanschlussregeln Hoch- und Höchstspannung*, August 2003 (Germany)
/6/ Eltra, Elkraft System, *Vindmøller tilsluttet net med spændinger under 100 kV*, Draft, May 2003 (Danmark)
/7/ NECA, *National Electricity Code*, Version 1.0 Amendment 8.0, 1999 – 2003 (Australia)
/8/ Thomas Krüger, Jens Birk, *Metode til kontrol af vindturbine under perioder med afbrydelse af elnettet,* Patent DK 174411 B1, February 2003
/9/ Vestas internal Documentation
/10/ Sigrid M. Bolik, Jens Birk, Björn Andresen, Joh G. Nielsen, *Vestas Handles Grid Requirements: Advanced Control Stradegy for Wind Turbines,* EWEC'03, Juni 2003, Madrid, Spain

Analytical Generator Model for fault simulation of Wind Turbines

Sigrid M. Bolik
Research & Development
Vestas Wind Systems A/S
E.F. Jacobsens Vej 7, 6950 Ringkøbing, Denmark
Aalborg University, Istitute of Energy Technology/ Dept. of Electrical Energy Conversion
Pontoppidanstraede 101, 9220 Aalborg East, Denmark
Phone +45 9730-1446 Fax +45 9730-1308 E-Mail: Sigrid.Bolik@IEEE.org

***Abstract* - Wind turbine modelling became an important part in the study of control, design and production of wind turbines. Thereby doubly-fed induction machine modelling as a part of variable speed wind turbines plays an important role. Therefore this paper is dealing with an introduction of a detailed analytical three-phase induction machine model. The model uses only a minimum set of parameters. The simulation accuracy is dramatically improved by including the saturation of main and leakage inductances. In the end of the paper experimental measurements at an 850 kW test bench for model validation are included and a simulation of a three-phase short circuit on a variable speed wind turbine with doubly fed generator is shown.**

I. INTRODUCTION.

The electrical power produced from wind has dramatically increased in the last years. Therefore today's wind turbines have a significant influence on the power production [1]. On one side the network operators have to ensure well function power transmission and supply to their customers and on the other side wind turbine manufacturers have to design a high quality product for a reasonable price. In order to determine the impact of the existing wind turbines as well as planed wind turbines on the grid and ensure the proper functioning of the wind turbine, wind turbine models have to be developed /84/ - /88/. The models today are made for research of control strategies and stability behaviour. The recent field of interest is the behaviour during fault conditions, like short circuit and voltage drop /84/. The generator as the energy converter in a wind turbine has the most influence on the electrical system. Detailed modelling of the generator is therefore crucial in order to gain realistic behaviour of the wind turbines during faults. However, research in the field of generator modelling for wind turbines studies has been driven by finding a simplified model to shorten simulation time /42/, /61/, /20/. These models are mainly developed for research of the interaction of the wind turbines and the electrical grid or control purposes, where there is no need for very detailed models. Wind turbine manufacturers have a different interest on wind turbines models. Their main interest is the precise knowledge about the influence of certain grid conditions to the wind turbine itself. Detailed knowledge about e.g. the torque on the wind turbine shaft caused by faults in the grid or transient current rises is important for the estimation of the load on the wind turbines. An accurate as possible knowledge is ensuring the availability of the turbine for the estimated life time and low costs. Since the most wind turbine manufacturers don't produce their own generators, there is only a minimum access to data. Representing a range of generators in a model, facing the additionally variation in each generators dimensions and material detailed FEM studies of the generator are not sufficient.

The purpose of the presented work is to find an analytical generator model for the simulation of fault conditions on variable speed Wind Turbines e.g. asymmetrical voltage supply or 1- ,2- , 3-phase short circuit using the program Matlab/ Simulink®.

II. MODEL DEVELOPMENT

A. Model development of the doubly fed induction generator (DFIG)

As stated in the introduction the developed generator model will be used for the study of fault conditions like short-circuits or asymmetrical supply. Since the machine is used in variable speed wind turbines the rotor of the generator will be coupled to power electronics. Furthermore the model will represent a range of generators from 600kW up to 3MW from different manufacturers. The generator is connected in star and as well as in delta.
In general the data provided by machine suppliers are the parameters of the one-phase equivalent diagram Fig. 1 under rated conditions and the magnetizing curve. In some cases a set of one-phase equivalent parameters in saturated conditions is accessible as well.
The in Fig. 1 shown one-phase equivalent diagram, is a well-known representation of an induction machine with stator resistance R_s, rotor resistance $R_r^{'}$, stator leakage inductance $L_{\sigma s}$, rotor leakage inductance $L_{\sigma r}^{'}$, main or magnetizing inductance L_m, iron loss resistance R_m, slip s, stator voltage U_s and rotor voltage $U_r^{'}$ related to the stator side of the machine .

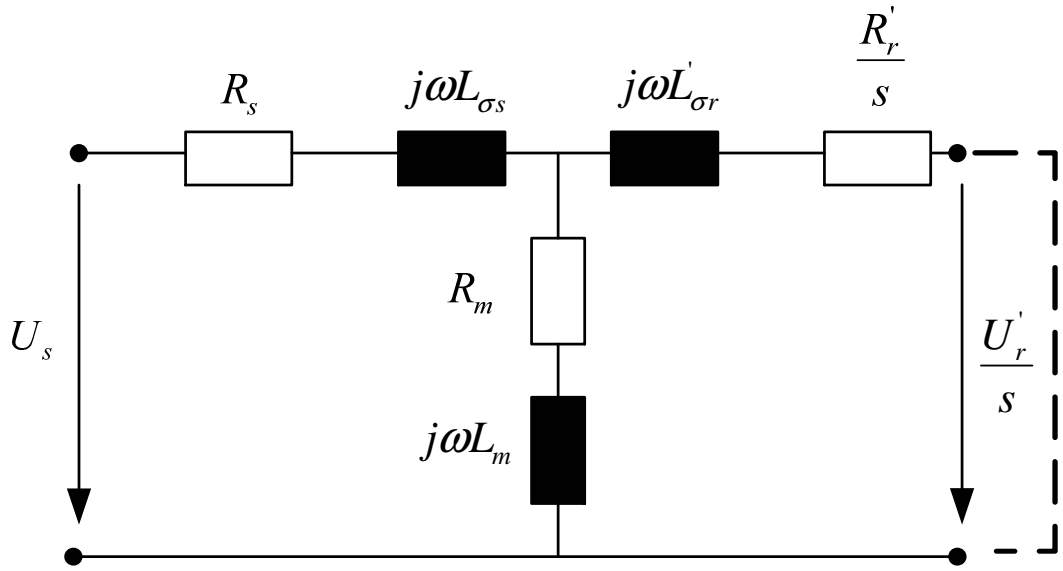

Fig. 1 One phase equivalent circuit diagram of a DFIG

The development of a three-phase ABC/abc generator model is a challenge under the given circumstances. Though it is worth the effort, since a three-phase ABC/abc generator model gives the possibility to look at each phase separately as well as the coupling between the phases /104/ Thereby the ABC/abc model is not limited by conditions of symmetry of either supply voltages or phase impedances /79/. The three-phase analytical model can be easily improved with accessibility of more input parameters, without complete model changes. All these advantages are improving the simulation result.
The basic equations for developing a three phase model can be found in various books

about electrical machines and drives /67/, /50/ and is shown in Figure 45. The variables of the machine are defined in vectors, where each element is represented per phase:

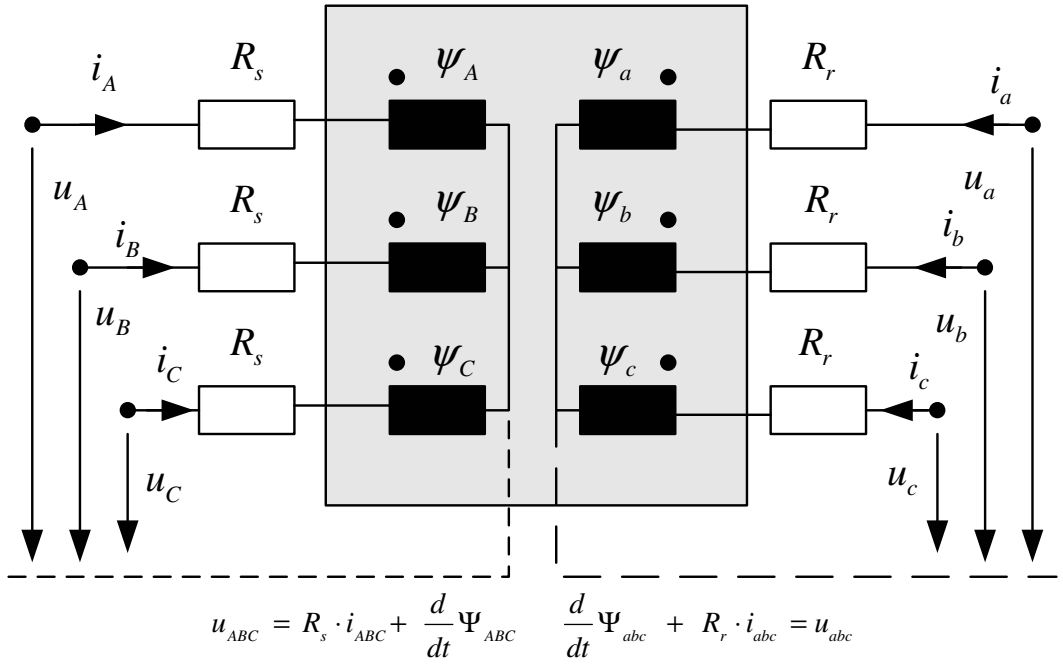

Fig. 2 Three phase equivalent ABC/abc circuit diagram of a doubly fed induction machine

The voltage (1) for each stator and rotor phase of the machine with voltages u, the currents i and flux ψ are vectors by (2), (3), (4).

$$u = R \cdot i + \frac{d}{dt}\psi \tag{1}$$

$$u = [u_A \quad u_B \quad u_C \quad u_a \quad u_b \quad u_c]^T \tag{2}$$

$$i = [i_A \quad i_B \quad i_C \quad i_a \quad i_b \quad i_c]^T \tag{3}$$

$$\psi = [\psi_A \quad \psi_B \quad \psi_C \quad \psi_a \quad \psi_b \quad \psi_c]^T \tag{4}$$

The flux can be expressed as a product of the inductance matrix L /79/ and the current vector i.
Thereby the inductances $M_{..} \ldots M_{..}$ represent the self or mutual inductances of stator and rotor in the inductance matrix and the variables $L_{\sigma A} \ldots L_{\sigma c}$ represent the leakage inductances for each phase. All inductances are a function of the electrical angle between the phases $f_{AA} \ldots f_{cc} = f_{AA}(\theta) \ldots f_{cc}(\theta)$.

$$L = \begin{pmatrix} L_{\sigma A}+M_{AA}\cdot f_{AA} & M_{AB}\cdot f_{AB} & M_{AC}\cdot f_{AC} & M_{Aa}\cdot f_{Aa} & M_{Ab}\cdot f_{Ab} & M_{Ac}\cdot f_{Ac} \\ M_{BA}\cdot f_{BA} & L_{\sigma B}+M_{BB}\cdot f_{BB} & M_{BC}\cdot f_{BC} & M_{Ba}\cdot f_{Ba} & M_{Bb}\cdot f_{Bb} & M_{Bc}\cdot f_{Bc} \\ M_{CA}\cdot f_{CA} & M_{CB}\cdot f_{BC} & L_{\sigma C}+M_{CC}\cdot f_{CC} & M_{Ca}\cdot f_{Ca} & M_{Cb}\cdot f_{Cb} & M_{Cc}\cdot f_{Cc} \\ M_{aA}\cdot f_{aA} & M_{aB}\cdot f_{aB} & M_{aC}\cdot f_{aC} & L_{\sigma a}+M_{aa}\cdot f_{aa} & M_{ab}\cdot f_{ab} & M_{ac}\cdot f_{ac} \\ M_{bA}\cdot f_{bA} & M_{bB}\cdot f_{bB} & M_{bC}\cdot f_{bC} & M_{ba}\cdot f_{ba} & L_{\sigma b}+M_{bb}\cdot f_{bb} & M_{bc}\cdot f_{bc} \\ M_{cA}\cdot f_{cA} & M_{cB}\cdot f_{cB} & M_{cC}\cdot f_{cC} & M_{ca}\cdot f_{ca} & M_{cb}\cdot f_{cb} & L_{\sigma c}+M_{cc}\cdot f_{cc} \end{pmatrix} \tag{6}$$

The inductance matrix is expressing the coupling of the flux in the stator and rotor windings. It takes a central position in the machine modelling.
Depending on the form of the inductance matrix the machine model is more or less

detailed. Symmetrical build machine and a displacement between the stator and rotor phases of 120° the function of the electrical angle between the phases becomes a function of the displacement angle ρ between stator and rotor as shown in (7) /79/. The functions of the electrical angle between the stator phases are constant and so are replaced by $f_{AA} \dots f_{CC} = 0$ as well as the functions of the electrical angle between the rotor phases are constant and set to $f_{aa} \dots f_{cc} = 0$. The functions of the electrical angle between the stator and rotor phases are dependant on the rotor position angle. There exist three different dependencies (7) which can be expressed by $f_{aA}, f_{bB}, f_{cC}, f_{Aa}, f_{Bb}, f_{Cc} = f_1$, $f_{aC}, f_{bA}, f_{cB}, f_{Ab}, f_{Bc}, f_{Ca} = f_2$ and $f_{Ac}, f_{Ba}, f_{Cb}, f_{aB}, f_{bC}, f_{cA} = f_3$.

$$f_1 = \cos\rho\,,\ f_2 = \cos\ (\rho + 2\pi/3)\,,\ f_3 = \cos\ (\rho - 2\pi/3) \tag{7}$$

When developing an analytical induction machine model for the purpose of e.g. short circuit simulation it is important to include saturation effects. The saturation of the field can be expressed as a change in magnetising and leakage inductance /30/. Thereby the change of magnetizing inductances as well as the leakage inductances is important. The variation of the magnetising inductance is achieved from the measured no load magnetizing curve Fig. 3, which depict the dependency of the no load voltage U_0 and no load current I_μ (stator current). The no load situation can be obtained with running a rotor short circuit induction machine with the synchronous speed ω_0. With (8) the variation of the magnetizing inductance due to the magnetizing current can be calculated Fig. 4.

$$L_m \cdot \omega_0 = \sqrt{\frac{U_0^{\,2}}{3 \cdot I_\mu^{\,2}} - (R_s + R_m)^2} - L_{\sigma s} \cdot \omega_0 \tag{8}$$

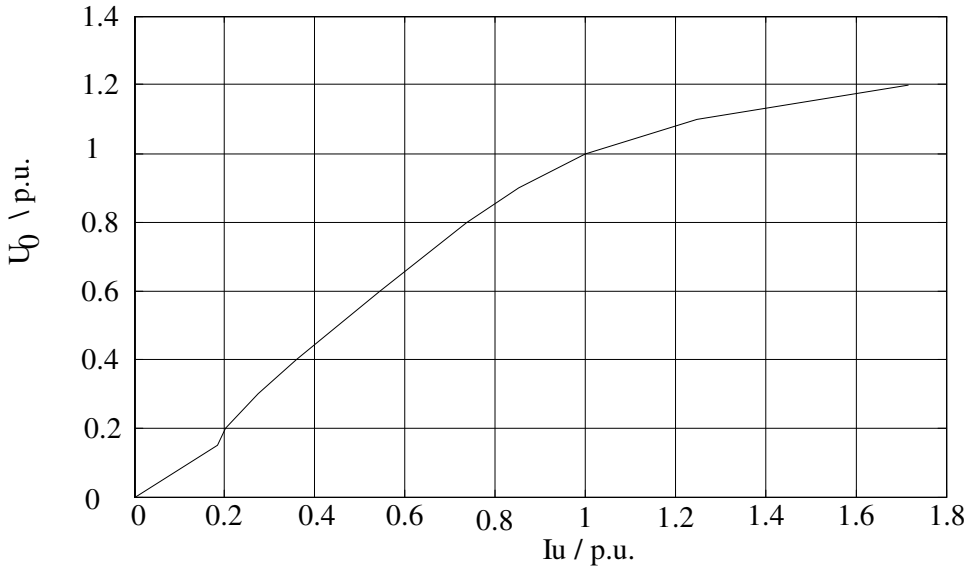

Fig. 3 Measured no load curve for modelling the saturation of magnetizing inductance

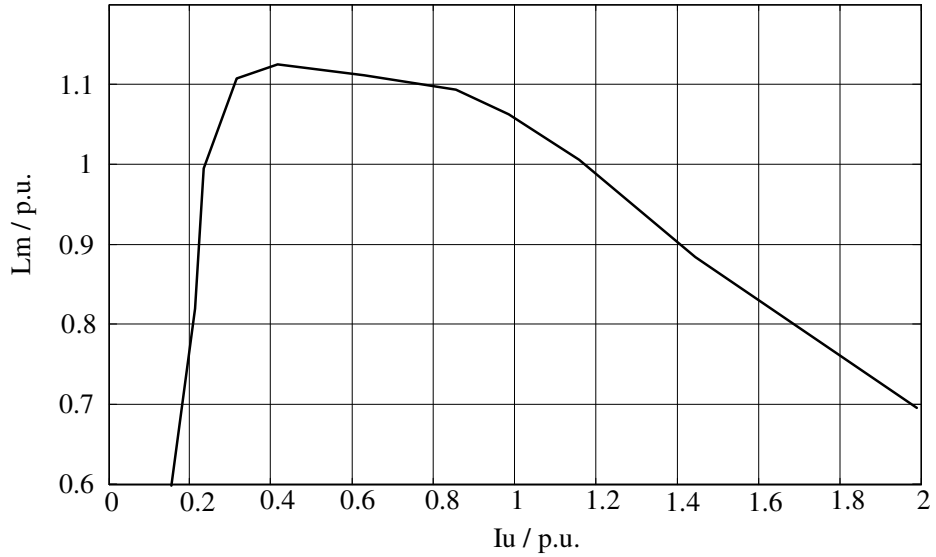

Fig. 4 Magnetizing inductance depending on magnetizing current

For the variation of the leakage inductance two points, the rated and saturated value, of one phase equivalent parameters is used. Using the stator current as a reference a modification of the leakage inductances per phase is possible as indicated in Table 1 and shown in Fig. 5.

TABLE 1
Leakage inductance saturation reference

Stator Current	Leakage inductance
0	rated value
rated value	rated value
blocked rotor current	saturated value of slip=1
10 x blocked rotor current	saturated value of slip=1

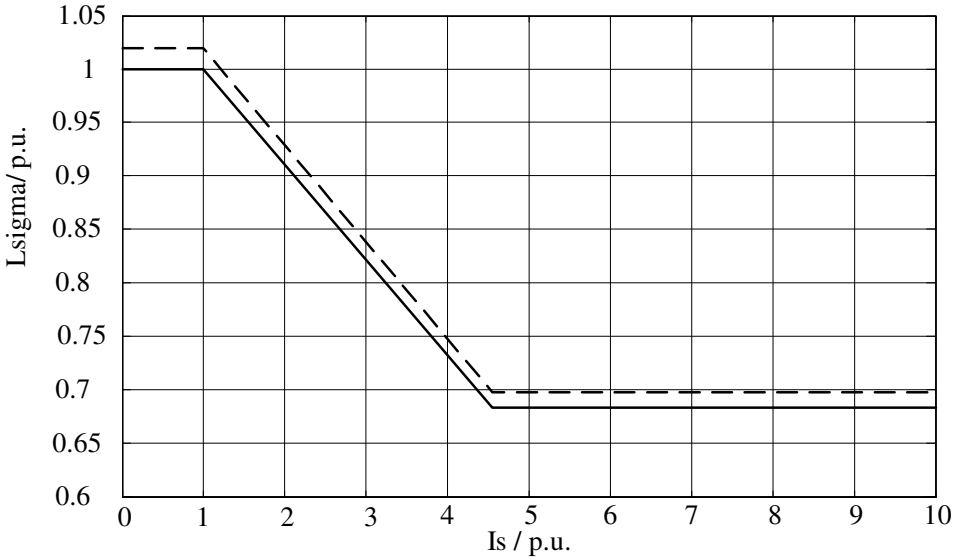

Fig. 5 Example for stator (solid line) and rotor (dashed line) leakage inductance depending on stator current

Since the model will be used for asymmetrical simulations a per phase variation of the parameters in the inductance matrix is used (9), as opposed to the common use of variation of the inductances using the slip as reference, which does initiate a variation in all three phases with the same value.
Thereby the following groups can be defined.

$$M_{AA}, M_{AB}, M_{AC}, M_{aa}, M_{ab}, M_{ac} = M_{sA;ra} = L_m\left(i_{\mu Aa}\right) \quad M_{Aa}, M_{Ab}, M_{Ac}, M_{aA}, M_{aB}, M_{aC} = M_{srAa} = \frac{2}{3} L_m\left(i_{\mu Aa}\right)$$

$$M_{BA}, M_{BB}, M_{BC}, M_{ba}, M_{bb}, M_{bc} = M_{sB;rb} = L_m\left(i_{\mu Bb}\right) \quad M_{Ba}, M_{Bb}, M_{Bc}, M_{bA}, M_{bB}, M_{bC} = M_{srBb} = \frac{2}{3} L_m\left(i_{\mu Bb}\right)$$

$$M_{CA}, M_{CB}, M_{CC}, M_{ca}, M_{cb}, M_{cc} = M_{sC;rc} = L_m\left(i_{\mu Cc}\right) \quad M_{Ca}, M_{Cb}, M_{Cc}, M_{cA}, M_{cB}, M_{cC} = M_{srCc} = \frac{2}{3} L_m\left(i_{\mu Cc}\right)$$

$$L = \begin{pmatrix} L_{\sigma sA} + M_{sA} & -0.5M_{sA} & -0.5M_{sA} & M_{srAa} \cdot f_1 & M_{srAb} \cdot f_2 & M_{srAc} \cdot f_3 \\ -0.5M_{sB} & L_{\sigma sB} + M_{sB} & -0.5M_{sB} & M_{srBa} \cdot f_3 & M_{srBb} \cdot f_1 & M_{srBc} \cdot f_2 \\ -0.5M_{sC} & -0.5M_{sC} & L_{\sigma sC} + M_{sC} & M_{srCa} \cdot f_2 & M_{srCb} \cdot f_3 & M_{srCc} \cdot f_1 \\ M_{sraA} \cdot f_1 & M_{sraB} \cdot f_3 & M_{sraC} \cdot f_2 & L'_{\sigma ra} + M_{ra} & -0.5M_{ra} & -0.5M_{ra} \\ M_{srbA} \cdot f_2 & M_{srbB} \cdot f_1 & M_{srbC} \cdot f_3 & -0.5M_{rb} & L'_{\sigma rb} + M_{rb} & -0.5M_{rb} \\ M_{srcA} \cdot f_3 & M_{srcB} \cdot f_2 & M_{srcC} \cdot f_1 & -0.5M_{rc} & -0.5M_{rc} & L'_{\sigma r} + M_{rc} \end{pmatrix} \tag{9}$$

Completing the model of the machine the torque is calculated from the three phase stator flux and stator current in (10). The equation of motion, including friction losses takes the form (11).

$$T_e = \frac{p_p}{\sqrt{3}} \cdot \left(i_A\left(\Psi_C - \Psi_B\right) + i_B\left(\Psi_A - \Psi_C\right) + i_C\left(\Psi_B - \Psi_A\right)\right) \tag{10}$$

$$\ddot{\rho} = \frac{p_p}{J} \cdot \left(T_e - T_m - D\omega_r\right) \tag{11}$$

Where

T_e air gap torque

T_m load torque

p_p number of pole pairs

D friction, windage loss factor

J generator inertia

ω_r rotor angular velocity

$\ddot{\rho}$ second derivative of displacement angle

B. Connection Conditions

Considering the connection conditions of the machine a further simplification of the inductance matrix can be achieved, which gives the possibility of simplify the computing of the inverse matrix like proposed by Pillay /79/ and Goldemberg /30/. Assuming e.g. a YY connected machine with no external accessible star point and take equation (12) into account, the induction matrix takes the following form (13).

$$i_A + i_B + i_C = 0\,,\; i_a + i_b + i_c = 0 \tag{12}$$

$$L = \begin{pmatrix} L_{\sigma s}+1.5M_s & 0 & 0 & M_{sr}\cdot f_1 & M_{sr}\cdot f_2 & M_{sr}\cdot f_3 \\ 0 & L_{\sigma s}+1.5M_s & 0 & M_{sr}\cdot f_3 & M_{sr}\cdot f_1 & M_{sr}\cdot f_2 \\ 0 & 0 & L_{\sigma s}+1.5M_s & M_{sr}\cdot f_2 & M_{sr}\cdot f_3 & M_{sr}\cdot f_1 \\ M_{sr}\cdot f_1 & M_{sr}\cdot f_3 & M_{sr}\cdot f_2 & L'_{\sigma r}+1.5M_r & 0 & 0 \\ M_{sr}\cdot f_2 & M_{sr}\cdot f_1 & M_{sr}\cdot f_3 & 0 & L'_{\sigma r}+1.5M_r & 0 \\ M_{sr}\cdot f_3 & M_{sr}\cdot f_3 & M_{sr}\cdot f_1 & 0 & 0 & L'_{\sigma r}+1.5M_r \end{pmatrix} \tag{13}$$

All parameters are still achievable from the one phase equivalent diagram. Though notice, that the stator and rotor mutual inductances M_s, M_r are calculated to $2/3L_m$.

In case of a ΔY connected machine the coupling of the rotor phases can be simplified as shown above in the YY example, while leaving the stator phases untouched. The inductance matrix for a ΔY connected machine takes the form shown in (14).

$$L = \begin{pmatrix} L_{\sigma s}+M_s & -0.5M_s & -0.5M_s & M_{sr}\cdot f_1 & M_{sr}\cdot f_2 & M_{sr}\cdot f_3 \\ -0.5M_s & L_{\sigma s}+M_s & -0.5M_s & M_{sr}\cdot f_3 & M_{sr}\cdot f_1 & M_{sr}\cdot f_2 \\ -0.5M_s & -0.5M_s & L_{\sigma s}+M_s & M_{sr}\cdot f_2 & M_{sr}\cdot f_3 & M_{sr}\cdot f_1 \\ M_{sr}\cdot f_1 & M_{sr}\cdot f_3 & M_{sr}\cdot f_2 & L'_{\sigma r}+1.5M_r & 0 & 0 \\ M_{sr}\cdot f_2 & M_{sr}\cdot f_1 & M_{sr}\cdot f_3 & 0 & L'_{\sigma r}+1.5M_r & 0 \\ M_{sr}\cdot f_3 & M_{sr}\cdot f_3 & M_{sr}\cdot f_1 & 0 & 0 & L'_{\sigma r}+1.5M_r \end{pmatrix} \tag{14}$$

Leaving the magnetic coupling of the stator phases in the original allows the stator currents to flow in a circle. This gives a more realistic result than the usually used method of assuming a magnetically YY connected machine and afterwards calculation of the electrical delta coupling of the stator windings, which is shown in the following example. A

delta coupled generator experiences a 2-phase line to line short circuit at the terminals.

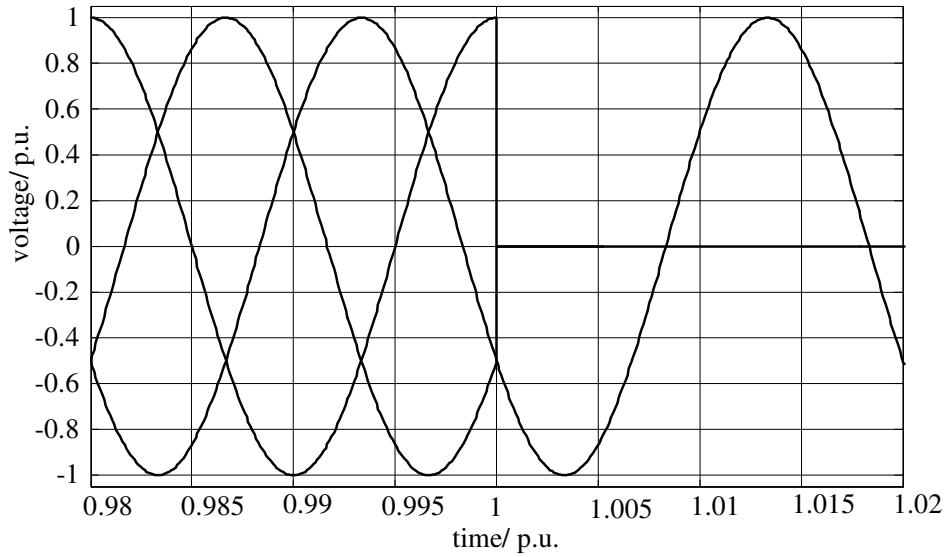

Fig. 6 Voltage at generator stator terminal during a two-phase short circuit

While there is no difference between the simulated stator current under symmetrical conditions before the short circuit, the difference between the models can be seen in the asymmetrical condition Fig. 7. The current modeled with the star connected machine model and a calculated delta coupling shows difference in phase and amplitude to the current simulated with the delta connected machine model.

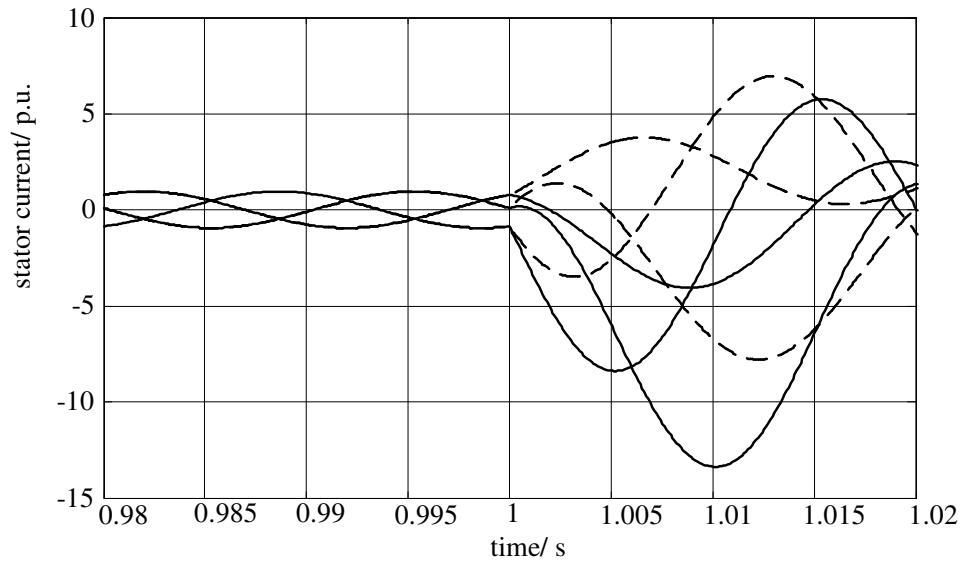

Fig. 7 Stator currents of the generator dashed line – star modeled machine with calculated delta coupling and solid lines – delta modeled machine

III. MODEL VALIDATION AND RESULTS

A. Model validation with Direct On Line start measurement

Different machine models have been validated by comparing a Direct On Line (DOL) start of an YY coupled machine. The DOL start has been chosen to produce high currents and achieve saturation effects in the machine, since real short circuits for validation of the machine model is not feasible in the researched machine size of 850kW to 3MW. As input for the simulation the measured per phase voltage (Fig. 8) of the machine is used. The voltage is dropping immediately while connecting the machine. Because the generator is not designed for DOL start, there is very little starting torque developed. Consequently the machine has a long time starting period. This gives the possibility to use it for validation. There exist an asymmetrical transient and a quasi stationary part during the DOL start of the machine.

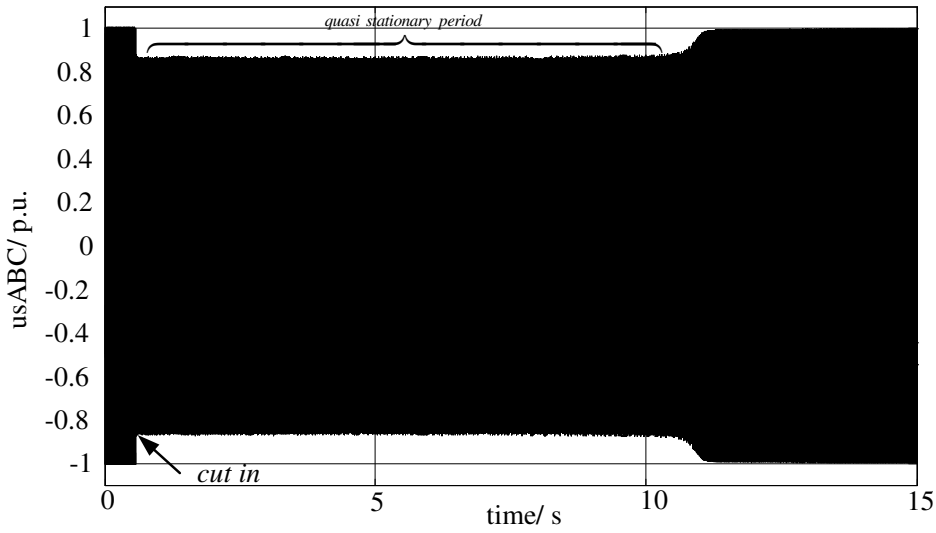

Fig. 8 Stator voltages during the DOL start in p.u.

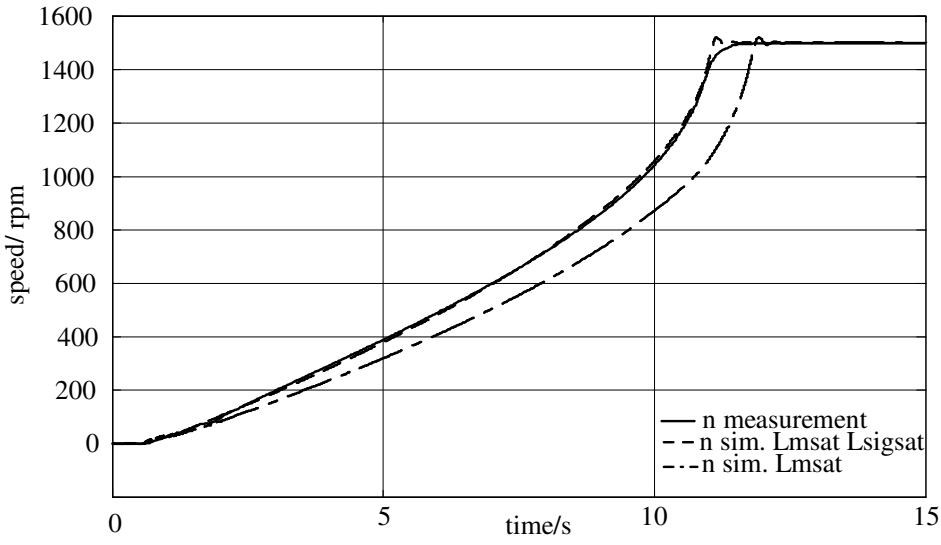

Fig. 9 Speed of the machine during DOL start

In Fig. 9 increasing speed during the DOL start is shown. Here the impact of saturation of leakage inductances is visible. The dotted line, which is simulated with the model including saturation of main and leakage inductance, is very close to the measured speed (solid line). The simulation using the model without leakage saturation and only main saturation are very close together. There is a big discrepancy between the simulated and the measured speed.

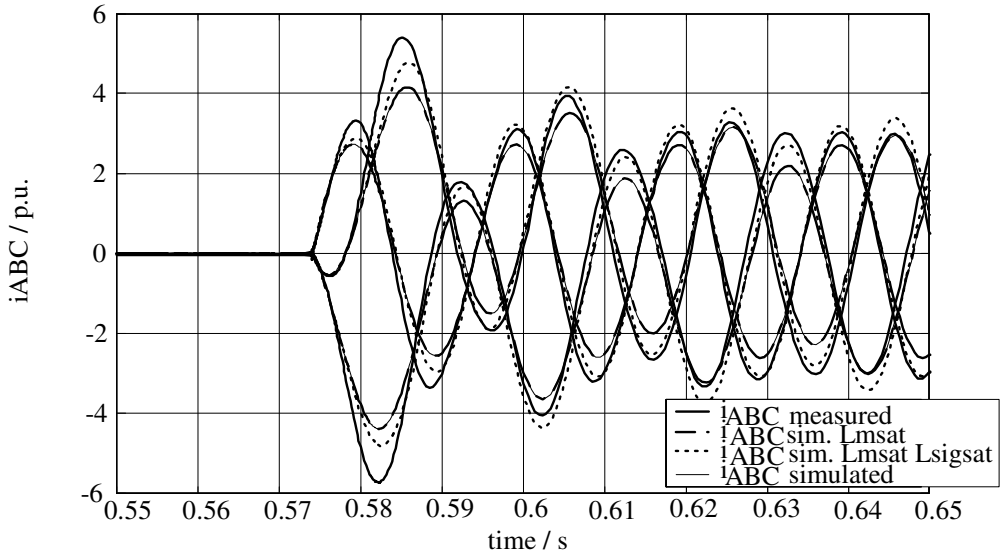

Fig. 10 Three-phase stator current transients during cut in of the machine

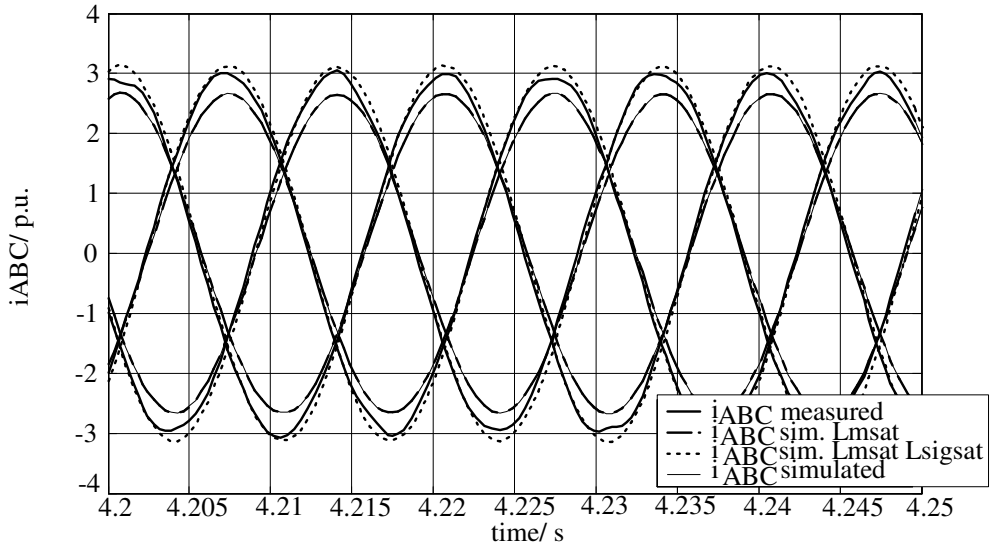

Fig. 11 Three-phase stator currents during quasi stationary period

Using the simulation model including main and leakage saturation the error by simulating the highest stator current peak value at start up is minimized about 10%. The improvement by using a model included main saturation to a model without saturation at all is less than 1%. In the quasi stationary period the error using the model including main and leakage saturation is reduced by 5%.

A. Machine model used for simulating a Wind Turbine

The developed model is now applicable for fault simulation of a Wind turbine. As example a three phase short circuit on the transformer primary winding terminal of a variable speed 1.8MW Vestas OptiSlip Wind Turbine Fig. 12 is simulated. The generator is a double fed induction generator of the type with delta connection in the stator windings and star connection in the rotor. At the rotor terminals a controlled resistance is connected, which allows a speed variation of 10%. The used model of the wind turbine is a complete model of the whole turbine, which imply a model of the drive train, aerodynamics and the total wind turbine control.

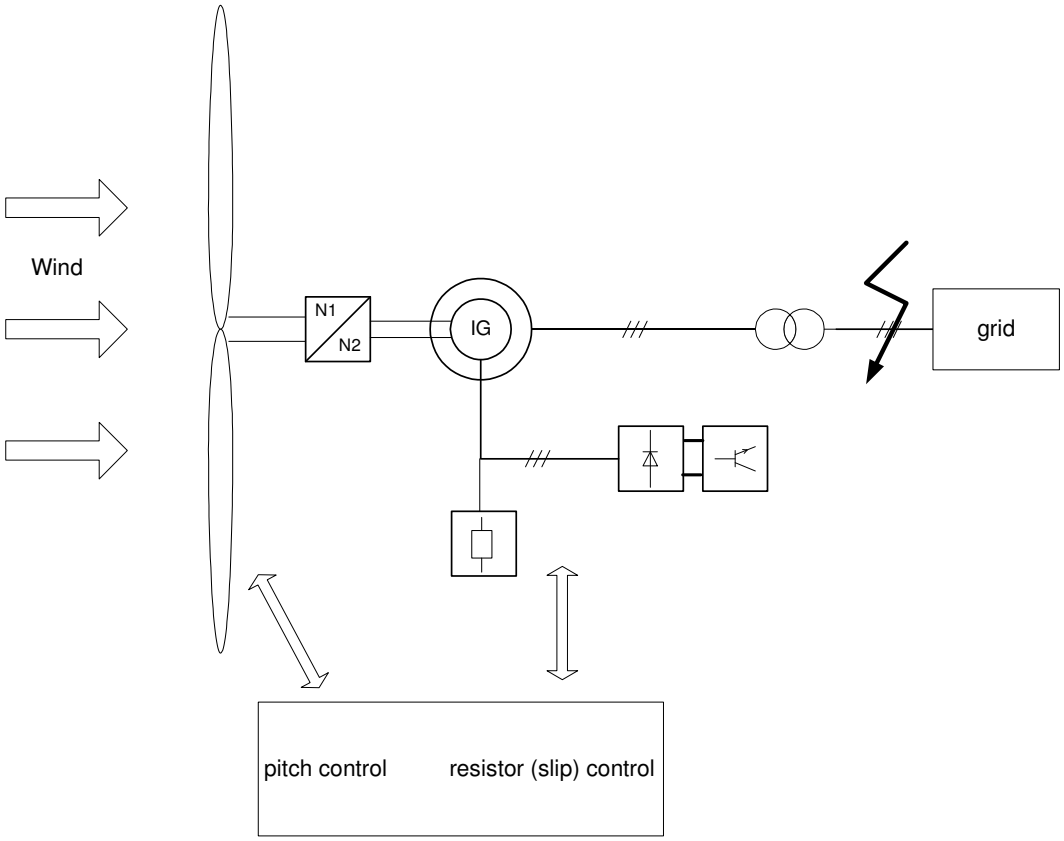

Fig. 12 Outline of the Vestas OptiSlip variable speed wind turbine

With this model two simulations have been made with two different generator models (with and without saturation effects), while the rest of the model remains untouched.

At time 2s a three-phase short circuit occurs at the primary side of the transformer. The wind turbine is operating at rated conditions at this time. The voltage on the secondary side of the transformer, which is seen as stator voltage at the generator terminals is shown in Fig. 13 and is therewith the input of the generator model.

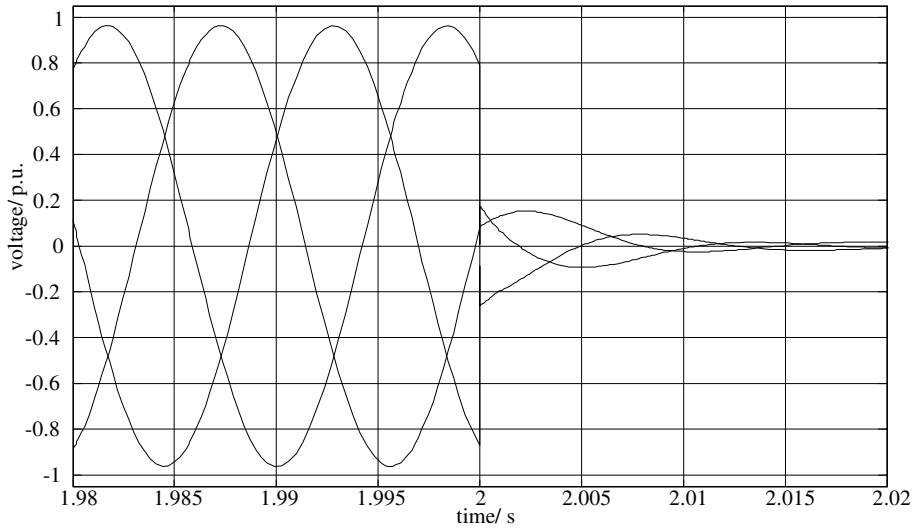

Fig. 13 Voltage at generator stator terminals during a three-phase short circuit at the turbine

Due to the transformer impedance the voltage after the transformer is not immediately dropping to zero. The generator experiences therefore only a voltage drop to 20% rest voltage, which minimizes the short circuit contribution.
A further influence on the system is the controlled resistor, placed at the rotor terminals of the generator (Fig. 14). After the short-circuit occurrence the control increases the resistance to reduce the rotor current of the system. The rise of the resistance includes a huge damping in the system and minimizes short circuit contribution further.

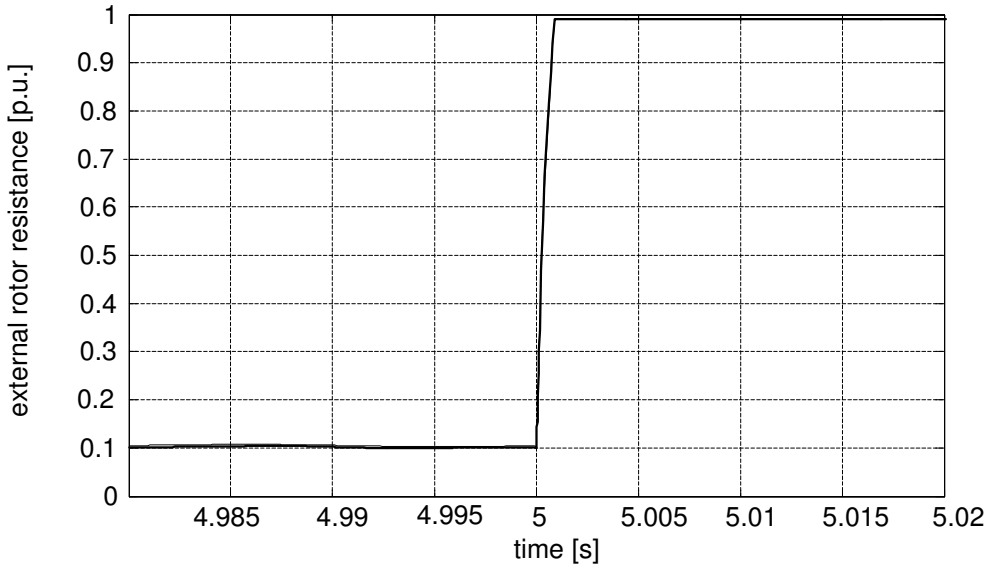

Fig. 14 external controlled rotor resistor

Despite all these described influences the effect of different generator models can be still seen in the generator stator currents Fig. 15. The current amplitude of the model with saturation effects shows a 4% higher value compared to the model without saturation effects on the highest peak.

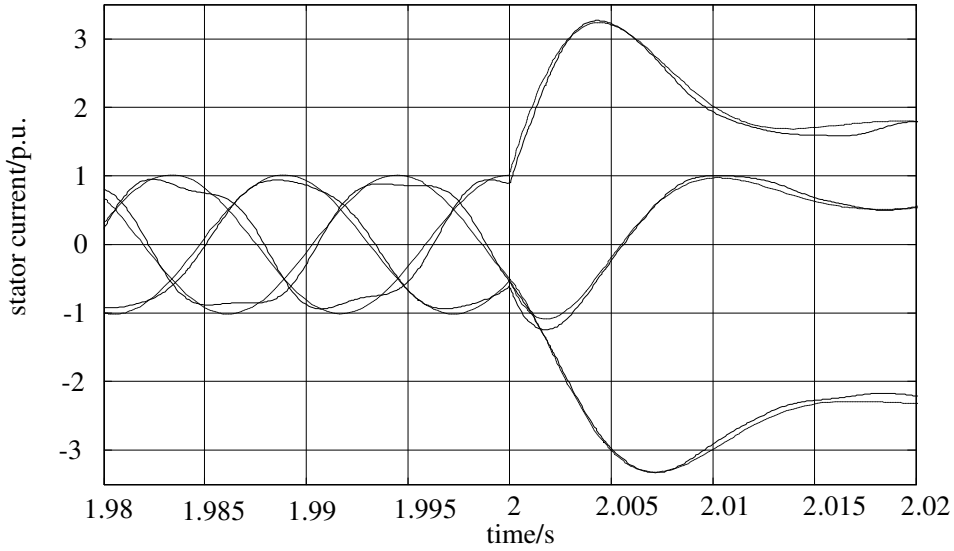

Fig. 15 generator stator current of model with saturation effects (solid line) and model without saturation effects (dashed line)

The 4% higher amplitude of the current is important for the design of the protection system of the turbine. It might just be the critical contribution, which decides to upgrade the components of the turbine.

CONCLUSION

There are many different ways of machine modeling, but as the machines are designed for there application, the model has to be developed for the expected use and the reality. The in this paper presented three-phase model has been made for the purpose of fault simulation of Vestas variable speed wind turbines. Thereby it has been shown, that different analytical description of the e.g. connection of the machine phases have an increased importance, while looking at asymmetrical conditions. Leakage saturation has an important influence, while looking at short circuit contribution to the grid, which plays an important role for grid connection of the turbine. On the other hand the effect of main saturation is almost negligible. The ABC/abc machine model is beneficial to use, because it simplifies the inclusion of connection condition influence, per phase variability of saturation and it can be easily expanded for other simulation purposes e.g. asymmetry in the machine parameters or harmonics.

REFERENCES

[1] S.Bolik, “Grid Requirements challenges for Wind Turbines”, *Fourth International Workshop on Large-Scale Integration of Wind Power and Transmission Networks for Offshore Wind farms, Billund 2003*

[2] I. Serban, F. Blaabjerg, I. Boldea, Z. Chen, ”A study of the Doubly-Fed Wind Power Generator Under Power System Faults”, proceed. of *EPE’03,2003*

[3] F. Iov, F. Blaabjerg, A.D. Hansen, P. Sørensen, ”Analysis of reduced order models for large squirrel-cage induction generators in wind turbine applications”,Proceed. of *EPE’03,2003*

[4] J. Morren, S.W.H. de Haan, P. Bauer, J.T.G. Pierik, J. Bozelie, “Comparison of complete and reduced models of a wind turbine with Doubly-Fed Induction Generator”, Proceed. of *EPE’03, 2003*

[5] J.B. Ekanayake, L. Holdsworth, N.Jenkins, “Comparation of 5th order and 3th order machine models for doubly fed induction generator (DFIG) wind turbines”, *Elsvier Power System Research 67, 2003, pp. 207-215*

[6] F. Iov, A.D. Hansen, F. Blaabjerg, ”A New Matlab/ Simulink Toolbox for Wind Turbine Applications”, *Proceed. Nordic MATLAB Conference 2003 in Copenhagen*

[7] T. Petru, “Modeling of Wind Turbines for Power System Studies”, *Thesis*, *Chalmers University of Technology, 2003*

[8] P. Sørensen, A. Hansen, L. Janosi, J. Bech, B. Bak-Jensen, ”Simulation of Interaction between Wind Farm and Power System”, *Risø National Laboratory, Roskilde, Dec. 2001*

[9] Zhongming Ye, Bin Wu, “Simulation of Electrical Faults of Three Phase Induction Motor Drive System”, *Power System Technology, Proceed. of. PowerCon 2000 , Vol. 2 pp. 789 -794*

[10] P. Pillay, V. Levin, “Mathematical models for induction machines”, *Proceed. of IAS-95, Vol.X.pp.606-616*

[11] C. Goldemberg, A. de Arruda Penteado, F. A. M. Salotti, “Induction motor analysis in the ABC/abc refernce frame including saturation effects”, *Proceed. of the ICEM 2000,pp.397-401*

[12] D. W. Novotny, T. A. Lipo, “Vector Control and Dynamics of AC Drives”, *Oxford University Press, 1996, ISBN 0198564392*

[13] P. C. Krause, O. Wasynczuk, S. D. Sudhoff, **“**Analysis of electrical Machinery”*, IEEE PRESS, 1994 ISBN 0-7803-1101-9*